

*Suban Viorel*

# **FAST DYNAMICS RESPONSE OF SENSORLESS CONTROL OF HIGH SPEED SURFACE PERMANENT MAGNET SYNCHRONOUS MOTOR DRIVES**

Teză destinată obținerii  
titlului științific de doctor inginer  
la  
Universitatea "Politehnica" din Timișoara  
în domeniul INGINERIE ELECTRICĂ  
de către

**Ing. Răzvan Ancuți**

UNIV "POLITEHNICA"	
TIMIȘOARA	
BIBL:	ELSA
Nr. vol:	674/13
Dulap:	ET / LR Ancu

Conducător științific:  
Referenți științifici:

prof.dr.ing. Ion Boldea  
prof.dr.ing. Ioan Adrian Viorel  
prof.dr.ing. Mircea Rădulescu  
prof.dr.ing. Gheorghe-Daniel Andreescu

Ziua susținerii tezei: 31.10.2008

Seriile Teze de doctorat ale UPT sunt:

- |                        |   |
|------------------------|---|
| 1. Automatică          | 7. Inginerie Electronică și Telecomunicații |
| 2. Chimie              | 8. Inginerie Industrială                    |
| 3. Energetică          | 9. Inginerie Mecanică                       |
| 4. Ingineria Chimică   | 10. Știința Calculatoarelor                 |
| 5. Inginerie Civilă    | 11. Știința și Ingineria Materialelor       |
| 6. Inginerie Electrică |   |

Universitatea „Politehnica” din Timișoara a inițiat seriile de mai sus în scopul diseminării expertizei, cunoștințelor și rezultatelor cercetărilor întreprinse în cadrul școlii doctorale a universității. Seriile conțin, potrivit H.B.Ex.S Nr. 14 / 14.07.2006, tezele de doctorat susținute în universitate începând cu 1 octombrie 2006.

Copyright © Editura Politehnica – Timișoara, 2008

Această publicație este supusă prevederilor legii dreptului de autor. Multiplicarea acestei publicații, în mod integral sau în parte, traducerea, tipărirea, reutilizarea ilustrațiilor, expunerea, radiodifuzarea, reproducerea pe microfilme sau în orice altă formă este permisă numai cu respectarea prevederilor Legii române a dreptului de autor în vigoare și permisiunea pentru utilizare obținută în scris din partea Universității „Politehnica” din Timișoara. Toate încălcările acestor drepturi vor fi penalizate potrivit Legii române a drepturilor de autor.

România, 300159 Timișoara, Bd. Republicii 9,  
tel. 0256 403823, fax. 0256 403221  
e-mail: editura@edipol.upt.ro

# PREFACE

The present thesis represents an approach, based on high speed permanent magnet synchronous machine with one directional inverter, for control of the variable speed electric drives.

## Motivation

In industry more than 60% of electrical energy is consumed by electrical drives. That's why the demanding of more motor efficiency is increasing year after year. Three phase motors are wide-spread almost anywhere in: industry, electric traction, road vehicles, ships, aircrafts, military equipment, medical equipment etc.

D.c. commutator was the first motor chosen to drive systems at variable speed. After 1970s vector control methods with new generations of inverters became an alternative solution. In last 10 years the importance of permanent magnet motors technology has significantly increased since the price of rare earth permanent magnet has decreased steadily. In this situation the permanent magnet motor replaces more and more, where it is possible, the induction motor.

High speed permanent magnet machines are used in applications such as pumps, centrifugal compressors, dental drills, aerospace technologies, etc. However, the control of these machines involves some issues. The control without motion sensor is mandatory for reasons of costs and reliability. The on line computation cycle decreases meanwhile the speed increases. Any observer, feedback control loops or coordinates transformation introduces undesirable time delays. The target of the thesis was to offer concrete solutions for advanced control of high speed electric machines.

**Ancuți, Răzvan**

**Fast dynamics response of sensorless control of high speed surface permanent magnet synchronous motor drives**

Teze de doctorat ale UPT, Seria 6, Nr. 9, Editura Politehnica, 2008, 214 pagini, 129 figuri, 5 tabele.

ISSN: 1842-7022

ISBN: 978-973-625-734-6

Keywords:

Frequency control, Frequency stability, High speed surface permanent magnet synchronous motors, Sensorless control, Voltage control.

**Abstract**

The present thesis is dedicated to the performant control of high variable speed permanent magnet synchronous motors. Thus, the thesis is focused on two solutions in order to control this machine for pumps, micro-turbine started generation units, centrifugal compressors, grinding machines, textile machines, drill, dental drills, aerospace technologies etc.

In order to use permanent magnet synchronous machines in motor drives for heating, ventilating, and air conditioning applications, simple, low cost control methods are also important. The particular requirement of the control of permanent magnet synchronous machines is the synchronization of the a.c. excitation frequency with rotational speed. Usually a shaft-mounted position sensor is required for achieving this. This position sensor increases the cost and reduces the reliability in the drive system. This makes it undesirable for these applications.

The objective of this research project is to investigate sensorless control methods of permanent magnet synchronous machines with particular attention for high speed applications requirements.

Since high dynamic performance is a demand for this kind of high speed applications, a suitable control approach for permanent magnet machines is proposed.

The new control is based on standard V/f control with two supplementary stabilizing loops. This control becomes more reliability with evident advantages beside standard V/f control with superior stability and dynamic. Much more the power computation is inferior to vector control but with similar speed dynamics and steady state errors.

Beside the new control, the vector control performance is also discussed in the thesis. The control structure and the design of the controllers for field orientation control drive system are described. Four angle and rotor position estimators for sensorless operation of the field oriented controlled drive system are studied in detail.

# ACKNOWLEDGEMENTS

I wish to thank to my supervisor Prof. Ion Boldea from the "Politehnica" University of Timisoara, Romania. His guidance and support made this work possible.

I would like to thank also Prof. Frede Blaabjerg from the Institute of Energy Technology, Aalborg University, Denmark for his support and for the discussions during and after my three months researching period in Aalborg.

Many thanks to Prof. Gheorghe Daniel Andreescu from the Faculty of Automation and Computers, "Politehnica" University of Timisoara, Romania. His advices and numerous inputs during the experimental work were very helpfully.

I want to thank also to Assoc. Prof. Lucian Tutelea and to all of those who contributed to my engineering education and also to my colleagues from Intelligent Motion Control Laboratory at Faculty of Electrical Engineering, Timisoara.

Finally I want to thank my parents and my girlfriend for their support and understanding.

Timișoara, Septembrie, 2008

Răzvan Ancuți

# Objectives of the thesis

The major objectives of the thesis are:

- offer an overview of the variable speed permanent magnet electric machines and their control for power applications and systems;
- develop simulation models for the complete system with high speed SPMSM;
- testing rotor position and speed estimators for surface mounted synchronous permanent magnet motors for sensorless control;
- finding a sensorless vector control strategy, robust and accurate which will startup under synchronous operation working with one tested estimator;
- finding a novel sensorless control system for high-speed SPMSM with performance almost as good as the ones in vector control and some possible improvements;
- simulation of different proposed controls and comparisons between them and vector control are the goal of an entire thesis;
- implementation details and comprehensive test results on a developed system are expected;
- advantages and drawbacks of the new control system and comparison results with the same system tested with vector control will be done;

# Outline of the thesis

The thesis is organized in 7 chapters following the above-presented objectives.

The *first chapter* presents a comprehensive overview of actual variable speed permanent magnet electric machines and their control. Detailed information is given for all actual solutions.

In the *second chapter* the vector control simulation models developed for analysis of the surface permanent magnet synchronous machine system are described and discussed. In this chapter four rotor position and speed estimators for surface mounted synchronous permanent magnet motors were tested.

In the *third chapter*, experimental results of sensorless control, low-voltage, high speed surface permanent magnet system are illustrated in detail. The importance of voltage drop compensation of the inverter semiconductor devices was demonstrated, especially at startup and low speeds.

In the *forth chapter* the simulation investigation introduces a novel set of two stabilizing loops to correct the voltage amplitude and phase in V/f control of SPMSM. Two solutions are introduced and both of them reduce speed oscillations, having fast speed responses.

In the *fifth chapter* the experimental investigations of the new proposed control system are presented. The dynamics are similar to the vector control system dynamics. Experimental results confirm the simulation results from the above chapter.

In the *sixth chapter* the test rig used for the whole experimental work is presented and commented and in the *seventh chapter* the work is summarized and the conclusion, contributions and the future perspectives are stressed.

# Table of Contents

<b>PREFACE .....</b>	<b>3</b>
MOTIVATION.....	3
ABSTRACT.....	4
ACKNOWLEDGEMENTS.....	5
OBJECTIVES OF THE THESIS .....	6
OUTLINE OF THE THESIS .....	7
<b>NOMENCLATURE .....</b>	<b>13</b>
<b>CHAPTER 1 INTRODUCTION .....</b>	<b>15</b>
1.1. PERMANENT – MAGNET ELECTRIC MACHINES.....	15
1.2. CLASSIFICATION OF PM ELECTRIC MACHINES .....	18
1.3. PERMANENT MAGNET SYNCHRONOUS MACHINES .....	20
1.4. PMSMS VERSUS INDUCTION MACHINES.....	21
1.5. BASIC SINUSOIDAL CONTROL METHODS.....	23
1.5.1. <i>V/f control</i> .....	23
1.5.2. <i>Closed-loop speed and torque control</i> .....	24
1.6. ROTOR POSITION SENSOR ELIMINATION.....	25
1.7. SUPER-HIGH SPEED PMSMS.....	28
1.7.1. <i>Inverter with high switching frequency at high power ratings..</i>	29
1.7.2. <i>Fast feedback loops in controller</i> .....	30
1.8. CONCLUSION .....	31
<b>REFERENCES .....</b>	<b>32</b>
<b>CHAPTER 2 SIMULATION OF VECTOR CONTROL FOR THE SYNCHRONOUS MACHINE WITH SURFACE PERMANENT MAGNETS .</b>	<b>34</b>
2.1. INTRODUCTION.....	34
2.2. MATHEMATICAL MODELS AND CONTROL PROPERTIES.....	35



2.2.1. <i>SPMSM model in space vector form</i> .....	35
2.2.2. <i>Voltage equations in stationary stator reference frame</i> .....	36
2.2.3. <i>Voltage equations in rotor reference frame</i> .....	38
2.3. THE CONTROL STRUCTURE OF THE DRIVE SYSTEM.....	40
2.3.1. <i>Overall simulated system description</i> .....	41
2.3.2. <i>Coupling in rotor d, q reference frame</i> .....	43
2.3.3. <i>Decoupling in current controllers</i> .....	44
2.3.4. <i>Validation of the current and speed controller design</i> .....	45
2.4. FOUR ROTOR POSITION AND SPEED SIMPLIFIED ESTIMATORS FOR VECTOR CONTROL STRATEGY.....	46
2.4.1. <i>Theoretical background of the speed and position estimators</i> ..	46
2.4.2. <i>Rotor position and speed estimators for encoderless control</i> ...	49
2.4.3. <i>Rotor speed estimator for encoderless control</i> .....	55
2.4.4. <i>Simulations results of angle and speed estimators</i> .....	56
2.5. SENSORLESS PMSM VECTOR CONTROL SIMULATION .....	60
2.6. SENSORLESS PERFORMANCE OF THE COMPLETE DRIVE SYSTEM.....	62
2.7. CONCLUSION .....	66
<b>REFERENCES .....</b>	<b>68</b>
<b>CHAPTER 3 VECTOR CONTROL – MOTION SENSORLESS CONTROL EXPERIMENTAL RESULTS .....</b>	<b>73</b>
3.1. INTRODUCTION.....	73
3.2. EQUATIONS USED IN ESTIMATOR DESIGN .....	74
3.3. MOTION SENSORLESS CONTROL SYSTEM.....	75
3.4. BACK-EMF ANGLE ESTIMATOR FOR DYNAMIC OPERATING MODE.....	77
3.5. START-UP STRATEGY.....	80
3.6. PARTICULARITY OF THE CONTROL SYSTEM.....	84
3.7. EXPERIMENTAL RESULTS.....	85
3.7.1. <i>No Load Start-Up at 10,000 rpm</i> .....	86
3.7.2. <i>Load Start-Up at -10,000 rpm and Reversal at +10,000 rpm</i> ..	89

3.7.3. <i>No Load Start-Up at 15,000 rpm Followed by a Step Torque Load</i> .....	92
3.7.4. <i>No Load Start-Up at 20,000 rpm</i> .....	94
3.7.5. <i>No Load Start-Up at 2,000 rpm and Speed Reversal, Followed by a Step Torque Load</i> .....	97
3.8. CONCLUSION .....	100
<b>APPENDIX .....</b>	<b>100</b>
<b>REFERENCES .....</b>	<b>101</b>
<b>CHAPTER 4 SENSORLESS V/F CONTROL OF SURFACE PMSM WITH STABILIZING LOOPS – BASICS AND SIMULATION RESULTS .....</b>	<b>106</b>
4.1. INTRODUCTION.....	106
4.2. V/F CONTROL WITH FLUX AND POWER ANGLE STABILIZING LOOPS.....	107
4.3. DIGITAL SIMULATIONS RESULTS .....	111
4.4. SENSORLESS V/F CONTROL OF PMSM WITH TWO NOVEL STABILIZING LOOPS FOR HIGH SPEED DYNAMICS FOR ZERO INTERIOR REACTIVE POWER.....	119
4.4.1. <i>Proposed V/f control with two stabilizing loops</i> .....	119
4.4.2. <i>Overall simulated system description</i> .....	121
4.4.3. <i>Simulation results</i> .....	125
4.5. CONCLUSION .....	130
<b>APPENDIX .....</b>	<b>131</b>
<b>REFERENCES .....</b>	<b>132</b>
<b>CHAPTER 5 SENSORLESS V/F CONTROL OF SURFACE PMSM WITH TWO NOVEL STABILIZING LOOPS FOR HIGH SPEED DYNAMICS: IMPLEMENTATION AND TEST RESULTS .....</b>	<b>136</b>
5.1. INTRODUCTION.....	136
5.2. BASIC CONTROL SYSTEMS FOR SPMSM.....	137
5.3. PROPOSED V/F CONTROL, WITH TWO STABILIZING LOOPS .....	139

---

5.4. INTERNAL REACTIVE POWER CALCULATOR.....	142
5.5. START-UP STRATEGY .....	144
5.6. EXPERIMENTAL RESULTS.....	145
5.6.1. <i>No Load Start-Up to 10,000 rpm</i> .....	146
5.6.2. <i>On Load Start-Up at and Speed Reversal at +10,000 rpm</i> ....	148
5.6.3. <i>No Load Start-Up to 15,000 rpm</i> .....	153
5.6.4. <i>No Load Start-Up to 20,000 rpm</i> .....	155
5.6.5. <i>No Load Start-Up to 2,000 rpm and Speed Reversal with Step             Torque Load</i> .....	158
5.7. CONCLUSION .....	160
<b>APPENDIX .....</b>	<b>161</b>
<b>REFERENCES .....</b>	<b>162</b>
<b>CHAPTER 6 THE TEST BENCH SETUP .....</b>	<b>165</b>
6.1. INTRODUCTION.....	165
6.2. HARDWARE SPECIFICATIONS.....	167
6.2.1. <i>The twin permanent magnet synchronous machines</i> .....	167
6.2.2. <i>dSpace DS1103</i> .....	168
6.2.2.1. <i>I/O Units</i> .....	171
6.2.2.2. <i>DSP Subsystem</i> .....	171
6.2.2.3. <i>CAN Subsystem</i> .....	171
6.2.2.4. <i>Master PPC Slave DSP Slave MC</i> .....	171
6.2.3. <i>Position sensor</i> .....	174
6.2.4. <i>Interface system</i> .....	179
6.3. SOFTWARE.....	180
6.3.1. <i>Matlab Simulink</i> .....	180
6.3.1.1. <i>Measure and protection software</i> .....	180
6.3.1.2. <i>Control and estimation algorithms</i> .....	182

6.3.2. "Control Desk" Developer specialized real time interface software .....	183
6.4. FROM SIMULATION TO PRACTICAL IMPLEMENTATION .....	184
6.5. THE SYSTEM TUNING.....	187
6.5.1. Current and voltage sensors tuning.....	187
6.5.2. Phase A Voltage Back Emf synchronization with incremental encoder .....	187
6.5.3. Start up issues .....	189
6.5.3.1. Optical fiber.....	189
6.5.3.2. The congruence between the current sensors and the motor phases.....	189
6.5.3.3. Position sensor errors.....	191
6.6. CONCLUSION .....	192
<b>REFERENCES .....</b>	<b>193</b>
<b>CHAPTER 7 CONCLUSION AND CONTRIBUTIONS .....</b>	<b>195</b>
7.1. MATHEMATICAL MODEL AND CONTROL PROPERTIES .....	195
7.2. SENSORLESS VECTOR CONTROL.....	195
7.3. SENSORLESS V/F CONTROL WITH TWO STABILIZING LOOPS.....	196
7.4. COMPARISON OF CONTROL METHODS.....	197
7.5. ORIGINAL CONTRIBUTIONS.....	198
7.6. FUTURE WORK .....	199
SUMAR .....	200
ORGANIZAREA TEZEI.....	202
CONTRIBUTIILE TEZEI.....	204
AUTHOR'S PAPERS RELATED TO THE PH. D. THESIS.....	205
AUTHOR'S CV .....	206
<b>APPENDIX .....</b>	<b>207</b>

# NOMENCLATURE

## Symbols

$B_m$	Viscous friction coefficient;
$E_m$	Magnitude of the rotor permanent-magnet flux induced voltage vector in steady state;
$E_s$	Magnitude of the stator flux linkage induced voltage vector in steady state;
$I_s$	Magnitude of the stator current vector;
$i_a, i_b, i_c$	currents of stator phases a, b, and c;
$I_\alpha, I_\beta$	stator currents in $\alpha, \beta$ stator reference frame;
$I_d, I_q$	stator currents in $d, q$ rotor reference frame;
$J$	Inertia of the motor shaft and the load system;
$L_s$	stator total inductance;
$L_m$	magnetizing inductance;
$R_s$	stator resistance;
$p$	number of pole pairs;
$T_e$	electromagnetic torque;
$T_L$	load torque;
$Q_\alpha^j, Q_\beta^j$	internal reactive power in $\alpha, \beta$ stator reference frame;
$Q_d^j, Q_q^j$	internal reactive power in $d, q$ rotor reference frame;
$\bar{V}_s$	voltage stator vector;
$V_\alpha, V_\beta$	stator voltage in $\alpha, \beta$ stator reference frame;
$V_{DC}$	DC-link voltage;
$n_{mec}$	mechanical speed;
$f_e$	electrical frequency;
$\omega_{er}$	electrical rotor speed;
$\theta_{er}$	electrical rotor position;

$\theta_i$	stator current vector angle;
$\theta_v$	stator voltage vector angle;
$\lambda_s$	total stator flux;
$\lambda_{PM}$	rotor permanent magnet flux;
$\gamma$	total flux to current angle;
$\delta$	load angle;

### Abbreviations

a.c.	Alternating current;
d.c.	Direct current;
DSP	Digital signal processor;
EMF	Electromotive force;
LPF	Low-pass filter;
PI	Proportional-Integral control;
PM	Permanent magnets;
PLL	Phase-locked loop;
PWM	Pulse width modulation;
SM	Synchronous machine;
SPMSM	Surface permanent-magnet synchronous machine;
SVM	Space vector modulation;

# Chapter 1

## Introduction

### 1.1. Permanent – magnet electric machines

Synchronous machines are doubly excited electric machines.

In the conventional type - d.c. commutation machines and synchronous machines - both of magnetic fields are produced by currents that flows through windings connected to external electrical sources.

For the PM electric machines, one of the winding is replaced with permanent-magnets so one of the external sources is eliminated [1].

The replacement of the copper winding in the SM's with permanent magnets brings the following advantages:

- higher efficiency because the copper losses are reduced;
- lower weight and reduced dimensions;
- more compact construction;

As main disadvantages of PMSMs we should mention here the following two:

- the excitation field cannot be controlled so easy as in conventional synchronous machine by directly controlling the field current;
- the permanent magnets of very good quality are very sensitive to the temperature consequently the machine design and cooling should be adequate

Permanent magnet machines have numerous applications. The areas where this electrical devices start to be successfully used are mentioned below [2]:

### • **Medium power alternators**

The configuration of PM alternator is similar to a conventional synchronous alternator where the electric excitation system is replaced by permanent magnets. The main advantage of this arrangement is removing the brush/slipping system and, as disadvantage, losing of field control and reducing of flexibility of the operation have to be mentioned.

### • **Automotive motors and generators**

The actual trend in the automotive industry and especially in modern automobiles and trucks construction is the replacement of the rare-earth magnets with PM machines. Consequently, this industry becomes the largest user of the PM machines.

### • **Applications in Textile and Glass Industries**

In the synthetic fiber and glass industries, it is often important that the speed of different machines to be identical and exactly related to the supply frequency. This capability of synchronous machines gives them an advantage in such applications related to induction machines.

This fact leads to an increased utilization of variable speed drivers in the textile and glass industries similar to the automotive applications noted above. Here, reluctance and PM motors have been used with power semiconductor controllers.

### • **Small Appliance**

These applications have traditionally been of the a.c. series or “universal” configuration for house appliances. Commutation problems are generally more severe in a.c. series machines than d.c. machines of similar size. However, in certain applications where a more constant speed with load is desirable, the conventional PM may offer a reduced cost and reduced maintenance due to improved commutation.



## • Control Motors

In many types of d.c. control and instrumentation applications, including control motors, instrument drives, servomotors, revolvers, torque motors and tachometers. Reluctance sensors are also requiring PM excitation. Magnetic encoders are PM-excited.

## • Computer and Robotics Applications

PM motors are used in this domain in large applications because of noise level reduction, speed and torque control and flexibility of shape. An example, the so called spindle motor that is driving the most computer disks, is presented in Fig. 1.1

They combine advantages of synchronous motor technology with operational characteristics of asynchronous motors, providing high torque. Cooling system is enclosed within stator, and motor windings are protected against thermal overload by integrated temperature sensors.

The main requirements of these motors are high starting torque and very precise speed regulation.

PM motors are used mostly in other computer applications, such as printers and type drives, where controlled motion is required. Another domain of applications is the area of robotics.

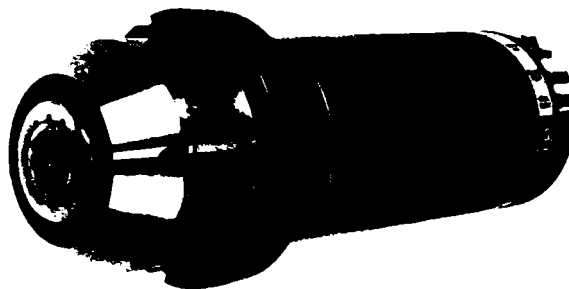


Fig. 1.1 Spindle motor with three-phase-wound stator and permanent-magnet rotor

## • Printed Circuit Motors

Special constructions of the PMSMs are the so named "Printed Motors". The name "printed circuit motor" was adopted to describe the special construction of

these PMSMs whose armature winding were formed through a technological process which is in essence a photochemical printing similar to the one used for some types of PC board. These circuits can be also formed by stamping process.

In control applications, printed-circuit motors have very high acceleration capabilities compared to cylindrical motor and can operate at higher speed since their rotor inertia is very low.

## 1.2. Classification of PM electric machines

Depending on the hardware design, electrical machines can be with d.c. or a.c. excitations. So, in the below paragraph, the most wide-spread machines are presented.

Permanent magnet (PM) electric machines classification is:

- d.c. commutator motor (PMDC)
- brushless motor (a.c. and d.c synchronous):
  - sinusoidal excited or a.c. brushless motor (BLAC or PMSM)
    - surface magnets type (SPMSM)
    - interior magnets type (IPMSM)
  - trapezoidal type or d.c. brushless motor (BLDC)
- stepping motor

The construction of a PMDC commutator motor is similar to a d.c. motor with the electromagnetic excitation system replaced by PMs.

PM d.c brushless and a.c. synchronous motors have practically the same construction: with polyphase stator and PMs located on the rotor. The only difference is in the control and shape of the excitation voltage: an a.c. synchronous motor is fed (excited) with more or less sinusoidal waveforms which in turn produce a rotating magnetic field. In PM d.c. brushless motors the armature current has a square (trapezoidal) waveform, only two phase windings (for Y connection) conduct the current at the same time. The current switching pattern for such a machine is synchronized with the rotor angular position (electronic commutation). A comparison between PM d.c brushless and a.c. synchronous motors is presented in [3] and [4].

It should be mentioned that PMACs are not built with damper windings in rotor mainly due to the high manufacturing cost. This kind of construction will cause some control issues.

The PMSMs are synchronous machines whose field is generated by permanent-magnet located in the rotor.

The commutation and brushes missing makes the machine structure very simple and eliminates the commutation problems associated to PMDC. This is important particularly where the machine is used in a relatively inaccessible location – such an outer space or in many automotive vehicle locations and for computer applications. Due to its simplicity and compactness the PMAC machines are the most attractive machines from all of the PM electric machines.

The rotor topology of PMSMs depends on how the magnets are placed in the rotor, as is presented in references [5] and [6].

The two common types, namely, surface permanent magnets and interior permanent magnets types are shown in Fig. 1.2. In the case of the surface permanent magnets synchronous motors (SPMSMs) the magnets are placed on the rotor core surface in the air gap, which results larger than for a classical machine. For the interior permanent magnets synchronous motors (IPMSMs) the permanent magnets are placed inside the rotor core. A particular case of this construction is the one with concentrated flux topology when the PMs are magnetized tangential not radial and the ratio of the pole area to PMs active area is larger than unity.

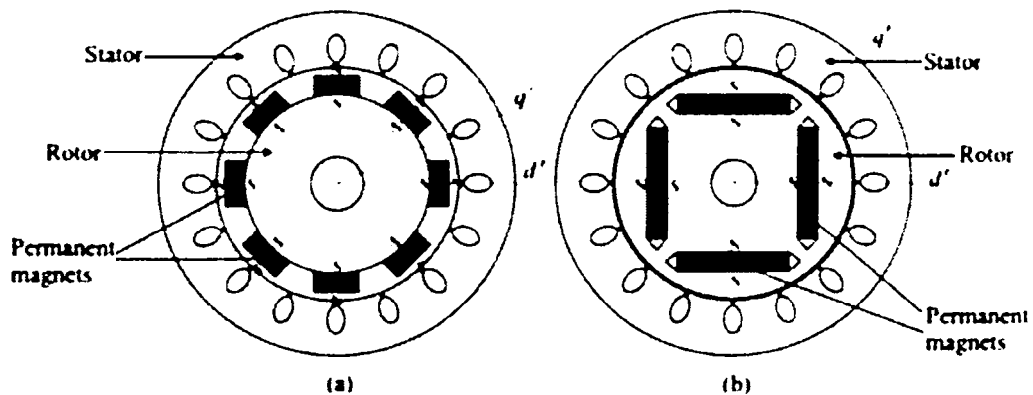


Fig. 1.2 Permanent magnets synchronous machines with surface magnets type (a) and interior magnets type (b)

Stepping motor drive consists of an input controller, a logic sequencer and a driver. The input controller is a logic circuit that produces the required train of pulses. It can be a microprocessor or microcomputer which generates a pulse train to speed up and slow down the stepping motor. The logic sequencer is a logic circuit that responds to step-command pulses and controls the excitation of windings sequentially [9]. Output signals of a logic sequencer are transmitted to the input terminals of a power drive which turn on and turn off the stepping motor windings. The stepping motor converts electric pulses into discrete angular displacements.

### **1.3. Permanent Magnet Synchronous Machines**

PM synchronous machines generally have the same operating and performance characteristics as synchronous machines operation at synchronous speed, a single or polyphase source of a.c. supplying, a power limit above which operation at synchronous speed is unstable, reversible power flow etc. The configuration can be almost identical to that of the conventional synchronous machine with the absence of the slip rings and a field winding and of course this is the principal merit of the PM synchronous machines. In general, synchronous machines are power reversibles, i.e., one configuration can be operated in either the motoring or generating mode.

The PM synchronous machine is almost the simplest machine. Only reluctance machines are simpler in construction and in assembly production than PM machines, but reluctance machines, generally, develop less torque per unit of current and per unit of weigh. Therefore regarding of power output per unit of weight the PM synchronous machine is superior to all other brushless synchronous machines but PM motors are generally more complex than several other types of synchronous brushless machines, such as the reluctance and inductors machines. In terms of cost per unit power output it is also lower than all because the prices of the rare earth magnets decreased satisfactorily enough in the last years.

## 1.4. PMSMs versus induction machines

Due to the relatively high cost of the permanent magnets, the PM synchronous machines were introduced recently. However, once the cost of the permanent magnets was decreasing, PM synchronous machines became more sell than the induction machine, which have a lower cost, but a poor efficiency.

Thus, making a comparison between the relatively high power system (20 kW) of a PMSM and the one of an induction machine, the following benefits for the former system result [10]:

- the efficiency is increased with 10 to 15 percent compared to current a.c. systems;
- variable speed capability with a proper command inverter keeps efficiency high while matching changes in demand;
- all the PMSM systems should repay initial costs installation drive in few months: 12 to 30 months in the case of changing of an old induction machine drive system with a performant PM synchronous machine drive system and in at least 6 months in the case of choosing a PM synchronous machine drive system in the favor of an induction machine drive system;
- using rare earth permanent magnet materials, permanent magnet motors are significantly smaller and quieter than traditional a.c. motors;
- at 50 kg, the lighter, smaller, and quieter drive offers significant installation savings compared to conventional a.c. package units with 250 kg compressors.

Alternating current (AC) induction motors, also known as “squirrel cage” motors, drive compressor systems used in conventional packaged air conditioners. Pressure to advance technologies in areas such as efficiency and environmental impact, however, are leading to the development of new technologies for the air conditioner market.

PMSMs have permanent magnets in the rotor so do not require current magnetization component in the stator like induction motors and the efficiency is higher (no loses in the copper rotor winding as in the conventional type). This

characteristic improves significantly the efficiency in PMSMs compared with asynchronous machines.

These machines have higher torque and/or output power per volume than using electromagnetic excitation; have higher magnetic flux density in the air gap – better dynamic performance than motors with electromagnetic excitation.

The PMSMs are also attractive because can be designed with less weight and volume in contrast with induction machines. Moreover, they have high torque to inertia ( $T_e/J$ ) ratio, which is attractive for applications that demand fast dynamic response.

PMSM systems also have a very high capability to suppress heat generation, particularly in rotors.

Cage induction motors have been the most popular electric motors in the 20<sup>th</sup> century. The main advantages of the cage induction motors are their simple construction, simple maintenance, no commutator or slip rings, low price and moderate reliability. The disadvantages are their small air gap, the possibility of cracking the rotor bars due to hot spots and plugging and reversal, and lower efficiency and power factor than synchronous motors [12].

The entire electrical energy is consumed in motor drive in special for pumps and fans driving. The fans and pumps with slow torque response driven by PMSMs contribute to reduce the total energy consumption.

Since PMSMs are synchronous machines without damping cage their control should have incorporated self synchronization concepts. This demand is not required for induction machine control since it is an asynchronous machine. That's way the control concept is different between induction machines and PMSMs.

The use of PMSM motors has become a more attractive option than the induction motor. Rare earth permanent magnets improve the motor's steady state performance and the power density (output power-to-mass ratio), dynamic performance and quality.

On the market, the price of rare earth magnets is going down which is making these motors cheaper and more popular.

Due to the fact that rotor has lower inertia, there is a high gap magnetic flux and no-speed dependency of current limitation, the motor can reach a very good dynamic performance [13].

## 1.5. Basic sinusoidal control methods

By sinusoidal control of permanent magnet synchronous motors results that the drive has low torque perturbations and high dynamic performance. These motors have distributed windings which produce sinusoidal or quasi-sinusoidal mmf wave having very low harmonic contents.

### 1.5.1. V/f control

The problem of this control is caused by the missing of the damper windings (if the control is used for a PMSM). Thus, the open-loop V/f control without any improvements is hard to achieve fast dynamic response. Practically this control is fitting for applications that do not require fast dynamic response.

However, if we use a machine with damper winding, this control can be used. The asynchronous torque produced by rotor squirrel windings during asynchronous operation can damp the oscillations so the behavior of the PMSM is like an asynchronous machine in transitory periods. This makes possible to use simple open-loop V/f control algorithm for this type of IPMSMs as shown in Fig. 1.3. For this kind of machine (with damping windings) the standard V/f control will be used again only for applications such pumps or fans that do not require fast dynamic responses.

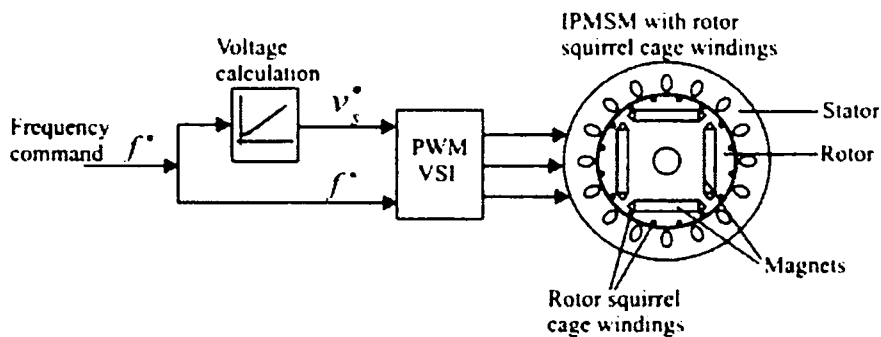


Fig. 1.3 Open loop V/f control, which can be used for IPMSMs with rotor squirrel cage windings [11]

Fig. 1.3 shows the V/f control approach for PMSMs with rotor cage windings which is similar to the one used for induction machine. However, one advantage of the PMSM drive is that the rotor speed is dependent only on the machine excitation frequency and it does not require slip compensation it does the induction machine drive.

To control the PMSMs without having rotor cage is a difficult job. This means that machine does not guarantee the synchronization between a.c. excitation frequency and rotor frequency. Much more, the system will oscillate or it can not be driven. The instability and oscillatory power associated with the open loop schemes are highlighted. Furthermore, a closed-loop sensorless vector control scheme could be developed to acquire the accurate rotor position for the entire speed range.

### 1.5.2. Closed-loop speed and torque control

In contrast with V/f control, the closed-loop speed and torque control is much better. The control can be achieved incorporating in the drive controller of the machine the torque and speed control elements. The drive control structure with torque and speed controller is shown in Fig. 1.4. The torque control is related with stator currents control requiring by stator currents feedback. Moreover, as described in this paragraph, to achieve self-synchronization, the rotor angular position feedback is also essential for the torque controller as opposed to induction machine, in those case this synchronization does not happened.

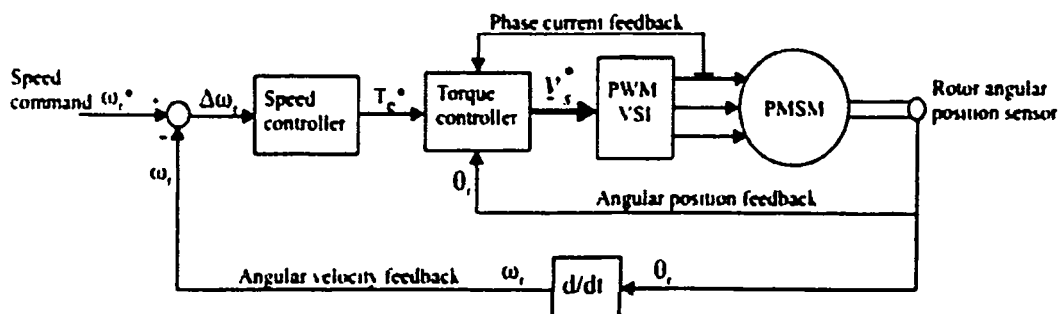


Fig. 1.4 Block diagram of PMSM control scheme incorporating torque and speed controller

The speed control can be achieved closing the speed feedback loop outside the inner torque control loop, so it can be said that speed loop is slower than torque



loop. The speed loop can be derived from the same angular position sensor; which is used to obtain the rotor position feedback.

Direct torque control (DTC) of PMSMs is the best control method, but requires fast computation time so an expensive drive controller. Accurate flux estimation and torque estimation are also required for DTC.

## 1.6. Rotor position sensor elimination

Position sensorless control has become popular for reliability improvement and cost reduction for any electric machine. The cost reduction is more evident at small motors where the encoder is an important part of the total cost of the system. For the super-high speed PMSM systems, sensorless position is needed for performance improvement. Issues occur when exceeding a certain speed because it is very difficult to install and maintain a mechanical shaft position sensor for super-high speed operations. A better solution is to replace the encoder with two Hall sensors, but these do not deliver the precise position of the shaft which is very important for the PMSM control.

The position sensor mounted on the shaft is not desirable in the control due to many reasons:

- is expensive and considerably increase the cost of the drive system;
- extra signals wires are required from the sensor to the controller;
- a special arrangement has to be made for mounting the sensor on the shaft;
- some sensor types are temperature sensitive;
- all are vibration sensitive;

The reasons given above, lead to eliminate the shaft mounted rotor angular position sensor, which is conventional used for self-synchronization in the control system.

To achieve fast torque control, direct torque control (DTC) of PMSMs is another method to drive the machine [14] [15]. This strategy involves accurate flux and torque estimation and fast computation time.

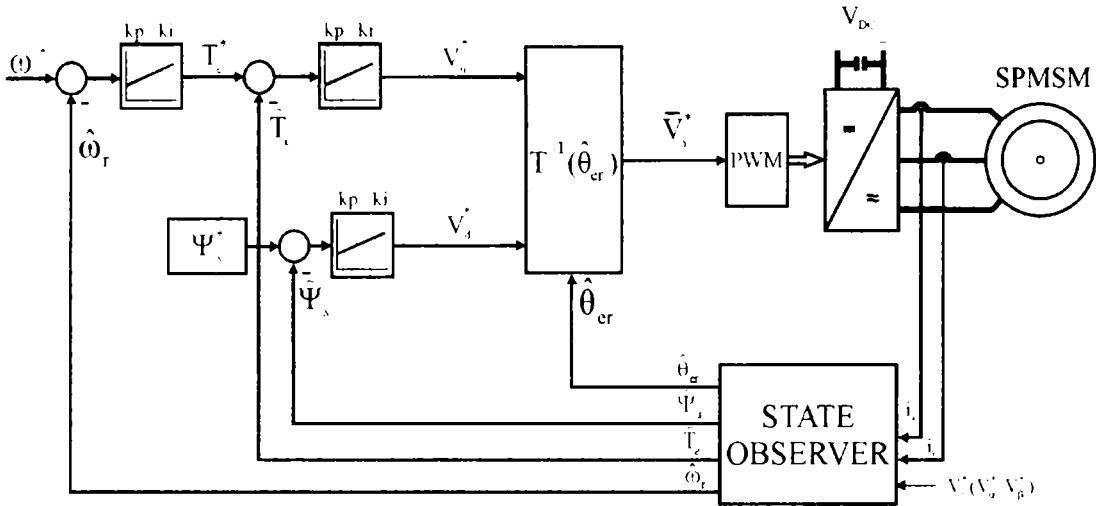


Fig. 1.5 Block diagram of DTFC control system without rotor angular position sensor

The other method to drive the machine is the standard vector control strategy presented in Fig. 1.6.

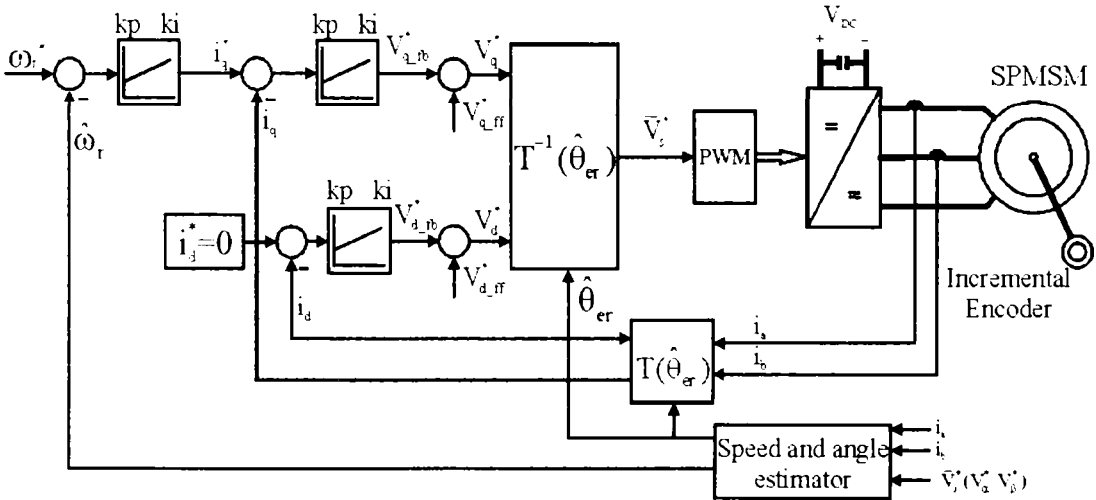


Fig. 1.6 Block diagram of sensorless vector control system without rotor angular position sensor

The field oriented control systems are presented in Fig. 1.5 and Fig. 1.6. In the special literature, these methods are considered the most performant close loop control strategies.

These strategies have in common the fact that the information delivered by the position sensor is not used. The rotor position, required in the control, is provided by an estimator. Furthermore this estimator can observe (estimate) other parameters like torque and flux which are needed in the control system.

Alternatively, in the special literature there are a few proposed controls as the one based on the standard V/f control (Fig. 1.4), but at which stabilizing loops are attached [11]. Fig. 1.7 presents a control system that uses a stabilizing loop on the frequency prescription. The correction is performed by analyzing the variation of the inverter d.c. link or the active power variation.

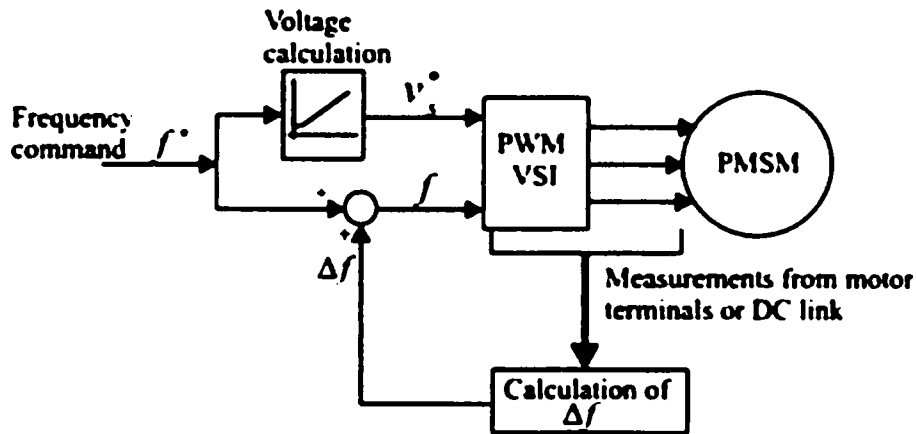


Fig. 1.7 V/f control approach for PMSMs with one stabilizing loop and without using rotor position sensor[11]

A stabilizing loop on the voltage module can also be introduced. Control systems using either one or other or both stabilizing loops can be proposed.

However, there is an important difference on how the stabilizing loops are design. Depending on the chosen strategy, in some cases, these corrections could lead to small improvements by reducing the pulsations in the speed waveform occurred in standard V/f control and, in other cases, they could lead to more improvements compared with the results achieved with the vector control.

## 1.7. Super-High Speed PMSMs

High speed motors develop mechanical speeds exceeding 10,000 rpm. Super-high speed PMSMs (> 50,000 rpm) are of great significance in a broad range of applications, such as pumps, micro-turbine started generation units, centrifugal compressors, grinding machines, textile machines, drill, dental drills, aerospace technologies, etc. Typical super-high speed PMSM is presented in Fig. 1.8.

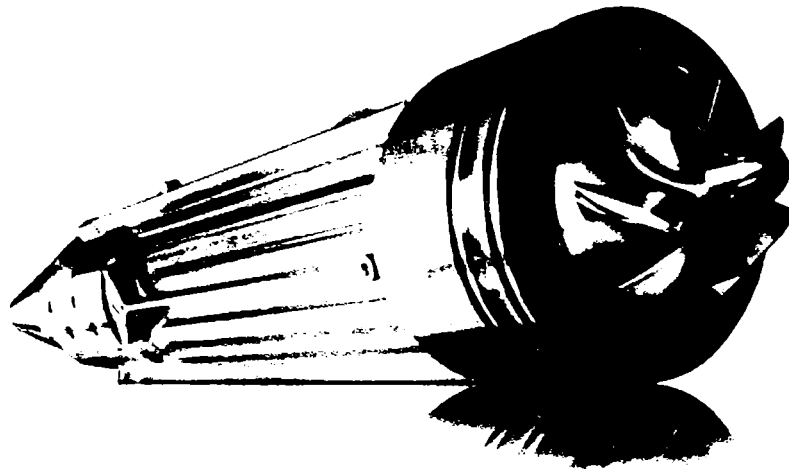


Fig. 1.8 Super High speed PMSM

Remarkably small size and light weight are the most distinctive features of super-high speed PMSMs, which lead to the high ratios of power to mass and power to volume.

The main demands for high speed electrical are [16]:

- increased bearing robustness as a result of high mechanical stress
- high efficiency cooling system to reach the highest output power-to-volume ratio comparable with standard machine;
- suitable lubrication system in order to get high quality behavior and mirror friction problems;
- capability to work in different positions;

Since the centrifugal force ( $F$ ) acting on a rotating mass is proportional to the linear velocity ( $v$ ) squared and inversely proportional with rotation radius ( $R$ ) (1.1), the rotor must be designed with a small diameter and must have a very high mechanical integrity to resist to high centrifugal force, and a very good static and dynamic balance. Even very small unbalance can produce high vibration which becomes stronger with speed increasing.

$$F = \frac{mv^2}{R} \quad (1.1)$$

The developed power is basically proportional with to the speed and the volume of the rotor. But this power is limited by thermal and mechanical constrains placed in the machine volume. The stator volume is limited by winding losses and heat dissipation. So the design of a high speed permanent magnet machine should take into consideration many aspects and, of course, does not have a simple solution.

Compared to a conventional speed PMSM system, the super-high speed PMSM system poses many challenges for its variable-speed operation over a wide speed range:

- inverter with high switching frequency at high power ratings;
- fast feedback loops in controller;
- necessity of position sensorless algorithm.

### **1.7.1. Inverter with high switching frequency at high power ratings**

A super-high speed PMSM system operates in the speed range from a few rpm to 50,000 rpm and above, with an excitation frequency from several to a few thousand hertz. So it is required that the switching frequency of the inverter to be as high as possible around 20 kHz. The designer of the inverter has to choose between MOSFET and IGBT. In practice, around this switching frequency, there are no single solutions. The choice will depend on the intrinsic transistor characteristics and the requirements of the application. The topology of the inverter and the d.c.

input voltage will affect the choice [7]. Additionally, a super-high speed PMSM features a very small resistance and inductance of stator windings, which make extremely difficult the stator current regulation and will affect the final selection.

### 1.7.2. Fast feedback loops in controller

Since the super-high speed PMSM is running with fundamental frequency between few Hz and 20 kHz, corresponding to a speed from a few rpm to 50,000 rpm, the digital controller should use a very short sampling cycle to acquire feedback signals (if these exist), process data and execute algorithms to produce control commands promptly. So if we fix the PWM frequency at 20 kHz, then all the computations have to be done in max 50  $\mu s$ .

$$f_{cycle} \leq \frac{1}{f_{PWM}} = \frac{1}{20.000} = 50 \mu s \quad (1.2)$$

$$f_{cycle} \leq f_{PWM} = 50 \mu s \quad (1.3)$$

Taking into account all the above mentioned conditions, the control system can be implemented only if there is an adequate mathematical algorithm and an expensive microprocessor such as the response is available in a time period lower than the cycle time.

Of course, if the microprocessor is not powerful enough then the implementation of some control algorithms which require a longer computation cycle time can be limited. To avoid limitation, a powerful microprocessor has to guarantee (1.2).

Anyway, at this high speed, extra fast digital signal processor is obviously needed or else "real time" control will be lost. Normally, the speed and current loops for the PMSM system has to be executed within several tens of microseconds to ensure online real time control. In such conditions, a general purpose microprocessor can not meet the required control speed and computing complicity simultaneously [8].

## 1.8. Conclusion

In this chapter, a review of the existent permanent magnet machines is presented.

The contrasts and the similarities between each machine are here highlighted.

Also the areas where these electrical devices are successfully used are presented.

Then the differences between an induction machine and a synchronous machine are presented.

The advantages of using a system incorporating a PM synchronous machine are here accentuated.

The PM synchronous machines have their weight and the volume net superior than induction machines.

Higher efficiency of the PM synchronous machines involves higher cost, which however can be damped in few months.

Then an overview of the sinusoidal control methods is presented. The way each control acts is highlighted.

Here the alternatives of the vector control using encoder are also presented. V/f control with stabilizing loops can be one of these alternatives.

At last, the difficulties occurred in the construction and in the control of the high speed machines are presented.

## References

- [1] S. A. Nasar, "Handbook of Electric Machines", McGraw-Hill Book Co., New York, 1987
- [2] Boldea, Nasar "Permanent Magnet Reluctance and Self Synchronous Motors" CRC Press 1993
- [3] Pillay P., Krishnan R., "Application Characteristics of Permanent Magnet Synchronous and Brushless dc Motors for Servo Drives", *IEEE Trans. On Ind. Appl.*, vol.27, nr.5, Septembrie/Octombrie 1991
- [4] Monajemy R., Krishnan R. "Performance Comparison for Six-Step Voltage and Constant Back EMF Control Strategies for PMSM", IEEE 1999
- [5] Thomas M. Jahns, "Variable Frequency Permanent Magnet AC Machine Drives", Chapter 6 in Power Electronics and Variable Frequency Drivesm Technology and Applications, B. K. Bose, Ed., IEEE Press, 1997.
- [6] Gordon R. Slemon, "Electrical Machines for Drives", Chapter 2 in Power Electronics and Variable Frequency Drives, Topology and Applications, B. K. Bose, Ed., IEEE Press, 1997.
- [7] B. Maurice, G. Izzo, T. Castagnet "Comparison of Mosfet and Igbt Transistors in Motor Drive Applications" <http://www.st.com/stonline/products/literature/an/3717.pdf>
- [8] Longya Xu and Changjiang Wang, "Implementation and Experimental Implementation of Sensorless Control Schemes for PMSM Drives", *IEEE Trans. Ind. Appl.*, vol. 39, no. 3, pp. 783–791, May-June 2003.
- [9] Kenjo T. "Power Electronics for the Microprocessor Control". Oxford: Clarendon Press. 1990
- [10] Martins, C.A.; Carvalho, A.S. "Technological Trends in Induction Motor Electrical Drives" Power Tech Proceedings, 2001 IEEE Porto, vol.2.
- [11] P. D. C. Perera, F. Blaabjerg, J. K. Pedersen, and P. Thogersen, "A Sensorless, Stable V/F Control Method For Permanent-Magnet Synchronous Motor Drives", *IEEE Trans. Ind. Appl.*, vol. 39, no. 3, pp. 783–791, May/Jun. 2003.
- [12] Gieras J.F., Wing M. "Permanent Magnet Motor Technology". Designs and Applications. 2002



- [13] Mongeau P. "High Torque/High Power Density Permanent Magnet Motors". Naval Symp on Electr Machines, Newport, RI, USA, 1997
- [14] M. Fu, L. Xu, "A sensorless direct torque control technique for PM synchronous motors", *Conf. Rec. 34<sup>th</sup> IEEE IAS Annual Meeting*, 1999, Vol. 1, pp. 159-164
- [15] C. Bian, S. Ren, L. Ma, "Sensorless DTC of super high-speed PMSM", *Proc. 2007 IEEE Int, Conf. Automat. Logist.*, pp. 3060-3064
- [16] A. Boglietti, M. Pastorelli, and F. Profumo, "High Speed Brushless Motors For Spindle Drivers", *Int. Conf. on Synchronous Machines SM100*, vol 3, Zurich, Switzerland, 1991, pp. 817-882.

# Chapter 2

## Simulation of Vector Control for the Synchronous Machine with Surface Permanent Magnets

### Abstract

This chapter presents the mathematical models for SPMSM control systems for high speed application. The models are developed taking into account the SPMSM, power converter and the control block and in each case a complete description of the components and required commands is given. The operation of the control system under normal conditions of the power grid is presented and discussed.

Four speed and angle estimators are discussed and then the sensorless simulation results with the best estimator are presented.

### 2.1. Introduction

Asynchronous ac machines are the most widespread motors, known as being the workhorse in industrial drives, and large efforts are still made to improve their efficiency and to develop new kinds of motors for industrial applications [1]. A good alternative for this kind of applications are the surface permanent-magnet synchronous machines (SPMSM), which have many advantages such as high power density, torque to inertia ratio and energy efficiency [2], and make them feasible candidates for direct drive systems.

For a better control of synchronous machines with fast speed (torque) response, an encoder is necessary to be used to synchronize the rotor position with the stator currents. Thus, using an adequate control system, the synchronous motors can successfully replace the asynchronous motors and d.c. machines in various working conditions, maintaining in the same time the advantages presented above. The major encoder drawbacks are its relatively high cost and performance degradation due to vibration or humidity [3].

Another alternative is to outfit the machine with Hall sensors. Unfortunately, this method does not confer good dynamics because the Hall sensors give low resolution angle information that is not sufficient for complete operation range [4].

The most reasonable control of this kind of motor is without encoder. The first importance in this case is the rotor construction. Thus, from the control viewpoint, at low speeds, it matters if  $L_d$  is equal to  $L_q$  or not, so the motor design is very important when good operation at low speeds is desired [5] and [6].

Generally, in sensorless control of SPMSM ( $L_d=L_q$ ), position and speed estimators based on emf begin to act properly only from speed values greater than 10% rated speed. The main drawback of these estimators is low and zero speed operation, where they fail since the back-emf information is too low [7]. They need also very well known parameters. Fortunately, in high-speed applications, self-starting over light load is frequent, and low-speed operation is scarce. Finally, limited on-line computing cycles are available in the control of high-speed drives, so simplified, but reliable, position/speed estimations are required. References [8] to [20] present different strategies of sensorless control for PMSMs, each with its merits and demerits.

## 2.2. Mathematical Models and Control Properties

The understanding of the machine physics is the key requirement for any type of electrical machine control. Some detail can be found in [21].

Below are presented the surface permanent magnet synchronous machine equations written in the two known rotor and stator reference frames.

### 2.2.1. SPMSM model in space vector form

The SPMSM space vector model in stator reference frame is:

$$\bar{V}_s^s = R_s \bar{I}_s^s + \frac{d\bar{\lambda}_s^s}{dt} \quad (2.1)$$

$$\bar{\lambda}_s^s = L_s \bar{I}_s^s + \bar{\lambda}_{PM}, \quad \bar{\lambda}_{PM} = \lambda_{PM} e^{j\theta_r}, \quad \bar{I}_s^s = I_s e^{j\theta_i} \quad (2.2)$$

The vectors in (2.1) represent the stator values for the three stator phase voltages and currents  $a$ ,  $b$  and  $c$  in stator reference frame:

$$\begin{aligned}\bar{V}_s^s &= \frac{2}{3} \left( v_a + v_b e^{j\frac{2\pi}{3}} + v_c e^{-j\frac{2\pi}{3}} \right) \\ \bar{I}_s^s &= \frac{2}{3} \left( i_a + i_b e^{j\frac{2\pi}{3}} + i_c e^{-j\frac{2\pi}{3}} \right)\end{aligned}\quad (2.3)$$

and

$$\bar{\lambda}_s^s = \frac{2}{3} \left( \lambda_a + \lambda_b e^{j\frac{2\pi}{3}} + \lambda_c e^{-j\frac{2\pi}{3}} \right)\quad (2.4)$$

where the flux linkage space vector  $\bar{\lambda}_s^s$  can be obtained from the current space vector  $\bar{I}_s^s$  and the permanent magnet flux vector  $\bar{\lambda}_{PM}$  [22].

### 2.2.2. Voltage equations in stationary stator reference frame

The space vector approach discussed in the above section can be represented in a suitable reference frame.

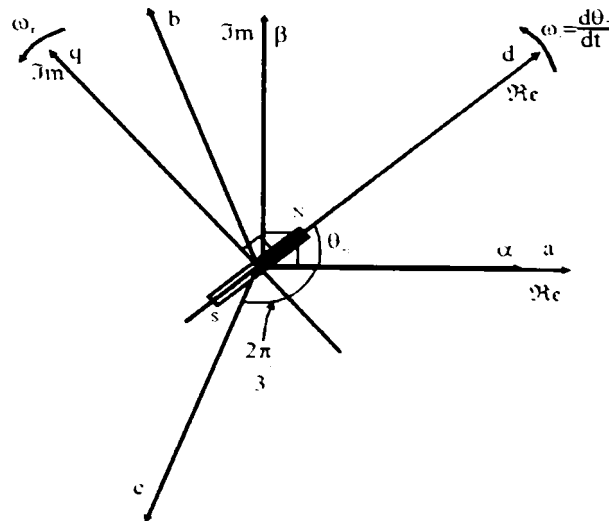


Fig. 2.1 Stator three phases axes ( $a, b, c$ ), stator ( $\alpha, \beta$ ) and rotor ( $d, q$ ) reference frame.

Fig. 2.1 shows the axes of the reference frame for the three stator phases  $a$ ,  $b$ , and  $c$ . In the above figure the stator reference frame  $(\alpha, \beta)$  is used. The  $\alpha$  axis of this reference frame has the same direction as phase  $a$  axis.

Taking account of the below equations:

$$\bar{\lambda}_S^S = L_S \bar{I}_S^S + \lambda_{PM} e^{j\theta_{er}} \quad (2.5)$$

$$\frac{d\bar{\lambda}_S^S}{dt} = L_S \frac{d\bar{I}_S^S}{dt} + \frac{d}{dt} (\lambda_{PM} e^{j\theta_{er}}) \quad (2.6)$$

$$\frac{d\bar{\lambda}_{PM}}{dt} = \frac{d}{dt} (\lambda_{PM} e^{j\theta_{er}}) = \bar{E} \quad (2.7)$$

the machine voltage equations from (2.1) can be written as:

$$\begin{aligned} V_\alpha &= R_S I_\alpha + L_S \frac{dI_\alpha}{dt} + E_\alpha \\ V_\beta &= R_S I_\beta + L_S \frac{dI_\beta}{dt} + E_\beta \end{aligned} \quad (2.8)$$

Taking into consideration (2.2):

$$\bar{I}_S^S = I_S e^{j\theta_i} \quad (2.9)$$

where  $\theta_i$  is the current angle with respect to  $\alpha$  axis. For the steady state:

$$\frac{d\theta_i}{dt} = \frac{d\theta_{er}}{dt} = \omega_r \quad (2.10)$$

and from (2.9) and (2.10) the current derivative becomes:

$$\frac{d\bar{I}_S^S}{dt} = j\omega_r (I_\alpha + jI_\beta) \quad (2.11)$$

The permanent magnet flux can be written as:

$$\bar{\lambda}_{PM} = \lambda_{PM} \cos \theta_{er} + j\lambda_{PM} \sin \theta_{er} = \lambda_{PM\alpha} + j\lambda_{PM\beta} \quad (2.12)$$

so the permanent magnet flux derivative becomes:

$$\frac{d\bar{\lambda}_{PM}}{dt} = \omega_r (-\lambda_{PM\beta} + j\lambda_{PM\alpha}) = -\omega_r \lambda_{PM} \sin \theta_{er} + j\omega_r \lambda_{PM} \cos \theta_{er} = \bar{E} \quad (2.13)$$

With (2.11) and (2.13) in (2.8) the voltage equations in stationary stator reference frame for steady state can be written in many ways, one is given below:

$$\begin{aligned} V_\alpha &= R_S I_\alpha - L_S \omega_r I_\beta - \omega_r \lambda_{PM} \sin \theta_{er} \\ V_\beta &= R_S I_\beta + L_S \omega_r I_\alpha + \omega_r \lambda_{PM} \cos \theta_{er} \end{aligned} \quad (2.14)$$

### 2.2.3. Voltage equations in rotor reference frame

Fig. 2.1 also shows a rotating set of  $d, q$  axes, where  $d$  axis is phase shifted with an angle  $\theta_{er}$  with respect to  $\alpha$  axis.

Variables along  $a, b$  and  $c$  axis can be referred to the  $d$  and  $q$ -axes by the expression:

$$f_d = \frac{2}{3} \left[ f_a \cos(\theta_{er}) + f_b \cos\left(\theta_{er} - \frac{2\pi}{3}\right) - (f_b + f_c) \cos\left(\theta_{er} + \frac{2\pi}{3}\right) \right] \quad (2.15)$$

$$f_q = -\frac{2}{3} \left[ f_a \sin(\theta_{er}) + f_b \sin\left(\theta_{er} - \frac{2\pi}{3}\right) - (f_b + f_c) \sin\left(\theta_{er} + \frac{2\pi}{3}\right) \right] \quad (2.16)$$

where,  $f$  represent any of the three phases stator variables such as voltage, current or flux linkage.

From (2.1) we may translate them into rotor reference frame:

$$\bar{V}_s^r e^{j\theta_{er}} = R_s \bar{I}_s^r e^{j\theta_{er}} + \frac{d}{dt} \left( \bar{\lambda}_s^r e^{j\theta_{er}} \right) \quad (2.17)$$

Taking into consideration that:

$$\frac{d}{dt} \left( \bar{\lambda}_s^r e^{j\theta_{er}} \right) = \frac{d\bar{\lambda}_s^r}{dt} e^{j\theta_{er}} + j\omega_r \bar{\lambda}_s^r e^{j\theta_{er}} \quad (2.18)$$

the equation (2.17) becomes:

$$\bar{V}_s^r e^{j\theta_{er}} = R_s \bar{I}_s^r e^{j\theta_{er}} + \frac{d\bar{\lambda}_s^r}{dt} e^{j\theta_{er}} + j\omega_r \bar{\lambda}_s^r e^{j\theta_{er}} \quad (2.19)$$

Dividing (2.19) by  $e^{j\theta_{er}}$ , results:

$$\bar{V}_s^r = R_s \bar{I}_s^r + \frac{d\bar{\lambda}_s^r}{dt} + j\omega_r \bar{\lambda}_s^r \quad (2.20)$$

but:

$$\bar{\lambda}_s^r = \lambda_{PM} + L_s \bar{I}_s^r = \lambda_{PM} + L_s (I_d + jI_q) \quad (2.21)$$

for steady state (2.20) becomes:

$$\bar{V}_s^r = R_s \bar{I}_s^r + j\omega_r \bar{\lambda}_s^r \quad (2.22)$$

The equation (2.22) is equivalent to:

$$\begin{aligned} V_d &= R_s I_d - \omega_r L_s I_q \\ V_q &= R_s I_q + \omega_r L_s I_d + \omega_r \lambda_{PM} \end{aligned} \quad (2.23)$$

To the above presented electrical equations should be added the mechanical equation:

$$T_e = \frac{3}{2} p [\lambda_d I_q - \lambda_q I_d] \tag{2.24}$$

The simulation of the SPMSM control system implies first to develop a model for the simulated motor. This model infers the direct and the inverse Park transformations but also the mathematical motor equations (2.23) and (2.24) written in stationary stator coordinates. Implementing the above mentioned equations the simulated model of the synchronous machine is obtained (Fig. 2.2).

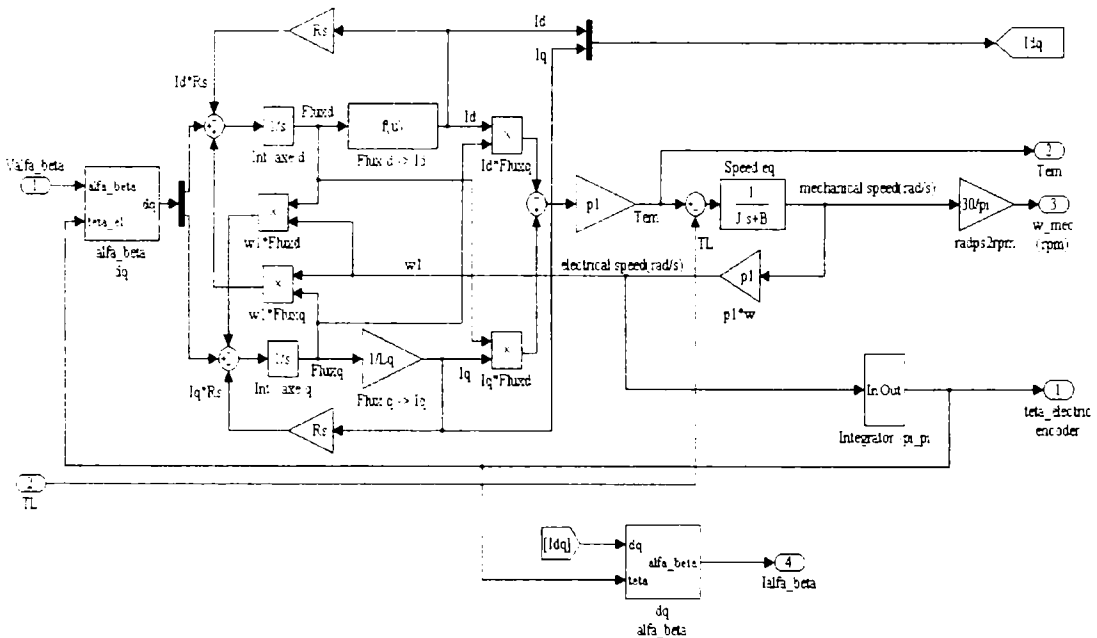


Fig. 2.2 Surface permanent magnet d - q motor model

### 2.3. The control structure of the drive system

Here the investigation of a variable-speed PMSM system in high speed operation is studied. A wide range of speed (2,000 – 10,000 rpm) and extremely low value of stator time constant pose special challenges to the associated power converter and control. Additionally, position sensorless control is necessary to test the four rotor position angle estimators.



### 2.3.1. Overall simulated system description

The entire simulated control was developed in Matlab Simulink. Fig. 2.3 shows the overview control structure of the simulated drive system.

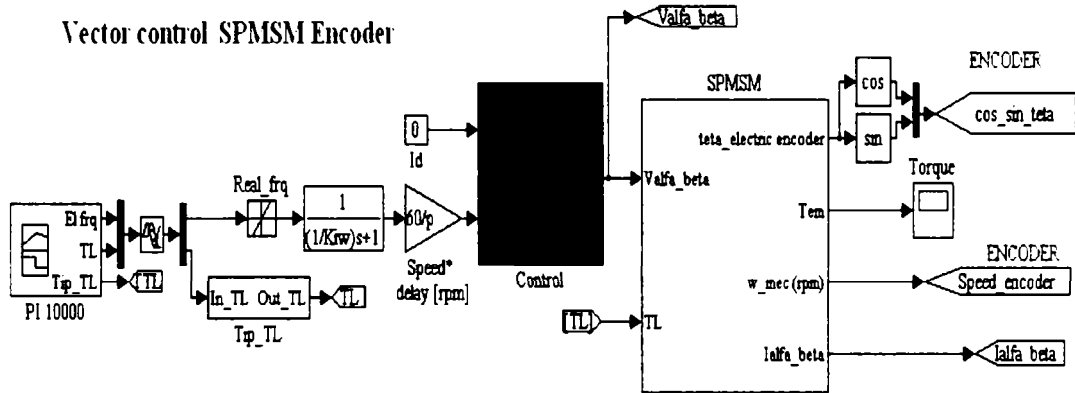


Fig. 2.3 High speed PMSM simulated system overview.

Both speed and torque can be prescribed using a dedicated block from Matlab (see the left side in Fig. 2.3). The prescribed signals have step waveform. To avoid the oscillations the reference speed is delayed by using a PT1 regulator.

For this control strategy, the minimum stator current magnitude can be imposed to the machine for a required electromagnetic torque. In fact, the strategy, for this machine,  $L_d=L_q$ , supposes  $I_d=0$ .

The control block consists of a speed controller and  $dq$  current controllers with emf compensator.

The speed controllers generate the torque command through the  $I_q$  current (see [23] to [31]). So the torque control is achieved by controlling the current in rotor reference frame. The rotor reference frame current commands ( $I_d^*$  and  $I_q^*$ ) are provided to the machine by the current controllers in order to achieve the machine required speed. The current controllers consist of two PI controllers as shown in Fig. 2.5. The actual currents ( $I_d$  and  $I_q$ ) in rotor reference frame, used in current control, could be obtained by measuring two phase currents and then transforming them from stator coordinates in to rotor coordinates using the relationship:

$$I_d = \frac{2}{3} \left[ I_a \cos(\theta_{er}) + I_b \cos\left(\theta_{er} - \frac{2\pi}{3}\right) - (I_b + I_c) \cos\left(\theta_{er} + \frac{2\pi}{3}\right) \right] \quad (2.25)$$

$$I_q = -\frac{2}{3} \left[ I_a \sin(\theta_{er}) + I_b \sin\left(\theta_{er} - \frac{2\pi}{3}\right) - (I_b + I_c) \sin\left(\theta_{er} + \frac{2\pi}{3}\right) \right] \quad (2.26)$$

where  $\theta_{er}$  is the electrical rotor position.

The control presented in Fig. 2.5 delivers voltages in rotor reference frame. These voltages, which are in fact the outputs of the current controllers, are transformed in to stationary stator reference frame (see Fig. 2.5) using the rotor position as follows:

$$V_d = V_d \cos\theta_{er} - V_q \sin\theta_{er} \quad (2.27)$$

$$V_\beta = V_d \sin\theta_{er} + V_q \cos\theta_{er} \quad (2.28)$$

These stationary reference frame voltage commands are used to generate the inverter control signals (see Appendix), so these voltage commands are applied to the machine phases.

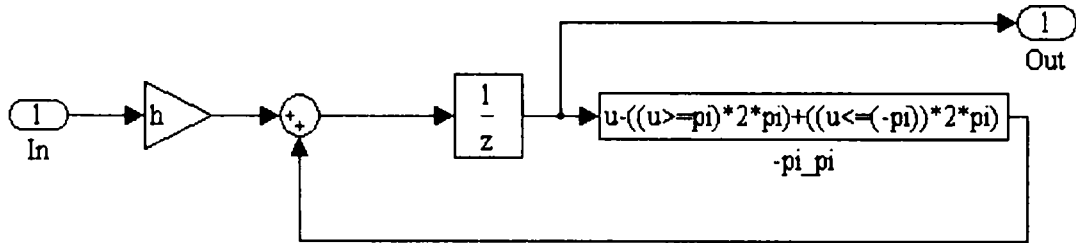


Fig. 2.4 Integrator with the output angle between  $-\pi \dots +\pi$

To avoid achieving a large value, that could saturate the digital registers, the rotor angle must be constrained to a value situated in the  $(-\pi \dots +\pi)$  domain. Fig. 2.4 implements in Matlab these limitations.

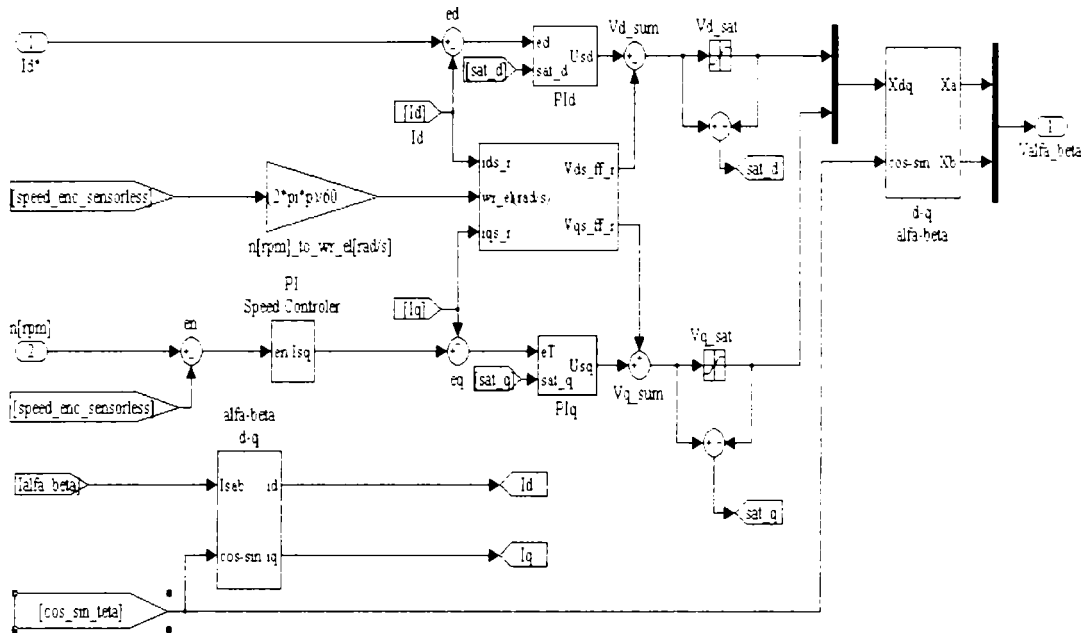


Fig. 2.5 Simulated vector control block

### 2.3.2. Coupling in rotor *d, q* reference frame

The steady state voltage equations in rotor reference frame (2.23) can be written as follows:

$$\begin{aligned}
 V_d &= R_s I_d - \omega_r L_s I_q \\
 V_q &= R_s I_q + \omega_r L_s I_d + \omega_r \lambda_p M
 \end{aligned}
 \tag{2.29}$$

The  $R_s$  can be omitted and thus (2.29) becomes:

$$\begin{aligned}
 V_d &= -\omega_r L_s I_q = V_{ds\_ff} \\
 V_q &= \omega_r L_s I_d + \omega_r \lambda_p M = V_{qs\_ff}
 \end{aligned}
 \tag{2.30}$$

Equations (2.30) can be implemented by the block diagram shown in Fig. 2.6. These equations (see [33]) are feedforward voltage decoupling used in vector control system presented in Fig. 2.5.

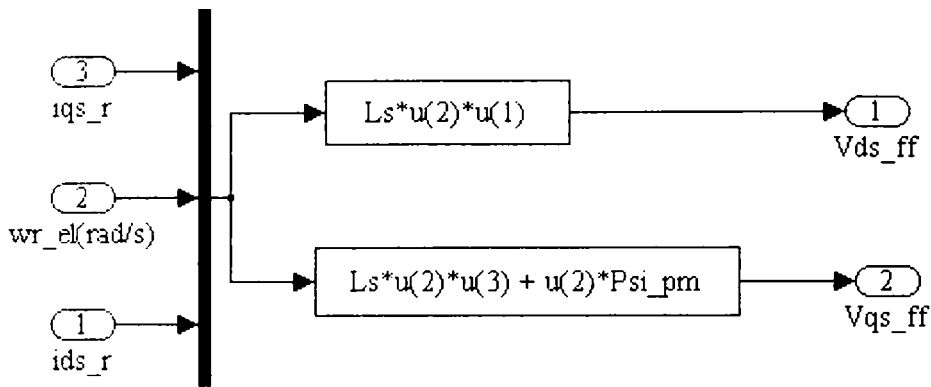


Fig. 2.6 Block diagram feedforward voltage-decoupling implementation

### 2.3.3. Decoupling in current controllers

The currents in rotor reference frame in Fig. 2.5 become dc values in steady state [34] and [35]. Consequently PI controllers can be used to control these currents with zero steady state error, because the current error at the input of the controller becomes zero in steady state.

The  $d$ ,  $q$  currents cannot be controlled independently, due to cross coupling as shown in Fig. 2.5. In order to control  $I_d$  when  $V_d$  is changed the  $I_d$  is changed as desired, but this causes to change also the  $V_q$ , and therefore the  $I_q$ , which is not desirable. This degrades the control performance of the current control. To obtain better performance in current control the  $I_d$  and  $I_q$  must be controlled independently. This can be achieved by decoupling the cross coupling in rotor  $d$ ,  $q$  circuits. The speed (measured or estimated), measured stator currents and machine parameters are used in the decoupling equations. If the decoupling equations are used in the control, the PI controllers have to correct errors occurred in the system.

It is important to say that the control is working satisfactorily without these decoupling equations proven by simulations.. In this situation the PI controllers should reconstruct the designated voltages. Of course this could be possible only if proper controller P and I coefficients, chosen especially for this purpose, are used.

### 2.3.4. Validation of the current and speed controller design

Dynamic analyses of current regulators are presented in [36]. In order to validate the design of the current controller, the step response of the rotor  $d$  and  $q$  axes currents are measured in the drive system (see Fig. 2.7).

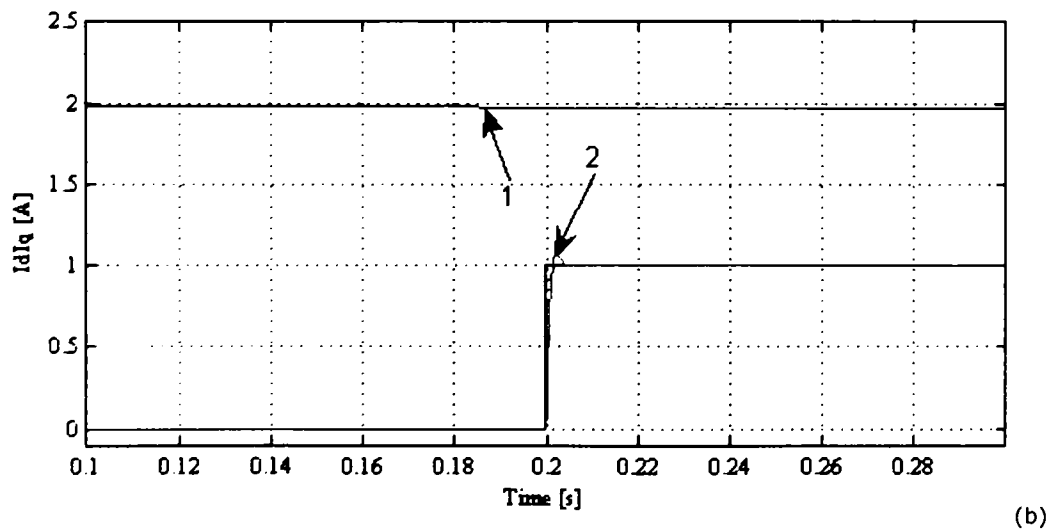
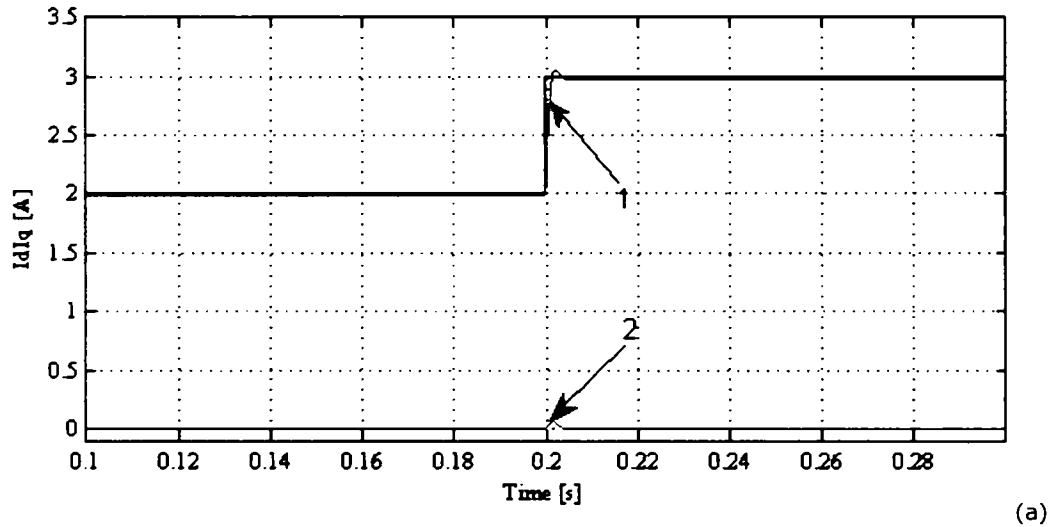


Fig. 2.7 Measured current step response for the controllers in the vector control strategy  
 (a)  $I_d$  step response with  $I_d$  reference fixed at zero (a)  $I_d$  step response with  $I_q$  reference fixed at 2A (1)  $I_q$  current (2)  $I_d$  current

For these tests, the outer speed loop is disabled and the controller is operated only with the current loop. The measured current responses at step prescription are shown in Fig. 2.7. In order to see the  $I_q$  step response,  $I_q$  reference is stepped from zero to 2 A and to 3 A with  $I_d$  reference fixed at zero. For  $I_d$  step response, the  $I_d$  reference is stepped from zero to 1 A with  $I_q$  reference fixed at 2 A.

The PI current controllers with the transfer function  $k_p(1 + 1/k_i)$  are designed with  $k_p = 0.3$  and  $k_i = 1500$  for both current controllers. To compensate the electrical time constant  $\tau = L_s/R_s \approx 0.5$  ms the internal constant is chosen around  $k_i \approx 1/\tau = 2000$ . These coefficients are the same as the ones used in the experimental setup presented in Chapter 3.

As it can be seen from the simulations presented in Fig. 2.7, the rise time for the current step response is around 1 ms which is quite enough for this kind of motor.

## **2.4. Four rotor position and speed simplified estimators for vector control strategy**

Four position and speed estimators are presented. They can be used in the control of ac machines, in particular for SPMSM. A background theory for these estimators is presented in [16], [37] and [41].

### **2.4.1. Theoretical background of the speed and position estimators**

The SPMSM is generally assumed to have three balanced phases connected in Y or  $\Delta$  configuration. The SPMSM model in stator coordinates is presented in (2.1) and (2.2).

Since the rotor permanent magnet flux is aligned with the rotor d-axis in the PMSM, the permanent magnet flux induced voltage (i.e. back emf  $\bar{E}$ ) always lies on the rotor q-axis. Therefore, in the stationary reference frame, the position of the back-emf vector indicates the rotor position angle  $\theta_{er}$ . This is shown in Fig. 2.8.

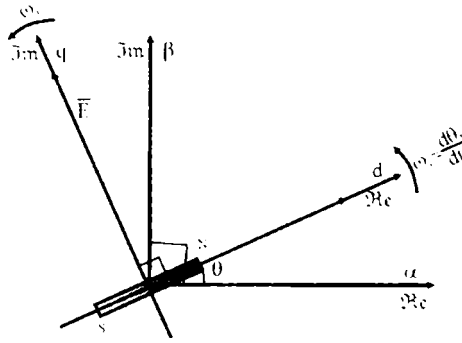


Fig. 2.8 Back – emf vector in the stationary reference frame

If it is possible to calculate the position of the back-emf vector in stator stationary reference frame, then the rotor position is known.

The back-emf vector  $\bar{E}$  in (2.13) is given by:

$$\bar{E} = \frac{d\bar{\lambda}_{PM}}{dt} = \omega_r \lambda_{PM} e^{j(\theta_r + \pi/2)} \quad (2.31)$$

where  $\omega_r$  is the electrical rotor speed.

By inserting (2.2) and (2.31) in (2.1), the machine voltage equation becomes:

$$\bar{E} = \bar{V}_s^s - R_s \bar{I}_s^s - L_s \frac{d\bar{I}_s^s}{dt} \quad (2.32)$$

In steady state, the current vector speed  $\omega_i = \omega_r$ , and therefore by using (2.11), equation (2.32) can be written as:

$$\bar{E} = \bar{V}_s^s - R_s \bar{I}_s^s - j\omega_r L_s \bar{I}_s^s \quad (2.33)$$

In the next paragraph, for simplicity, the superscript<sub>s</sub> notation will not be anymore used, so (2.32) and (2.33) will become:

$$\bar{E} = \bar{V}_s - R_s \bar{I}_s - L_s \frac{d\bar{I}_s}{dt} \tag{2.34}$$

$$\bar{E} = \bar{V}_s - R_s \bar{I}_s - j\omega_r L_s \bar{I}_s \tag{2.35}$$

Equations (2.1), (2.34) and (2.35) for SPMSM in stator stationary reference frame will be used in position and speed estimators from the next paragraph.

The SPMSM phasor diagram is illustrated in Fig. 2.9.

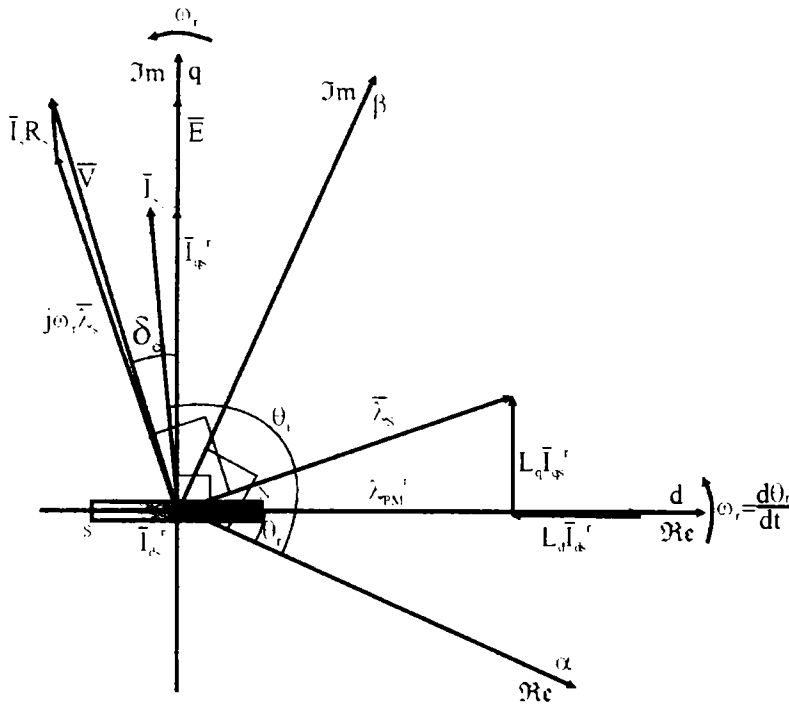


Fig. 2.9 Space vector diagram of SPMSM

The SPMSM control structure in Fig. 2.10 uses speed control with position encoder, and employs standard current-vector PI control algorithm ( $I_d^* = 0$ ) with two voltage-decoupling loops presented in (2.30) and (2.36).

$$V_{dq\_ff}^* = -L_s \omega_r I_q^* + j\omega_r (\lambda_{PM} + L_s I_d^*) \tag{2.36}$$



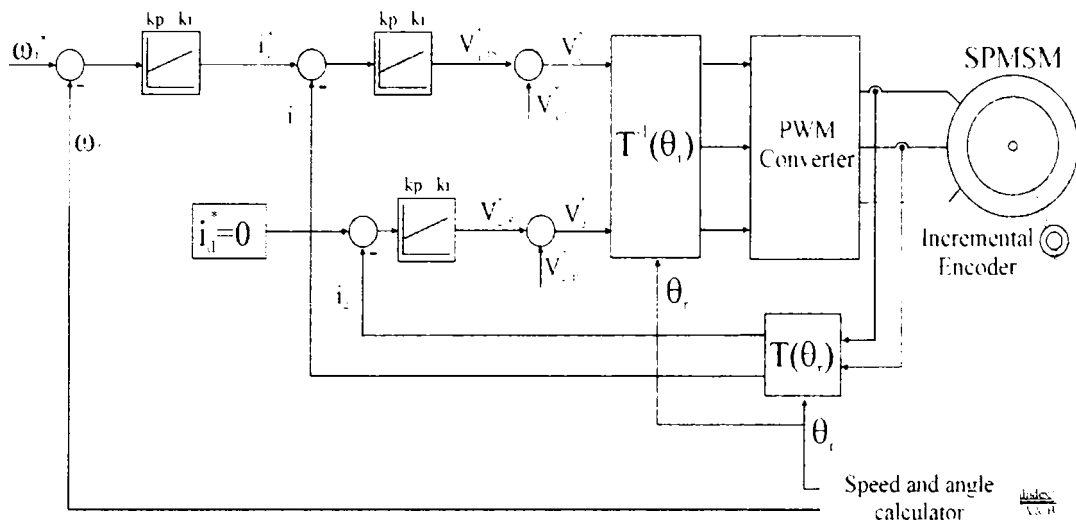


Fig. 2.10 Block diagram of vector control scheme with encoder position sensor

### 2.4.2. Rotor position and speed estimators for encoderless control

The main feature of the proposed sensorless control techniques is that all of them use only current sensors. The input voltages ( $V_a$ ,  $V_b$ ,  $V_c$ ) or ( $V_{\alpha}$ ,  $V_{\beta}$ ) are replaced by the inverter reference voltages ( $V_a^*$ ,  $V_b^*$ ,  $V_c^*$ ), respectively ( $V_{\alpha}^*$ ,  $V_{\beta}^*$ ). Without voltage sensors, some approximations can be made for the back-emf. In fact this means to neglect voltage harmonics, delay of time response due to power switches commutations and voltage drop on power switches. For SPMSMs and IPMSMs, using the electrical equations of the machine, the possibility of calculating the position of the back-emf vector in stator stationary reference frame is investigated below.

Four rather simple rotor position estimators suitable for high-speed applications are introduced.

#### 2.4.2.1. Permanent-magnet flux angle estimator

The PM-flux vector angle is identical with the rotor position  $\theta_r$ . The estimator based on PM-flux vector  $\bar{\lambda}_{PM}$  (Fig. 2.11) consists of 3 parts (see [38] and [39]). The 1<sup>st</sup> part estimates the stator flux vector  $\bar{\lambda}_S$  using the voltage model in stator

reference frame (2.1) without using the superscript  $s$  notation with a PI loop compensator for dc offset compensation:

$$\begin{aligned}\bar{\lambda}_S &= \int (\bar{V}_S - \bar{I}_S R_S - \bar{V}_{comp}) dt, \\ \bar{V}_{comp} &= (k_p + \frac{k_i}{s}) \bar{\lambda}_S.\end{aligned}\quad (2.37)$$

The 2<sup>nd</sup> part estimates  $\bar{\lambda}_{PM}$  from (2.2):

$$\bar{\lambda}_{PM} = \bar{\lambda}_S - L_S \bar{I}_S \quad (2.38)$$

The 3<sup>rd</sup> part gives the PM-flux module  $\lambda_{PM}$  and the rotor position by  $\sin\theta_r$  and  $\cos\theta_r$ , which are directly used in rotation operators.

As the torque and flux response of the machine is faster than the speed response, the angle  $\hat{\theta}_r$  may be calculated as:

$$\cos \hat{\theta}_r = \frac{\lambda_{PM\alpha}}{\lambda_{PM}}; \quad \sin \hat{\theta}_r = \frac{\lambda_{PM\beta}}{\lambda_{PM}} \quad (2.39)$$

in the situation when the flux and the torque reference do not experience step variations.

The stator voltage phase, the currents and the stator resistance should be known in order to estimate the flux components from (2.37). Integration drift becomes an issue when using (2.37) for flux estimator and should be avoided using proper techniques [32]. The concept can be used both for SMPMSMs and IPMSMs. In order to avoid the integrator drift during flux estimation, the estimated flux is corrected in the algorithm using a feedback loop as Fig. 2.11 shows. Almost the same concept is used in [17] for the sensorless operation of a SPMSM drive above zero speed.

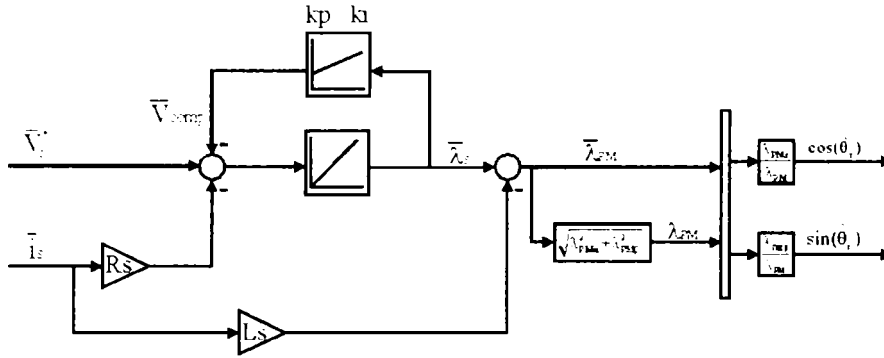


Fig. 2.11 Rotor position estimator based on PM-flux vector.

The machine parameters are used in these rotor position estimation algorithms, and therefore, the control system is sensitive to parameters variations.

**2.4.2.2. Back-emf angle estimator for dynamic operating mode**

The back-emf vector  $\vec{E}$  is phase shifted with exactly  $\pi/2$  from the  $d$  axis (2.31)

The back-emf vector  $\vec{E}$  is calculated from (2.35). It is valid for transients and has the components:

$$\begin{aligned} E_\alpha &= V_\alpha - R_S I_\alpha - L_S dI_\alpha / dt \\ E_\beta &= V_\beta - R_S I_\beta - L_S dI_\beta / dt \end{aligned} \tag{2.40}$$

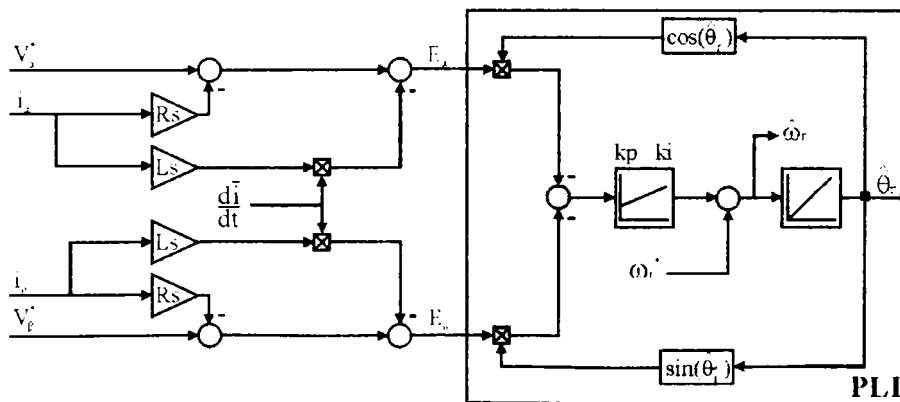


Fig. 2.12 Rotor position and speed estimator based on back-emf in dynamic operating mode

To reduce noise in current derivatives  $d\bar{i}_s/dt$ , a filter-based derivative estimator (Fig. 2.13) is used [11].

Overall, this scheme has shown good accuracy over the whole speed range and also during the start-up procedure.

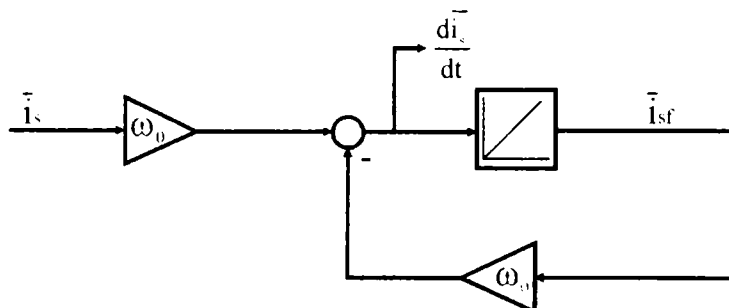


Fig. 2.13 Derivative estimator based on filter technique.

#### 2.4.2.3. Back-emf angle estimator in steady-state operating mode

The estimator-version in Fig. 2.14 is closed to the one in Fig. 2.12, but the computation of  $\bar{E}$  is in steady-state (2.33):

$$\begin{aligned} E_\alpha &= V_\alpha - R_S I_\alpha + L_S \omega_r I_\beta, \\ E_\beta &= V_\beta - R_S I_\beta - L_S \omega_r I_\alpha. \end{aligned} \quad (2.41)$$

A phase-locked loop (PLL) state-estimator extracts the rotor position and speed from  $\bar{E}$  vector. Other PLL is presented in [40].

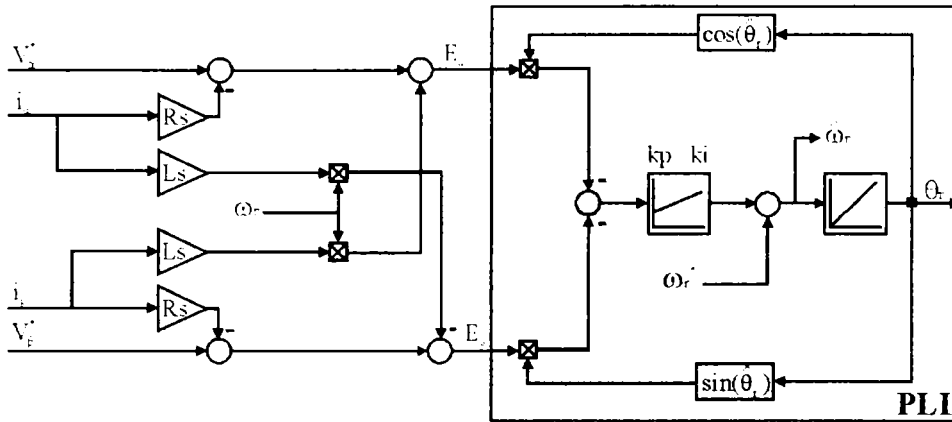


Fig. 2.14 Rotor position and speed estimator based on back-emf in steady-state operating mode.

The PLL error  $\mathcal{E}$  is calculated as a difference described by the below equation:

$$\varepsilon = -E_{\alpha} \cos \hat{\theta}_r - E_{\beta} \sin \hat{\theta}_r \quad (2.42)$$

The error  $\mathcal{E}$  is used to extract the rotor speed and position using a phase-locked loop (PLL) technique (Fig. 2.14). The output of the PI compensator gives the estimated rotor speed  $\hat{\omega}_r$  and after the integration, the estimated rotor position  $\hat{\theta}_r$  is obtained:

$$\hat{\omega}_r = \left( K_{P\_PLL} + \frac{K_{I\_PLL}}{s} \right) \varepsilon + \omega_r^*; \quad \hat{\theta}_r = \int \hat{\omega}_r dt \quad (2.43)$$

The optimal parameters of the PI compensator were chosen making a compromise between the speed of the PLL, especially during transients, and the level of oscillations in the speed estimation, especially at low speeds.

The best parameters seem to be:  $K_{P\_PLL} = 3$ , and  $K_{I\_PLL} = 7000$ .

### 2.4.2.4. Voltage-based angle estimator

This type of estimator uses the voltage vector represented in two references: stator and rotor reference frames (see Fig. 2.9). Thus, in each moment, if both  $(V_\alpha, V_\beta)$  and  $(V_d, V_q)$  computed voltages at the previously sampling period are known, the voltage angles with respect to the axis  $\alpha_r$ , respectively, axis  $d$  can be estimated as:

$$\begin{aligned} V_d &= V_\alpha \cos \theta_r - V_\beta \sin \theta_r \\ V_q &= V_\alpha \sin \theta_r + V_\beta \cos \theta_r \end{aligned} \quad (2.44)$$

$$\theta_r = (\theta_r + \pi/2 + \delta) - (\pi/2 + \delta) \quad (2.45)$$

Computing the difference between the two angles in (2.45), the rotor position can be estimated. The implementation of this estimator is shown in Fig. 2.15.

The implementation of the position and speed estimator can be also made in the way presented in [7] and [8]. It is shown (see Fig. 2.10) that the output of the current regulator  $V_{d\_fb}^*$  has unexpectedly bad results. Even more, the drawback of this method is that it employs, together with vector control or another control method, the transformation  $\alpha\beta \rightarrow dq$  that requires rotor position  $\theta_r$ . Note that for the estimators presented above, the estimators 1 to 3 do not use rotation operators, while the estimator 4 uses them.

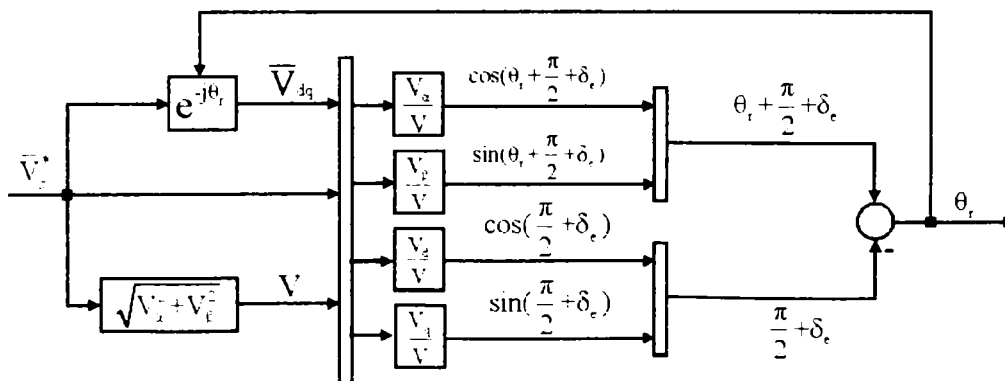


Fig. 2.15 Voltage angle calculation with respect to  $\alpha$  and  $d$  axes.

None of the presented estimators can detect the initial rotor position, and therefore, the starting performance can degrade unless another technique is used to detect the initial rotor position.

### 2.4.3. Rotor speed estimator for encoderless control

The rotor speed  $\omega_r$  can be estimated from the rotor position  $\theta_r$ . All estimators previously presented estimate rather well the rotor position. The estimators 2 and 3 contain the speed estimation, which can be used efficiently in control. For the estimators 1 or 4 which give rotor position estimation, a phase-locked loop (PLL) speed estimator was introduced as in Fig. 2.16.

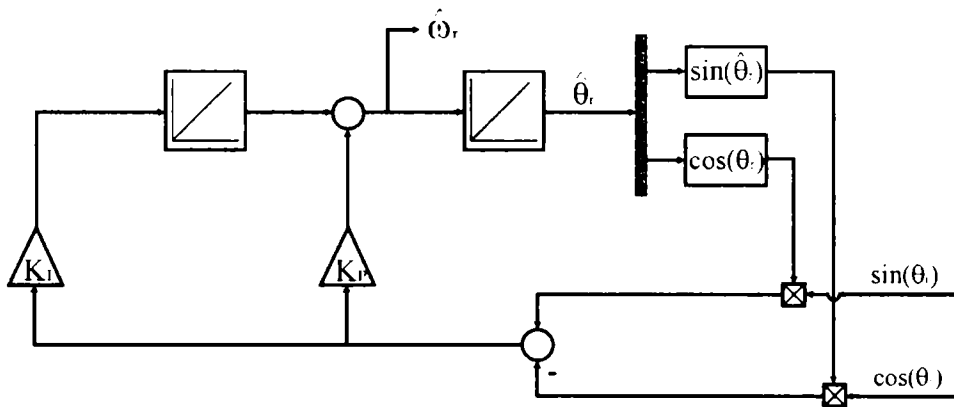


Fig. 2.16 Speed estimator based on rotor position given by the estimators 1 or 4.

The gains  $k_p$  and  $k_i$  could be computed, for example, using the pole placement method. Thus, if the system poles are  $p_1$  and  $p_2$  then:

$$k_p = -(p_1 + p_2), \quad k_i = p_1 p_2. \quad (2.46)$$

This method is an analytical one, but a trial and error method can also be applied [10] with good results, even if the system is very complex and computation delays should be taken into account.

### 2.4.4. Simulations results of angle and speed estimators

For a good image over the estimators work a very relevant test has been performed: 100% step rated-load perturbation torque at 10,000 rpm followed by unload and speed reversal from -10,000 rpm to +10,000 rpm, without load.

For the first test, the reference and the actual speeds are presented in Fig. 2.17.

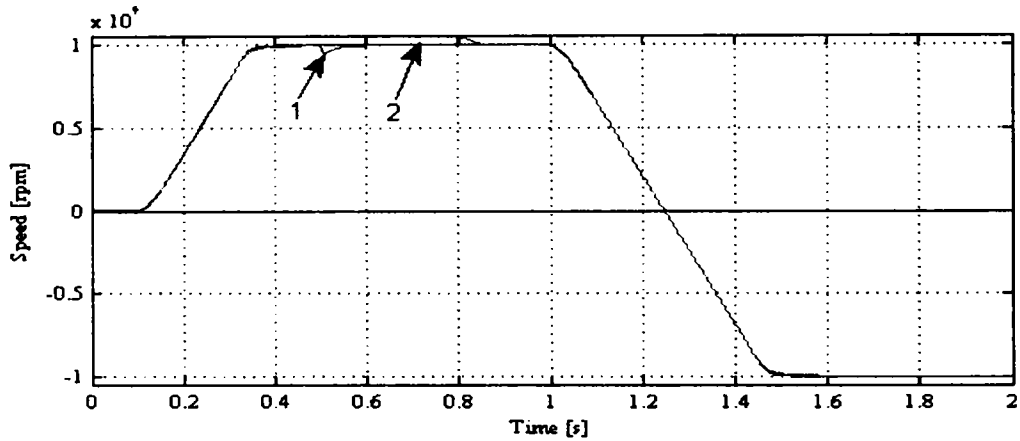


Fig. 2.17 (1) Reference (red line) and (2) machine speed (blue line) unloading start-up at 10.000 rpm followed by 100 % loading at 0.5 s, unloading at 0.8 s, reverse speed from 10.000 rpm to -10.000 rpm at 1 s

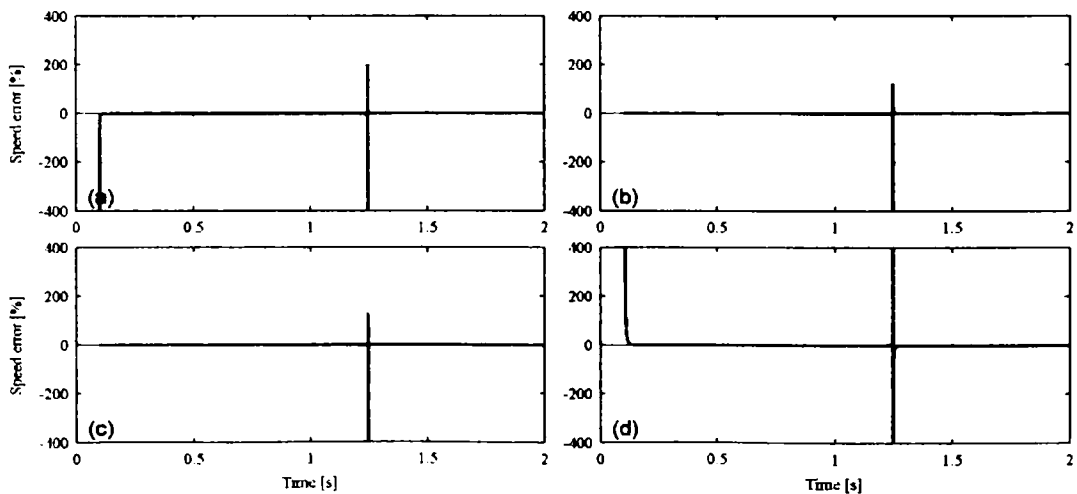


Fig. 2.18 Speed estimation versus encoder errors for estimators:  
1(a), 2(b), 3(c), 4(d) for  $\pm 10$  krpm, no load.



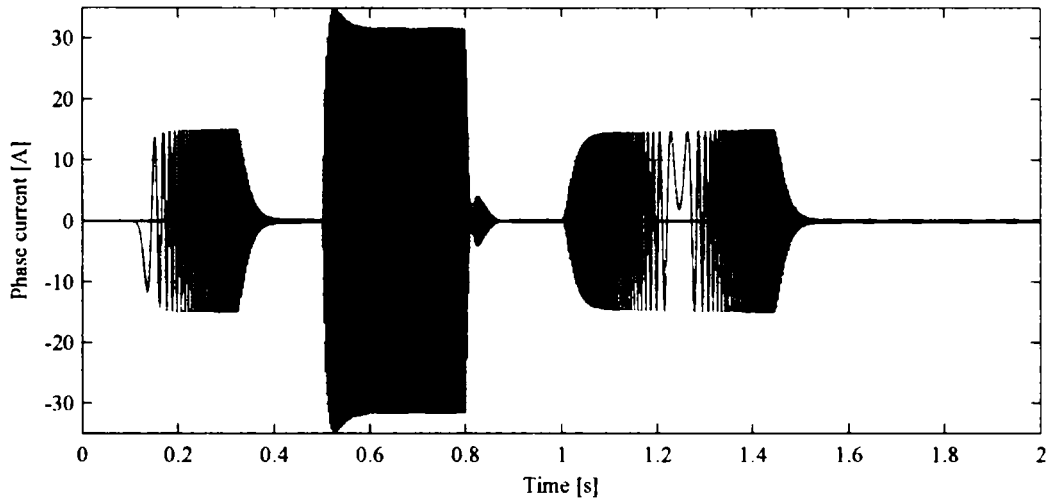


Fig. 2.19 Actual current during tests presented in Fig. 2.17

Fig. 2.18 illustrates the speed error [%] of all the four estimators in comparison with the speed feedback computed from encoder. Notable errors for estimator 1 and small errors for estimators 2 and 3 are visible at very low speed. The worst case is for the estimator 4.

Fig. 2.19 shows the actual current for the speed reversal in Fig. 2.20. As it can be seen the currents do not exceed the maximum possible current value.

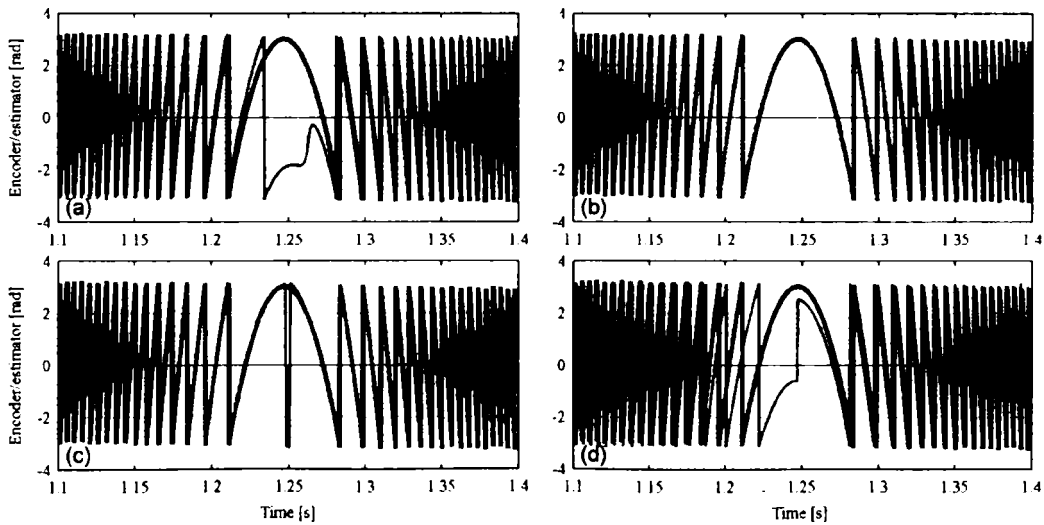


Fig. 2.20 Position estimation (blue thin line) versus encoder (black thick line)

1(a), 2(b), 3(c), 4(d), during tests presented in Fig. 2.17

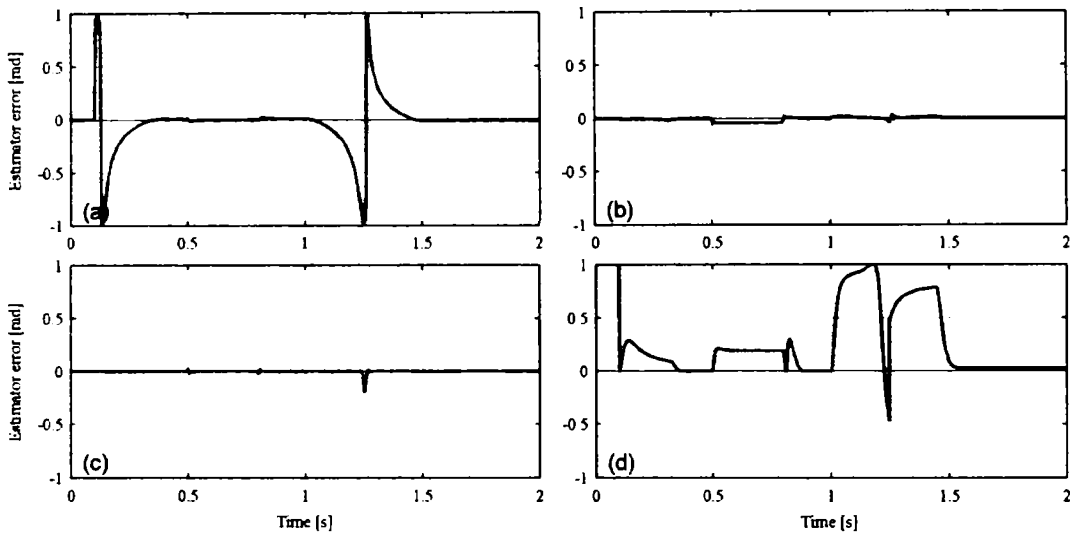


Fig. 2.21 Electric angle error between encoder and estimator:  
 1(a), 2(b), 3(c), 4(d), during tests presented in Fig. 2.17

The rotor position response of all estimators, in speed reversal during transient interval [1.1-1.4] s, is shown in Fig. 2.20. As can be seen, all estimators follow very closely the actual encoder position. Nevertheless, the absolute error could not be observed here, except for around zero speed and at start-up.

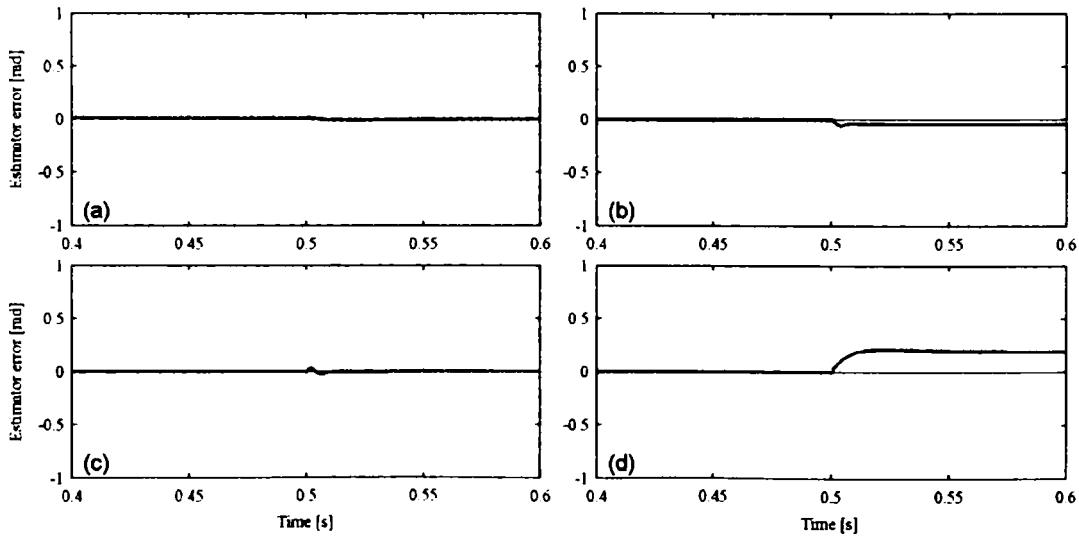


Fig. 2.22 Zoom of electric angle error between encoder and estimators:  
 1(a), 2(b), 3(c), 4(d), during loading test presented in Fig. 2.17

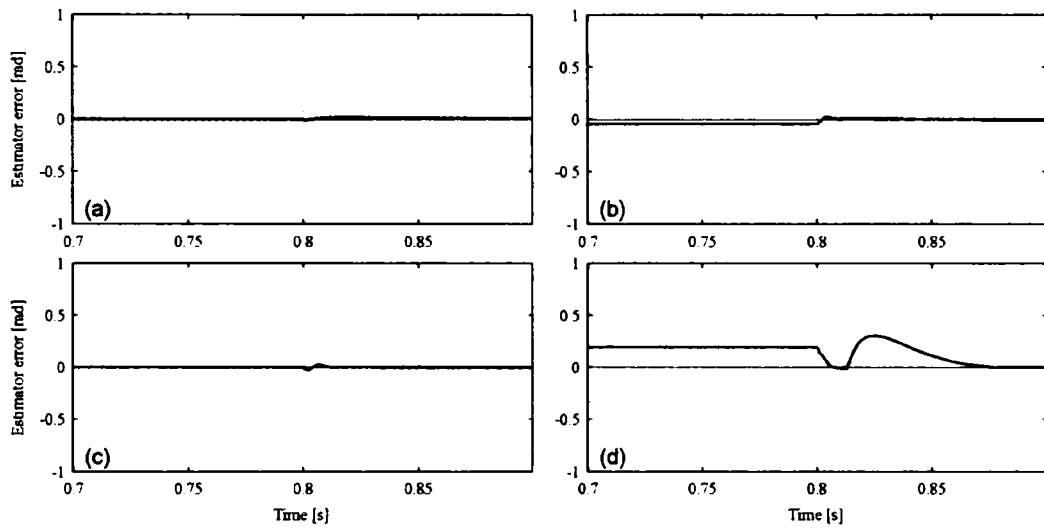


Fig. 2.23 Zoom of electric angle error between encoder and estimators:  
 1(a), 2(b), 3(c), 4(d), during unloading test presented in Fig. 2.17

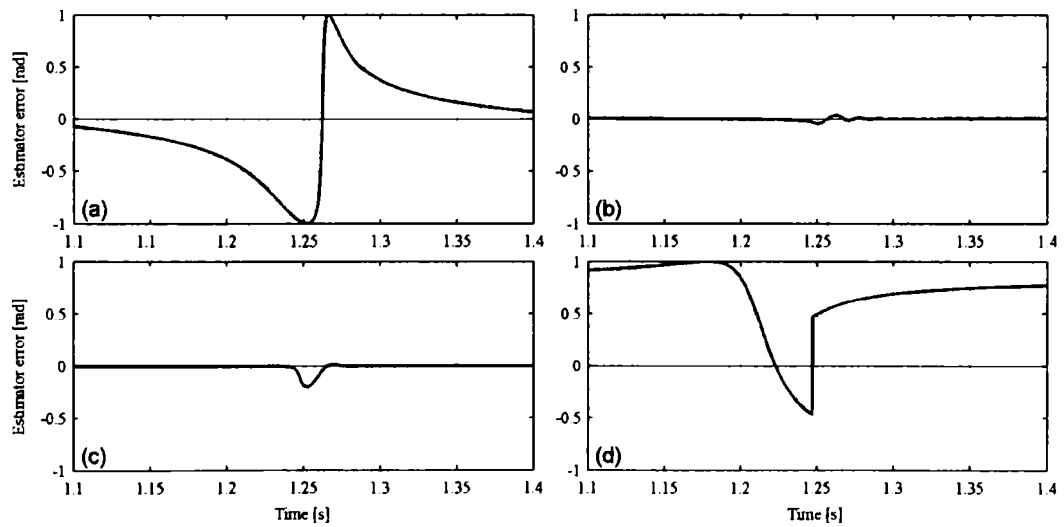


Fig. 2.24 Zoom of electric angle error between encoder and estimators:  
 1(a), 2(b), 3(c), 4(d), during speed reversal test presented in Fig. 2.17

For more clarity the position errors for all four position estimators are given separately in Fig. 2.21, Fig. 2.22, Fig. 2.23 and Fig. 2.24, during loading, unloading and no load speed reversal  $\pm 10,000$  rpm tests. All estimator errors are within 1 electrical radian. Only estimator 2 shows a zero average (steady state) error, though oscillatory (Fig. 2.24 (b)). Small differences can be seen during loading and unloading tests. During unloading tests the estimator 4 has the worst behavior, having the largest dynamic errors, especially during speed reversal.

All estimators operate with acceptable parameter values and have small errors. For high-speed encoderless system, a rotor position estimator with small oscillations should be used in implementation. In encoderless systems, the duration of position angle computation is decisive. If the estimated angle has large oscillations comparatively with the encoder angle, then the system will not operate properly. This is visible at high-speed motors, where the position angle estimator should be very fast and without large oscillations. In this case, the estimators 2 and 3 should be selected.

## **2.5. Sensorless PMSM vector control simulation**

In order to eliminate the rotor position sensor in the rotor permanent magnet vector controlled drive system, a rotor position and velocity estimation technique is studied (see [11] to [14]). Only motor phase currents are measured and this information is used in the estimators.

In the above sections four position estimations were presented. Any of them can drive the PMSM system. For the sensorless control system, the back-emf angle estimator for dynamic operating mode was chosen.

In Fig. 2.3 the encoder device is replaced with an angle and velocity estimator. Fig. 2.25 presents the entire sensorless control used to drive the system.

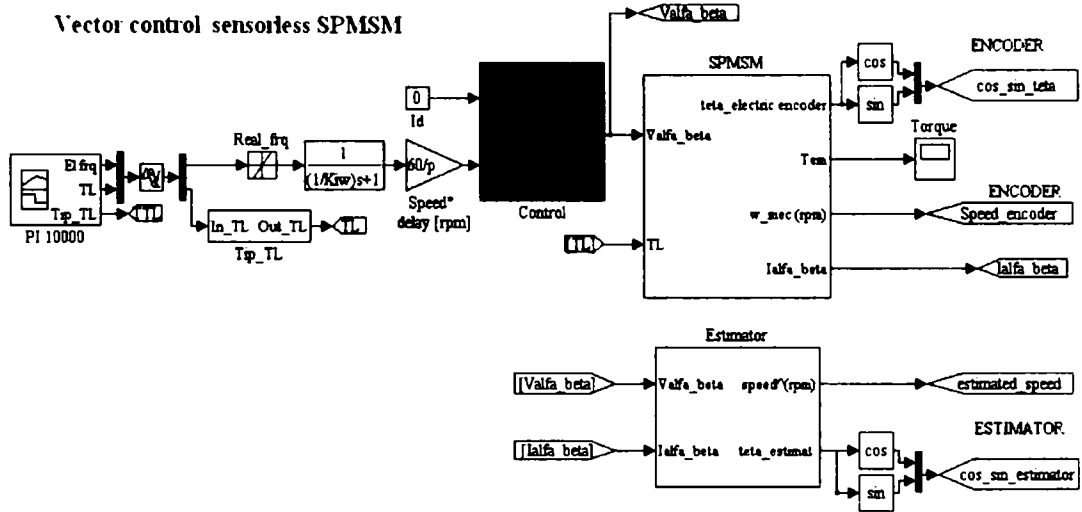


Fig. 2.25 High speed PMSM simulated sensorless system overview.

Fig. 2.26 presents the implementation of the speed and angle estimator from Fig. 2.12.

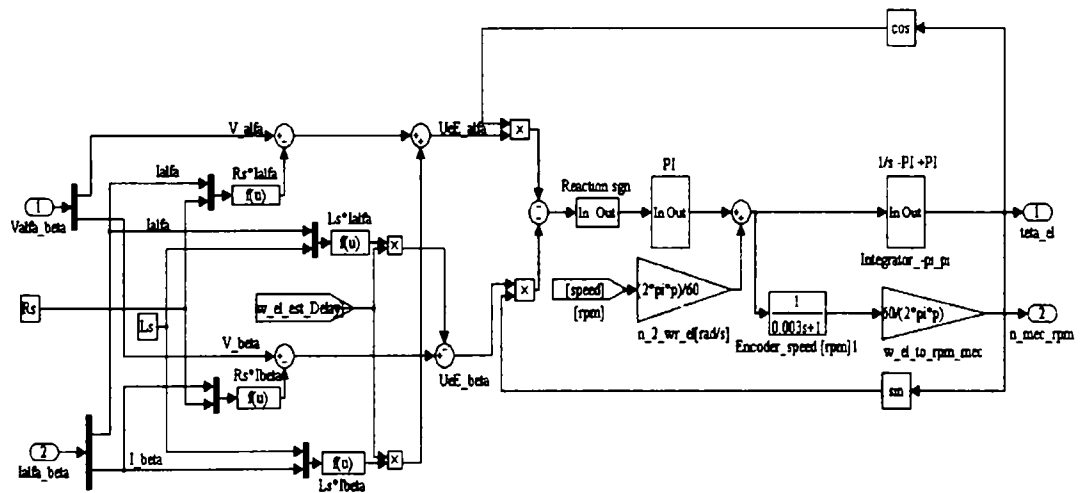


Fig. 2.26 Speed and velocity estimator

## 2.6. Sensorless performance of the complete drive system

For simulations a constant d.c. link voltage was assumed. Initially, the actual rotor position of the machine was used in the controller. So in Fig. 2.27 the drive system using an encoder is presented. Some startup details are provided in [15].

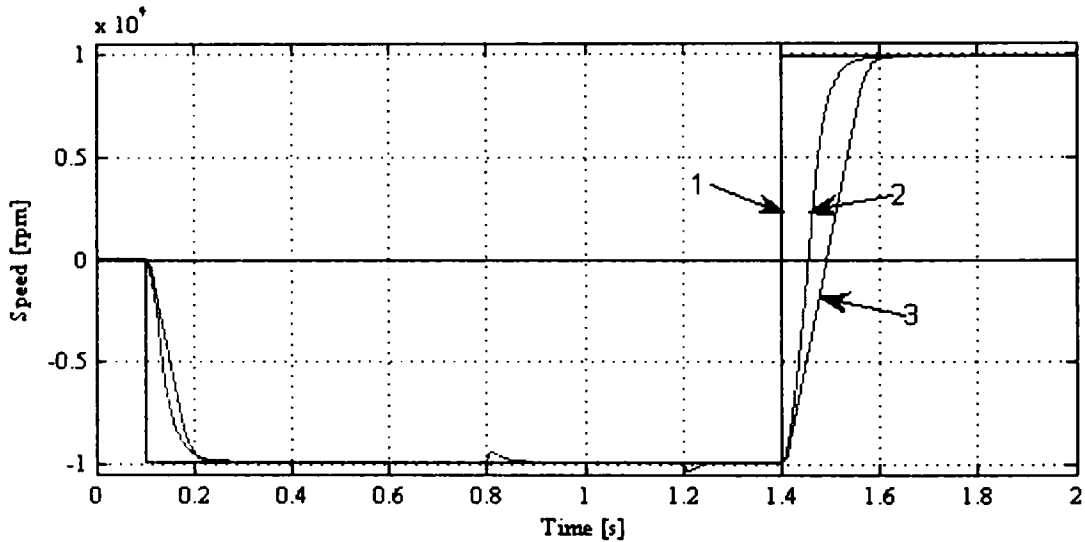


Fig. 2.27 No-load start-up at -10,000 rpm, followed by loading at 0.8 s, unloading again at 1.2 s, reverse speed from -10,000 rpm to 10,000 rpm at 1.4 s  
1) designated speed; 2) filtered designated speed; 3) encoder speed

Fig. 2.27 presents the way the motor reacts when the vector control is used with the information provided by an encoder. As we said before, the vector control could be considered a reference control, due to the good results obtained in the case of its application. The above figure illustrates how the motor speed follows the reference speed. The motor dynamics is an excellent one and is the maximum dynamics that this motor could give. The acceleration time is less than 0.1 s, the speed reversal is less than 0.2 s and the loading and the unloading tests produce a very small error and for a very short period of time in the speed waveform.

The performance of the drive under sensorless control is given in Fig. 2.28. All the next figures (Fig. 2.29 to Fig. 2.33.) present the results obtained under sensorless control.

In the sensorless control, when the speed crosses the zero point during speed reversal from -10,000 rpm to 10,000 rpm some problems occur; meaning by this, there are oscillations in the speed waveform, as it can be seen in Fig. 2.28. These oscillations are derived from  $\text{sgn}(\omega_r)$  in the mathematical expression of the PLL in Fig. 2.14 and Fig. 2.12, which interferes with the estimator. Thus, it is possible that the rotor speed sign to be changed and the estimator do not take it into consideration.

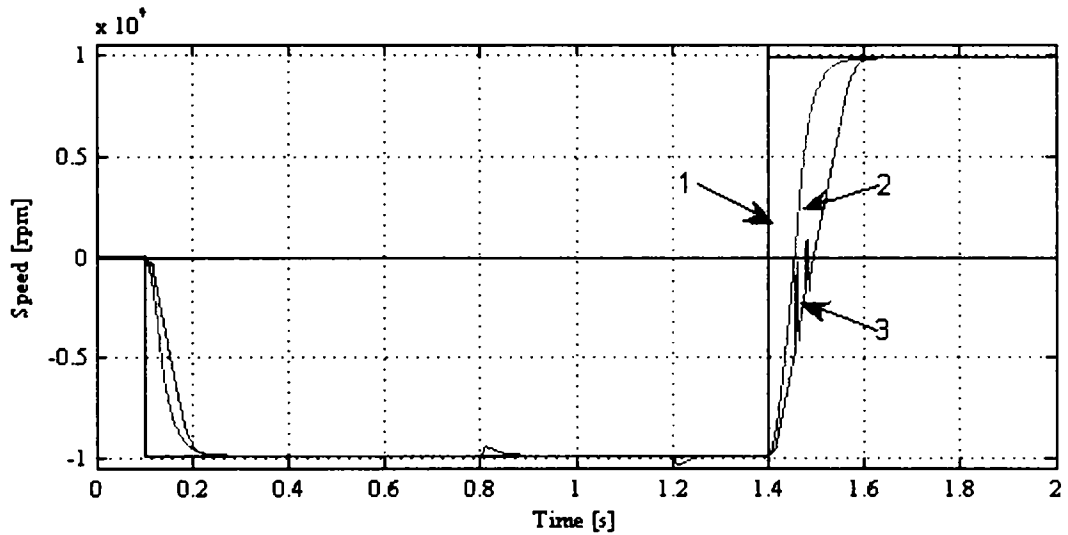


Fig. 2.28 No-load start-up at -10,000 rpm, followed by loading at 0.8 s, unloading again at 1.2 s, reverse speed from -10,000 rpm to 10,000 rpm at 1.4 s

1) designated speed; 2) filtered designated speed; 3) encoder speed under sensorless control

For the sensorless control system it is well known the fact that during speed reversal some problems occur. These are also due to the very small mechanical time constant (see Chapter 7).

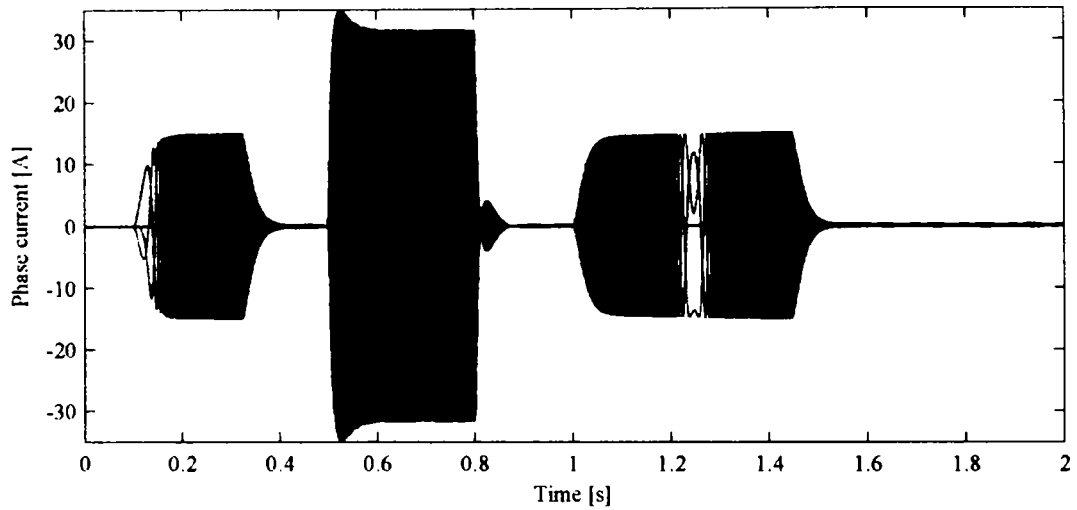


Fig. 2.29 Three phase stator currents in sensorless control in Fig. 2.28.

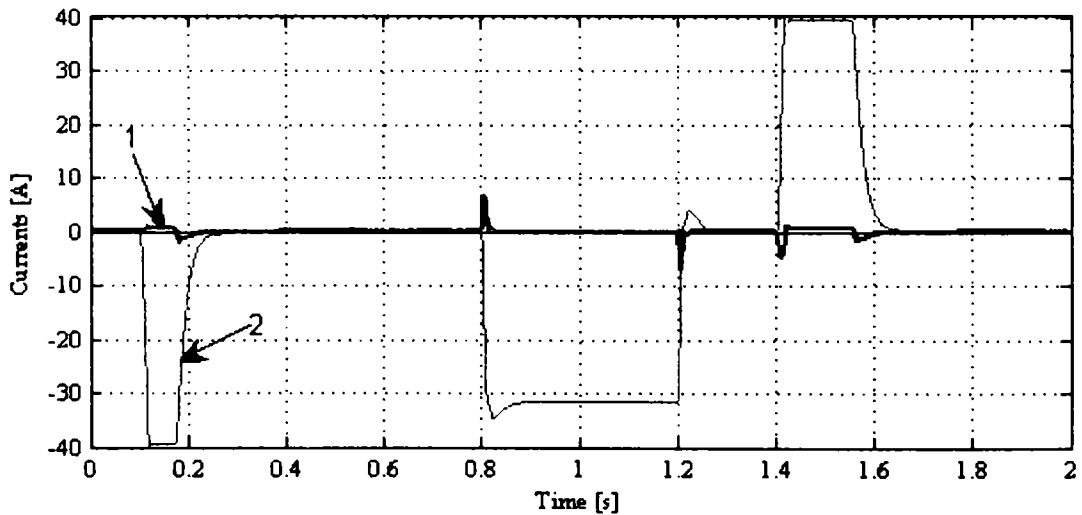


Fig. 2.30 Stator currents in rotor reference frame.  
 $I_d$  current (1) and  $I_q$  current (2).

Fig. 2.29 and Fig. 2.30 illustrate the currents waveforms during tests presented in Fig. 2.28. As it can be seen in the former one, the currents are not larger than the admitted ones. In the second figure, the current value  $I_d$  is maintained to zero during the entire simulation time. Even more, the oscillations are almost invisible.

Fig. 2.31 illustrates the torque waveform developed by the machine (1).



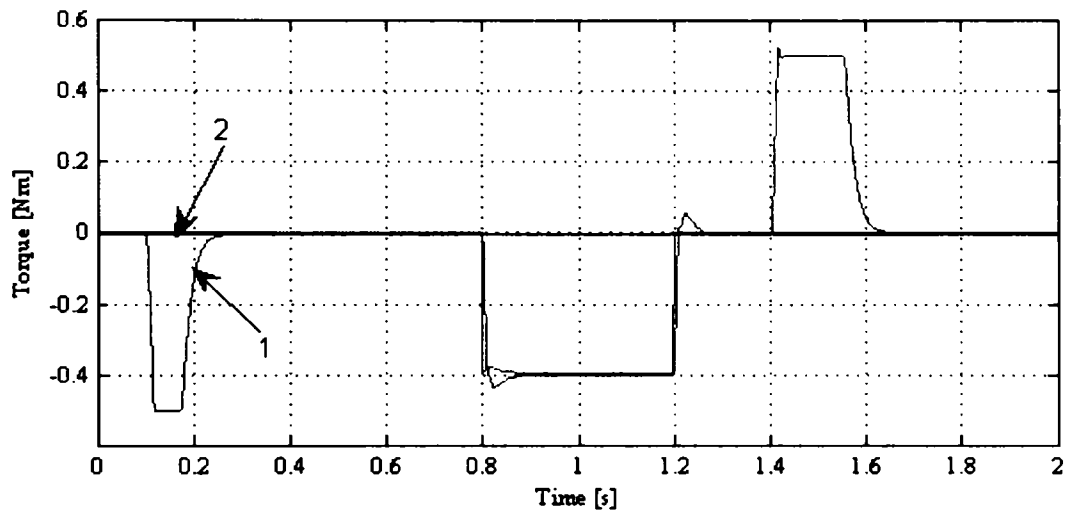


Fig. 2.31 Load torque  $T_l$  (2) and electromagnetic torque  $T_e$ (2) in sensorless control in Fig. 2.28.

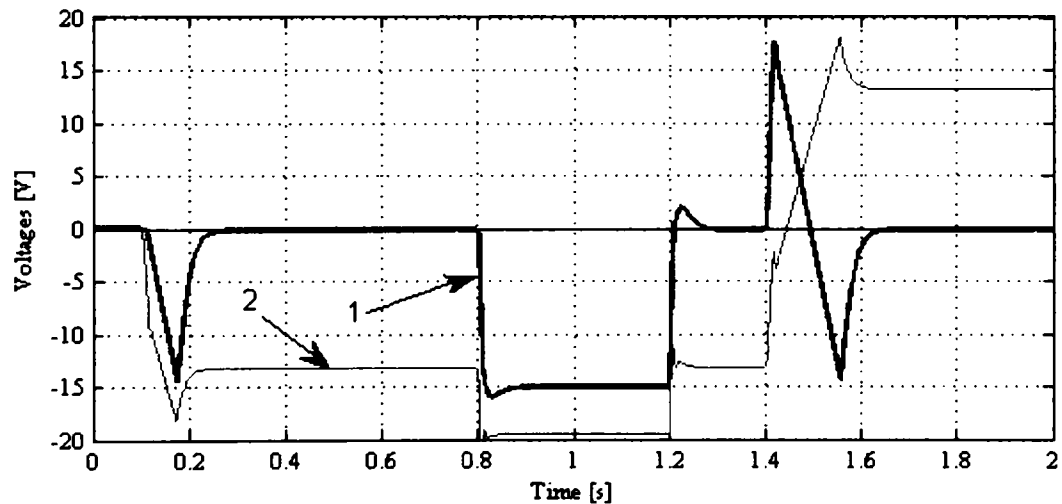


Fig. 2.32 Voltage vector in rotor reference frame  $V_d$  (1) and  $V_q$  (2);

The voltage waveforms in stator reference frame are presented in Fig. 2.32.

Fig. 2.33 illustrates the actual (provided by the encoder) and the estimated rotor position angle. Only at startup a small difference between the two waveforms (actual and estimated) can be observed.

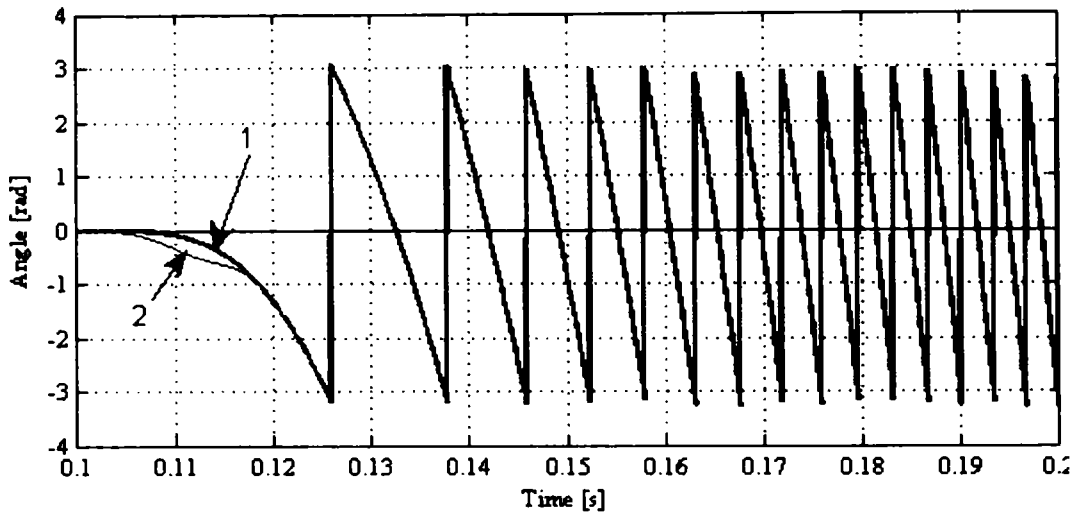


Fig. 2.33 Zoom of encoder (1) and estimated (2) angle

## 2.7. Conclusion

A high speed SPMSM was driven with and without encoder.

In the case of encoderless control system, it is clear that the obtained dynamic is the best which can be for this system, taking into account the small electrical time constant of the motor.

To see which estimator fits better with the motor in the same operating conditions, four rotor position and speed estimators for surface mounted synchronous permanent magnet motors (SPMSMs) were tested. All of them operate for acceptable parameter values and have small errors. For high-speed encoderless system, a rotor position estimator with small oscillations should be implemented. In encoderless systems, the duration of position angle computation, is decisive. If the estimated angle has large oscillations comparatively with the encoder angle, then the system will not operate properly. This is visibly at high-speed motors, where the angle estimator should be very fast and without large oscillations.

All rotor position and speed estimators have problems at low and especially zero speed. So, in sensorless control, an addition starting control strategy is required.

In the next step the rotor speed sensor and position sensor was eliminated.

Simulations confirm that the proposed method gives a good tracking performance for different speeds with and without load.

The presented results demonstrate a good behavior of the simulated sensorless control system.

Now, looking at the above presented simulation results, one can expect that the control system will have at least the same good behavior during the practical implementation (with and without encoder).

## References

- [1] Montesinos, D, Galceran, S., Sudria, A., Gomis, O., Blaabjerg, F.: "Low cost Sensorless Control of Permanent Magnet Motors - An Overview and Evaluation". In: Proc. IEEE Int. Conf. on Electric Machines and Drives, IEMDC 2005, San Antonio, TX, May 2005, pp. 1681-1688.
- [2] Chi, S., Xu, L., Zhang, Z.: "Sliding Mode Sensorless Control of PM Synchronous Motor for Direct-Driven Washing Machines". In: Conf. Record of IEEE-IAS 2006, Tampa, FL, Vol. 2, Oct. 2006, pp. 873-879.
- [3] Kim, J.-S., Sul, S.-K.: "New Approach for High-Performance PMSM Drives without Rotational Position Sensors". In: IEEE Trans. on Power Electronics, Vol. 12, No. 5, Sept. 1997, pp. 904-911.
- [4] Urlep, E., Horvat, J., Jezernik, K.: "Pseudo Sensorless Control of PMSM". In: Proc. 12th Int. Power Electronics and Motion Control Conf., EPE-PEMC 2006, Portoroz, Aug. 2006, pp. 1950-1955.
- [5] Bumby, J.R., et al: "Electrical machines for Use in Electrically Assisted Turbochargers". In: Proc. 2nd Int. Conf. on Power Electronics Machines and Drives, PEMD 2004, Vol. 1, March 2004, pp. 344-349.
- [6] Bianchi, N., Bolognani, S.: "Influence of Rotor Geometry of an Interior PM Motor on Sensorless Control Feasibility". In: Conf. Record of IEEE-IAS 2005, Hong Kong, Vol. 4, Oct. 2005, pp. 2553-2560.
- [7] Seok, J.-K., Lee, J.-K., Lee, D.-C.: "Sensorless Speed Control of Nonsalient Permanent-Magnet Synchronous Motor Using Rotor-Position-Tracking PI Controller". In: IEEE Trans. on Industrial Electronics, Vol. 53, No. 2, April 2006, pp. 399-405.
- [8] Bae, B.-H., Sul, S.-K., Kwon, J.-H., Byeon, J.-S.: "Implementation of Sensorless Vector Control for Super-High-Speed PMSM of turbo-compressor". In: IEEE Trans. on Industry Applications, Vol. 39, No. 3, May-June 2003, pp. 811-818.
- [9] Lorenz, R.D., Van Patten, K.W.: "High-Resolution Velocity Estimation for All-Digital, AC Servodrives". In: IEEE Trans. on Industry Applications, Vol. 27, No. 4, July-Aug. 1991, pp. 701-705.

- 
- [10] Ziegler, J.G., Nichols, N.B.: "Optimum Settings for Automatic Controllers". In: Trans. of American Society of Mechanical Engineers (ASME), Vol. 64, Nov. 1942, pp. 759-765.
- [11] Sakamoto, K.; Iwaji, Y.; Endo, T.; "Position Sensorless Vector Control of Permanent Magnet Synchronous Motors for Electrical Household Appliances" Power Conversion Conference - Nagoya, PCC '07 2-5 April pp. 1119 - 1125
- [12] Yamanaka, K.; Ohnishi, T.; Hojo, M.; "A Novel Position Sensorless Vector Control of Permanent-Magnet Synchronous Motors" Power Conversion Conference - Nagoya, PCC '07 2-5 April pp. 290 - 295
- [13] Yu, J.S.; Lee, B.K.; Won, C.Y.; "Sensorless Vector Control for Non-salient Permanent Magnet Synchronous Motors using Programmable Low Pass Filter" IEEE Power Electronics Specialists Conference, PESC '06. 18-22 June 2006 pp. 1 - 6
- [14] Ahmad, G.; Tsuyoshi, H.; Teruo, T.; "A novel implementation of low speed sensorless vector control of synchronous reluctance motors with a new online parameter identification approach" IEEE Applied Power Electronics Conference and Exposition, APEC '06. 19-23 March 2006
- [15] Ahmad, Ghaderi; Tsuyoshi, Hanamoto; "Very Low Speed Sensorless Vector Control of Synchronous Reluctance Motors with a Novel Startup Scheme" IEEE Applied Power Electronics Conference, APEC 2007 - Feb. 25 -March 1 pp. 396 - 402
- [16] Andreescu G.D.: "Estimatoare în sisteme de conducere a acțiunilor electrice - Aplicații la MSMP (Estimators in Control of Electric Drives -Applications to MSMP)", Editura Orizonturi Universitare, Timișoara, 1999.
- [17] Ostlund, S., Brokemper, M.: "Sensorless Rotor-Position Detection from Zero to Rated Speed for an Integrated PM Synchronous Motor Drive", In: IEEE Trans. on Industry Applications, Vol. 32, No. 5, Sept.-Oct. 1996, pp. 1158-1165.
- [18] Chung, D.-W., Kang, J.-K., Sul, S.-K.: "Initial Rotor Position Detection of PMSM at Standstill without Rotational Transducer". In Int. Conf. Electric Machines and Drives, IEMD'99, Seattle, WA, May 1999, pp. 785-787.
- [19] Nakashima, S., Inagaki, Y., Miki, I.: "Sensorless Initial Rotor Position Estimation of Surface Permanent-Magnet Synchronous Motor". In IEEE Trans. on Industry Applications, Vol. 36, No. 6, Nov.-Dec. 2000, pp. 1598-1603.

- [20] Silva, C., Asher, G.M., Sumner, M.: "Hybrid Rotor Position Observer for Wide Speed-Range Sensorless PM Motor Drives Including Zero Speed". In IEEE Trans. on Industrial Electronics, Vol. 53, No. 2, April 2006, pp. 373-378.
- [21] Burgos, R.P.; Kshirsagar, P.; Lidozzi, A.; Wang, F.; Boroyevich, D.; "Mathematical Model and Control Design for Sensorless Vector Control of Permanent Magnet Synchronous Machines" IEEE Computers in Power Electronics, COMPEL '06. 16-19 July 2006 pp. 76 - 82
- [22] Paul C. Krause, Oleg Wasynczuk, and Scott D. Sudhoff, "Linearized Equation of Induction and Synchronous Machine", Chapter 7 in Analysis of Electric Machinery, IEEE Press 1995.
- [23] Yong Zhang; Keran Shao; Lan Li; Xinhua Li; "Theory and simulation of vector control based on rotor position orientation of rare-earth permanent magnet motor", ICEMS 2003. 9-11 Nov. 2003 pp. 530 - 533 vol.2
- [24] Azadi, M.; Rahideh, A.; Safavi, A.A.; Mahdiyari, O.; "Wavenet Based Vector Control of a Permanent Magnet Synchronous Motor Drive" Electric Machines & Drives Conference, IEMDC '07. 3-5 May 2007 pp. 1663 - 1668
- [25] Burzanowska, H.; Sario, P.; Stulz, Ch.; Joerg, P.; "Redundant Drive with Direct Torque Control (DTC) and dual-star synchronous machine, simulations and verification", Power Electronics and Applications, 2-5 Sept. 2007 pp. 1 - 10
- [26] Vamsidhar, S.; Fernandes, B.G.; "Hardware-in-the-loop simulation based design and experimental evaluation of DTC strategies", PESC 04, 20-25 June 2004, Vol.5, pp. 3615 - 3621
- [27] Diamantis, G.; Prousalidis, J.M.; "Simulation of a ship propulsion system with DTC driving scheme" ,PEMD 2004, 31 March-2 April 2004, Vol.2, pp. 562 - 567
- [28] Castoldi, M.F.; Aguiar, M.L.; "Simulation of DTC Strategy in VHDL Code for Induction Motor Control", IEEE Industrial Electronics, July 2006, Vol. 3, pp. 2248 - 2253
- [29] E. Erdem; Y. Tatar; S. Sunter; "Modeling and Simulation of Matrix Converter Using Space Vector Control Algorithm", EUROCON 2005, Vol. 2, pp. 1228 - 1231
- [30] Szabo, C.; Imecs, Maria; Incze, I. I.; "Vector control of the synchronous motor operating at unity power factor" OPTIM 2008. May 2008 pp. 15 - 20

- 
- [31] Lin Hua; Zou Yunping; He Bi; "The Vector Control Strategies for Multiphase Synchronous Motor Drive Systems" IEEE Industrial Electronics, July 2006 pp. 2205 - 2210
- [32] Markku Niemela, Juha Pyrhonen, Olli Pyrhonen and Julius Luukko "Drift Correction Methods of the Stator Flux Linkage in DTC Synchronous Motors Drives", In IEEE Proc. of European Conf. of Power Electronics and Applications, 1999.
- [33] Shuhui Li; Haskew, T.A. "Transient and Steady-State Simulation Study of Decoupled d-q Vector Control in PWM Converter of Variable Speed Wind Turbines", IEEE IECON 2007 5-8 Nov. 2007, pp. 2079 - 2086
- [34] Dal Y. Ohm and Richard J. Oleksun, "On Practical Digital Current Regulators Design for PM Synchronous Motor Drives", In IEEE Proc. on APEC'98, vol 1, pp. 56-63, 1998.
- [35] Shigeo Morimoto, Masayuki Sanada and Yoji Takeda, "Wide-Speed Operation of Interior Permanent Magnet Synchronous Motor with High-performance Current Regulators Practical Digital Current Regulators", IEEE Trans. On Ind. Appl., Vol. 30, No. 4, pp. 920-926, July/August 1994.
- [36] F. Briz del Blanco, M.W. Degner, R.D. Lorenz, "Dynamic Analysis of Current Regulators for AC Motors Using Complex Vectors", IEEE TRANS. IND. APPL., VOL. 35, NO. 6, 1999.
- [37] Acarnley P. P., Watson, J.F. "Review of Position-Sensorless Operation of Brushless Permanent-Magnet Machines", IEEE Trans. on Ind. Electronics, vol. 53, Nr. 2, Aprilie, 2006
- [38] Shinnaka, S. "New sensorless vector control using minimum-order flux state observer in a stationary reference frame for permanent-magnet synchronous motors" IEEE Industrial Electronics, Trans. April 2006 pp. 388 - 398
- [39] Incze, I. I.; Szabo, Cs.; Imecs, Maria; "Flux identification for vector control of the synchronous motor drives" Automation, Quality and Testing, Robotics, AQTR 2008. 22-25 May 2008 pp. 105 - 110
- [40] Burgos, Rolando P.; Kshirsagar, P.; Lidozzi, A.; Jang, Jihoon; Wang, Fred; Boroyevich, Dushan; Rodriguez, Pedro; Sul, Seung-Ki; "Design and Evaluation of a PLL-Based Position Controller for Sensorless Vector Control of Permanent-

Magnet Synchronous Machines" IEEE Industrial Electronics, IECON - Nov. 2006 pp. 5081 - 5086

[41] R. Ancuti, G.-D. Andreescu, and I. Boldea, "Four rotor position and speed simplified estimators for vector control of high-speed SPMSM with test comparisons", Journal of Electrical Engineering, JEE, vol. 7, no. 4, Politehnica Publishing House, Timisoara, 2007 (in press).



# Chapter 3

## Vector control – motion sensorless control experimental results

### Abstract

Cost and reliability reasons lead to motion sensorless control of high speed PMSM drives. This chapter presents a novel emf based observer for rotor position and speed estimation that provides very fast starting from pre-produced zero initial position (less than 100 milliseconds from zero to 10 krpm in a 750 W surface PMSM) with very good dynamic response to large step torque perturbations. Implementations and test results fully validate the proposed control solution.

### 3.1. Introduction

In the recent years, the demand for high-speed permanent magnet synchronous motors (PMSM) has increased due to the advanced technology and reduced cost, replacing the induction machines. To this category also belong the surface permanent-magnet synchronous machines (SPMSM) that have many advantages such as high power density, torque to inertia ratio and energy efficiency. They are cost effective and simpler to manufacture than embedded magnet based machines [1].

In ultra-high-speed applications, PMSMs offer the advantage of high efficiency compared to other types of motors since there are no excitation power loss in the rotor, and low eddy current loss in the stator and rotor [2].

These motors can be controlled with an encoder mounted on their shaft. But for high-speed PMSM drive, the speed sensor is costly and easy to be damaged, and it is difficult to build. The most reasonable control of this kind of motors is without encoder (sensorless control) [3], [4]. In this case, of prime importance is the way how the rotor is built. Thus, from the control point of view, at low speeds, it matters if  $L_d$  is equal to  $L_q$  or not, so the motor design is very important when good operation at low speeds is desired.

For sensorless control of PMSM drives, a starting voltage sequence in rotor coordinates [5], V/f and I-f control with one stabilizing loop has been proposed [6], [7]. More strategies of scalar control were investigated in [8]. Four simplified position and speed estimators, good for sensorless vector control at high speed, were successfully tested in [11].

This chapter presents the principles, the implementation and the test results up to 10,000 rpm of a 6 slot /4 pole SPMSM motion sensorless drive with current vector control, including a start-up strategy, rotor position and speed estimator, without dc or ac voltages feedback. Inverter nonlinearities are compensated for safe and fast response (100 ms from zero to 10,000 rpm) repetitive starting.

### 3.2. Equations used in estimator design

According to voltage equations in space vector form presented in Chapter 2 and ignoring the  $s$  superscript notation, the space-phasor SPMSM model in stator coordinates can be described as:

$$\bar{V}_S = R_S \bar{I}_S + \frac{d\bar{\lambda}_S}{dt} \quad (3.1)$$

$$\begin{aligned} \bar{\lambda}_S &= L_S \bar{I}_S + \bar{\lambda}_{PM} \\ \bar{\lambda}_{PM} &= \lambda_{PM} e^{j\theta_{er}} \\ \bar{I}_S &= I_S e^{j\theta_i} \end{aligned} \quad (3.2)$$

where  $\bar{V}_S$ ,  $\bar{I}_S$  and  $\bar{\lambda}_S$  are the stator voltage, current and flux vectors, respectively,  $\bar{\lambda}_{PM}$  is the PM-flux vector,  $R_S$ ,  $L_S$  are the stator resistance and inductance,  $\theta_{er}$  is the electrical rotor position, and  $\theta_i$  is the stator current vector angle.

The back-emf vector  $\bar{E}$  is given [12] by:

$$\bar{E} = \frac{d\bar{\lambda}_{PM}}{dt} = \omega_r \lambda_{PM} e^{j(\theta_{er} + \pi/2)} \quad (3.3)$$

where  $\omega_r$  is the electrical rotor speed.

The SPMSM phasor diagram is illustrated in Fig. 3.1.

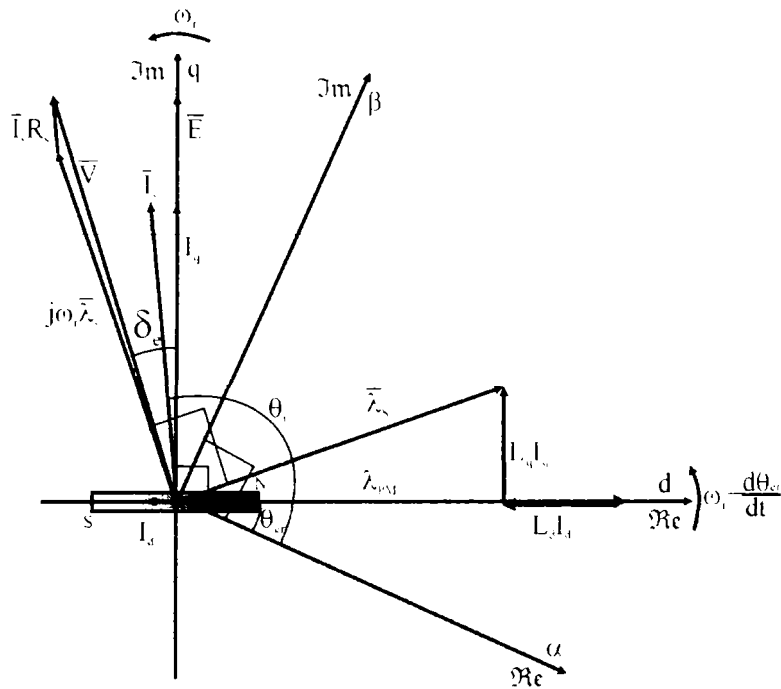


Fig. 3.1 Space vector diagram of SPMSM

By inserting (3.2) in (3.1) and using (3.3), the back-emf vector  $\bar{E}$  is obtained:

$$\bar{E} = \bar{V}_s - R_s \bar{I}_s - L_s \frac{d\bar{I}_s}{dt} \tag{3.4}$$

The rotor position and speed estimator is based on (3.4).

### 3.3. Motion Sensorless Control System

The SPMSM sensorless control structure (Fig. 3.2) uses speed control without position encoder and without dc link voltage sensor, and employs standard

current-vector control algorithm ( $I_d^* = 0$ ) with feedforward voltage-decoupling according with (3.5).

$$\begin{aligned} V_{d\_ff}^* &= -L_s \omega_r I_q^* \\ V_{q\_ff}^* &= L_s \omega_r I_d^* + \omega_r \lambda_{PM} \end{aligned} \quad (3.5)$$

The current vector control consists in feedback loop ( $V_{d\_fb}$ ,  $V_{q\_fb}$ ) with feedforward correction ( $V_{d\_ff}$ ,  $V_{q\_ff}$ ). The control system without feedforward correction is also feasible, but in this case the PI controllers have to be operated faster to compensate the feedforward (3.5) by the integral component [10].

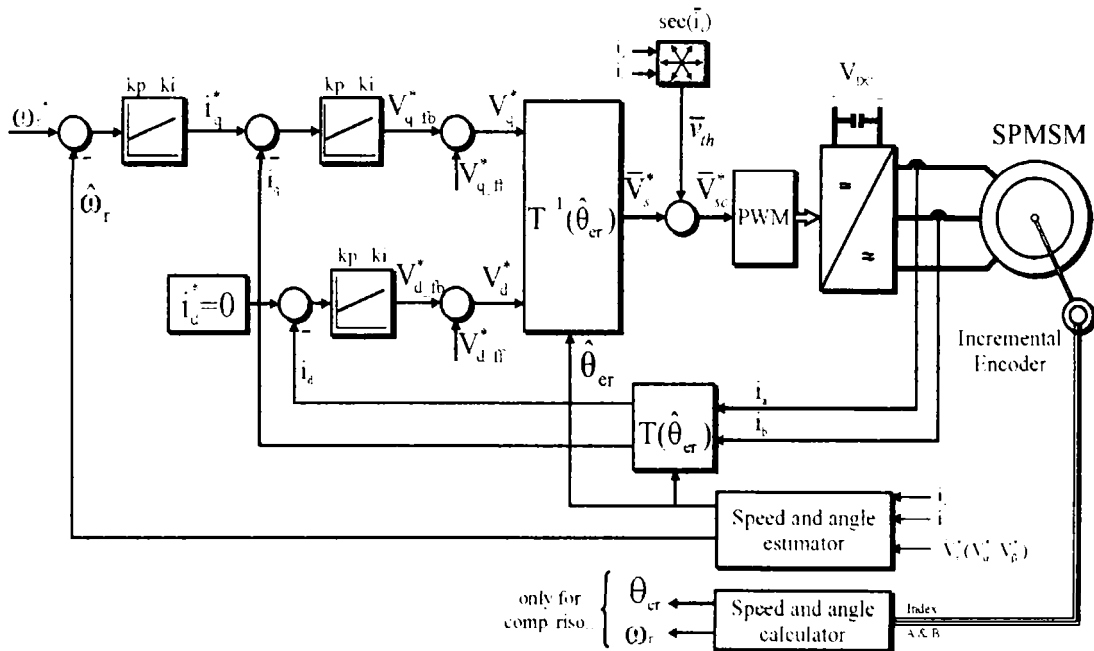


Fig. 3.2 Block diagram of sensorless vector control scheme.

Fig. 3.2 has a drawback at start-up. For the reason that the speed estimator has a large overshoot, which is transmitted also in the voltage reference by feedforward correction (3.5), the start-up operation could fail. Even more, the voltage provided by the feedback loop has to compensate errors introduced by (3.5) and thus a very fast controller has to be implemented. If you do not have a lot of

confidence in the speed estimator, then it is better not to introduce the feedforward correction (3.5) during start-up.

The maximum values for  $V_d^*$  and  $V_q^*$  provided by the control do not exceed 20 V (see the experimental results), values attained relatively easy, and quickly, by the PI controllers outputs.

The gains of PI current and speed controllers (3.6) for the investigated prototype are given in TABLE 3.1 in Appendix.

$$\Delta y = k_p(1 + k_i / s) \cdot \Delta x \quad (3.6)$$

The gains are a little changed from those in [11], in which they were tested having an encoder mounted on the shaft of the rotor.

The estimator coefficients were improved by a trial and error method, but first of all they were chosen using the Ziegler Nichols method [41] taking into account the given values of the machine parameters ( $R_s$ ,  $L_s$  and  $J$ ) in Chapter 6.

### 3.4. Back-EMF Angle Estimator for Dynamic Operating Mode

Due to the fact that the machine operates at relatively high speeds (experiments are done at 10,000 rpm) with high dynamics (acceleration to 10,000 rpm in 100 ms), it is necessary to use a fast estimator with very low errors. An estimator for sensorless control synchronous machine based on electromotive force is presented in [42], [43].

A phase-locked loop (PLL) state-estimator (Fig. 3.3) extracts the rotor position and speed estimations from  $\bar{E}$  vector according to equations (3.3) and (3.4) (see (3.13)). This estimator is the same as the one presented in Fig. 2.13, but written in another form. The estimator receives the measured stator currents ( $I_a$ ,  $I_b$ ), the reference voltages in stator coordinates ( $V_d^*$ ,  $V_q^*$ ) and the reference speed  $\omega_{fPT1}^*$ , and generates at the output both the rotor position  $\hat{\theta}_{er}$  and rotor speed  $\hat{\omega}_r$  estimations. No voltage sensors are used.

$\bar{E}$  is delayed with  $\pi/2$  degrees with respect to the permanent magnet flux vector  $\bar{\lambda}_{PM}$  (see Fig. 3.1), so:

$$\bar{E} = E \cdot e^{j(\theta_{er} + \pi/2)} \quad (3.7)$$

Multiplying (3.7) with  $e^{-j(\hat{\theta}_{er} + \pi/2)}$  :

$$E \cdot e^{j(\theta_{er} + \pi/2)} \cdot e^{-j(\hat{\theta}_{er} + \pi/2)} = E \cdot e^{j\Delta\theta_r} \quad (3.8)$$

The value of  $\Delta\theta_r$  is important for any PLL. In (3.8) the imaginary part is decisive. So the left part of the above equation becomes:

$$\begin{aligned} \text{Im}(E \cdot e^{j(\theta_{er} + \pi/2)} \cdot e^{-j(\hat{\theta}_{er} + \pi/2)}) &= \text{Im}[(E_\alpha + jE_\beta) \cdot e^{-j(\hat{\theta}_{er} + \pi/2)}] = \\ &= \text{Im}\left\{(E_\alpha + jE_\beta) \cdot [\cos(\hat{\theta}_{er} + \pi/2) - j\sin(\hat{\theta}_{er} + \pi/2)]\right\} = \\ &= \text{Im}\left\{(E_\alpha + jE_\beta) \cdot [-\sin\hat{\theta}_{er} - j\cos\hat{\theta}_{er}]\right\} = \\ &= -E_\beta \cos\hat{\theta}_{er} - E_\alpha \sin\hat{\theta}_{er} \end{aligned} \quad (3.9)$$

Thus, the right part of the equation (3.8) turns into:

$$\begin{aligned} \text{Im}(E \cdot e^{j\Delta\theta_r}) &= \text{Im}[E \cdot (\cos(\Delta\theta_r) + j\sin(\Delta\theta_r))] = \\ &= E \cdot \sin(\Delta\theta_r) \end{aligned} \quad (3.10)$$

For small angle values  $\sin(\Delta\theta_r) = \Delta\theta_r$ , so (3.10) becomes:

$$\text{Im}(E \cdot e^{j\Delta\theta_r}) = \text{Im}[E \cdot \sin(\Delta\theta_r)] = E \cdot \Delta\theta_r \quad (3.11)$$

From (3.8), (3.9) and (3.11) outcomes:

$$E \cdot \Delta\theta_r = -E_\beta \cos\hat{\theta}_{er} - E_\alpha \sin\hat{\theta}_{er} \quad (3.12)$$

Taking into account that  $E_\alpha = E \cdot \cos\theta_{er}$ ,  $E_\beta = E \cdot \sin\theta_{er}$  and  $E = \omega_r \lambda_{PM}$ , results:

$$\Delta\theta_r = -\text{sgn}(\hat{\omega}_r)[E_\alpha \cdot \cos(\hat{\theta}_{er}) + E_\beta \cdot \sin(\hat{\theta}_{er})] \tag{3.13}$$

The  $V_{dc}$  voltage is known only with approximation. It is provided by the four batteries connected in series and it can vary from 47 V to 51 V. However, in these conditions the system operates correctly. The encoder in Fig. 3.2 is used only for making comparisons with the test results.

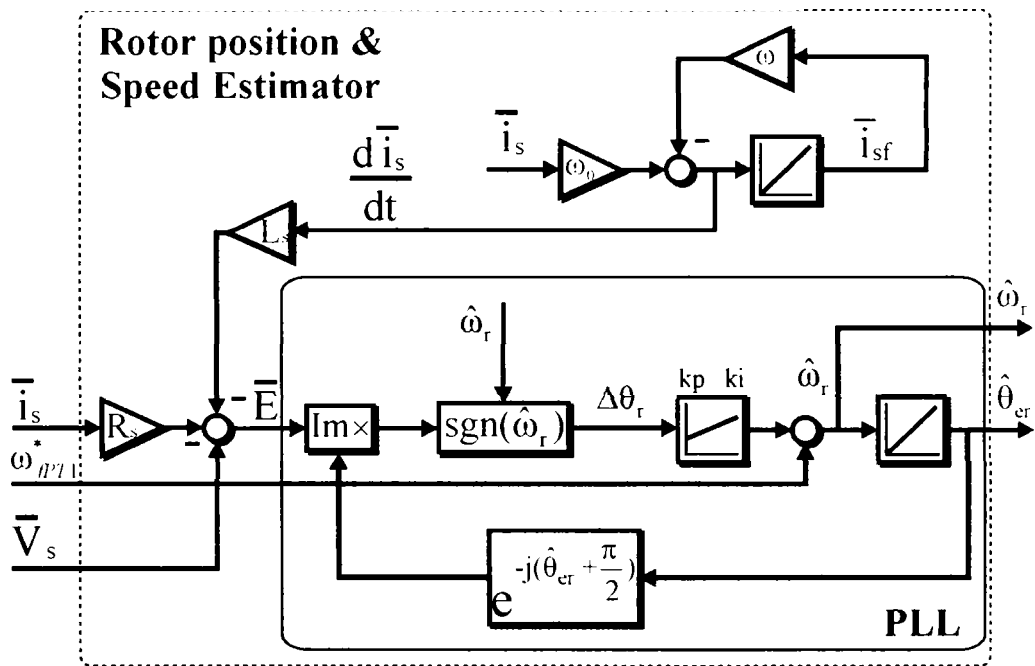


Fig. 3.3 Rotor position and speed estimator based on back-emf in dynamic operating mode.

For the sensorless start-up, it is crucial to know the right initial rotor position, which has to be introduced in the PLL integrator. This is done experimentally using a stator voltage sequence to align the rotor to a known position before start-up.

The hardest experimental test was the sensorless speed reversal. To accomplish such an operation, accurate speed estimation is required, whose aim is to change the PLL reaction sign (see  $\text{sgn}(\hat{\omega}_r)$  in Fig. 3.3. Otherwise, if the moment of time when the speed crosses zero is not exactly known,  $\hat{\theta}_{er}$  will be wrongly estimated and the system will have high chances to cease working.

To reduce noise in current derivative  $d\bar{I}_s/dt$ , a filter-based derivative estimator is used [40], as shown in the upper-right corner in Fig. 3.3.

### 3.5. Start-Up Strategy

When fast start-up without encoder or Hall sensors is desired, the initial rotor position has to be well known, otherwise the angle from the Park transformation is wrongly introduced and the system may not start (see [13], [14], [15] and [16]).

In the last decade, several solutions have been proposed to estimate the PMSM initial rotor position. Two basic methods are pulse signal injection, and sinusoidal carrier signal injection ([17] to [31]). The pulse signal injection methods are often based on estimating the minimum inductance location using a calculated value obtained during some form of iterative square wave voltage injection to arbitrary axes. Such methods can be applied to both surface (although it is a difficult task) and interior PMSMs.

Magnetic axis without polarity was estimated via a method named "INFORM" (Indirect Flux detection by On-line Reactance Measurement) and the polarity was detected by finding minimum inductance on the estimated magnetic axis [30]. In these methods, initial position estimation accuracy can be affected by additional spatial harmonics such as saturation of the stator teeth.

Another starting method is to apply, from the beginning of the start-up, a supplementary strategy of control (I-f or V/f control).

The method applied here is to align the rotor to a known direction, and thus the known initial rotor position is now introduced in the estimator. Usually, high-speed drives allow a little movement for such maneuver.

A drawback of these methods is that there is no warranty that the rotor will not move in wrong direction with a small angle before starting. Another drawback is that the system becomes more complex, and thus there are two control systems



working sequentially: one for robust start-up, and another for obtaining good speed and torque dynamics. The advantage is that this way a good starting is obtained.

Due to the fact that the motor has a very small electrical time constant ( $L_s/R_s = 0.5$  ms), the control is sensitive to any voltage variation. Thus, even if a zero stator vector voltage  $\vec{V}_s^* = 0$  is applied and the inverter is turned on, important oscillations of the rotor position can be detected by the position sensor (see Fig. 3.4).

In the case of  $\vec{V}_s^* = 0$ , by using space vector modulation (SVM), half of the sampling period the up-transistors are in conducting operation mode, while in the other half, the down-transistors are in conducting operation mode.

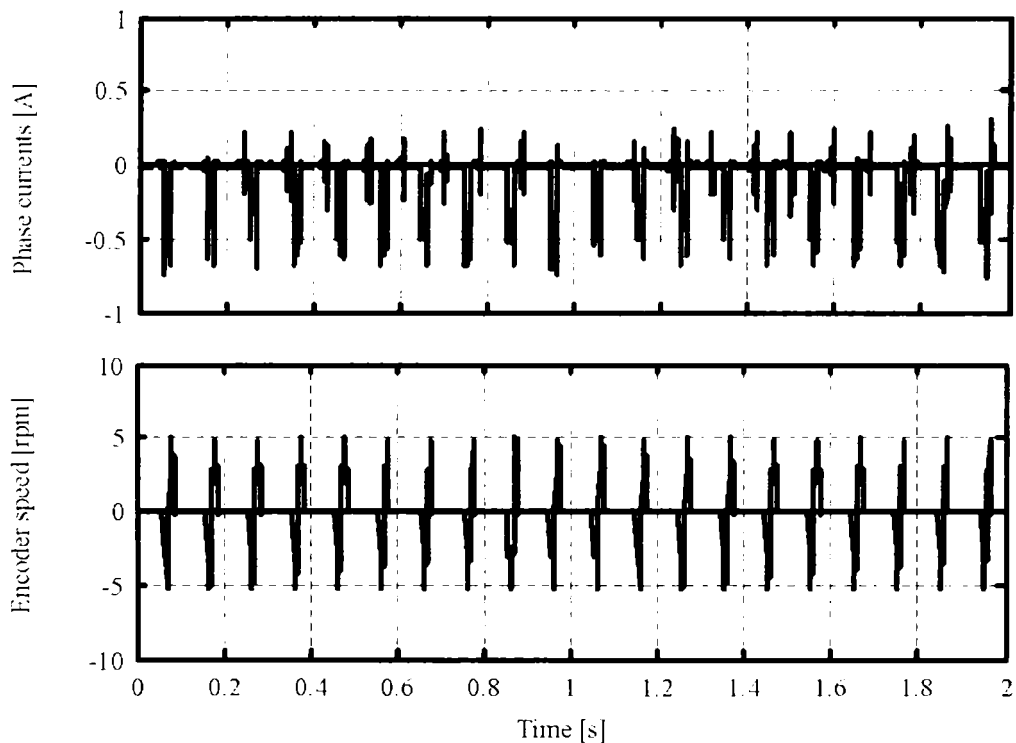


Fig. 3.4 Current and speed ripples when  $\vec{V}_s^* = 0$  is applied to inverter

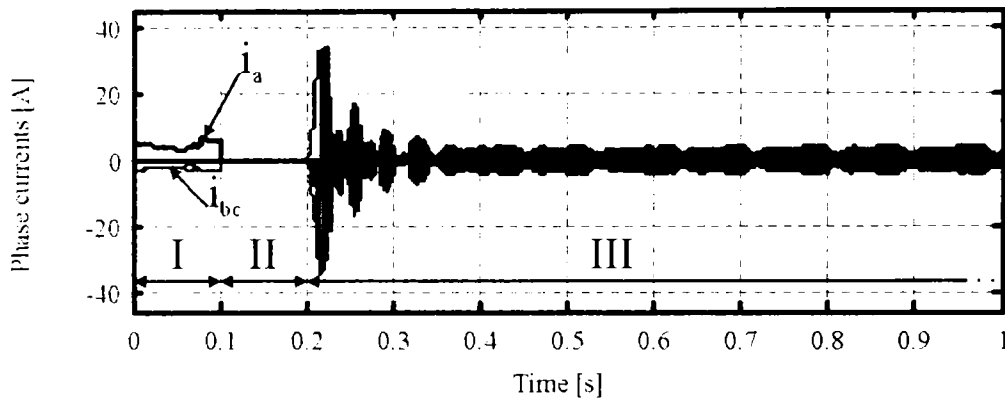


Fig. 3.5 Three steps start-up strategy

The oscillations from Fig. 3.4 are generated by using an inverter which have the rated current ten times larger than the motor rated current, combined with an inadequate chosen dead-time. Even if oscillations are present at  $\vec{V}_S^* = 0$ , the start-up is performed in three steps as in Fig. 3.5:

- i. the voltage vector  $\vec{V}_1(1,0,0)$  is applied, which aligns the rotor in a known position  $\theta_{er} = 0$
- ii. the inverter is turned off for a small interval of time;
- iii. the machine sensorless starts-up from known position.

The second step is necessary to guarantee the start-up from zero for all variables in the estimator.

In the start-up strategy the voltage drops on the semiconductor devices (6 transistors and 6 diodes) have been taken into consideration [32] to [36] to compensate inverter nonlinearity. These voltage drops depend not only on the stator current value, but on the sector in which  $\vec{i}_S$  is in that instant of time.

$$\bar{v}_{th} = v_{th} \sec(\bar{i}_S) \quad (3.14)$$

$$\sec(\bar{i}_S) = \text{sgn}(i_a) + a \cdot \text{sgn}(i_b) + a^2 \cdot \text{sgn}(i_c) \quad (3.15)$$

where  $a = e^{j2\pi/3}$ , and the value of  $v_{th} = 0.5 \dots 1 \text{ V}$ .

As it is shown in Fig. 3.6, if this compensation is not introduced, the real stator voltage vector  $\bar{V}_s$  applied to the motor is quite different from  $\bar{V}_s^*$ . This fact is very important during start-up and low speeds.

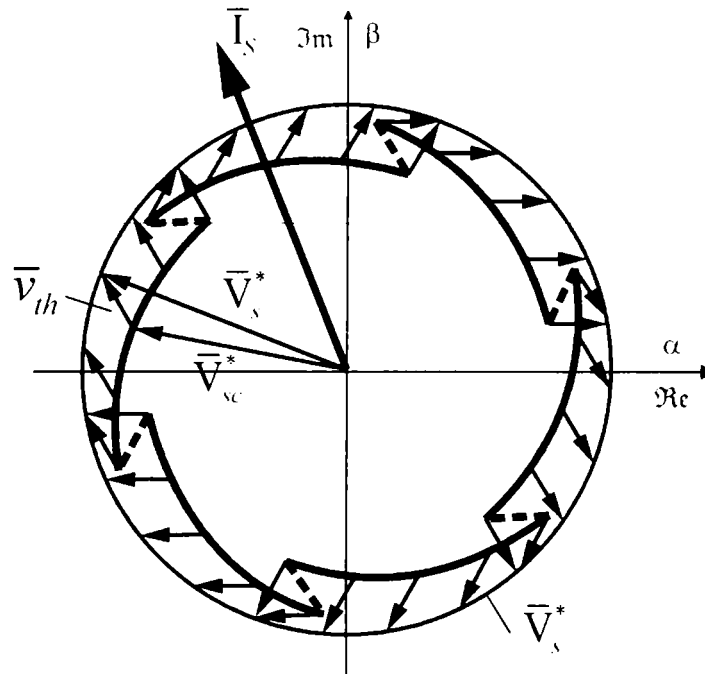


Fig. 3.6 Effect of inverter nonlinearity [33]

Even more, in the case of large current and small voltage motor, the problem discussed above is very important.

The speed reference for the speed controller and for the estimator differs a little. A first order lag PT1 (9) is used to filter the speed reference  $n_{PT1}^*$  for the speed controller, faster than  $n_{fPT1}^*$  applied to estimator, as in Fig. 3.7 for step speed reference  $n_r^*$ .

$$k_{PT1} / (T_{PT1} \cdot s + 1) \quad (3.16)$$

where  $k_{PT1} = 1$  and  $T_{PT1} = 0.018$  for  $n_{PT1}^*$ , and  $k_{fPT1} = 1$  and  $T_{fPT1} = 0.02$  for  $n_{fPT1}^*$ .

The estimator works with electrical rotor speed  $\omega_r$ , and thus the relation with the mechanical speed  $n$  [rpm] is given by:

$$\dot{\omega} = p_1 \cdot \frac{\pi}{60} \cdot \dot{n} \quad (3.17)$$

where  $p_1$  is the number of pole pair.

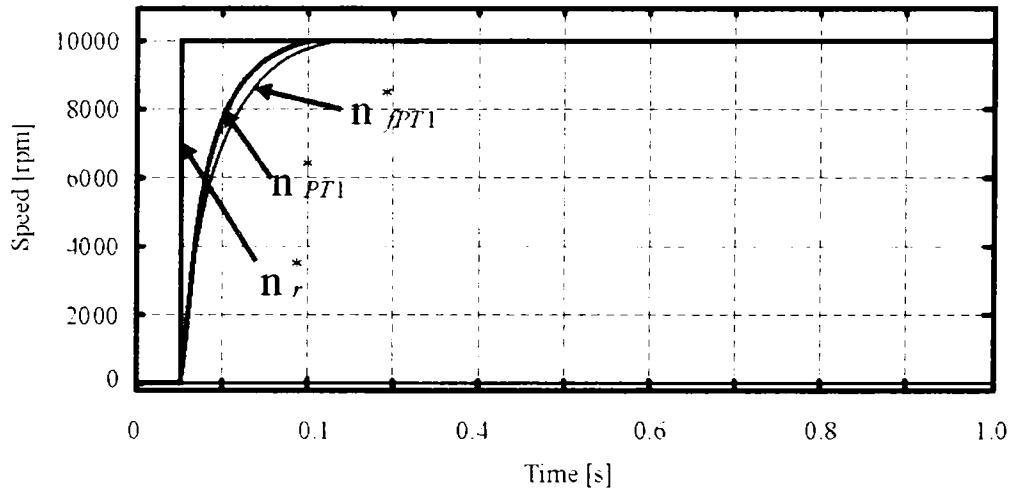


Fig. 3.7 Reference speed prescriptions

### 3.6. Particularity of the Control System

The control system is rather a standard current vector control presented in Fig. 3.2. It consists of two fast current loops on the  $d$  and  $q$  axes, and a not so fast speed loop. The Park operators [37], [38] are used to change  $\alpha\beta$  stator reference frame to  $dq$  rotor reference frame.

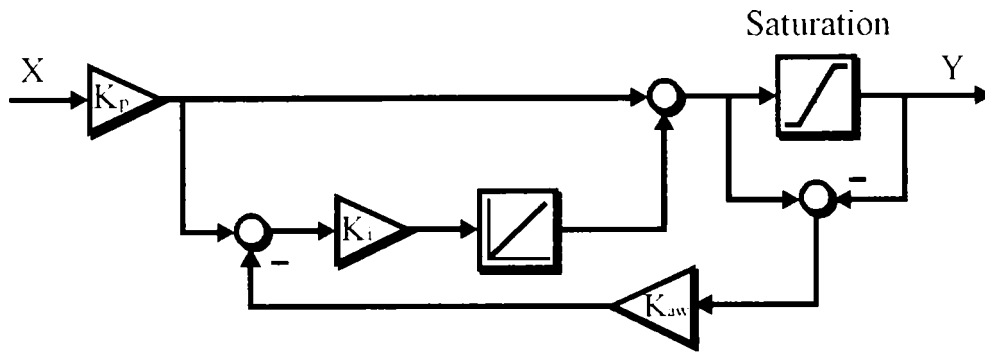


Fig. 3.8 PI controller with anti-windup

Following ideas are added to standard control system:

- a) taking into account the average voltage drop on the semiconductor switching devices (3.14);
- b) using the estimator presented in Fig. 3.3;
- c) using the anti-windup protection for PI controllers [39] (see Fig. 3.8).

The anti-windup strategy uses the saturation block to limit the PI output and to avoid the integrator saturation (Fig. 3.8). The gain  $k_{aw} = 1 \dots 10$  decides the system rapidity to overcome the saturation. The controllers gains used in experiments are given in TABLE 3.1 in Appendix.

### 3.7. Experimental Results

The SPMSM drive system for the laboratory prototype tests consists of two identical 0.8 kW, 20,000 rpm, 4 pole SPMSMs with sinusoidal back-emf mechanically coupled. The data for these motors are presented Chapter 6.

All experimental tests use sensorless control system, thus neither encoder, nor Hall sensors and voltage sensors are used in the control system.

For a good image of how the sensorless control work, three tests considered relevant have been performed, presented in Fig. 3.9, Fig. 3.11 and Fig. 3.16. All the experiments have at least three operating modes, which are representative for high-speed machine with very low electrical time-constant and inertia, in a speed range

from +20,000 rpm to 2,000 rpm (10% from the maximum speed tested) in both positive and negative direction.

### 3.7.1. No Load Start-Up at 10,000 rpm

This experiment consists in a fast acceleration at 10,000 rpm in a very short interval of time (100 ms). During this process the motor is not loaded. The  $I_q$  is soft limited to protect the motor, which develops maximum torque in this operation mode.

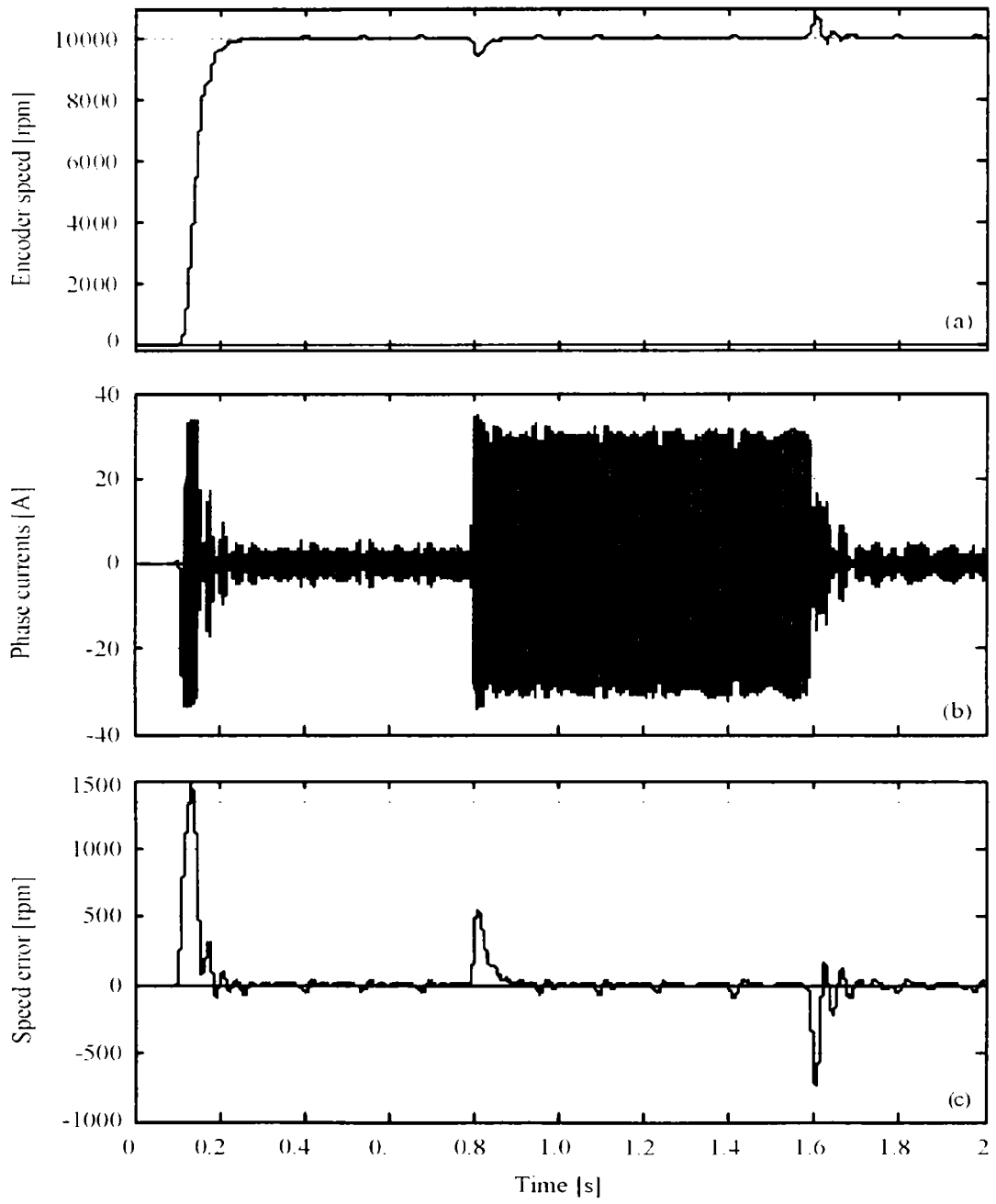
In steady-state operating mode the motor is instantly loaded at 80% rated torque, which represents the maximum value for the load, due to the fact that there is not enough dc voltage in inverter. To operate at maximum torque, the inverter has to be supplied by a voltage given by the value estimated in (3.18):

$$\left. \begin{array}{l} V_{rsmf} \cdot \sqrt{2} = 2/3 \cdot V_{DC}^d \\ V_{rsmf} \cdot \sqrt{3} = V_{rsmI} = 39 \text{ V} \end{array} \right\} \Rightarrow V_{DC}^d = \sqrt{\frac{3}{2}} \cdot 39 = 60 \text{ V} \quad (3.18)$$

Because it is not enough dc voltage in inverter, the motor could be loaded only in the ratio  $V_{DC}/V_{DC}^d = 0.8$  of the rated load.

During experiments, the voltages  $V_d$  and  $V_q$  are not going into limitation, fact that denotes a good dynamic response for flux and torque. The error between the actual angle and the estimated one, does not exceed 0.5 rad during fast transients. It is important to observe that the frequency of error oscillations is accordingly with Fig. 3.4.

It is possible that the machine, which is a synchronous permanent magnet motor with very small inductances and inertia, to be desynchronized if the angle estimator is not good enough. Thus, it is not so important that the estimated angle differs with few percents from the actual one, but is paramount to avoid the failure of the start-up. Due to this fact, it is necessary that the angle error does not exceed 0.5 rad, and for the rest of speed range to be reasonable and relatively constant.



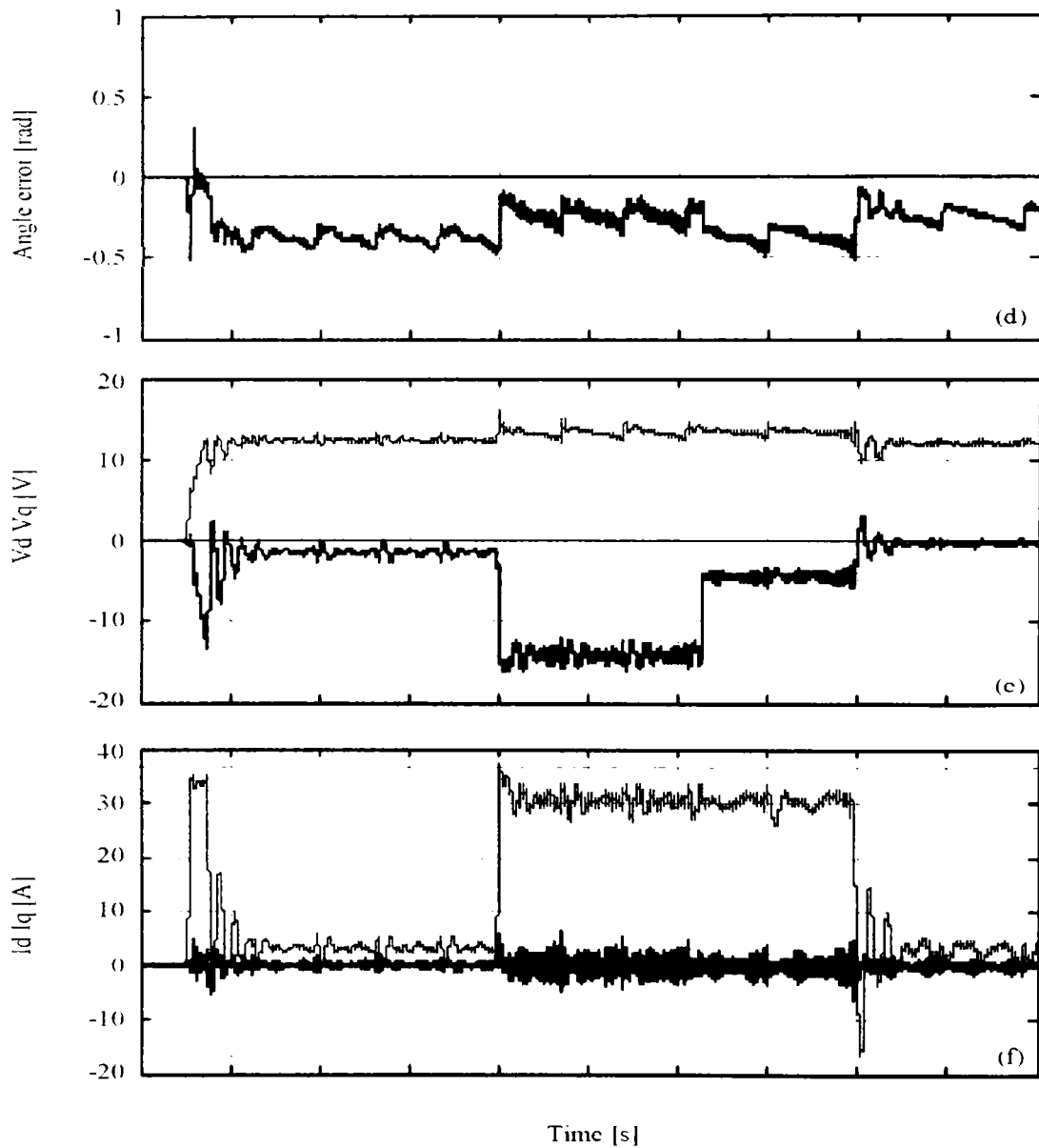


Fig. 3.9 No load start-up at 10,000 rpm followed by loading at 80% of nominal torque at 0.8 s and unloading at 1.6 s:

- a) Encoder speed; b) Three phase currents; c) Speed error between encoder & estimated speed; d) Angle error between encoder & estimated rotor angle;
- e) Voltage vector in rotor reference frame  $V_d$  (thick line) and  $V_q$ ;
- f) Current vector in rotor reference frame  $I_d$  (thick line) and  $I_q$



### 3.7.2. Load Start-Up at -10,000 rpm and Reversal at +10,000 rpm

The system starts up with load proportional to speed from 0 to -10,000 rpm (Fig. 3.11). The  $I_q$  is soft limited to protect the motor. This limitation produces a slower acceleration than before (acceleration process is longer: 0.15 s), but still good. During steady-state at 10,000 rpm, the load is instantly removed at 0.6 s, as it is shown in Fig. 3.11b and thus, slight oscillations in the current waveforms occur in the whole speed-range for both positive and negative directions of motion. This is due to the problems described before in Fig. 3.4 and thus, the spikes occurring in current waveforms, due to transistor commutations, become comparable with the required current value by the control.

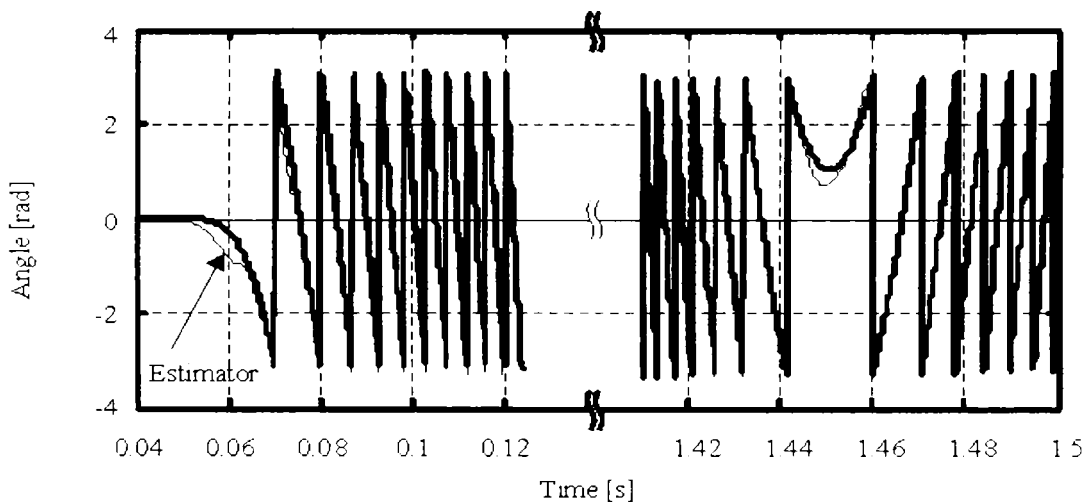
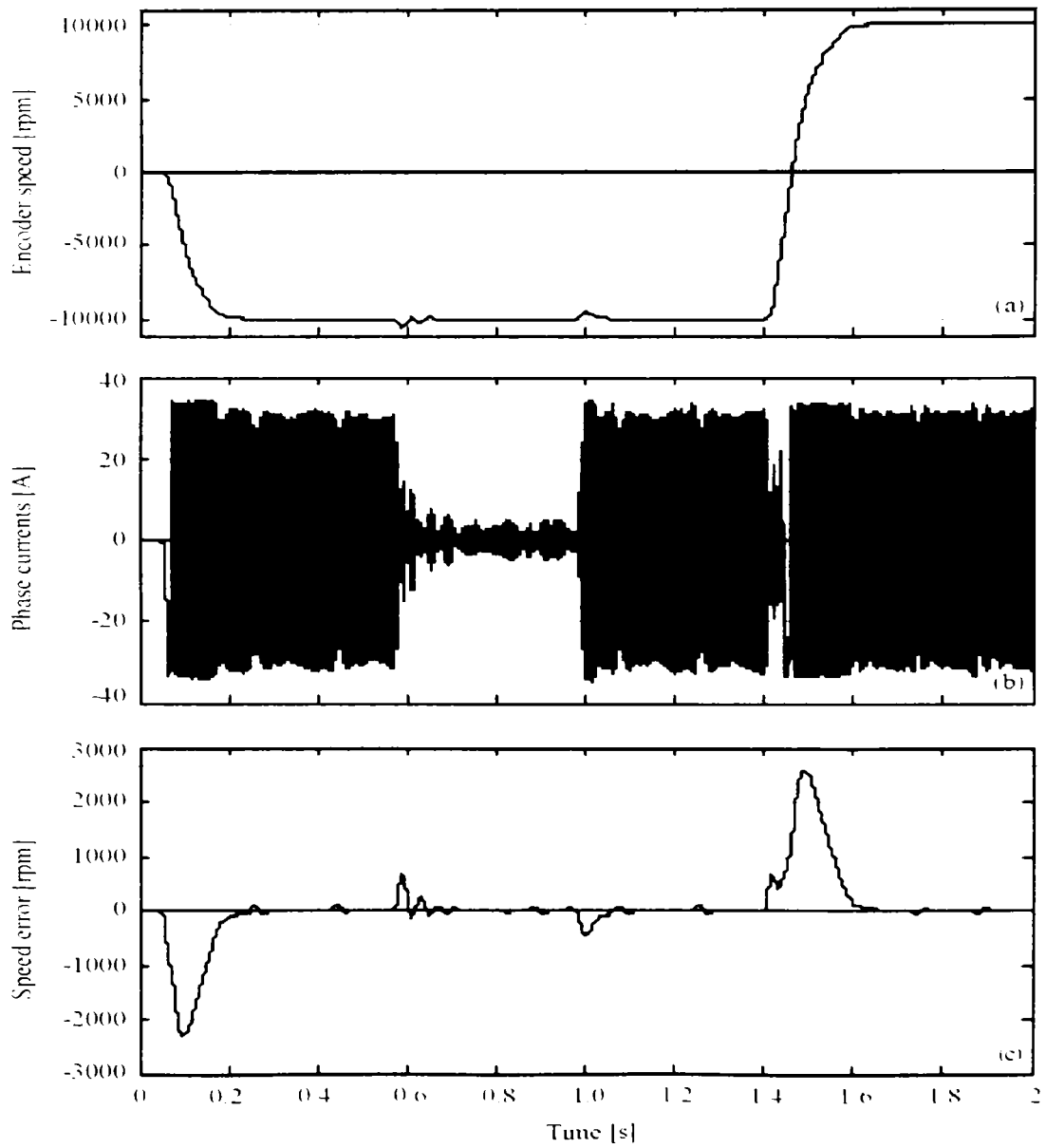


Fig. 3.10 Zoom of encoder and estimated (thin line) angle

The step torque load at 1 s is followed by a speed reversal from -10,000 rpm to +10,000 rpm at 1.4 s. The speed reversal is operated under full load and is achieved in a very short interval of time (smaller than 0.2 s). Fig. 3.10 presents a zoom of the two rotor angles (the actual and the estimated one) during the most critical instants of time: the start-up from 0 to -10,000 rpm and the speed reversal from -10,000 rpm to +10,000 rpm as it is shown in Fig. 3.11. It can be observed how well the estimated rotor angle (thin line) follows the actual one (thick line).

Fig. 3.11c illustrates a large transient speed error (2,500 rpm) at 1.4 s when the speed reversal occurs, and when the sign  $\hat{\omega}$ , changes in the speed estimator (see Fig. 3.3).



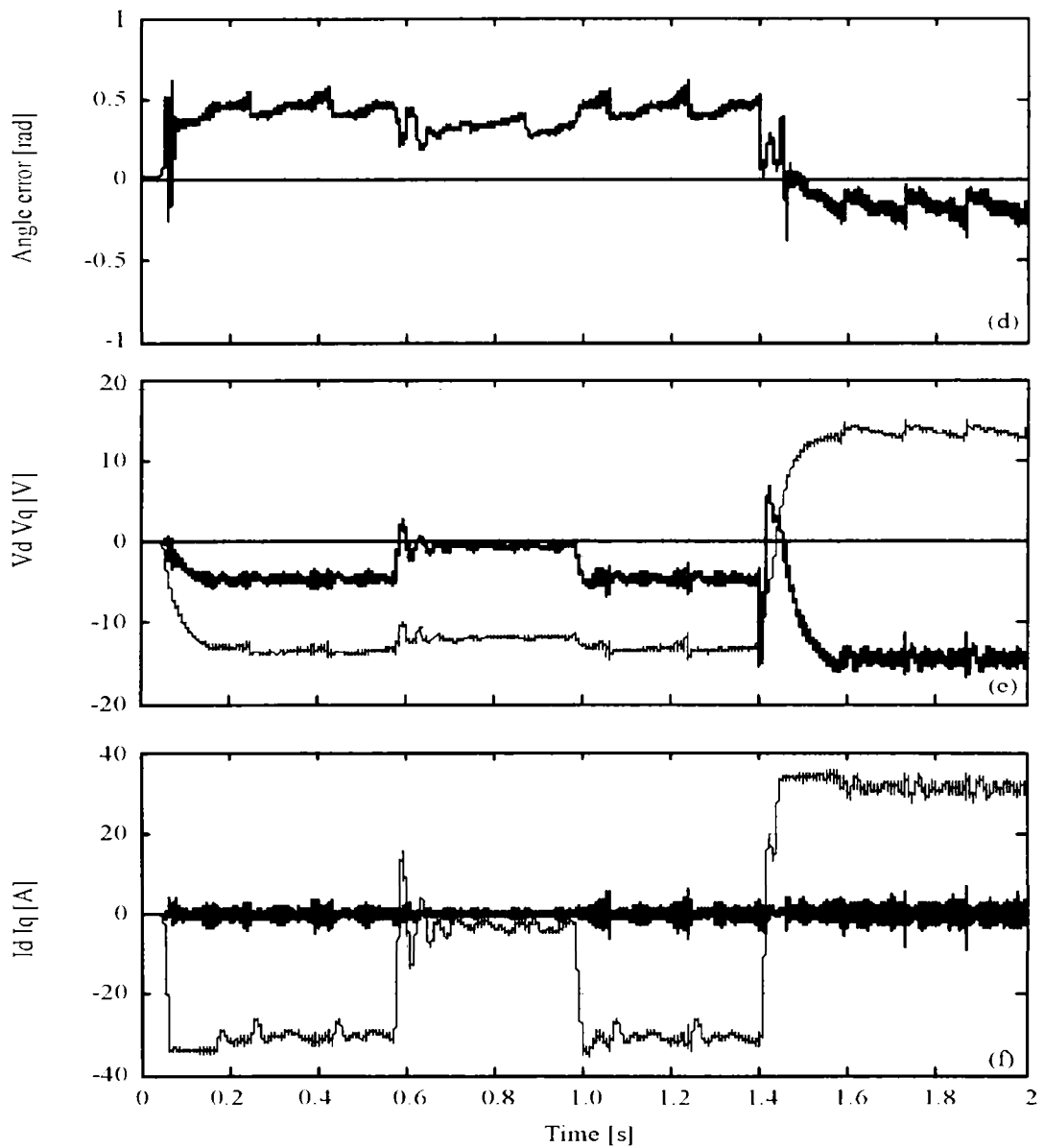


Fig. 3.11 80% loading start-up at -10,000 rpm followed by unloading at 0.6 s, reloading at 80 % of nominal torque at 0.8 s, reverse speed from -10,000 rpm to 10,000 rpm at 1.4 s: a) Encoder speed; b) Three phase currents; c) Speed error between encoder & estimated speed; d) Angle error between encoder & estimated rotor angle; e) Voltage vector in rotor reference frame  $V_d$  (thick line) and  $V_q$ ; f) Current vector in rotor reference frame  $I_d$  (thick line) and  $I_q$

If the motor speed is positive and the sign  $\hat{\omega}_r$  is not already changed in the estimator, then the control is not correct anymore and the protections are turn on (usually the over current protection). To avoid this, a good reference speed  $\omega_{PT1}^*$  (3.16) has to be prescribed to estimator.

### **3.7.3. No Load Start-Up at 15,000 rpm Followed by a Step Torque Load**

The motor was designed for speeds higher than the speed of 10,000 rpm. However, experimental tests at speeds close to its nominal speed are considered sufficient. Firstly, an experimental test at 15,000 rpm is performed. At this speed the motor is loaded at approximately 80% of nominal torque. For loads higher than 80% of nominal torque the available batteries voltage is insufficiently. Thus, after acceleration up to 15,000 rpm, at 0.8 s the motor is loaded at the torque value mentioned above. The acceleration was performed as it was expected under 0.2 s.

Fig. 3.12a illustrates the encoder speed. As it can be seen the encoder speed closely follows the reference speed. The speed error is presented in Fig. 3.12c. One can observe that this speed error is large only during startup than it is between normal values taking into account the motor dynamics.

The three stator currents of the motor are shown in Fig. 3.12a. These currents do not exceed the acceptable values due to the protections provided by the implemented software.

In conclusion, the behavior of the control system is very good, having excellent speed and torque dynamics.

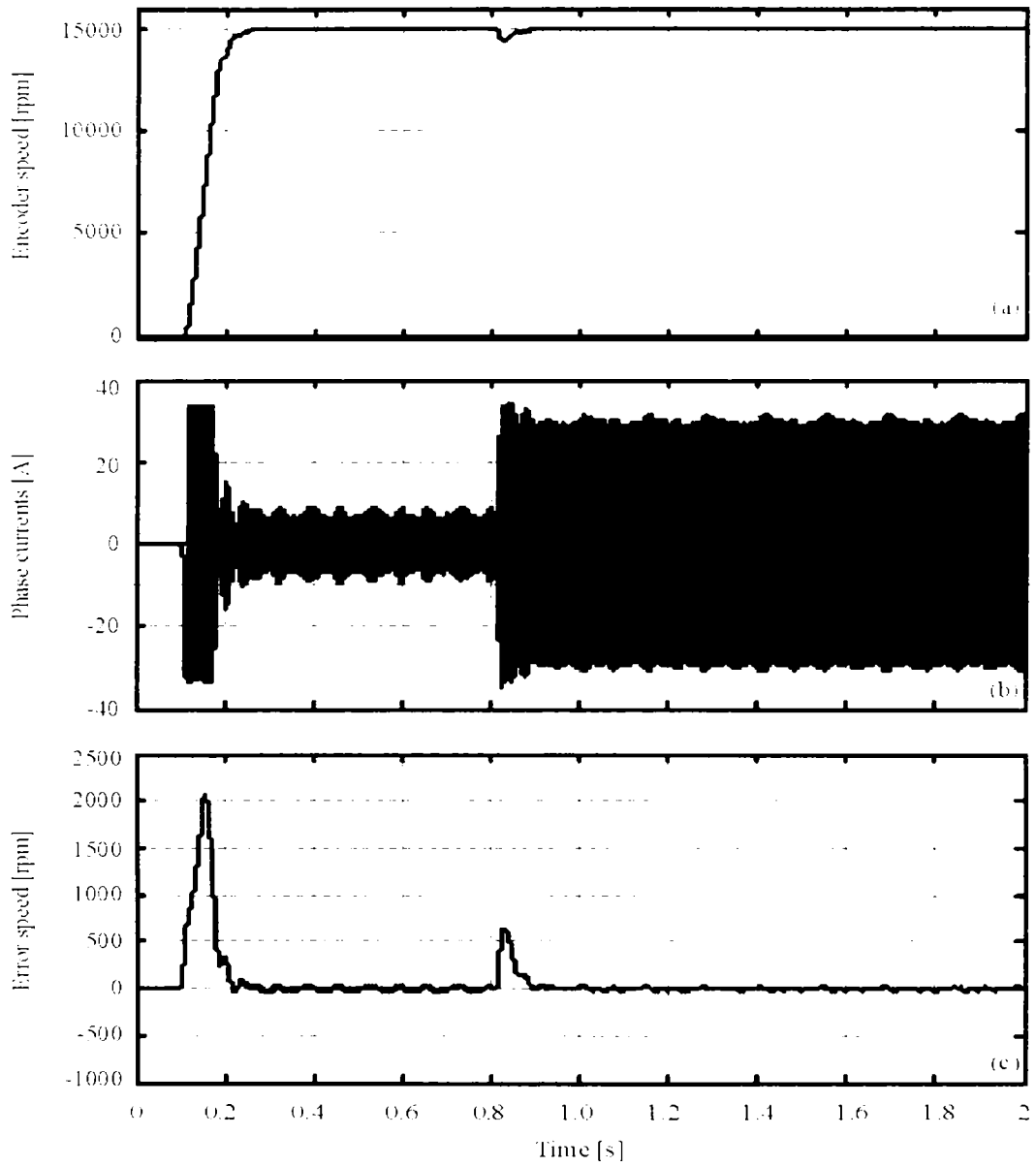


Fig. 3.12 No load start-up at 15,000 rpm followed by a step torque load:

a) Encoder speed; b) Three phase currents; c) Speed error between encoder & required speed;

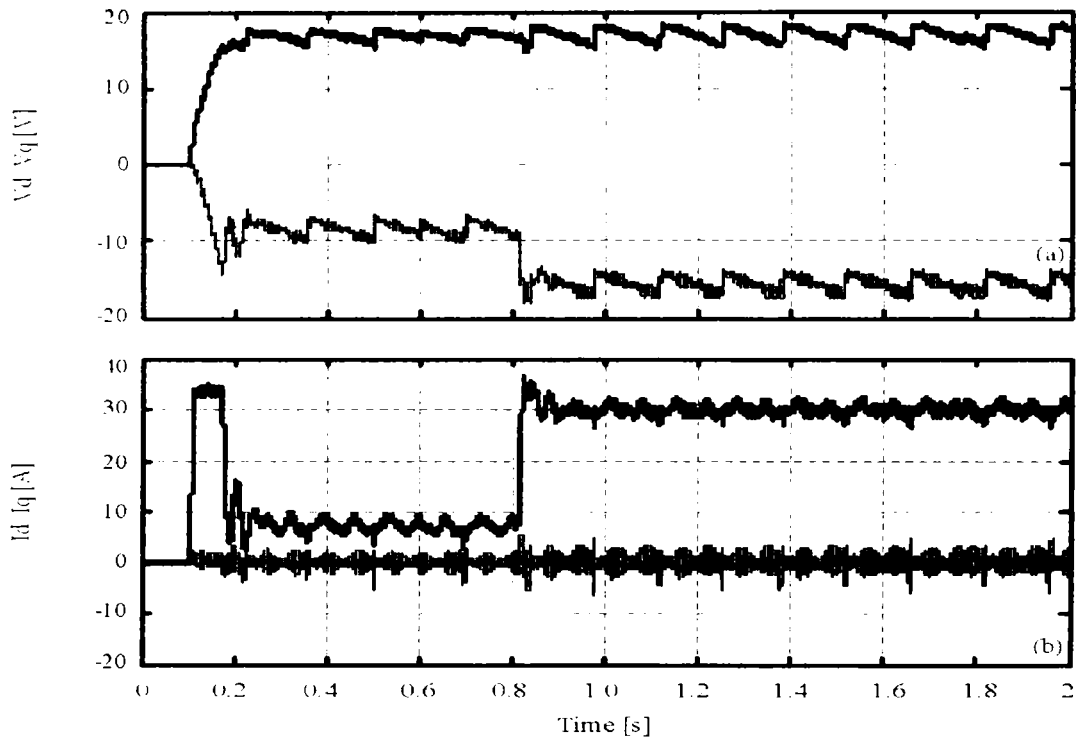


Fig. 3.13 Experiments results during dynamic tests in Fig. 3.12

a) Voltage vector in rotor reference frame  $V_d$  (thick line) and  $V_q$ ; b) Current vector in rotor reference frame  $I_d$  (thick line) and  $I_q$

Fig. 3.13 illustrates the currents and voltages in rotor reference frame. The same oscillations as in the currents waveforms in Fig. 3.12b can be also seen in Fig. 3.13. The  $I_d$  current is maintained zero.

### 3.7.4. No Load Start-Up at 20,000 rpm

As it can be seen from the motor data in Chapter 6 the nominal speed is 20,000 rpm. An experimental test at this speed is considered necessary to be performed. Thus, Fig. 3.14 illustrates a no load startup up to nominal speed. The startup is performed in 0.2 s.

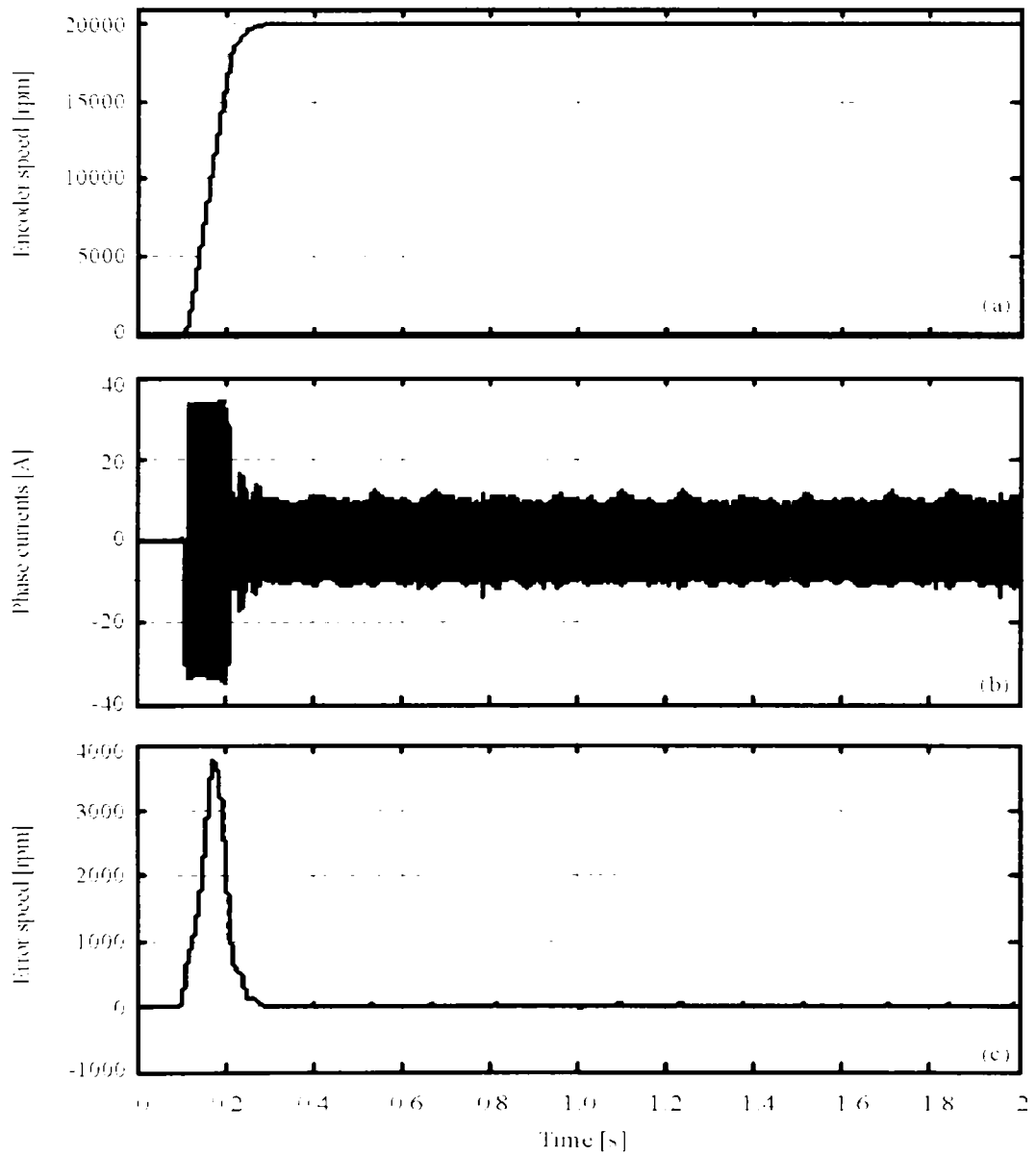


Fig. 3.14 No Load Start-Up at 20,000 rpm:  
a) Encoder speed; b) Three phase currents;  
c) Speed error between encoder & required speed;

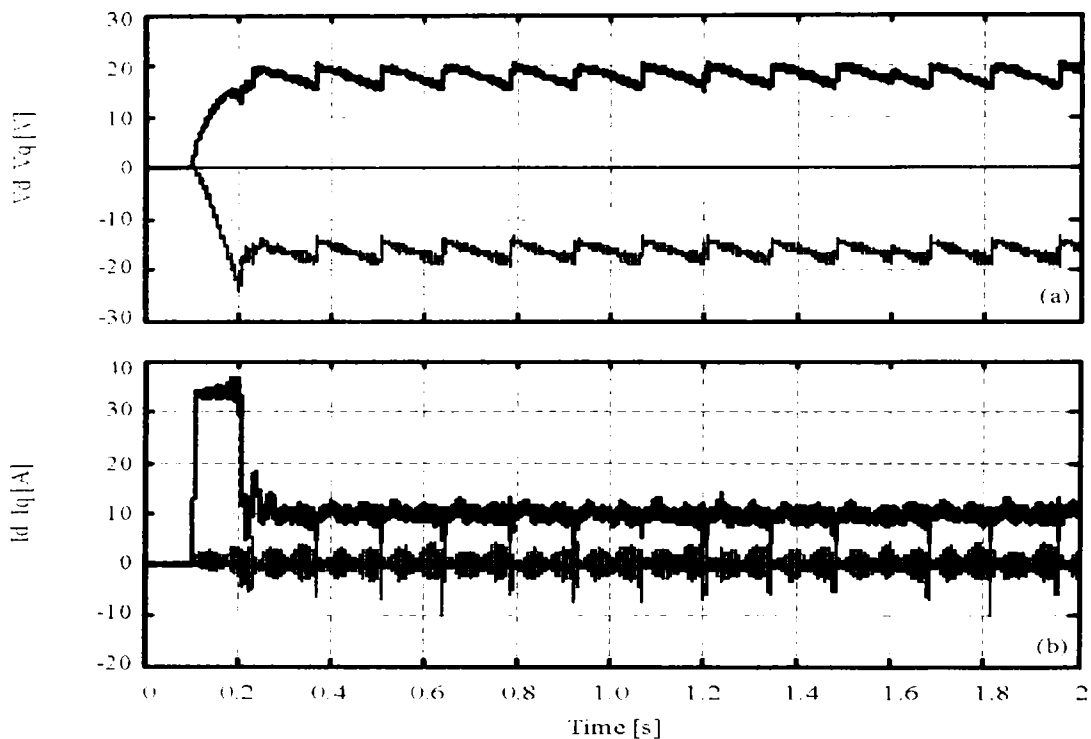


Fig. 3.15 Experiments results during dynamic tests in Fig. 3.14

a) Voltage vector in rotor reference frame  $V_d$  (thick line) and  $V_q$ ;

b) Current vector in rotor reference frame  $I_d$  (thick line) and  $I_q$

As it can be observed, even up to 20,000 rpm, the  $I_d$  current is maintained zero.

The occurred oscillations are repetitive and characteristic to the inverter used by this control. Thus, these oscillations will be present also within the next presented control using the same inverter. Probably an increased frequency of the MOSFET device represents a solution to improve the control and to have no oscillations.

Here again, we mention that the used setup consists of only four batteries and an oversized inverter. Thus, the test results are the best results which can be obtained implementing the control on this setup and using the considered motor.



### **3.7.5. No Load Start-Up at 2,000 rpm and Speed Reversal, Followed by a Step Torque Load**

Even if the motor is designed for high speeds, some applications require for it to operate also at low speeds (although for short time). The operation at low speeds involves small currents. When the currents are small (due to the explanation given before in Fig. 3.4), the control of the sensorless system becomes difficult. Note that it is better to start-up with the motor loaded than unloaded.

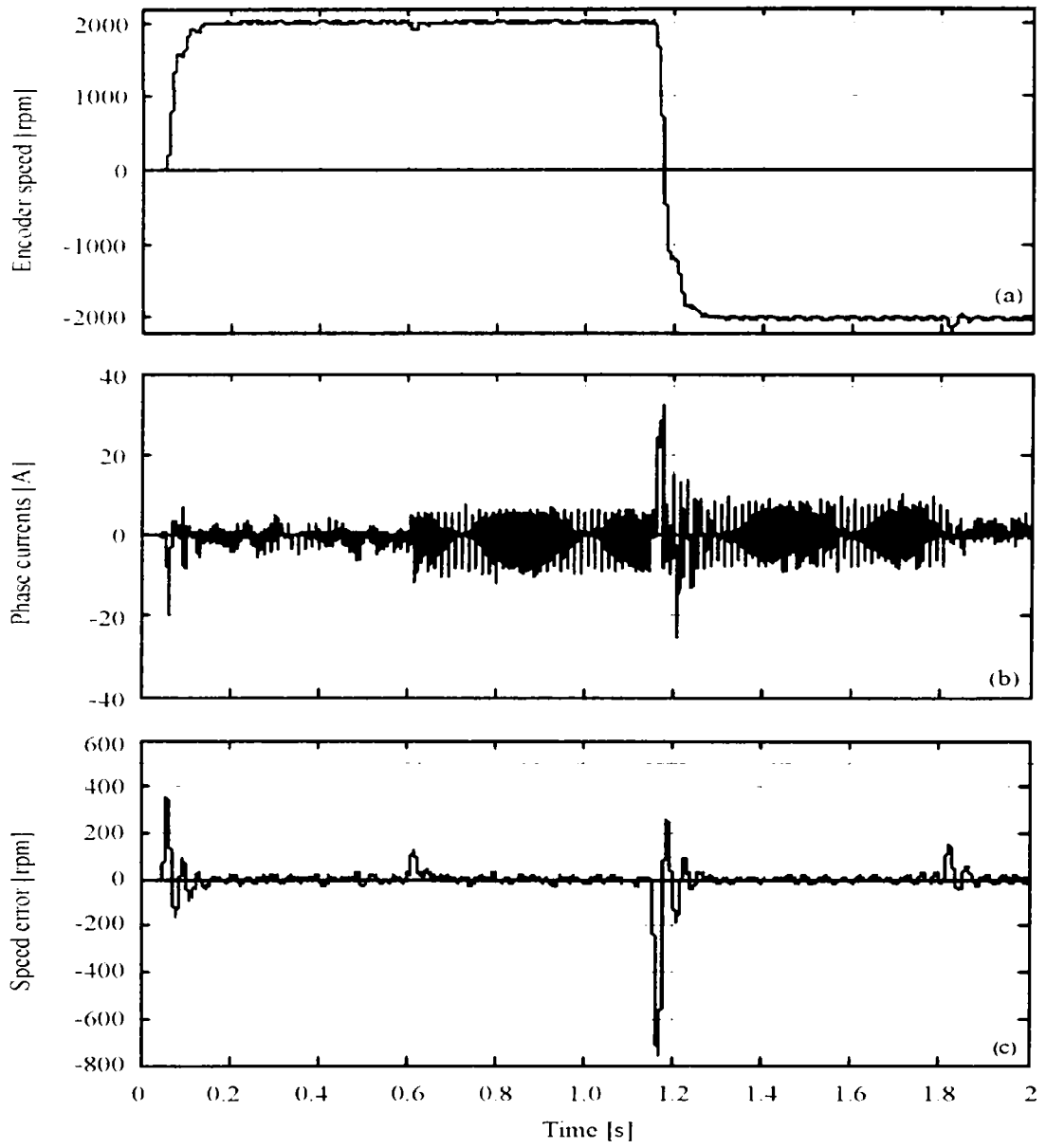
For the motor operating mode, a speed range between 20% and 100% rated speed is acceptable and desired for many high-speed applications. In this context, some experimental tests have been done.

The first event in Fig. 3.16 is acceleration up to 2,000 rpm. Here, it can be observed that the current oscillations are large and this instability is propagated in the whole system. Even if there are large oscillations, the currents are not limited because there is enough reserve in flux and torque. The induced emf is much smaller than that of the rated speed.

At 0.6 s the motor is instantly loaded at 25% rated torque. The reduction in speed to 2,000 rpm implies a reduction in voltage (Fig. 3.16e) and also in power.

At 1.2 s a speed reversal occurs. The speed error during speed transients is pretty large in Fig. 3.16c. The oscillations in the currents and speed waveforms are present also during negative direction of motion.

The final test consists in removing the load at 1.8 s.



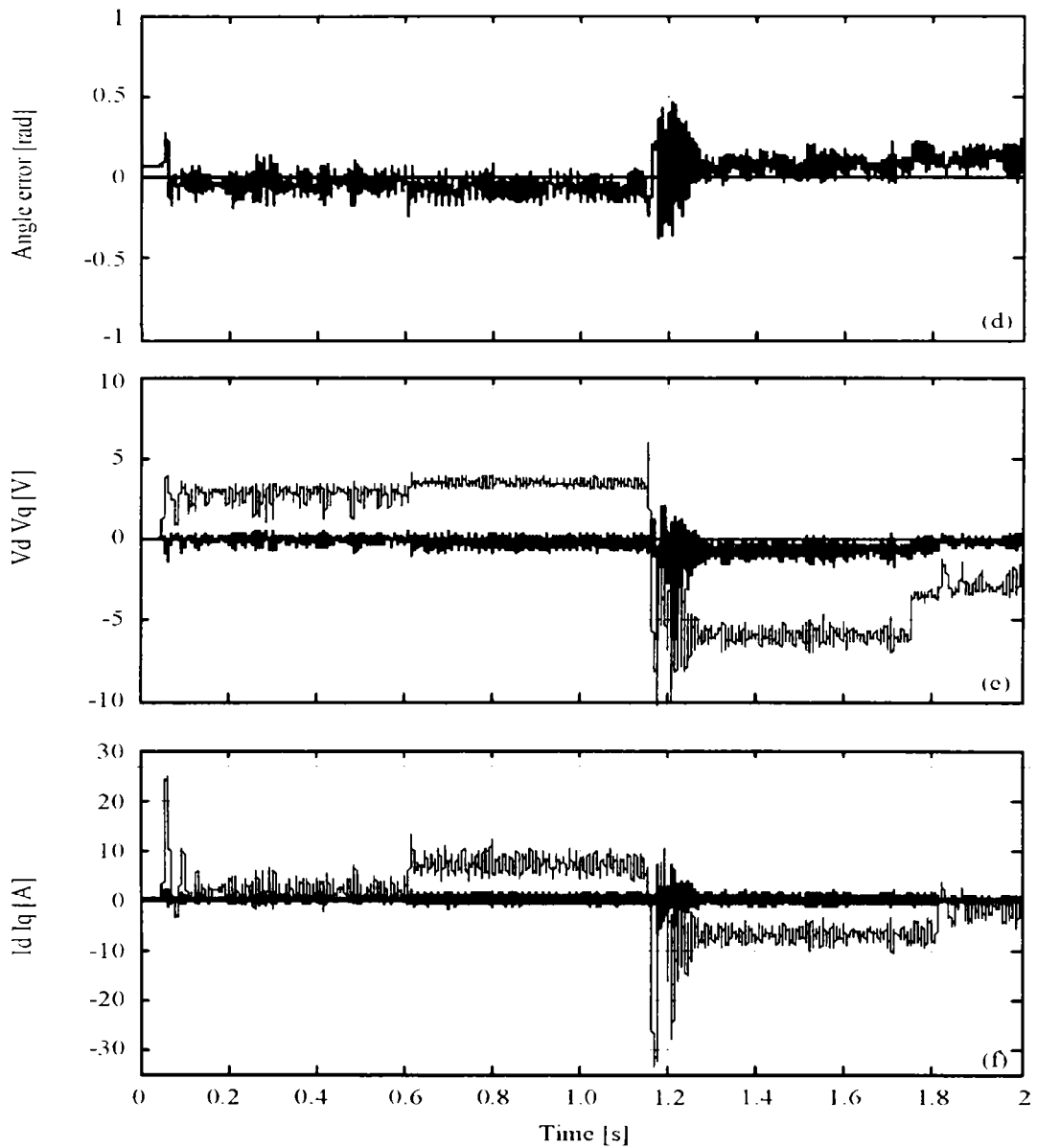


Fig. 3.16 No load start-up at 2,000 rpm, loading at 80% of nominal torque at 0.6 s, reverse speed from 2,000 rpm to -2,000 rpm at 1.2 s:

- a) Encoder speed; b) Three phase currents; c) Speed error between encoder & estimated speed; d) Angle error between encoder & estimated rotor angle;
- e) Voltage vector in rotor reference frame  $V_d$  (thick line) and  $V_q$ ;
- f) Current vector in rotor reference frame  $I_d$  (thick line) and  $I_q$

All these tests demonstrate that the operation in one direction of motion does not differ from the one in the reverse direction. So the control and the estimator are performing well for 5:1 speed range and heavy speed and torque transients.

### 3.8. Conclusion

In the experimental tests, the high-speed, low-voltage SPMSM drive, with very low electrical time-constant and inertia, has operated sensorless through current vector control.

Due to high-speed and small machine inductance and inertia, a fast model-based rotor position and speed estimator was employed.

Using this estimator the results were satisfactory in a relatively large speed range, from 2,000 rpm to 20,000 rpm, in both directions of motion.

The importance of voltage drop compensation of the inverter semiconductor devices was demonstrated, especially at start-up and low speeds.

PI speed and current controllers with anti-windup to avoid control saturation were used.

## Appendix

TABLE 3.1.

GAINS USED IN REAL CONTROL

PI speed control Fig. 3.2	$k_p$	0.05
	$k_i$	40
	$k_{iw}$	5
PI current controllers Fig. 3.2	$k_{p\_dq}$	0.3
	$k_{i\_dq}$	1500
	$k_{iw\_dq}$	5
PLL Fig. 3.3	$k_p$	1
	$k_i$	100
Derivative estimator Fig. 3.3	$\omega_0$	3500

## References

- [1] S. Chi, L. Xu, and Z. Zhang, "Sliding Mode Sensorless Control of PM Synchronous Motor for Direct-Driven Washing Machines", in *Conf. Record of IEEE-IAS 2006*, Tampa, FL, vol. 2, Oct. 2006, pp. 873–879.
- [2] W.L. Soong, G.B. Kliman, R.N. Johnson, R.A. White, and J.E Miller, "Novel High-Speed Induction Motor for a Commercial Centrifugal Compressor", *IEEE Trans. Ind. Appl.*, vol. 36, no. 3, pp. 706–713, May/June 2000.
- [3] A. B. Kulkarni and M. Ehsani, "A Novel Position Sensor Elimination Technique for the Interior Permanent-Magnet Synchronous Motor Drive", *IEEE Trans. Ind. Appl.*, vol. 28, no. 1, pp. 144–150, Jan./Feb. 1992.
- [4] J. S. Kim and S. K. Sul, "New Approach for the Low Speed Operation of PMSM Drives without Rotational Position Sensors", *IEEE Trans. Ind. Elec.*, vol. 11, no. 3, pp. 512–519, May 1996.
- [5] Bon-Ho Bae, Seung-Ki Sul, Jeong-Hyeck Kwon, and Ji-Seob Byeon, "Implementation of Sensorless Vector Control for Super-High-Speed PMSM of Turbo-Compressor", *IEEE Trans. Ind. Appl.*, vol. 39, no. 3, pp. 811–818, May/June 2003.
- [6] Longya Xu and Changjiang Wang, "Implementation and Experimental Implementation of Sensorless Control Schemes for PMSM Drives", *IEEE Trans. Ind. Appl.*, vol. 39, no. 3, pp. 783–791, May-June 2003.
- [7] P.D. Chandana Perera, F. Blaabjerg, J.K. Pedersen, and P. Thogersen, "A Sensorless, Stable V/F Control Method for Permanent-Magnet Synchronous Motor Drives", in *Conf. Record of APEC 2002*.
- [8] T. Halkosaari, "Optimal U/F-Control of High Speed Permanent Magnet Motors", in *Proc. IEEE Industrial Electronics Symposium, ISIE 2006*, vol. 3, July 2006, pp. 2303–2308.
- [9] J. Bumbyet, et al., "Electrical Machines for Use in Electrically Assisted Turbochargers", in *Proc. 2nd International Conf. on Power Electronics Machines and Drives, PEMD 2004*, pp. 344–349.
- [10] Olarescu V., Muşuroi S., "Enhanced Simplified Control Algorithm for Surface Mounted Permanent Magnet with Sinusoidal Excitation", *IPEMC 2004 China*, Vol. 2, pag. 1049-1053

- [11] R. Ancuti, G.-D. Andreescu, and I. Boldea, "Four Rotor Position and Speed Simplified Estimators for Vector Control of High-Speed SPMSM with Test Comparisons", *Journal of Electrical Engineering, JEE*, vol. 7, no. 4, Politehnica Publishing House, Timisoara, 2007 (in press).
- [12] I. Boldea and S.A. Nasar, "Electric Drives", 2nd Edition, Florida: CRC Press, Taylor & Francis, 2005.
- [13] Nakashima S., Inagaki Y., Miki I. "Sensorless Initial Rotor Position Estimation of Surface Permanent-Magnet Synchronous Motor", *IEEE Trans. On Ind. Appl.*, vol. 36, nr.6, Noiembrie/Decembrie, 2000
- [14] Tursini M., Petrella R., Parasiliti F. "Initial Rotor Position Estimation Method for PM Motors", *IEEE Trans. On Power Elec.*, vol. 39, nr.6, Noiembrie/Decembrie, 2003
- [15] Boussak M. "Implementation and Experimental Investigation of Sensorless Speed Control with Initial Rotor Position Estimation for Interior Permanent Magnet Synchronous Motor Drive", *IEEE Trans. On Power Elec.*, vol. 20, nr.6, Noiembrie, 2005
- [16] P. B. Schmidt, M. L. Gaspary, G. Ray, and A. H. Wijenayake, "Initial Rotor Angle Detection of a Nonsalient Pole Permanent Magnet Synchronous Machine", in *Conf. Rec. IEEE-IAS Annu. Meeting*, vol. 1, 1997, pp. 459-463
- [17] Noguchi T., Yamada K., Kondo S., Takahashi I. "Initial Rotor Estimation Method of Sensorless PM Synchronous Motor with No Sensitivity to Armature Resistance", *IEEE Trans. On Ind. Elec.*, vol. 45, nr.1, Februarie, 1998
- [18] Haque Md. E., Zhong L., Rahman M. F., "A Sensorless Initial Rotor Position Estimation Scheme for a Direct Torque Controlled Interior Permanent Magnet Synchronous Motor Drive", *IEEE Trans. On Power Elec.*, vol. 18, nr.6, Noiembrie, 2003
- [19] S. Kondo, A. Takahashi, and T. Nishida, "Armature Current Locus-Based Estimation Method of Rotor Position of Permanent Magnet Synchronous Motor without Mechanical Sensor", in *Conf. Rec. IEEE-IAS Annu. Meeting*, vol. 1, 1995, pp. 55-60
- [20] J.-I. Ha, K. Ide, T. Sawa, and S. Sul, "Sensorless Position Control and Initial Position Estimation of an Interior Permanent Magnet Motor", in *Conf. Rec. IEEE-IAS Annu. Meeting*, Chicago, IL, Sept./Oct. 2001, pp. 2607-2613.

- 
- [21] Y. Jeong, R. D. Lorenz, T. M. Jahns, and S. Sul, "Initial Rotor Position Estimation of an Interior Permanent Magnet Synchronous Machine Using Carrier-Frequency Injection Methods", in *Proc. IEEE IEMDC*, June 2003, pp. 1218–1223.
- [22] K. Tanaka, T. Yuzawa, R. Moriyama, and I. Miki, "Initial Rotor Position Estimation for Surface Permanent Magnet Synchronous Motor", in *Conf. Rec. IEEE-IAS Annu. Meeting*, Chicago, IL, Sept./Oct. 2001, pp. 2592–2597.
- [23] F. Philippen, "Position Estimation in PM Synchronous Machines Using Single Saliency-Tracking, Self-Sensing Methods", M.S. & Diplomarbeit thesis, Univ. Wisconsin, Madison, and Tech. Univ. Aachen, Germany, 1998.
- [24] S. Shinnaka, "New "Mirror-Phase Vector Control" for Sensorless Drive of Permanent-Magnet Synchronous Motor with Pole Saliency", *IEEE Trans. Ind. Appl.*, vol. 40, no. 2, pp. 599–606, Mar./Apr. 2004.
- [25] J. Holtz, "Initial Rotor Polarity Detection and Sensorless Control of PM Synchronous Machines", in *Conf. Rec. IEEE-IAS 2006 Annu. Meeting*, Tampa, FL, vol. 4, Oct. 2006, pp. 2040–2047.
- [26] D.-W. Chung, J.-K. Kang, and S. Sul, "Initial Rotor Position Detection of PMSM at Standstill Without Rotational Transducer", in *Proc. IEEE IEMDC*, May 1999, pp. 785–787.
- [27] P. L. Jansen, M. Corley, and R. D. Lorenz, "Flux, Position, and Velocity Estimation in AC Machines at Zero and Low Speed Via Tracking of High Frequency Saliencies", in *Proc. EPE Conf.*, 1995, pp. 154–160.
- [28] T. Takeshita and N. Matsui, "Sensorless Control and Initial Position Estimation of Salient-Pole Brushless DC Motor", in *Proc. Advanced Motion Control Workshop*, 1996, pp.18–23.
- [29] M. Corley and R. D. Lorenz, "Rotor Position and Velocity Estimation for a Permanent Magnet Synchronous Machine at Standstill and High Speeds", *IEEE Trans. Ind. Applicat.*, vol. 34, pp. 784–789, July/Aug. 1998.
- [30] M. Schroedl, "Sensorless Control of Ac Machines at Low Speed and Standstill Based on The "INFORM" Method", in *Conf. Rec. IEEE-IAS Annu. Meeting*, Oct. 6–10, 1996, pp. 270–277.

- [31] A. Consoli, G. Scarcella, and A. Testa, "Sensorless Control of PM Synchronous Motors at Zero Speed", in *Conf. Rec. IEEE-IAS Annu. Meeting*, Phoenix, AZ, Oct. 1999, pp. 1033–1040.
- [32] J. Holtz and J. Quan, "Sensorless Vector Control of Induction Motors at Very Low Speed Using a Nonlinear Inverter Model and Parameter Identification", *IEEE Trans. Ind. Appl.*, vol. 38, no. 4, pp. 1087–1095, July-Aug. 2002.
- [33] J. Holtz and J. Quan, "Drift- and Parameter-Compensated Flux Estimator for Persistent Zero-Stator-Frequency Operation of Sensorless-Controlled Induction Motors", *IEEE Trans. Ind. Appl.*, vol. 39, no. 4, pp. 1052–1060, July/Aug. 2003.
- [34] Th. Frenzke, F. Hoffman, and H.G. Langer, "Speed Sensorless Control of Traction Drives - Experiences on Vehicles", in *CD-ROM Proc. 8th European Conf. on Power Electronics and Applications, EPE '99*, Lausanne, Switzerland, 1999.
- [35] Schmirgel H., Krahn J. O. "Compensation of Nonlinearities in The IGBT Power Stage of Servo Amplifiers Through Feed Forward Control in The Current Loop", PCIM Europe, 2005
- [36] Munoz-Garcia A., Lipo T. A. "On-Line Dead Time Compensation Technique for Open-Loop PWM-VSI Drives", Research Report, 1998
- [37] D. W. Novotny and T. A. Lipo, "d, q Modeling of Induction and Synchronous Machines, in *Vector Control and Dynamics of AC Drives*", ch. 2, Oxford Univ. Press, London, U.K., 1998
- [38] P.P. Cruz, J.M. Aquino, and M.R. Elizondo, "Vector Control Using ANFIS Controller with Space Vector Modulation - Induction Motor Drive Applications", in *Proc. 39th International Universities Power Engineering Conf., UPEC 2004*, vol. 2, Sept. 2004, pp. 545–549.
- [39] G.D. Andreescu, "Nonlinear Observer for Position and Speed Sensorless Control of Permanent Magnet Synchronous Motor Drives", in *Proc. 6th International Conf. on Optimization of Electrical and Electronic Equipments, OPTIM '98*, vol. 2, May 1998, pp. 473–478.
- [40] G.D. Andreescu, "Estimatoare in Sisteme de Conducere a Actionarilor Electrice - Aplicatii la MSMP (Estimators in Control of Electric Drives - Applications to MSMP)", Editura Orizonturi Universitare, Timisoara, 1999.



- [41] J.G. Ziegler and N.B. Nichols, "Optimum Settings for Automatic Controllers", *Trans. of American Society of Mechanical Engineers (ASME)*, vol. 64, pp. 759–765, Nov. 1942.
- [42] Z. Chen, M. Tomita, S. Doki, and S. Okuma, "An Extended Electromotive Force Model for Sensorless Control of Interior Permanent Magnet Synchronous Motors", *IEEE Trans. Ind. Electron.*, vol. 50, no. 2, pp. 288–295, Apr. 2003
- [43] S. Morimoto, K. Kawamoto, M. Sanada, and Y. Takeda, "Sensorless Control Strategy for Salient Pole PMSM Based on Extended EMF in Rotating Reference Frame", *IEEE Trans. Ind. Appl.*, vol. 38, no. 4, pp. 1054–1061, Jul./Aug. 2002.

# Chapter 4

## Sensorless V/f Control of Surface PMSM with stabilizing loops – basics and simulation results

### Abstract

This chapter introduces a novel set of two stabilizing loops to correct the voltage amplitude and phase in V/f control of SPMSM. The proposed method is used to improve standard V/f control and is believed to be from the point of view of online computation, notably less time as compared to vector control as demonstrated by rather extensive comparisons of digital simulations for three alternative existing methods.

### 4.1. Introduction

Super high speed (above 30,000 rpm) drives control is hampered by the shortness of the online computation cycle and by the limited switching frequency in IGBT power converters. This is why, besides motion sensorless vector control – which anyway implies a starting sequence in rotor coordinates [1], V/f and I-f control with stabilizing loop has been proposed [2] to [4] for PMSM drives.

Speed observer with stabilizing loops is presented in [5].

In essence, open loop V/f control with d.c. link current pulsation driven correction of the reference frequency (speed) is successfully proven up to 200 rad/s in [3].

V/f control with frequency and voltage correction based on active current respectively reactive current (with efficiency optimization) is introduced in [4] and is used to calculate a V(f) on the base of fourth order polynomial equation.

Finally, [7] and [8] demonstrate the possibility to reach 45,000 rpm and respectively, 120,000 rpm in a brushless d.c. control, with startup sequence, by d.c. link voltage control via a chopper. The PWM converter is used only to commutate the phase sequences. For higher speed (120,000 rpm) we feel that sinusoidal

current control is needed to reduce both stator core and rotor losses, which tend to be too high for rectangular current control (see Fig. 10 of [6], on rotor temperature).

Dynamic current compensation has also been attached to V/f control at moderate speeds [6]. The present chapter uses digital simulations to assess some of the above mentioned methods up to 80,000 rpm and, in parallel, to propose a dual stability loop based on stator flux and power angle (stator flux, stator current control).

The proposed solutions are documented through digital simulations and compared with three existing solutions of lower and respectively higher complexity (vector control) and proved to perform almost as well as the more complex one.

## 4.2. V/f control with flux and power angle stabilizing loops

This paragraph deals with the comparisons between some control techniques existing in the literature and a novel proposed control. The simulations are performed on a motor model whose parameters are given in TABLE 4.1. The task of simulations is to develop a control system which can damp almost totally the oscillations

The  $dq$  model of the surface PMSM in rotor reference frame is presented in Chapter 2.

Based on this standard model the SPMSM [11] can be driven with standard V/f control scheme as shown in Fig. 4.1. This scheme can be used to achieve speed control in applications like pumps or fans where fast dynamic torque response is not needed.

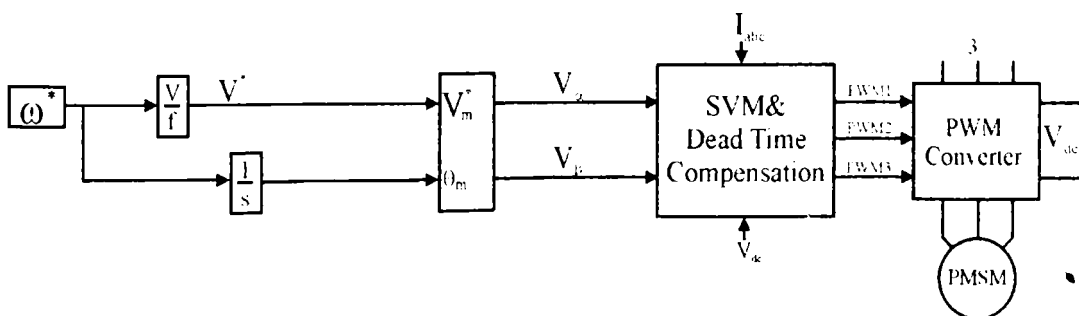


Fig. 4.1 Standard V/f control

This control system Fig. 4.1 does not allow the damping of the torque and speed ripples which mean an important deficiency. These inconveniences can be removed if PMSMs have a rotor with cage windings but this supposes supplementary costs and losses [1].

The solution shown in Fig. 4.2 [3] uses a stabilizing loop which depends on the d.c.-link power or current perturbations. The correction is performed by analyzing the variation of the inverter d.c. link or of the active power variation.

This solution works up to 200 rad/s but apparently does not work as well as it works at very high speeds as shown latter in this chapter.

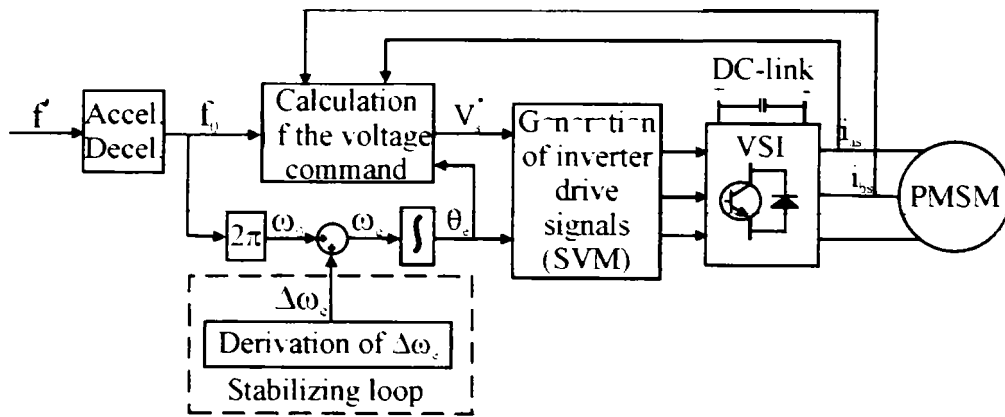


Fig. 4.2 V/f control with stabilizing loop [3]

Our solution, proposed here, corrects these deficiencies. The block diagram is shown in Fig. 4.3. This control scheme add to the standard V/f control two kinds of different loops: flux (voltage amplitude) and power angle regulators.

The flux observer is very simple and can be achieved from stator voltage and currents with a PI compensator to eliminate the input d.c. offset.

$$\begin{aligned} \bar{\lambda}_s &= \int (\bar{V}_s - \bar{I}_s R_s - \bar{U}_{comp}) dt \\ \bar{U}_{comp} &= (k_p + \frac{k_i}{s}) \bar{\lambda}_s \end{aligned} \tag{4.1}$$

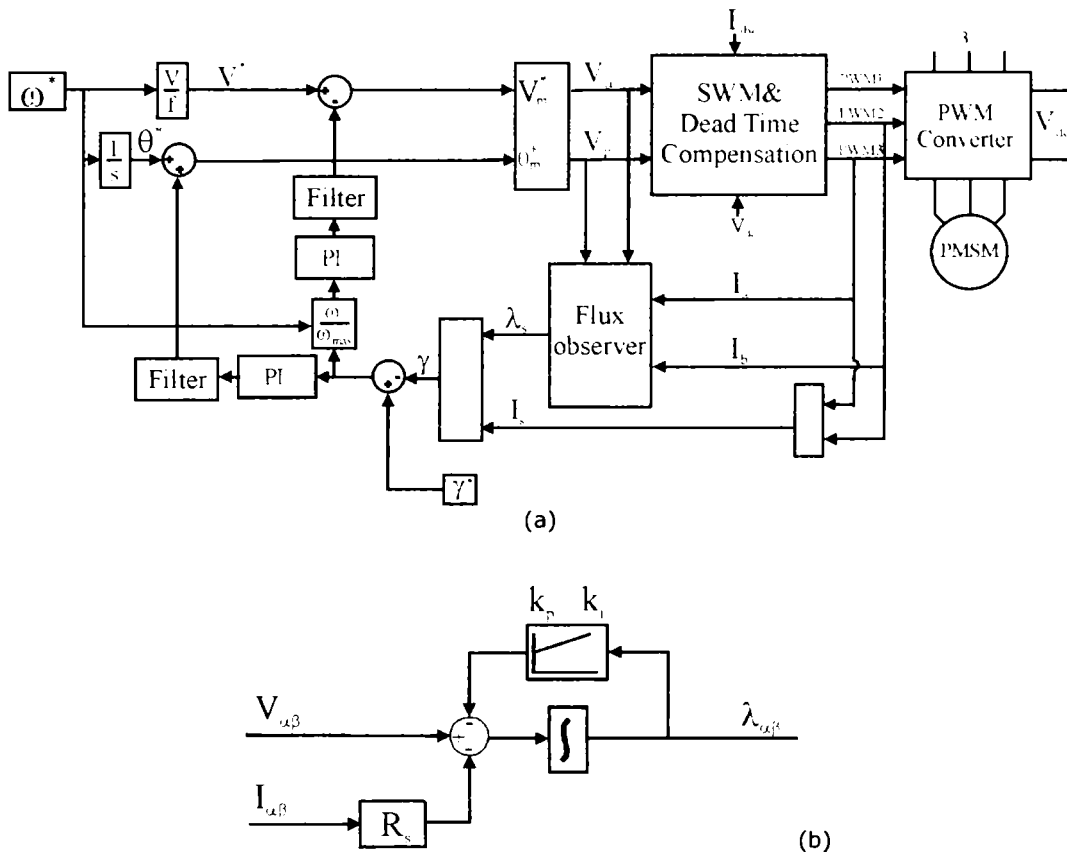


Fig. 4.3 V/f control with flux and power - angle stabilizing loops (a) with flux observer (b)

The angle between stator flux and stator current reference  $\gamma^*$  (Fig. 4.4) is used as a constant both during acceleration (start-up) and steady state. The actual angle between stator flux and stator current  $\gamma$ , called also the power angle, is obtained from a flux observer with the measured stator current  $I_{\alpha\beta}$  and the estimated stator flux  $\lambda_{\alpha\beta}$  in stator coordinates (Fig. 4.5).

The method principle consists of the stator flux  $\bar{\lambda}_s$  estimation (see Fig. 4.3b) and the stator current  $\bar{I}_s$  computation through two current sensors. The angle  $\gamma$  between the two above mentioned vectors can also be computed.

The angle  $\gamma$  should be greater than  $60^\circ$ . The error between the desired and the real angle is introduced in two PI regulators as in Fig. 4.3. It has to be noticed that the correction on the amplitude voltage loop is an adaptive one proportional with motor speed.

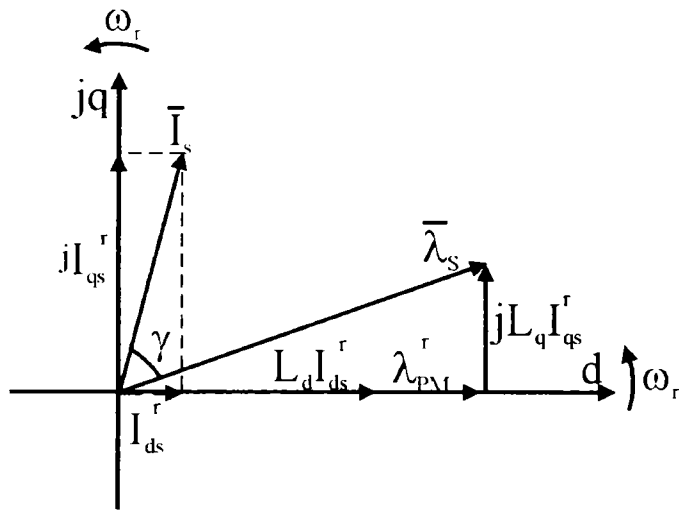


Fig. 4.4 Stator flux linkage and current vector in rotor reference frame

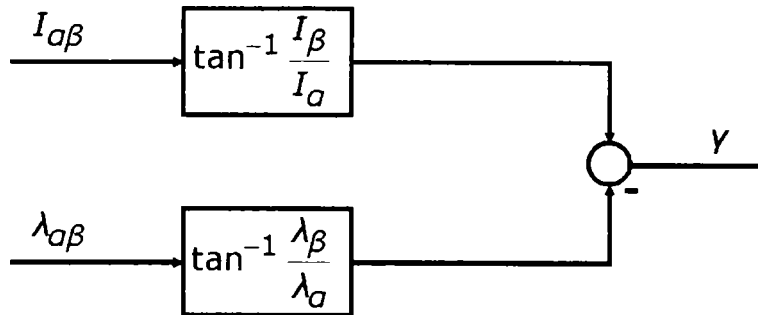


Fig. 4.5  $\gamma$  angle computation

$$\gamma = \tan^{-1} \frac{I_\beta}{I_\alpha} - \tan^{-1} \frac{\lambda_\beta}{\lambda_\alpha} \tag{4.2}$$

The reference value of the voltage  $V^*$  is limited to 75% of the nominal voltage of the inverter. The voltage is increased or decreased by the power angle loop feedback with up to +/- 25% of the nominal voltage which will lead to speed oscillations compensation. The power angle  $\gamma$  is corrected by the two PI regulators, having as outputs  $\Delta V$  and  $\Delta \theta$  and working together full time at any speed.

The flux voltage based observer is shown in Fig. 4.3b, and it is good enough at high speeds.

The coefficients of the flux observer controller are  $k_p=20$  and  $k_i=10$ . The coefficients on the correction loop of the voltage amplitude  $\Delta V$  are  $k_p=2$  and  $k_i=10$  and the ones on the correction loop of the voltage phase  $\Delta\theta$  are  $k_p=4$  and  $k_i=15$ .

The configuration in Fig. 4.3 is from the point of view of online computation notably less intensive as compared to vector control in existing implementation (Fig. 4.6) of approximately equivalent performance. The benefits of our method are related also to the elimination of two coordinate changers (Fig. 4.6), and their incumbent errors in delay time and rotor position [9].

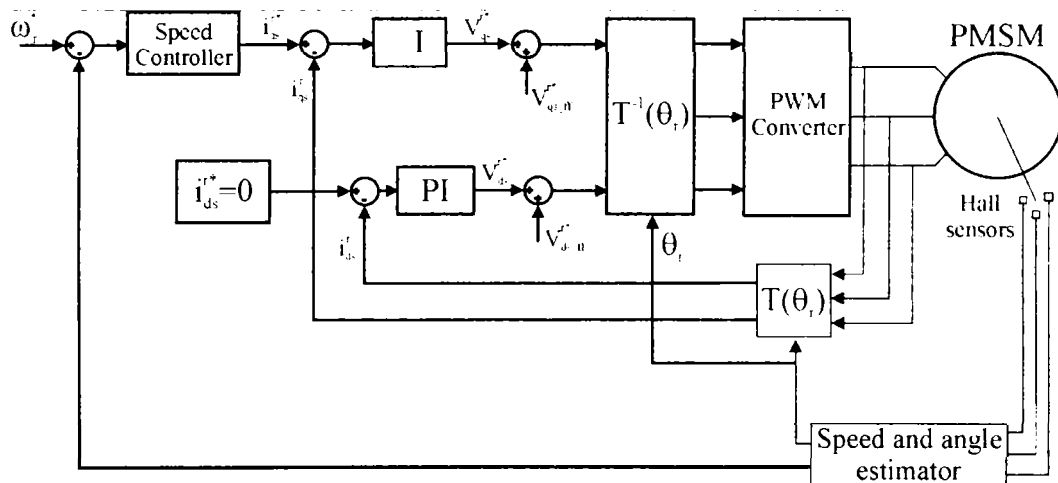


Fig. 4.6 PMSM – vector control scheme with three discrete Halls-effect sensors

### 4.3. Digital simulations results

Digital system simulations have been processed in Matlab Simulink for an easy translation into the dSpace. The motor data are given in the Appendix at the end of this chapter. Fig. 4.7 and Fig. 4.8 illustrate the performance of two existing solutions: classical V/f control and V/f control with d.c. link current (or power) oscillations correction loop. In V/f control the speed oscillations increase with load as no damping is provided but in the second case the speed oscillations decrease under similar circumstances. First, the speed is ramped to 80,000 rpm and V/f open loop

control was applied (Fig. 4.7) with a step load torque applied at  $t=12$  sec. The machine remains in synchronism, by this meaning that it oscillates around the designated speed with 100 rpm at 0.1 Nm torque load and with 300 rpm at 0.4 Nm load torque.

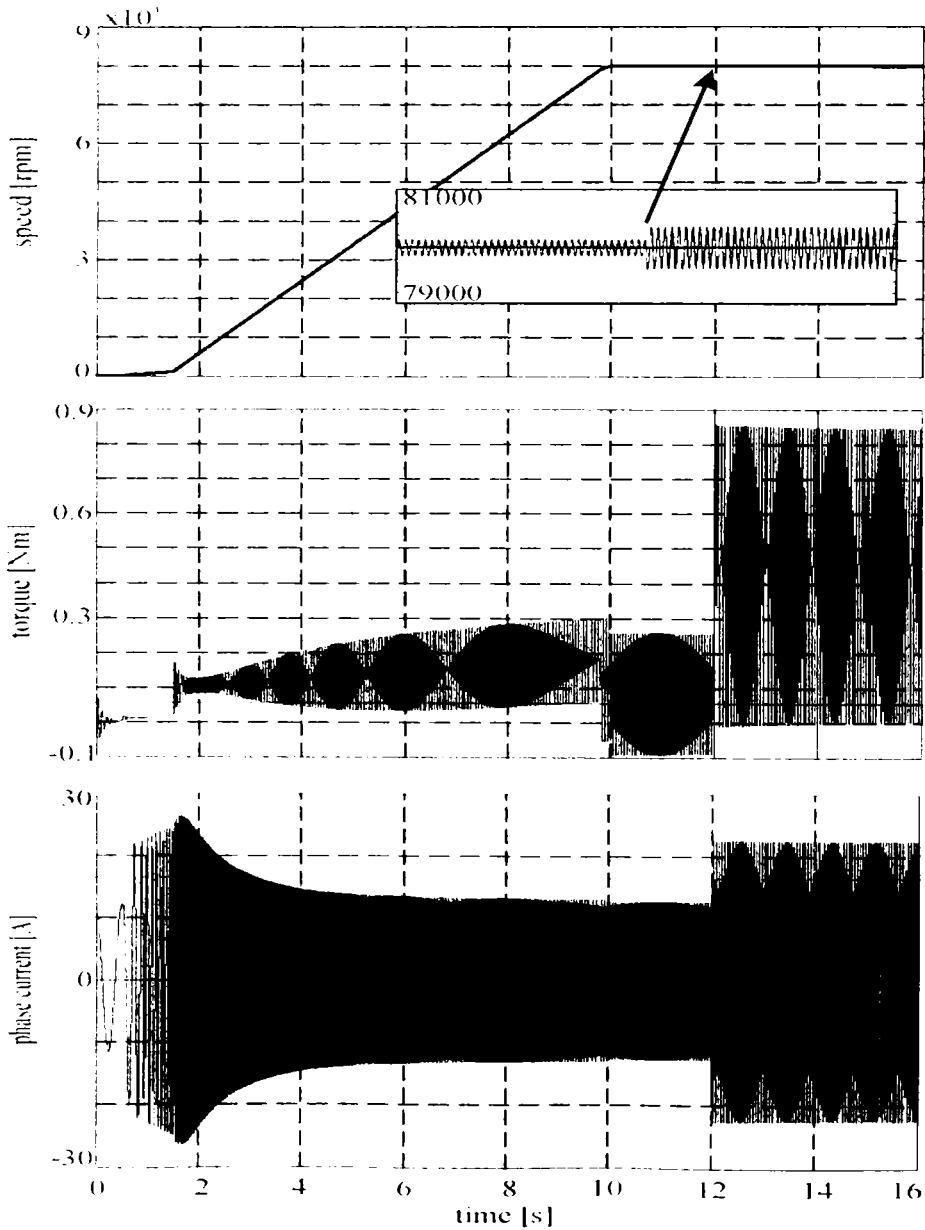


Fig. 4.7 PMSM Classical V/f control without any stabilization loop



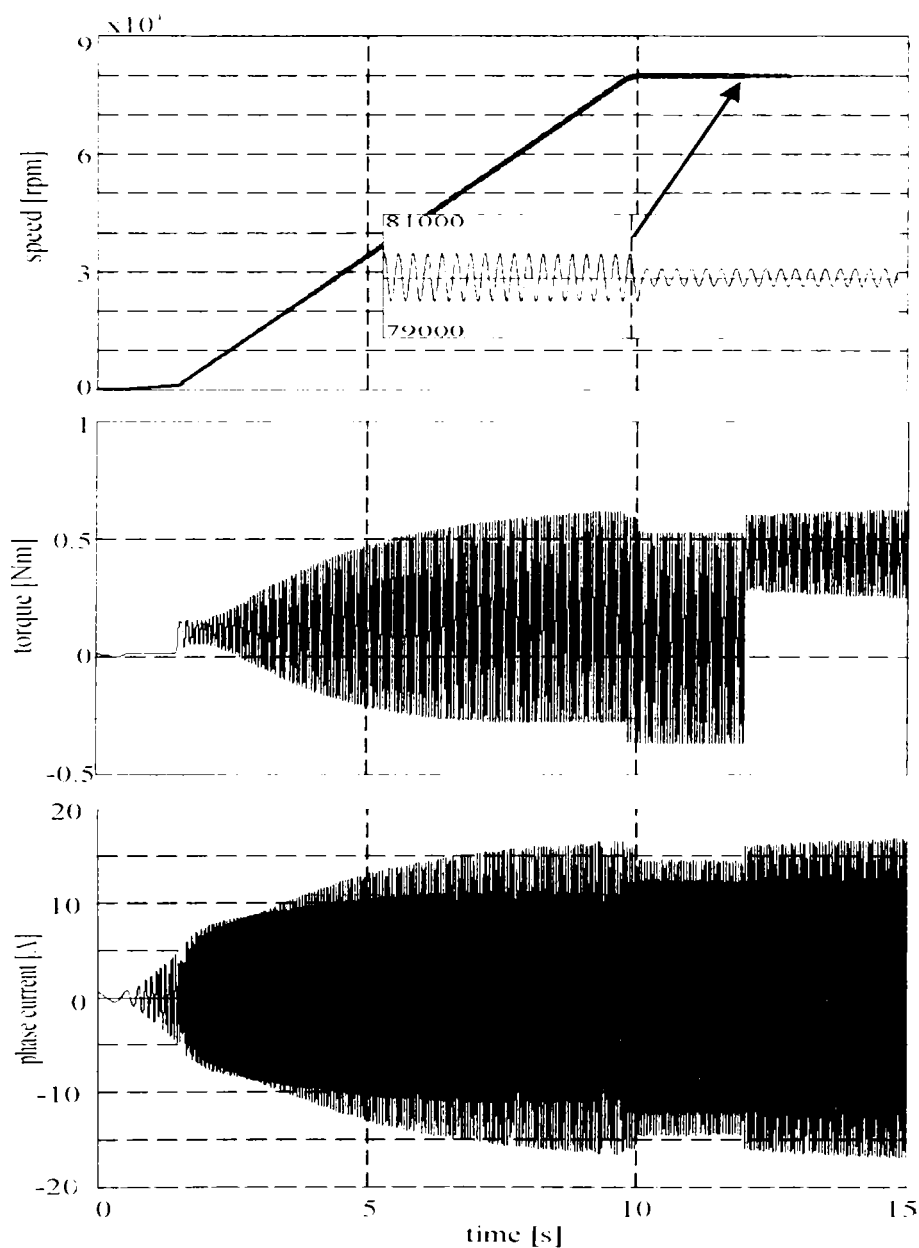


Fig. 4.8 V/f control with d.c. link current (or power) oscillations correction loop

The compensation loops work on limiting the oscillations under load as can be seen in Fig. 4.8. Both solutions have high speed and torque oscillations at 80,000 rpm which could not be acceptable.

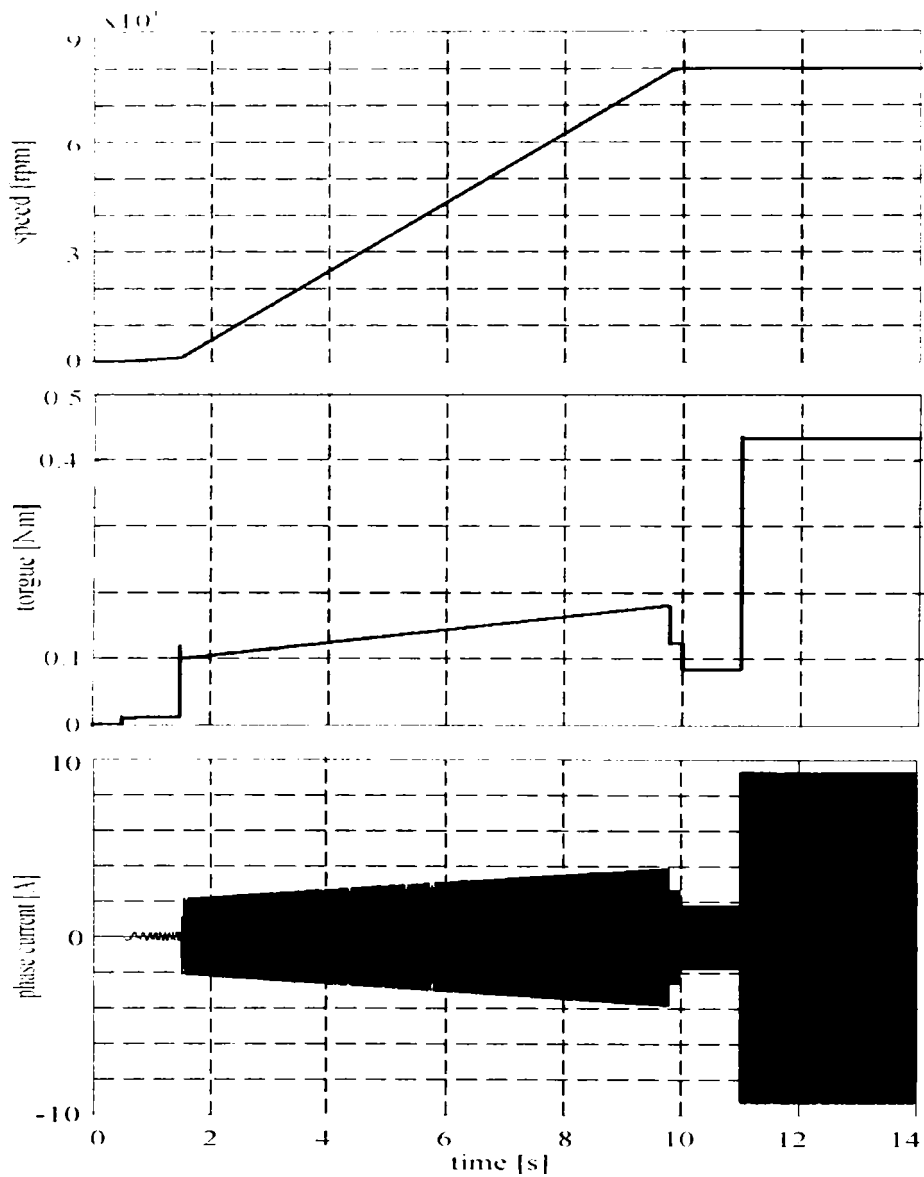


Fig. 4.9 Vector control transients

Vector control with speed and angle estimator and with synchronous current regulation based on [1] shows as expected smooth running and loading (Fig. 4.9) for same transient conditions.

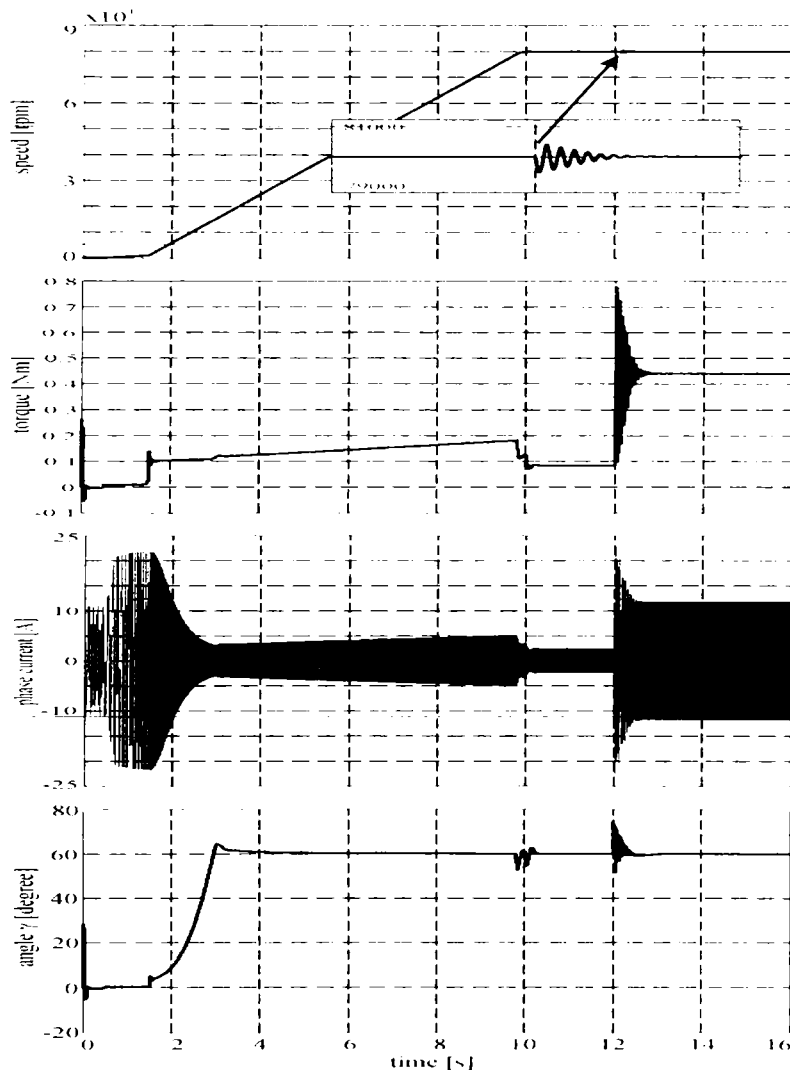


Fig. 4.10 V/f control with two stabilizing loops and full torque load

Fig. 4.10 illustrates the proposed V/f control with two stabilizing loops. The speed oscillations after step torque loading are very small, are damped in short time (as for vector control) and the speed recovery is swift. The transient power angle  $\gamma$  and its control around  $60^\circ$  is clearly visible in Fig. 4.10d. The reason to control the system maintaining an angle of  $60^\circ$  between the current vector and the stator flux vector is to obtain a good power factor. In these conditions,  $\varphi = 30^\circ$  and thus the power factor has an excellent value of 0.86.

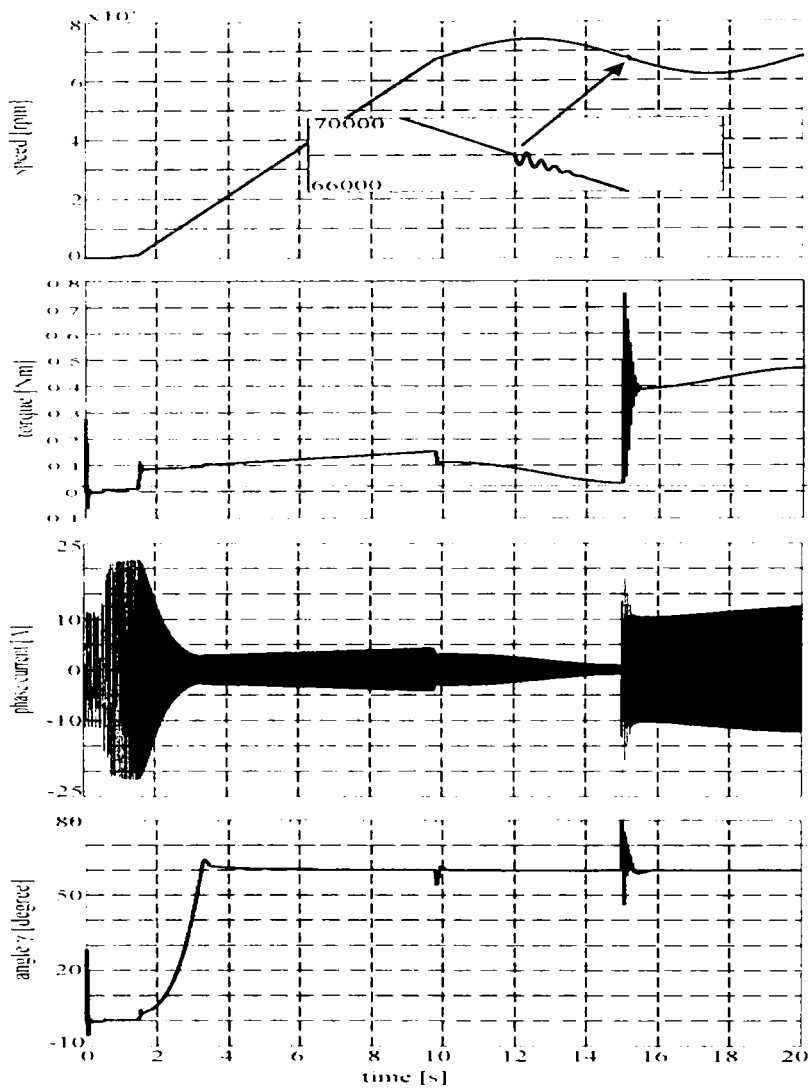


Fig. 4.11 1 Hz speed oscillations response with torque load ramp for the proposed control system

The response of the proposed system to 1 Hz frequency speed perturbations around 68,000 rpm is shown in Fig. 4.11. The reference and the actual speed are very close to each other.

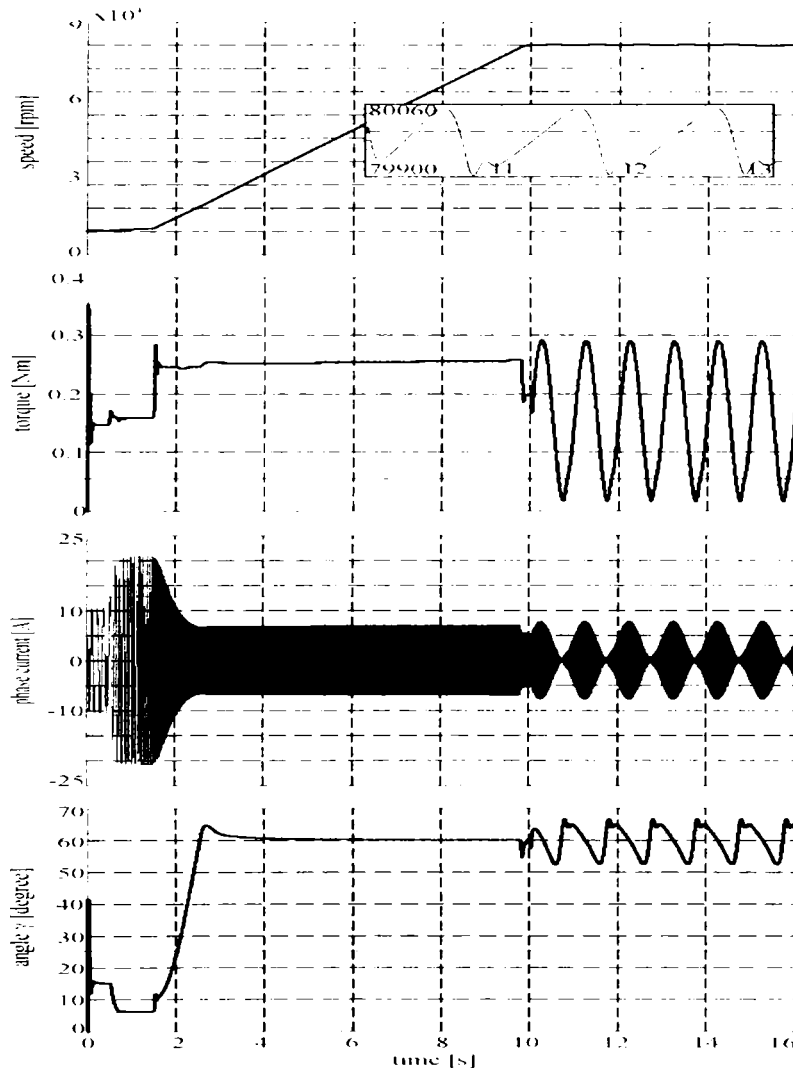


Fig. 4.12 1 Hz torque load oscillations response of proposed control system

Similar results are obtained with torque perturbations of sinusoidal character (Fig. 4.12).

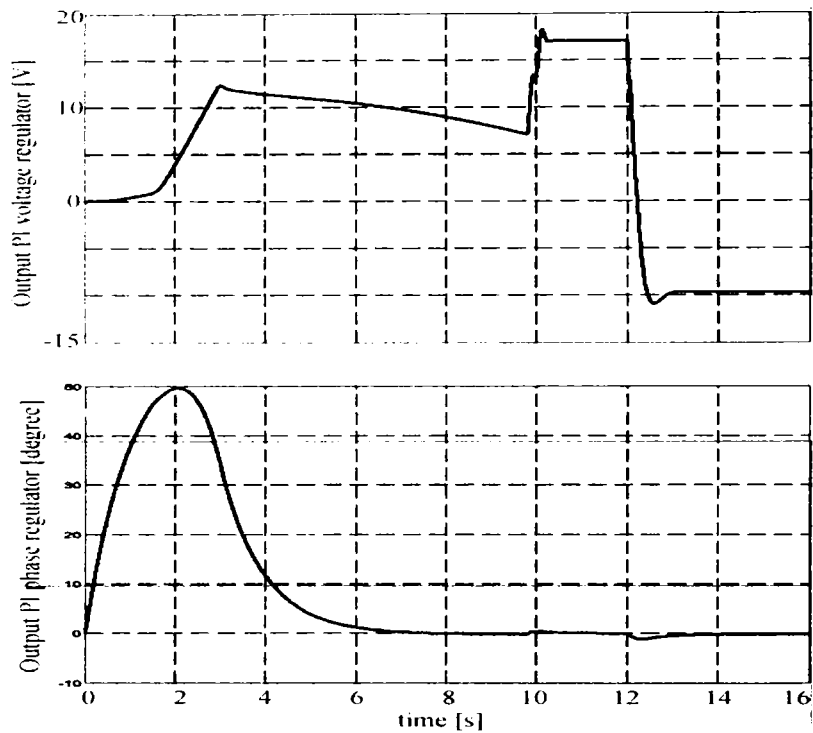


Fig. 4.13 Output of the PI regulators

To show the behavior of the power angle  $\gamma$  based on voltage and phase angle regulators, their outputs are shown in Fig. 4.13 for the transients given in Fig. 4.10.

It is obvious that the action of the two compensating loops is notable and, again, the quick and stable response after step load torque application at  $t=12s$  is highly visible.

## 4.4. Sensorless V/f Control of PMSM with Two Novel Stabilizing Loops for High Speed Dynamics for zero interior reactive power

This paragraph introduces two stabilizing loops to correct voltage amplitude and phase in V/f control of high speed PMSM based on a close loop that makes the machine interior reactive power zero (implicitly pure  $I_q$  control) (see [10]).

Details of the implementation with good load rejection properties and starting from any rotor position constitute the core of the paragraph. The solution should be especially instrumental for high speed drives where online computation time cycle is inherently very small.

### 4.4.1. Proposed V/f control with two stabilizing loops

Another V/f control with two stabilizing loops is proposed here in order to obtain high dynamic performance, which could place it between the standard V/f control and the standard vector control. Moreover, this proposed control strategy must be fast enough so that, at high speeds, the computation time should be sufficient.

The first idea is to reduce the computation time by eliminating the Park transformation between the  $\alpha\beta$  - stationary reference frame and  $dq$ - rotor reference frame [12]. This transformation, direct or inverse, uses trigonometric functions like  $\sin$  and  $\cos$  that need supplementary computation effort.

The proposed control strategy fulfills these restrictive conditions. It is best illustrated in connection with the vector diagram in Fig. 4.14, where  $\theta_{er}$  is the electrical rotor position.

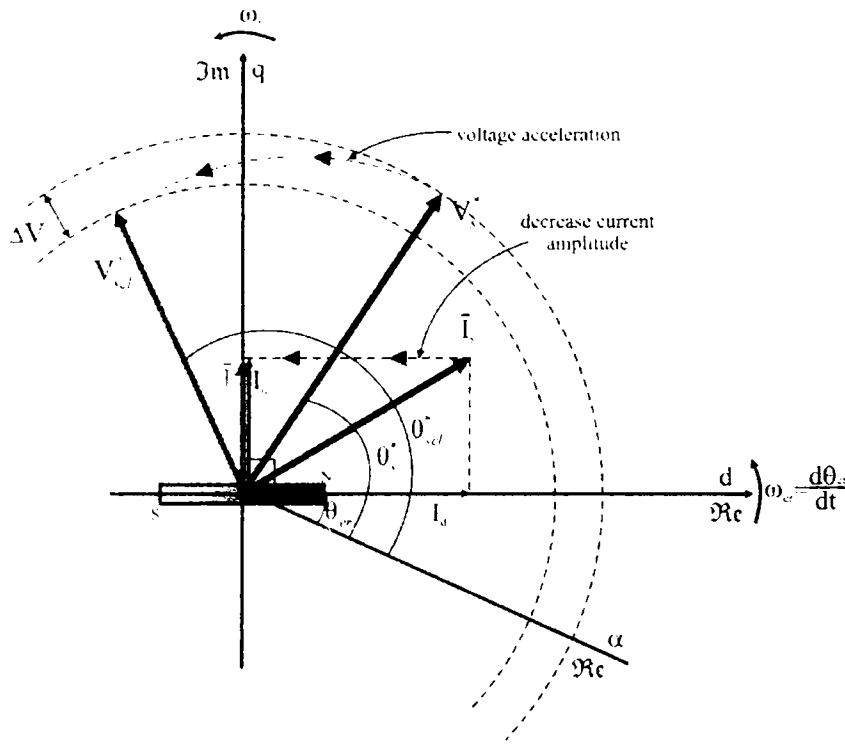


Fig. 4.14 Vector diagram of SPMSM for V/f control.

This control strategy is based on the vector diagram of voltage  $\bar{V}_s$  and current  $\bar{I}_s$  vectors for the V/f control and for the vector control, which operates with  $I_d = 0$  (surface PMSM) in ideal conditions. To achieve  $I_d = 0$ , the system will startup with the standard V/f control, while a parameter that indicates the orientation of current vector  $\bar{I}_s$  is monitored in closed loop. This current has the minimum value for a given torque only for  $I_d = 0$ .

In essence, the control strategy is based on the system property which consists in maintaining the same angle between the voltage  $\bar{V}_s$  and the current  $\bar{I}_s$  for a cvasi-constant load. Thus, to control the voltage  $\bar{V}_s$  means, in fact, to control the current  $\bar{I}_s$ . The voltage vector is accelerated or decelerated, while its amplitude is increased or decreased, depending on the case, until the current vector is aligned to the q axis. More details are given in Chapter 5 where the implementation of the control system on a SPMSM is presented.



#### 4.4.2. Overall simulated system description

As in the case of the precedent control strategy, this proposed novel control system was simulated in Matlab Simulink. To better understand this novel control strategy, the structure developed in Chapter 2 for the vector control is conserved, although some parameters like  $\theta_{er}$  and  $\sin\theta_{er}$  are not anymore used. The simulated control scheme is presented in Fig. 4.15.

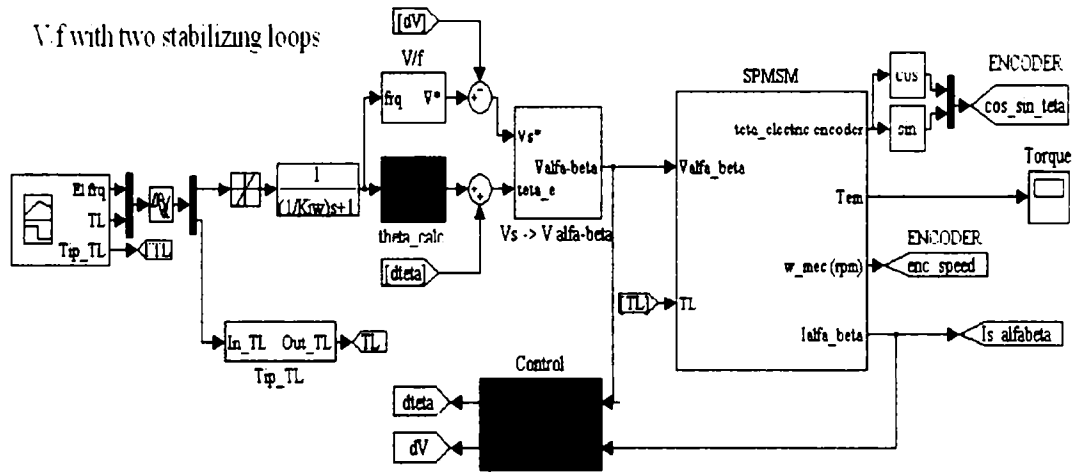


Fig. 4.15 High speed PMSM with two stabilizing loops - simulated system overview

This control scheme consists of the blocks presented below:

- The flux and torque reference (left part in Fig. 4.15) – is a special block from Matlab which can provide different signals needed in simulation;
- The block which prescribes the voltage amplitude for the standard V/f control (see Fig. 4.16). In fact it is a look-up table which takes into account the motor characteristics;
- The block which computes the voltage vector angle in the standard V/f control (see Fig. 4.17). It is also a look-up table which takes into account the motor characteristics;
- The SPMSM mathematical model is presented in Chapter 2;
- The control structure is presented in Fig. 4.18 and Fig. 4.19

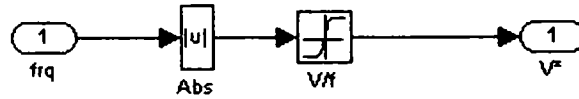


Fig. 4.16 Voltage amplitude computation in the standard V/f control

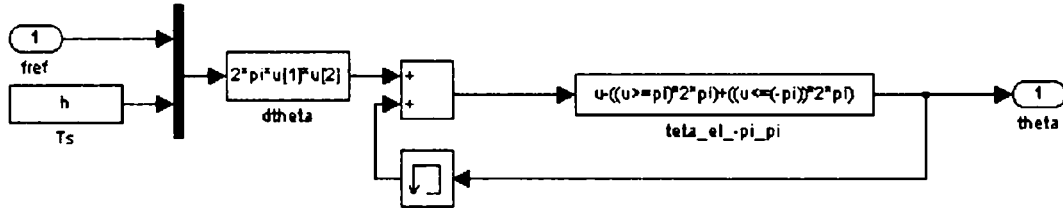


Fig. 4.17 Computation of the voltage vector angle in the standard V/f control

The block in Fig. 4.17 needs as input the reference frequency  $f^*$  and the control sampling time  $h$  which in our case is 100 ms.

This block also normalizes the rotor angle within  $(-\pi \dots +\pi)$  limits.

The control system is based on the fact that for a machine with  $L_d=L_q$  the current will be minimum for a given load only if  $I_d = 0$ . This was already implemented for the vector control in the precedent chapters. In what follows, the way the same conditions can be implemented in the novel strategy control is explained. Thus, the amplitude and phase of voltage vector  $\bar{V}^*$  will be modified until the current vector  $\bar{I}^*$  will fall along  $q$  axis, position for which the machine develops maximum torque.

This can be obtained in two ways:

1. Finding the rotor position of the sensorless drive and then imposing an angle of  $90^\circ$  electrical degrees between the current vector and the estimated rotor position ( see Fig. 4.18)
2. Monitoring an equivalent variable with the desideratum  $I_d = 0$  used in vector control. The chosen and computed variable was the internal reactive power symbolized by  $Q'_{\alpha\beta}$  (see Fig. 4.19).

Both inputs of the control blocks presented below have to be filtered in order to be able to manipulate the obtained output signals (see Fig. 4.21). The error on

the correction loop of the voltage magnitude must be multiplied by the speed sign (see Fig. 4.18 and Fig. 4.19).

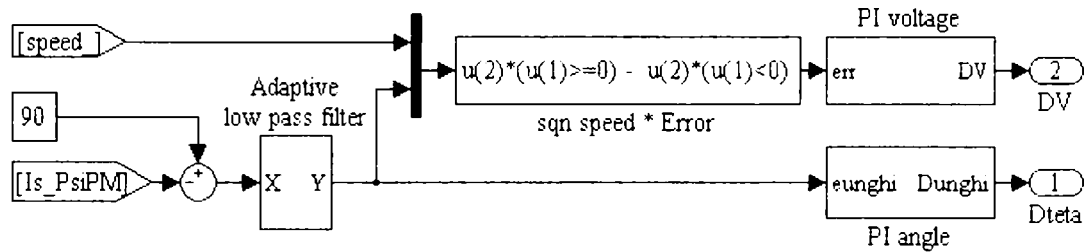


Fig. 4.18 Control block based on imposing an angle of 90° electrical degrees between the current vector and the estimated rotor position

Fig. 4.19 illustrates the block monitoring the internal reactive power  $Q_{\alpha\beta}^i$ . This internal reactive power and the arguments for its choose will be detailed in Chapter 5, in which the implemented experimental setup is presented.

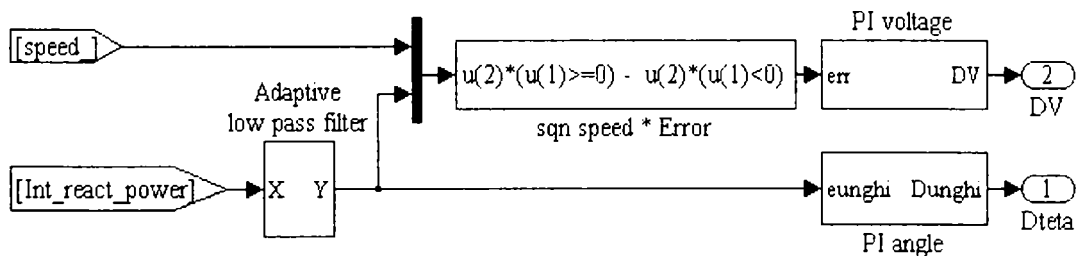


Fig. 4.19 Control block based on monitoring the internal reactive power

The expression which defines and computes the internal reactive power  $Q_{\alpha\beta}^i$  is (4.3):

$$Q_{\alpha\beta}^i = \frac{3}{2}(I_\alpha V_\beta - I_\beta V_\alpha) - \frac{3}{2}\omega_e^* L_s I_s^2 \tag{4.3}$$

Notice that this expression is very simple and easy to be implemented on any digital signal processor (DSP). However, the obtained values are not so exact during transients. This is the reason for which one can say that the system works with approximated values and the  $I_d$  value will not be the optimal one each time.

In conclusion, if we take into account the obtained results compared with vector control and the fact that the Park transformations are completed worthless, the advantages of the novel control strategy with two stabilizing loops are ahead of its disadvantages.

Details over the internal reactive power implementation are given in Fig. 4.20.

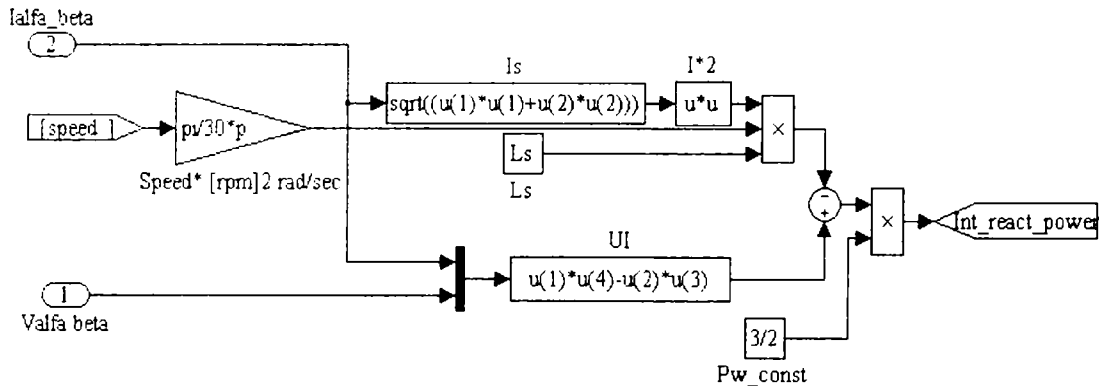


Fig. 4.20 Computation of the internal reactive power  $Q'_{\alpha\beta}$

The used filter is presented in Fig. 4.21. The filter is designed as a low pass filter (LPF), having the form:  $1/(k \cdot s + 1)$ .

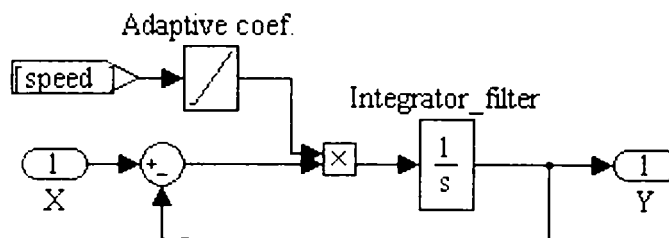


Fig. 4.21 Adaptive low pass filter (LPF)

The adaptive coefficient of the filter is  $k$ , which varies with speed from 0.2 (for low speed) to 0.05 (for high speed).

#### 4.4.3. Simulation results

It is important to point out some differences between the performance of vector control drive discussed in Chapter 2 and the investigated sensorless V/f control discussed above in this chapter. Data of the motor are presented in Chapter 6.

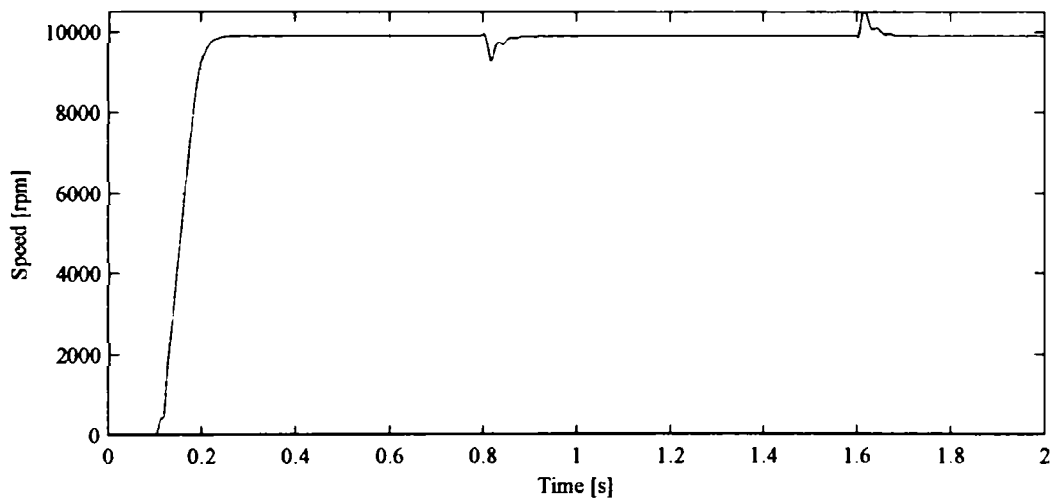


Fig. 4.22 Encoder speed during no load start-up at 10,000 rpm followed by loading at 100% of nominal torque at 0.8 s and unloading at 1.6 s

Fig. 4.22 shows the simulated speed response from the new above discussed system. A no load startup is made in 0.1 s, 100 % step load is added at 0.8 s and the entire system is unloaded at 1.6 s.

In Fig. 2.27 and Fig. 2.28 but also in Fig. 3.9a, it can be seen that the startup operation with and without encoder is achieved in maximum 0.1 s. One can say that speed waveform results from presented control in Fig. 4.22 have almost the same dynamic responses.

The control does not have problems with loading and unloading at 0.8 s and 1.6 s as it can be seen in Fig. 4.22. So the novel control system does not have major problems compared with vector control.

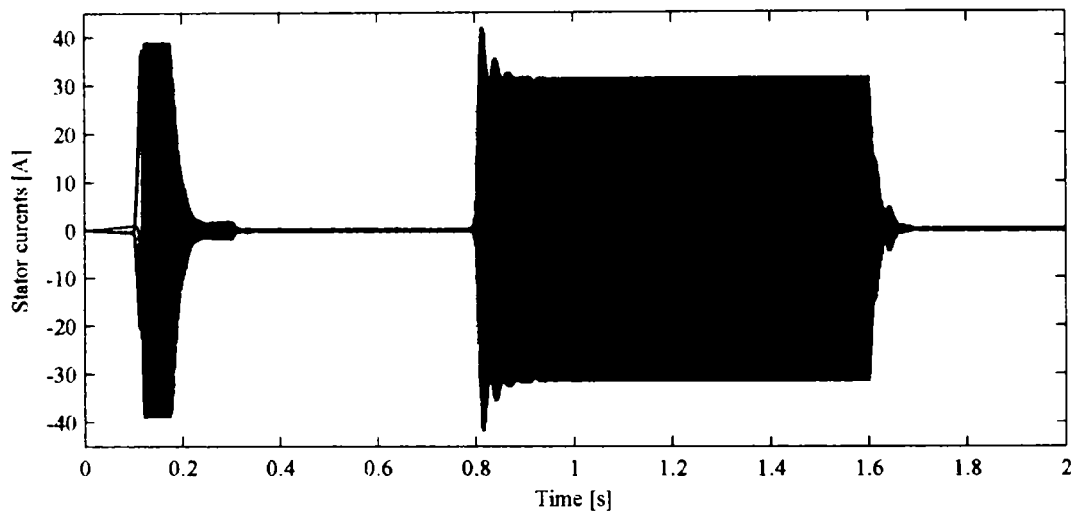


Fig. 4.23 Stator currents during tests in Fig. 4.22

The stator currents during simulation presented in Fig. 4.22 are illustrated in Fig. 4.23. The currents do not exceed the maximum available data given in Chapter 7.

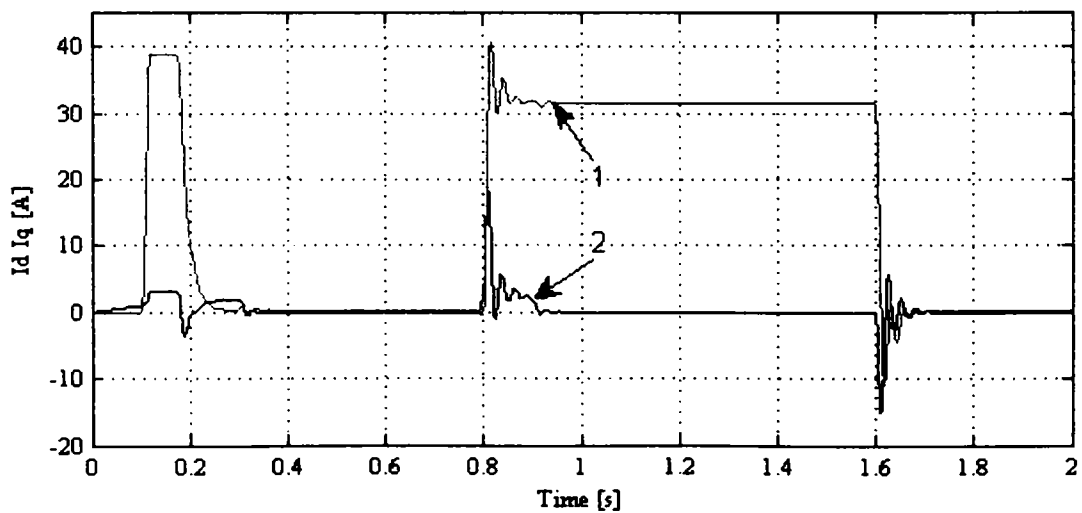


Fig. 4.24 Id Iq currents during simulation in Fig. 4.22

Fig. 4.24 illustrates the currents waveforms in rotor coordinates. The currents waveforms illustrated in Fig. 4.23 and also in Fig. 4.24 show the way the system responds to perturbations. The occurred problems are analyzed by comparing them with the experimental results illustrated in Fig 2.30. As it can be seen there are large oscillations occurred during loading or unloading operations, but these oscillations do not excessively affect the system performances.

It has to be noticed that the  $d$  axis currents are desired to be as small as they can be, especially in this case in which the  $d$  axis current has to be maintained zero and the torque expression depends only upon the  $q$  axis current. Even more, a larger value for the  $d$  axis current, even for a short period of time, in simulation tests, is undesirable.

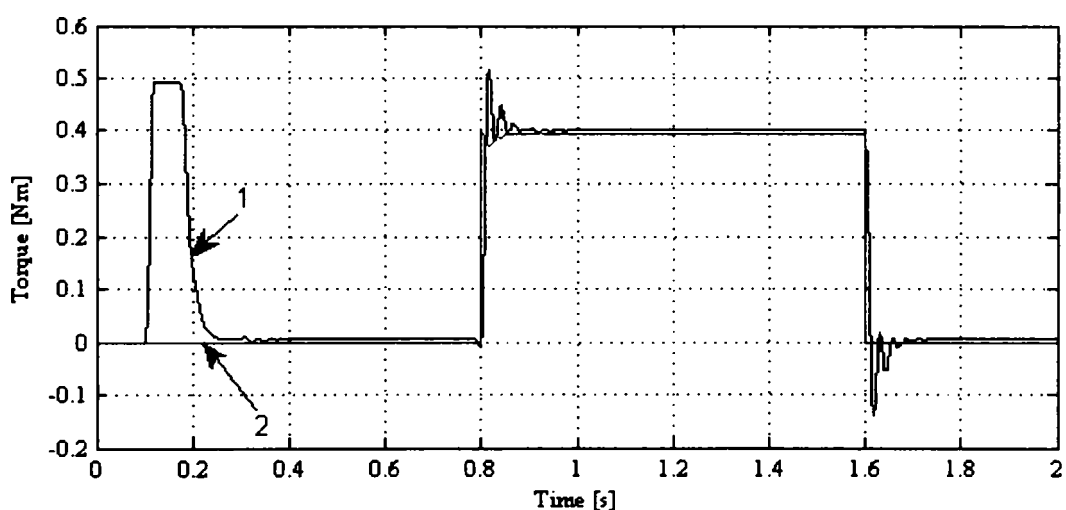


Fig. 4.25 Torque during simulation in Fig. 4.22

Fig. 4.26 illustrates the error between the actual and the reference speed. Thus, in simulation, the control does not use the speed provided by the machine model block and the necessary data are estimated using the machine currents and voltages.

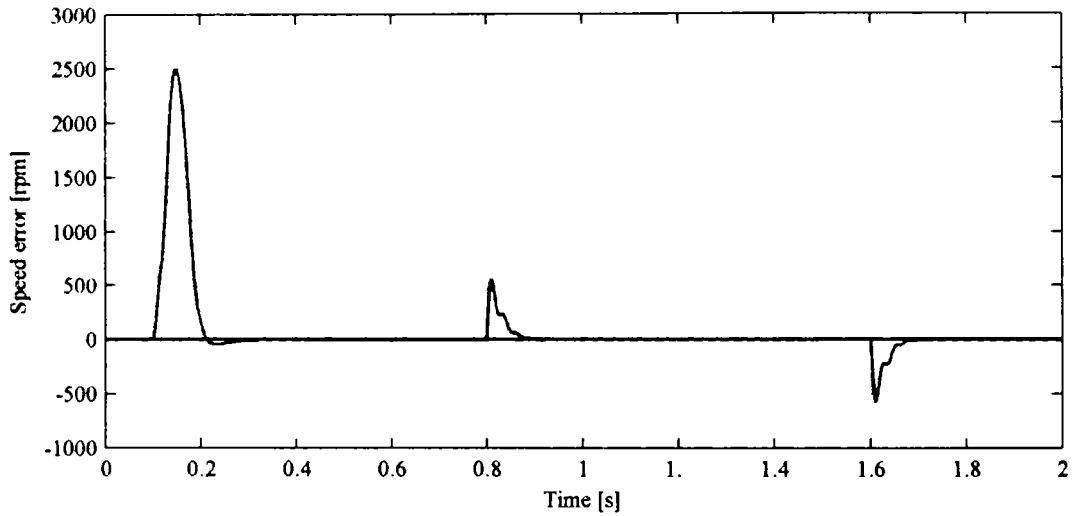


Fig. 4.26 Speed error during simulation in Fig. 4.22

The speed error is within acceptable limits, having large values only at startup. However, these errors are comparable with the ones obtained using the vector control and illustrated in Fig 3.9c.

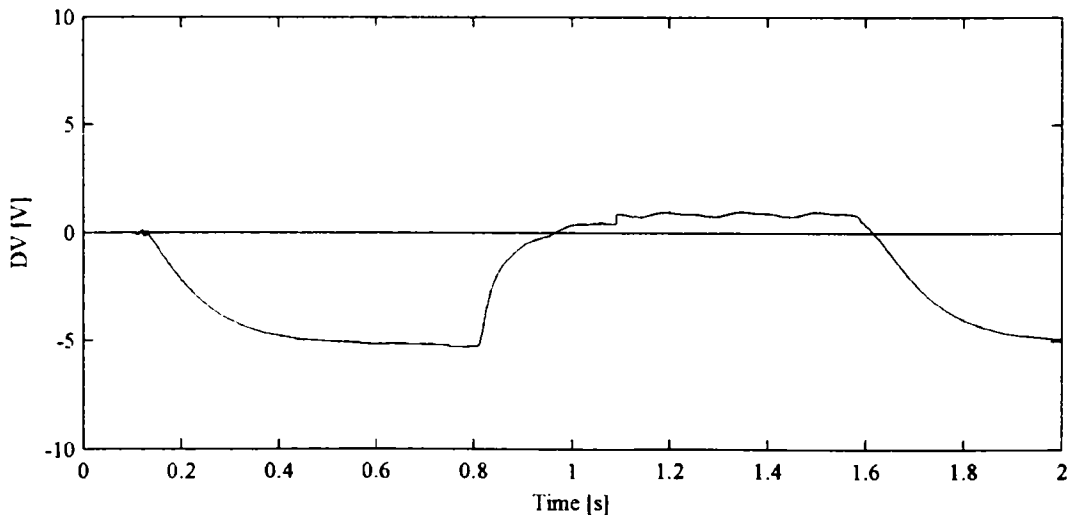


Fig. 4.27 DV during simulation in Fig. 4.22



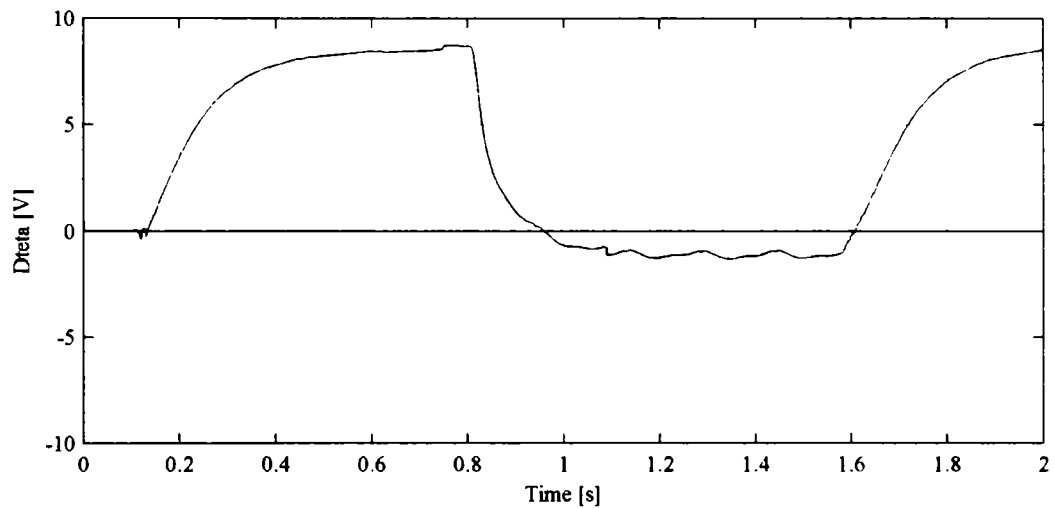


Fig. 4.28 Dtheta during simulation in Fig. 4.22

Fig. 4.27 and Fig. 4.28 illustrate the outputs of the voltage amplitude and angle controllers used in the control system. One can say that the two stabilizing loops are working together to control the entire system.

Thus, during acceleration within 0.1 s and 0.4 s, the voltage amplitude is decreased, while the voltage vector is accelerated. This can also be observed during loading (0,8 s) and unloading (1.6 s) operations. Thus, when the machine is loaded, the voltage amplitude is increased, while the voltage vector  $\bar{V}_s$  is slowly decelerated. The inverse process occurs when the machine is unloaded.

## 4.5. Conclusion

The goal of the present chapter was to analyze few control methods for high and super high speed SPMSM. Two novel control strategies for SPMSM with speed and torque fluctuations compensation have been introduced.

Both strategies act on the stator voltage vector  $\bar{V}_s$ . These strategies take into account some imposed angles in machine vector diagram and modify the voltage amplitude and phase (see Fig. 4.4 and Fig. 4.14). Thus, first strategy could impose for the angle  $\gamma$  (between the stator flux and stator current) a value around of  $60^\circ$ . The second strategy imposes an angle of  $90^\circ$  between the stator current  $\bar{I}_s$  and the permanent magnet flux  $\bar{\lambda}_{PM}$ , which is equivalent to  $I_d = 0$  in the vector control case.

Digital simulations proved that it is possible to obtain good performance both in steady state and transient regime.

The online computation effort is believed to be less intensive than for vector control.

## Appendix

TABLE 4.1.

### SPMSM SPECIFICATIONS

Number of pole pairs ( $p$ )	1
Rated power	3 kW
Rated speed	80.000 rpm
Rated frequency	1333 Hz
Rated torque	0.358 Nm
Rated phase to phase voltage	380 V(rms)
Rated phase current	20 A(rms)
Stator resistance per phase ( $R_s$ )	0.6 $\Omega$
d-axis inductance ( $L_d$ )	1 mH
q-axis inductance ( $L_q$ )	1 mH
Rotor permanent - magnet ( $\lambda_{PM}$ )	0.031 V s rad <sup>-1</sup>
Inertia of the rotating system ( $J$ )	10 <sup>-4</sup> kgm <sup>2</sup>
Viscous friction coefficient ( $B_m$ )	10 <sup>-5</sup> Nms/rad

TABLE 4.2.

### PI REGULATORS FOR VECTOR CONTROL

Regulator	$k_p$	$k_i$
Speed controller	0.2	10
Torque controller	30	10000
Flux controller	30	10000

## References

- [1] Bon-Ho Bae, Seung-Ki Sul, Jeong-Hyeck Kwon, Ji-Seob Byeon "Implementation of Sensorless Vector Control for Super-High-Speed PMSM of Turbo-Compressor", IEEE Trans. on Ind. Applicat., Vol.39, No. 3, May/June 2003.
- [2] Longya Xu, Changjiang Wang "Implementation and experimental implementation of sensorless control schemes for PMSM drives", IEEE Trans. on Ind. Applicat., vol 39, no3, 2003, pp. 783-791.
- [3] P. D. Chandana Perera, Frede Blaabjerg, John K. Pedersen and Paul Thogersen "A Sensorless, Stable V/f Control Method for Permanent-Magnet Synchronous Motor Drives", APEC 2002.
- [4] J. Oyama, T. Higuchi, T. Abe, K. Shigematsu, X. Yang, E. Matsuo "A Trial Production of Small Size Ultra-High Speed Drive System", IEMDC 2003.
- [5] Karel Jezernik, Aljaz Kapun, Milan Curkovic "Robust sensorless Control of PMSM" ISIE 2008
- [6] Jee-Hoon Jung, Gang-Youl. Jeong, Bong-Hwan Kwon "Stability Improvement of V/f-Controlled Induction Motor Drive Systems by Dynamic Current Compensator" IEEE Trans.on Ind. Vol. 51, no. 4, 2004, pp. 930-933
- [7] Kyeong-Hwa Kim, Myun-Joong Youn "DSP-Based High-Speed Sensorless Control for a Brushless D.C. Motor Using a D.C. Link Voltage Control" Electric Power Component and Systems, 2002 pp. 889 – 906.
- [8] J. X. Shen, S. Iwasake "Improvement of ASIC - Based Sensorless Control for Ultrahigh - Speed Brushless D.C. Motor Drive" IEMDC 2003
- [9] Pan C.-T., Sue S.-M. "A Linear Maximum Torque Per Ampere Control for IPMSM Driver Over Full-Speed Range", IEEE Trans. on Energy Conv., vol.20, nr.2, Iunie, 2005
- [10] M. Janaszek "New method of direct reactive energy and torque control for permanent magnet synchronous motor", Bulletin of The Polish Academy of Technical Sciences, Vol. 54, No. 3, 2006
- [11] Cui W., Chau K. T., Jiang J. Z., Fan Y., Wang Z. "Scalar Control of a New Phase-Decoupling Permanent Magnet Synchronous Motor for Servo Application", IEEE IAS, 2005

- 
- [12] D. W. Novotny and T. A. Lipo, "D, q modeling of induction and synchronous machines," in *Vector Control and Dynamics of AC Drives*, ch. 2, Oxford Univ. Press, London, UK, 1998.
- [13] Mineo Tsuji,; Shuo Chen,; Shin-ichi Hamasaki,; Xiaodan Zhao,; Eiji Yamada; "A novel V/f control of induction motors for wide and precise speed operation" International Symposium on Power Electronics, Electrical Drives, Automation and Motion, SPEEDAM, June 2008 pp. 1130 - 1135
- [14] Hoshino, T.; Itoh, J.-i.; Kaneko, T.; "Dead-Time Voltage Error Correction with Parallel Disturbance Observers for High Performance V/f Control" IEEE Industry Applications Conference, Sept 2007 pp. 2038 - 2044
- [15] Xiang-Dong Sun; Matsui, M.; Nakamura, Y.; "V/f Fuzzy Control of an Induction Motor for a DC Grid Power Leveling System Using a Flywheel Energy Storage Equipment" IEEE IECON Nov 2007 pp. 2092 - 2097
- [16] H. Luo, Q. Wang, X. Deng and S. Wan, "A novel V/f scalar controlled induction motor drives with compensation based on decoupled stator current," in *Proc. Industrial Technology Conf. IEEE-ICIT 2006*, Dec. 2006, pp. 1989-1994.
- [17] Grabner, C.; "Variable Speed Induction Drive System in V/f Control Mode - Numerical Calculation Versus Practical Measurement" Electrical and Computer Engineering, CCECE 2007. 22-26 April pp. 550 - 555
- [18] Pongpant, Jutarat; Po-ngam, Sakorn; Konghirun, Mongkol; "The Performance Improvement of Constant V/f Control of Induction Motor Drive in Low Speed Range" TENCON Nov 2006 pp. 1 - 4
- [19] Itoh, J.; Hoshino, T.; Kaneko, T.; "A Performance Improvement of V/f Control Using a Disturbance Observer" Power Electronics and Motion Control Conference, EPE-PEMC 2006. Aug. 2006 pp. 1167 - 1172
- [20] K. Suzuki, S. Saito, T. Kudor, A. Tanaka, and Y. Andoh, "Stability improvement of V/f controlled large capacity voltage-source inverter fed induction motor," in *Conf. Record IEEE-IAS 2006*, vol. 1, pp. 90-95, Oct. 2006.
- [21] Xianzhong Dai; Guohai Liu; Hao Zhang; Xinghua Zhang; "Neural network inverse control of variable frequency speed-regulating system in V/F mode" IEEE IECON Nov. 2005.

- [22] L. Zhao, C. H. Ham, Q. Han, T. X. Wu, L. Zheng, K. B. Sundaram, J. Kapat, and L. Chow, "Design of an optimal V/f control for a super high speed permanent magnet synchronous motor," in *Proc. IEEE-IECON 2004*, Nov. 2004, vol. 3, pp. 2260–2263.
- [23] Beig, A.R.; Narayanan, G.; Ranganathan, V.T.; "Space vector based synchronized PWM algorithm for three level voltage source inverters: principles and application to V/f drives" *Proc. IEEE, IECON Nov. 2002* vol.2 pp. 1249 – 1254.
- [24] Qingguang Yu; Qiang Song; Wenhua Liu; Yongqiang Li; "DSP LF2407 in NPC three-level inverter using constant V/f principle and SHE-PWM method" *Signal Processing, International Conference*, Aug. 2002 vol.2, pp. 1723 – 1726.
- [25] J.-I. Itoh, N. Nomura, and H. Ohsawa, "A comparison between V/f control and position-sensorless vector control for the permanent magnet synchronous motor," in *Proc. Power Conversion Conf. PCC Osaka 2002*, April 2002, vol. 3, pp. 1310–1315.
- [26] J.-I. Itoh, N. Nomura, and H. Ohsawa, "A comparison between V/f control and position-sensorless vector control for the permanent magnet synchronous motor," in *Proc. Power Conversion Conf. PCC Osaka 2002*, April 2002, vol. 3, pp. 1310–1315.
- [27] Grabner, C.; "Quality Improvement of a Variable Speed Drive in V/f Mode - Numerical Evaluation of Crucial Influences" *IEEE ISIE 2007* June 2007 pp. 1062 - 1067
- [28] Kumsuwan, Y.; Premrudeepreechacharn, S.; Oranpiroj, K.; Boonsai, T.; Toliyat, A.; "A Direct Torque Control of Induction Motor Using V/f PWM Technique" *Power Electronics and Drives Systems, PEDS 2005*, Jan. 2006 pp. 751 – 755.
- [29] Jung-Geun Kim; Young-Gook Jung; Seok-Hwan Na; Young-Choel Lim; "A new random PWM (SRP-PWM) technique for decreasing acoustic noise radiated from v/f controlled motor drives" *IEEE, IECON 2004*. 2-6 Nov, vol. 1, pp. 832 - 837
- [30] Fatu, Marius; Teodorescu, Remus; Boldea, Ion; Andreescu, Gheorghe-Daniel; Blaabjerg, Frede; "I-F' starting method with smooth transition to EMF based motion-sensorless vector control of PM synchronous motor/generator" *IEEE*

Power Electronics Specialists Conference, PESC 2008, 15-19 June 2008 pp. 1481 - 1487

- [31] Y. S. Kim, Y. K. Choi, and J. H. Lee, "Speed-sensorless vector control for permanent-magnet synchronous motors based on instantaneous reactive power in the wide-speed region," *IEEE Proc. - Electr. Power Appl.*, vol. 152, no. 5, pp. 1343-1349, Sept. 2005.
- [32] R. Ancuti and I. Boldea, "V/f control of PM-SM super high speed drives with flux and power angle stabilizing loops," in *Proc. OPTIM 2006, Brasov, May 2006*, CD-ROM.
- [33] R. Ancuti, I. Boldea, G. D. Andreescu and D. Iles "Fast Response Sensorless Control of High Speed Surface PM-SM: With Experiments" CNAE, Romania, Timisoara 2008

# Chapter 5

## Sensorless V/f Control of Surface PMSM with Two Novel Stabilizing Loops for High Speed Dynamics: implementation and test results

### Abstract

This chapter introduces a novel sensorless control of high-speed SPMSM drive based on two stabilizing loops to correct the voltage amplitude and phase in V/f control using a close loop for zero interior reactive power (implicitly pure  $I_q$  control). Implementation details and comprehensive test results with a 300 A, 50 Vdc MOSFET inverter and SPMSM are given. Speed reversal of  $\pm 10$  krpm within 160 milliseconds with good load rejection properties, 20 krpm no load startup and starting from any initial rotor position constitute the core of the chapter. The speed (torque) dynamics are similar to those of vector control method with encoder, but online computation effort is notably lower, with superior control robustness.

### 5.1. Introduction

An ultrahigh speed motor (500 krpm and 100 W) and three special commutation strategies for this high speed motor are presented in [1].

Super high-speed drives (over 150 krpm) have been obtained recently, focusing on stability rather than on control response quickness [2] with improved vector control dynamics [3]. Speed above 200 krpm are reported in [4] without control details.

However, V/f control systems with voltage amplitude [5] [6] and phase correction [7], for operation at high-efficiency constant power factor, have been also proposed. Other scalar or vector control strategies to improve stability at high speed are given in [8], [9] and [10]. Two stabilizing loops on top of V/f control ([11], [12]



and [13]) have led to speed oscillations reduction and good efficiency, but did not improve system dynamics.

For speeds between 60 krpm to 100 krpm, the hybrid V/f with position encoder and current control, but using Park transformation, has been proposed in [14]. Good dynamic performance up to 65 krpm with sensorless vector control are shown in [15], and comparisons between vector control and standard V/f control and given in [16]. V/f and  $I_f$  control up to large speeds is investigated in [17].

All the above methods either require large online computation effort for sensorless vector control, or show slow dynamics, i.e., large acceleration time to peak speed for V/f or  $I_f$  control with or without stabilizing loops.

The present chapter introduces two novel stabilizing loops based on the control to zero of the internal reactive power (in fact  $I_d=0$ ) for V/f control in order to:

- provide fast speed dynamics (both for startup from any rotor position and after torque perturbation);
- imply online computation effort and avoid stator resistance variation sensitivity;
- avoid both current and speed close loop regulators for control simplicity and robustness

## 5.2. Basic Control Systems for SPMSM

The SPMSM space-phasor model in stator coordinates is:

$$\bar{V}_s = R_s \bar{I}_s + \frac{d\bar{\lambda}_s}{dt} \quad (5.1)$$

$$\begin{aligned} \bar{\lambda}_s &= L_s \bar{I}_s + \bar{\lambda}_{PM} \\ \bar{\lambda}_{PM} &= \lambda_{PM} e^{j\theta_{er}} \\ \bar{I}_s &= I_s e^{j\theta_i} \end{aligned} \quad (5.2)$$

where  $\bar{V}_s$ ,  $\bar{I}_s$  and  $\bar{\lambda}_s$  are the stator voltage, current and flux vectors, respectively,  $\bar{\lambda}_{PM}$  is the PM-flux vector,  $R_s$ ,  $L_s$  are the stator resistance and inductance,  $\theta_{er}$  is the electrical rotor position, and  $\theta_i$  is the stator current vector angle.

The SPMSM can be driven by the following strategies met in literature: V/f, I<sub>f</sub>, vector control or DTC. Best results are obtained using the last two strategies when the system has an additional encoder. However, at high and very-high speeds, problems involving the computation time necessary for one control cycle occur. Even more, if no encoder is provided, the problems become more serious including startup, when initial position must be known. The machine parameters  $\lambda_{PM}$ ,  $R_s$ ,  $L_s$ , which are decisive terms in rotor position  $\hat{\theta}_{er}$  estimation must be also accurately known in order to provide a real rotor position, otherwise the motor will not start. All these problems were faced out in [18] using the vector control system, but we think that, using the method proposed in this chapter, most of them could be easier solved.

The standard V/f control strategy [12], shown in Fig. 5.1, prescribes a rotating voltage vector whose amplitude  $V^*$  is proportional to its frequency  $\omega_{er}^*$  and is smoothly modified.

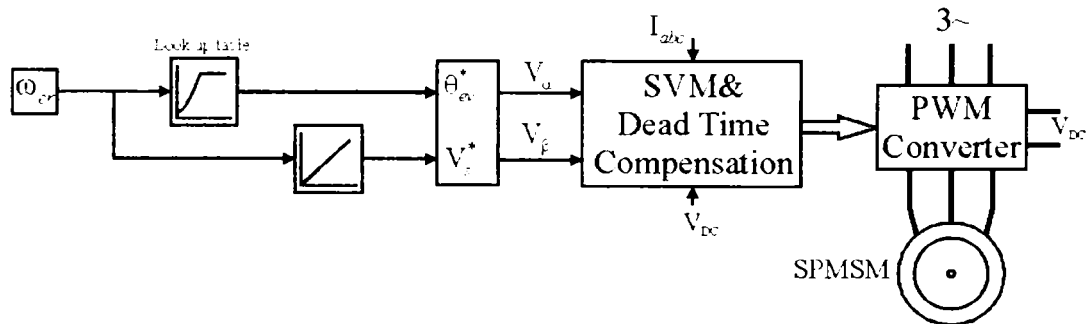


Fig. 5.1 Standard V/f control

One obvious disadvantage of this method is that the prescribed voltage amplitude has to be large enough to cover torque transient operations. Thus, the machine operates with the same voltage amplitude whatever the load is, because this voltage vector can not be modified very fast. Another disadvantage is the presence of speed large oscillations during steady state operation. Note that the machine reaches the rated speed in a sizeable time (see Fig. 5.7). Moreover, in some cases the rated speed can not be achieved, due to the large oscillations, which are amplified by the augmentation of speed. An abrupt frequency ramp will automatically lead to the stop of the control system by the overcurrent protection device, or by the machine loss of synchronization [12].

Another control strategy, this time a very performant one, is the vector control strategy [18] (see Fig. 5.2). The most essential characteristic of this

strategy is that the system is implemented in  $dq$  - rotor reference frame, with the advantage of good stability, notably when an encoder is provided. When the encoder is missing, some problems may occur and these will be presented when describing in detail the proposed control system.

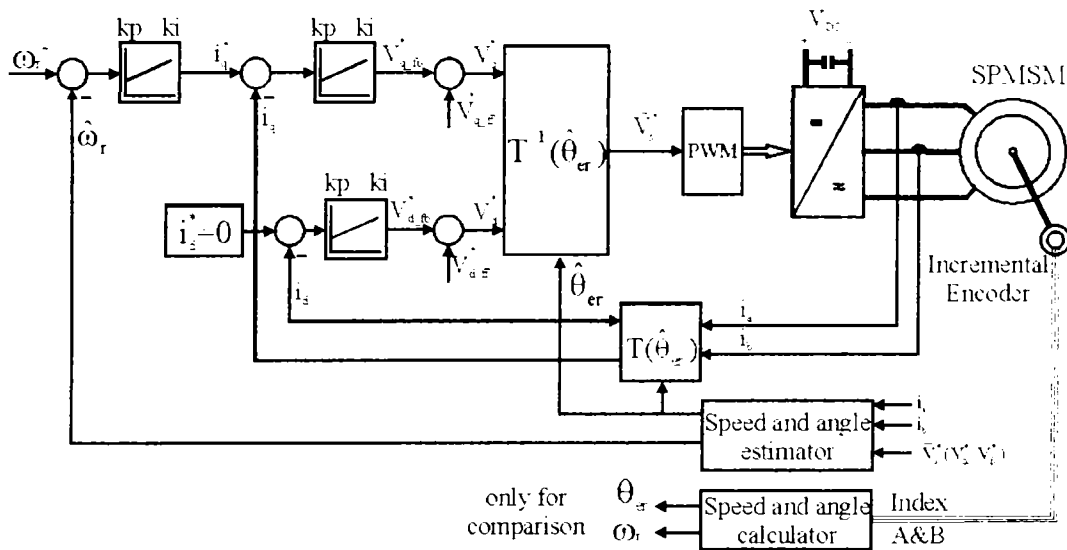


Fig. 5.2 Block diagram of sensorless vector control system.

### 5.3. Proposed V/f control with two stabilizing loops

The control strategy is similar with the one described in Chapter 4.

V/f control with two stabilizing loops is proposed here in order to obtain high dynamic performance, which could place it between the standard V/f control and the standard vector control described in Chapter 2, respectively in Chapter 3. Moreover, this proposed control strategy must be fast enough so that, at high speeds, the computation time should be sufficient to prescribe the next voltage vector  $\bar{V}_s$ .

The strategy control does not use the Park transformation between the  $\alpha\beta$  - stationary reference frame and  $dq$ - rotor reference frame [26]. This transformation, direct or inverse, uses trigonometric functions like  $\sin$  and  $\cos$  that need supplementary computation effort.

A second idea is to reduce the computation time by eliminating the rotor position and speed estimator.

The control strategy was described in Chapter 4 and is presented again in the vector diagram in Fig. 5.3, where  $\theta_{er}$  represents the electrical rotor position.

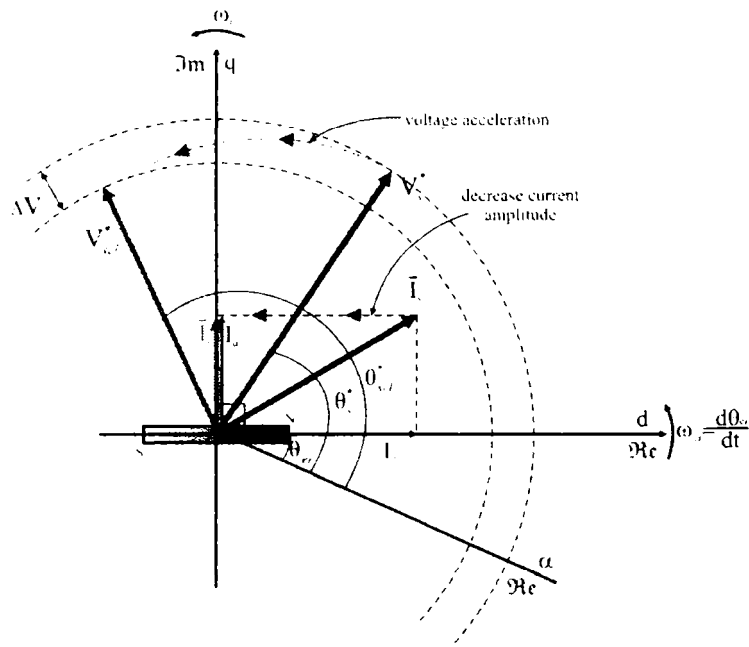


Fig. 5.3 Vector diagram of SPMSM for V/f control.

The vector diagram in Fig. 5.3 is related to the control scheme in Fig. 5.4. These two control schemes describe how the standard V/f control could be transformed in a performant control equivalent to vector control.

The system starts up with the standard V/f control and then  $I_d = 0$  has to be achieved by a proper control.

The chosen parameter to observe this is the internal reactive power  $Q'$ , which is zero when  $I_d = 0$ . More details of the internal reactive power will be presented subsequently.

Fig. 5.4 introduces the proposed V/f control scheme with two stabilizing loops:

i) for voltage amplitude correction  $\Delta V$ ,

ii) for voltage phase correction  $\Delta\theta$ , in order to lead to zero the internal reactive power.

Making allowance for the internal reactive power error, the voltage vector  $\bar{V}_s$  will be accelerated or decelerated (Fig. 5.3) and meanwhile its amplitude will be decreased or increased. The load angle between  $\bar{V}_s$  and  $\bar{I}_s$  remains roughly

constant, and thus, the voltage vector drags towards it the current vector, which will fall along the  $q$ -axis where the torque  $T_e$  is maximum for a given current. For SPMSM  $L_d = L_q$ , and thus

$$T_e = \frac{3}{2} \lambda_{PM} i_q \tag{5.3}$$

where the  $d$ - axis current  $I_d$  is worthless for torque production.

No Park transformation and no speed loop are used. The internal reactive power is computed from two measured stator currents and the reference stator voltage components. An incremental position encoder is used only for comparisons.

The input of the control system in Fig. 5.4 is the mechanical reference speed  $n_{mec}^*$  (given in rpm). Thus, the system operates at constant speed value.

The electrical speed  $\omega_{er}^*$  (rad/s) and the electrical frequency  $f_e^*$  (Hz) are computed from the mechanical speed  $n_{mec}^*$ . The two operating voltages are the computed voltage from the look up table  $V_s^*$  and the corrected voltage  $V_{sc}^*$ . In some extremely cases  $V_{sc}^*$  can be limited to  $V_{sc1}^*$ . This voltage is the maximum admitted voltage value for a demanded speed (frequency).

$\theta_s^*$  and  $\theta_{scl}^*$  (see Fig. 5.3 and Fig. 5.4) are the angles of the voltage vectors  $V_s^*$  and respectively  $V_{scl}^*$  with respect to  $d$  axis.

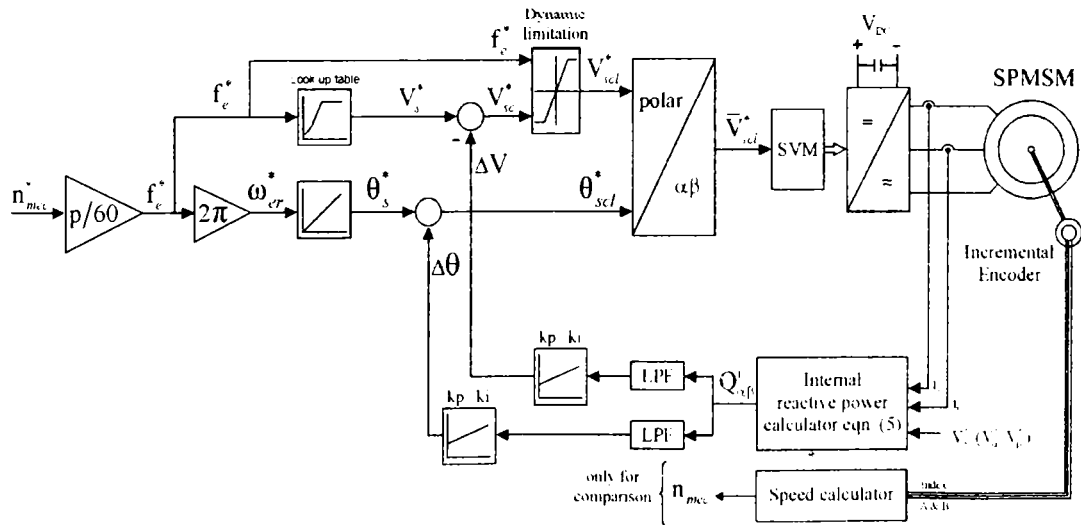


Fig. 5.4 Block diagram of the proposed V/f control with two stabilizing loops

## 5.4. Internal Reactive Power Calculator

The selected parameter to monitor the current vector alignment on  $q$ -axis, i.e.,  $I_d = 0$ , is the internal reactive power in stator coordinates  $Q_{\alpha\beta}^j$ .

The reactive power in rotor coordinates  $Q_{dq}^j$  has the expression (5.4) (see [19] to [25]), and it is zero when  $I_d = 0$ .

$$Q_{dq}^j = \frac{3}{2} \omega_e I_d \lambda_{PM} \quad (5.4)$$

This formula is a clock-like one, and it is valid both in steady state and transient regime. On the other hand, (5.4) contains the term  $I_d$ , employing the Park transformation, fact that must be avoided. Consequently, instead (5.4), the internal reactive power in stator coordinates (5.5) is used:

$$Q_{\alpha\beta}^j = \frac{3}{2} (I_\alpha V_\beta - I_\beta V_\alpha) - \frac{3}{2} \omega_e^* L_s I_s^2 \quad (5.5)$$

However, this formula is strictly valid during steady state and has some problems while may appear during transients and during generator regime. They will be discussed later.

Fig. 5.5 presents the two reactive powers described above estimated from speed reversal operation from 10,000 rpm to -10,000 rpm, using the standard vector control with encoder, implemented on the same setup. It should be noticed that the reactive power in rotor coordinates reaches zero faster than the reactive power in stator coordinates, as expected.

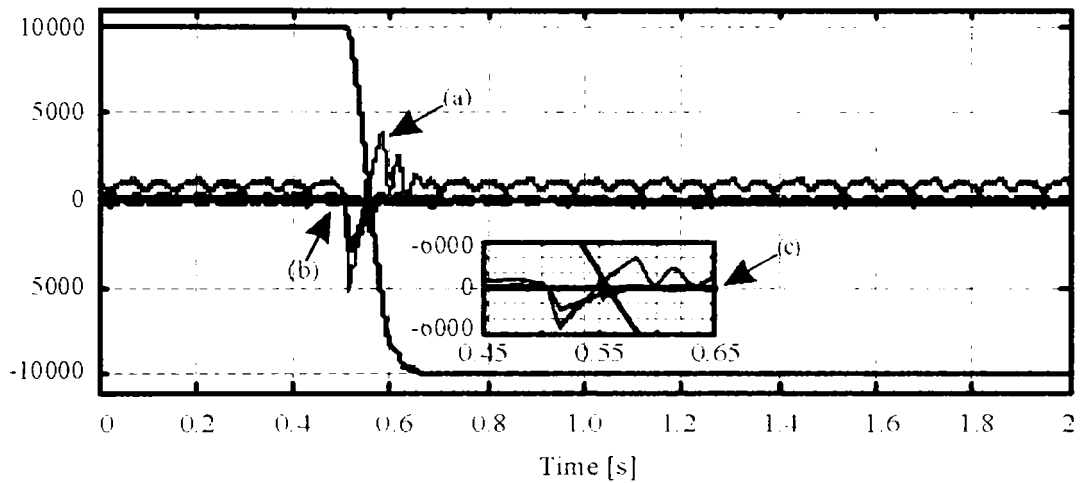


Fig. 5.5 Speed reversal from 10,000 rpm to -10,000 rpm vector control with encoder:

- a) reactive power  $Q'_{\alpha\beta}$  in stator coordinates multiplied by 10
- (b) reactive power  $Q'_{dq}$  in rotor coordinates multiplied by 10
- (c) Zoom of these reactive powers.

Therefore, in some situations the monitored  $I_d$  current will not be exactly zero as it is desired. For  $L_s$  an approximate value is also necessary. We could say that the whole system operates with approximate values. This is beneficial, because in sensorless vector control the rotor position and the machine parameters  $\lambda_{PM}$ ,  $R_{S1}$ ,  $L_s$  have to be accurately known; otherwise the machine will not start. Note that in (5.5), the stator resistance  $R_s$  influence gets cancelled. This is a special characteristic of the proposed control.

Due to the fact that the computed reactive power has notable noise disturbance, it has to be filtered. The filter constants are given in TABLE 5.1 in Appendix. These constants influence current dynamics, which, for short periods of time, have larger amplitudes than in vector control.

## 5.5. Start-up Strategy

A very well known problem in the case of synchronous machine startup is that the initial rotor position must be known. Moreover, in the case of SPMSM, when  $L_d=L_q$ , the signal injection can not be applied directly in order to find the initial rotor position, unless additional opposite voltage vectors are used subsequently for the scope. A simple solution is to align the rotor  $d$ -axis to a known position, by triggering a proper voltage vector, but the rotor will rotate a little bit in an indeterminate direction.

By using the proposed control system, the problem to determine the initial rotor position is eliminated, because in essence it is a V/f control. However, this is not an assurance that the rotor will not rotate in the opposite direction for a very short time, as it is suggestively presented in Fig. 5.6.

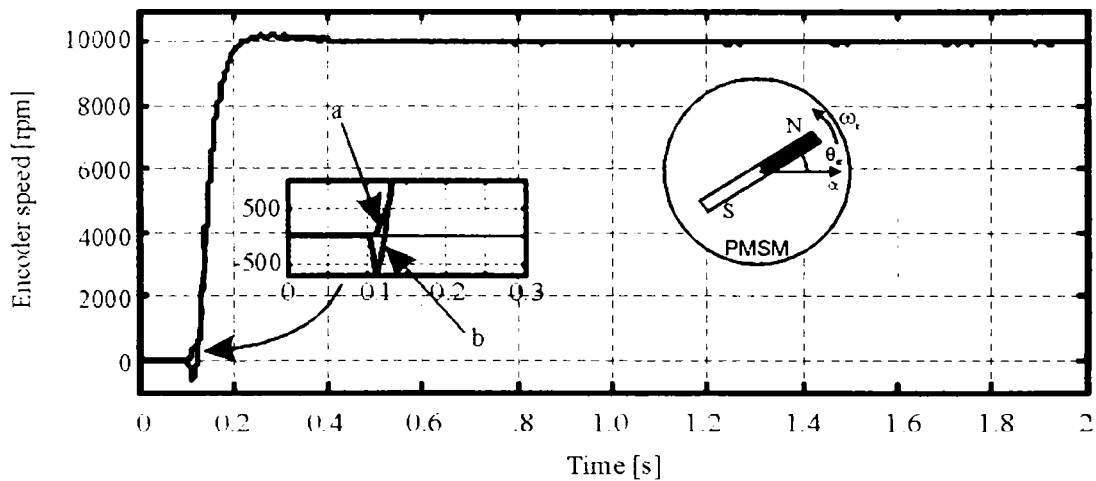


Fig. 5.6 Start-up problems to 10,000 rpm - experimental results

In the worst case, during acceleration from 0 to +10,000 rpm, the rotor initially turns into the negative direction reaching -600 rpm. Notice that the machine reaches the required speed in approximately the same time (0.1 s). Thus the total acceleration time remains about the same as the time for initial rotor position procedure is less than 20 ms.



The rotor rotates in the opposite direction after being deliberately placed in many different initial positions. Fig. 5.6 presents the worst case scenario.

## 5.6. Experimental Results

Fig. 5.7 presents the dynamics and the oscillations in the speed waveform, typical to standard V/f control.

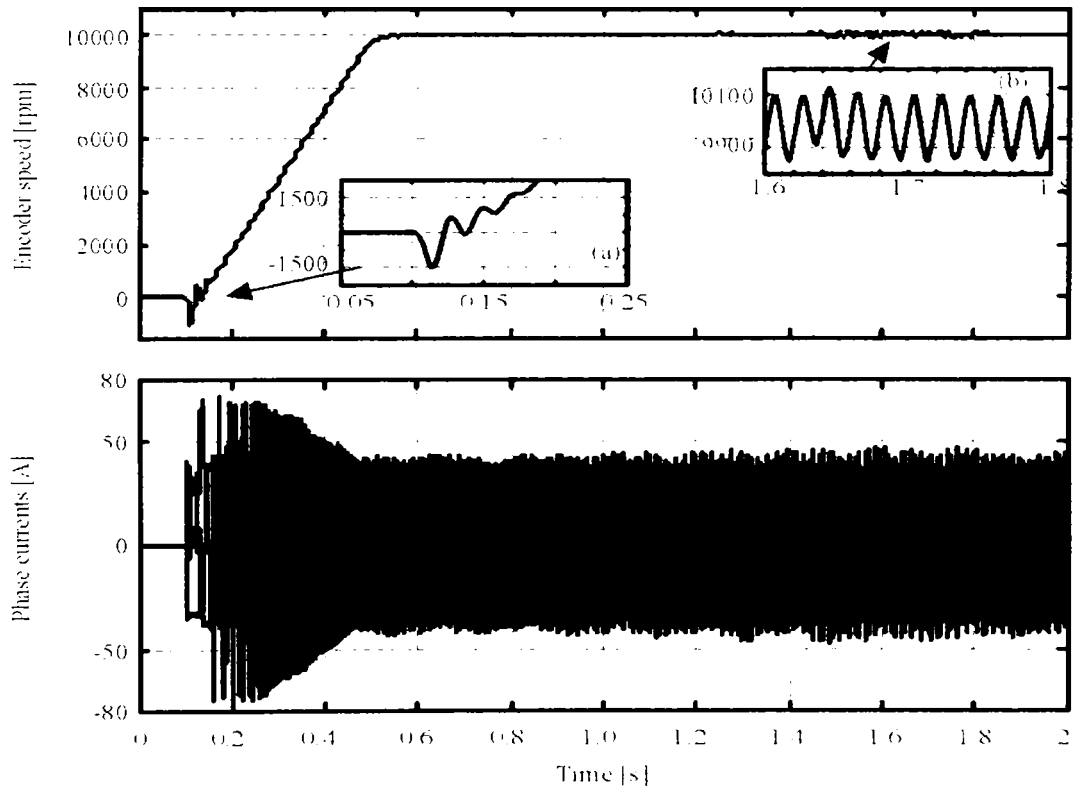


Fig. 5.7 No load start-up at 10,000 rpm with standard V/f control.

The motor operates at no load and the rated speed of 10,000 rpm is reached in 0.5 s. If large reference acceleration is applied, a loss of synchronization occurs. However, this acceleration can be slightly larger when the motor starts under a load torque proportional to speed, which acts as a damper cage and attenuate speed oscillations. Thus, the dynamics would be somewhat improved for

some load conditions ( $M_L=10\%M_{Ln}$ ) and the acceleration to 10,000 rpm could be achieved in 0.25 s; but this is still too much. V/f control in Fig. 5.7 shows speed pulsations and large current amplitudes irrespective to load.

The tests using the proposed V/f control system with two stabilizing loops are shown in parallel to those of the vector control system [18], in order to accentuate the similar performance of both control systems.

### 5.6.1. No Load Start-Up to 10,000 rpm

The first test consists in no load startup from 0 to +10,000 rpm. As it can be seen in Fig. 5.8, the dynamics are very good using the proposed control system, with the acceleration time of 0.1 s. These dynamics are similar to the vector control system dynamics with and without encoder. This is the minimum allowable acceleration time for this motor and it can also be theoretically derived from the mechanical equation of the system:

$$J \frac{d\omega_{mec}}{dt} = T_e - T_L - \omega B_m \quad (5.6)$$

where, for the machine parameters from Chapter 6 and for a speed from 0 to 10,000 rpm, a 0.1 s acceleration time is obtained. This acceleration time is close to the one obtained in the test results in Fig. 5.8.

The  $I_d$  current slowly reaches zero value because the used filters (LPF) have rather large time constant. This is also reflected in the startup current amplitude. Adequate current protection will ignore current spikes within a short time.

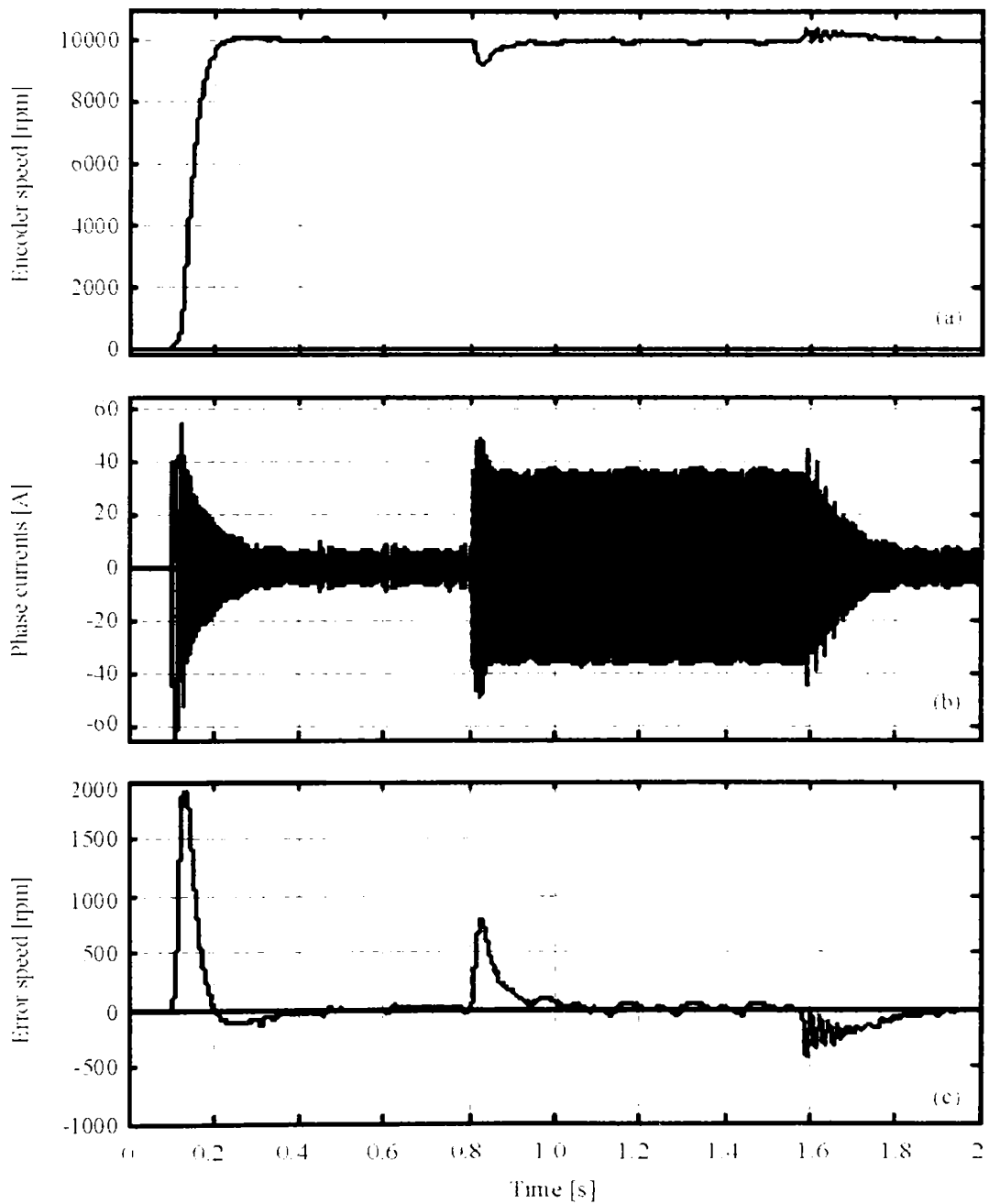


Fig. 5.8 No load start-up at 10,000 rpm followed by loading at 80% of rated torque at 0.8 s and unloading at 1.6 s: a) Encoder speed; b) Three phase currents; c) Speed error between encoder & required speed.

At 0.8s (Fig. 5.8) the motor is loaded with the rated torque value. Notice that, using the proposed control system, the motor accepts a load larger with 8 % than using the vector control in [18]. For the vector control system, when the mentioned load was reached, the motor lost synchronization due to unacceptable errors in rotor position  $\theta_{er}$ .

When the unloading occurs (at 1.6 s in Fig. 5.8) the speed oscillations are there, but they are quickly attenuated. The speed errors are acceptable and similar to the ones obtained using the vector control system [18].

The torque transients corresponding to the best results given in Fig. 5.8 are shown in Fig. 5.9. The torque response is very fast at 0.8 s. The torque oscillations, due to unloading process lead to oscillations in speed (see Fig. 5.8c). The step load torque is only 90% from the rated torque.

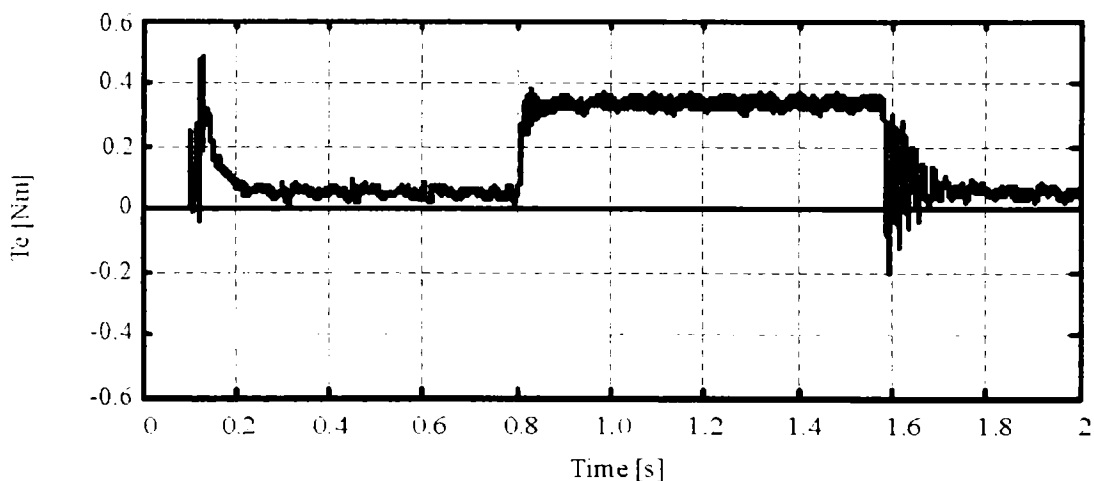


Fig. 5.9 Electromagnetic torque transients during tests in Fig. 5.8.

### 5.6.2. On Load Start-Up at and Speed Reversal at +10,000 rpm

Experiments at negative speeds have been also done, in order to demonstrate that the machine operates in the opposite direction too. Moreover, the startup in this direction has been done with the machine loaded (see Fig. 5.10). The system starts up with load proportional to speed from 0 to +10,000 rpm. The step load torque at 1 s is followed by a speed reversal from -10,000 rpm to +10,000 rpm at 1.6 s. The encoder speed presented in Fig. 5.10a is the machine real speed.

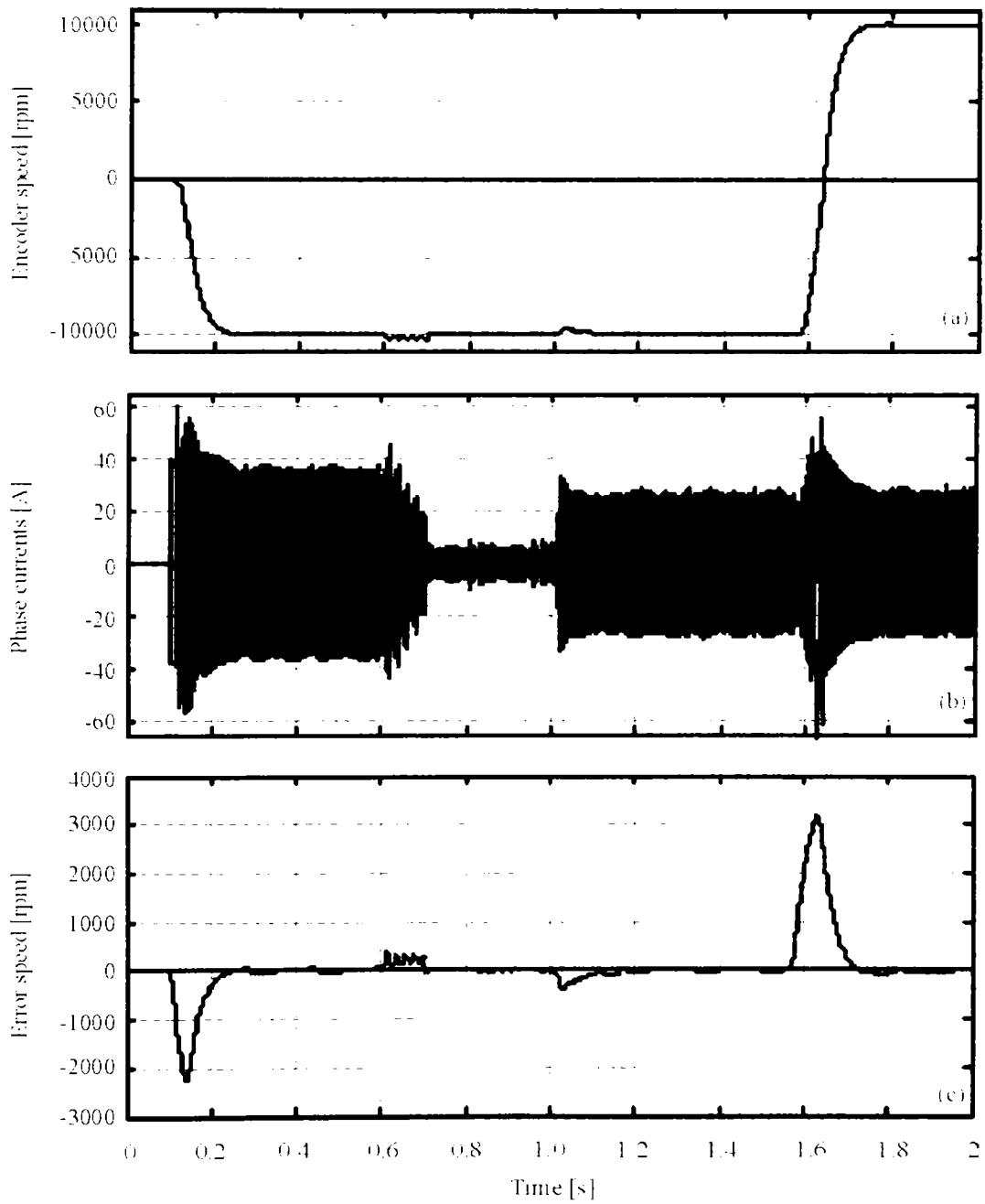


Fig. 5.10 On load start-up at -10,000 rpm followed by unloading at 0.6 s, reloading at 60 % of rated torque at 0.8 s, speed reversal from -10,000 rpm to 10,000 rpm at 1.4 s: a) Encoder speed; b) Three phase currents; c) Speed error between encoder & reference speed

For speed reversal operation, the machine is loaded only at 60% of rated torque value. This value could not be exceeded (see Fig. 5.11), for reasons still under investigation.

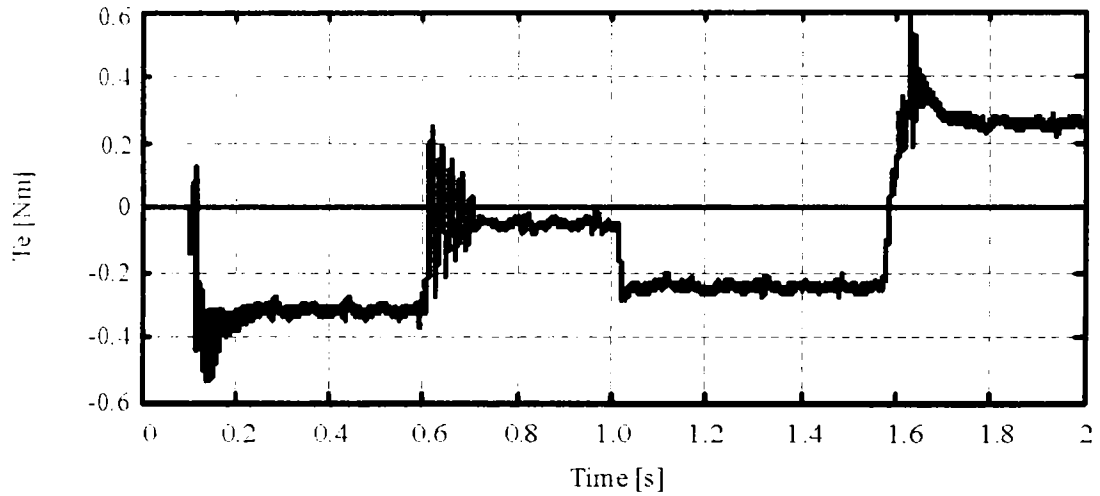


Fig. 5.11 Electromagnetic torque transients during tests in Fig. 5.10.

In Fig. 5.12, when the machine operates as generator, serious problems occur: at 0.6 s when the machine is abruptly unloaded, the current amplitude is not decreasing fast enough ( $i_d$  is not kept zero) and at 1.6 s, when the speed reversal occurs, the current amplitude is large again and thus the current protection has to be adjusted not to act in these conditions.

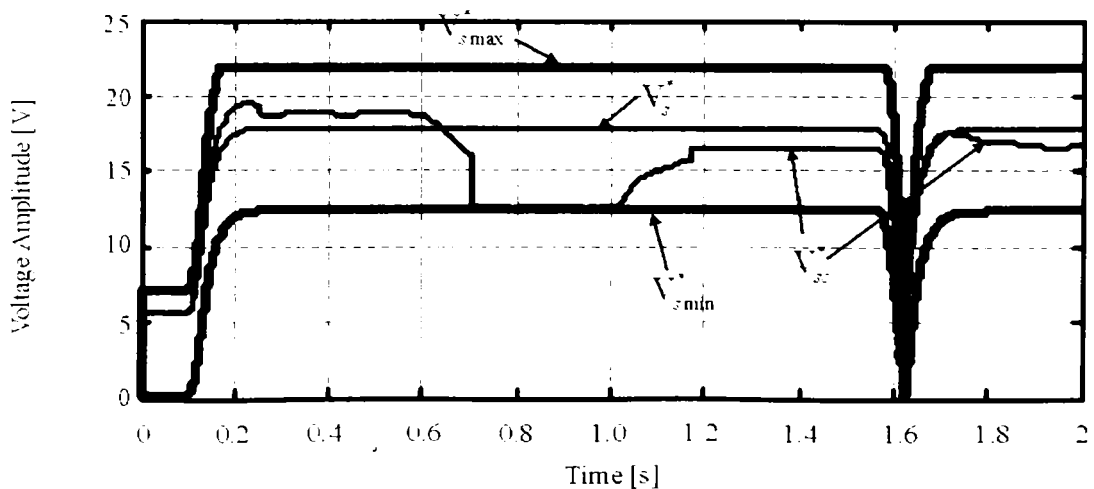


Fig. 5.12 Voltage amplitudes during dynamic tests in Fig. 5.10.

Around zero speed, instability occurs if operation with  $I_d=0$  is performed [27]. To avoid this and, thus, to secure safe speed reversal, the internal reactive power  $Q'_{\alpha\beta}$  signal was reduced when reference speed ramping was negative. This means that implicit positive  $I_d$  running was allowed.

In Fig. 5.12 the voltages amplitudes are presented.  $V_{s\max}^*$  and  $V_{s\min}^*$  are the voltage dynamic limitations.  $V_s^*$  is the voltage prescribed from the standard V/f control and  $V_{sc}^*$  is the real voltage amplitude applied to the control system.

It can be observed that the reference voltage  $V_s^*$  is notably adjusted by the control system to  $V_{sc}^*$  value. It is very important that this voltage never will be negative and also that it will not exceed the allowable maximum value for a given speed. These limitations were analytically computed from the feedforward loops of the vector control system, taking into account the  $I_d$  current which has to be zero:

$$\begin{aligned} V_{d\_ff}^* &= -L_s \omega_{er} i_q^* \\ V_{q\_ff}^* &= L_s \omega_{er} i_d^* + \omega_{er} \lambda_{PM} \end{aligned} \quad (5.7)$$

where  $V_{d\_ff}$  and  $V_{q\_ff}$  are the feedforward voltage corrections.

The most sensitive experimental test is the speed reversal operation (Fig. 5.10). For this experiment, the voltage has to be reduced close to zero, because the machine starts to operate as generator, and once the speed crosses zero, the voltage has to be increased. This increase is somehow artificial, because we also have to take into account that the internal reactive power  $Q'_{\alpha\beta}$  gives rather erroneous information for a short period of time. Thus, the control system operates properly if the voltage is large at the beginning and, after that, slowly reduced. This also may explain why, during transients, the currents amplitudes are rather large. Fig. 5.14 shows the effect of the amplitude and angle stabilizing loops controllers.

Fig. 5.13 illustrates the internal reactive power used in the control system during the tests in Fig. 5.10. The real power has large oscillations so it can not be used in the control. This is why it has to be filtered. In the same figure the filtered internal reactive power which is used in control is also presented. It can be observed that only when the filtered power is zero the motor speed reaches the reference speed.

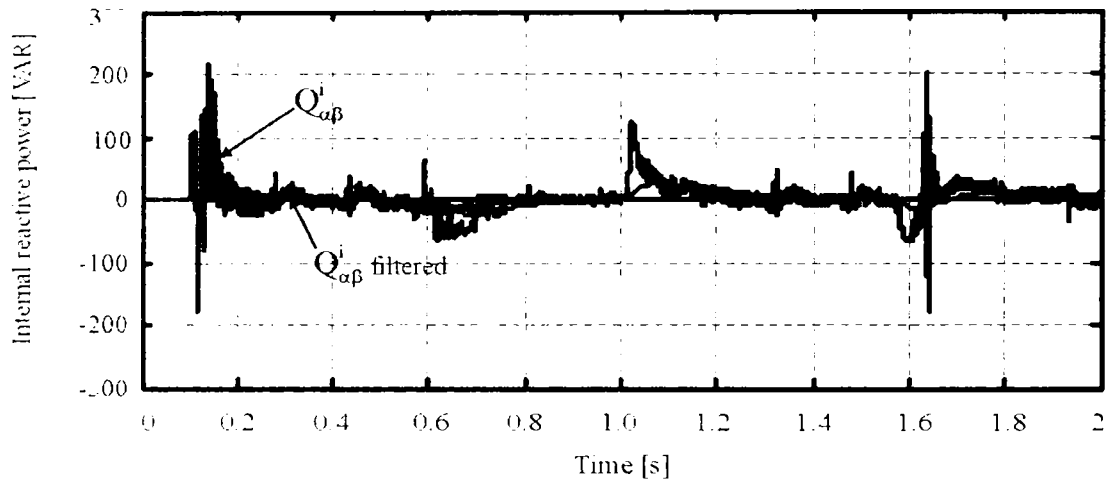


Fig. 5.13 Real and filtered internal reactive power during dynamic tests in Fig. 5.10.

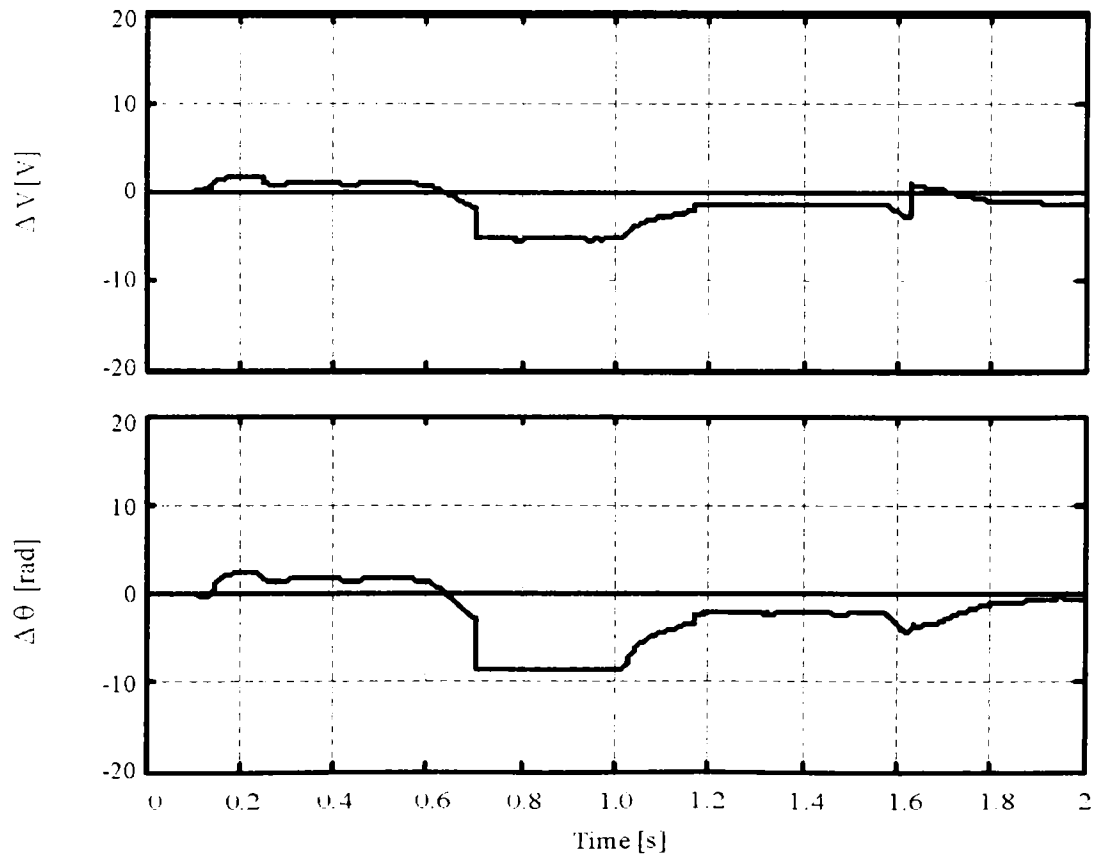


Fig. 5.14 Voltage amplitude and phase intervention of stabilizing loops regulators during dynamic tests in Fig. 5.10



Both corrections in Fig. 5.14 are rather similar, which means that, when the voltage vector  $\vec{V}_s^*$  is accelerated, a change in the voltage amplitude also occurs. There is still room for further investigation towards a good compromise between very good starting and performing running, with load perturbations.

With the proposed control system, the machine operates properly even at speeds higher than 10,000 rpm. If the sensorless vector control can have problems at speeds higher than 12,000 rpm, the proposed V/f control system with two stabilizing loops operates well at this speed.

However, the tested machine was build for high speeds. In these conditions, it was considered sufficiently to operate at machine rated speed. Only two experimental tests were realized at speeds over 10,000 rpm.

Thus, in the first test only 75 % of the rated speed was achieved, while in the second test the rated speed was attained.

The startup test from 0 to 15,000 rpm allowed the machine loading in same conditions as in the test presented in Fig. 5.10.

The startup test from 0 to 20,000 rpm was possible only in the no load condition because loading supposes having a larger voltage in the inverter dc link.

### 5.6.3. No Load Start-Up to 15,000 rpm

The experimental tests demonstrate that the drive is properly working even at high speeds.

The same experimental tests, in the same conditions, using the vector control were realized in Chapter 3.

The system starts up with no load from 0 to +15,000 rpm. Then the machine is loaded with a step load torque at 0.8s. The encoder speed presented in Fig. 5.15a is the machine real speed.

Fig. 5.15c illustrates the error between reference and actual speed. Notice that this error is not larger than 2500 rpm, which is very good.

Almost the same problems regarding the oscillations in the speed and currents waveforms can be observed in Chapter 3 (Fig. 3.12 and Fig. 3.13).

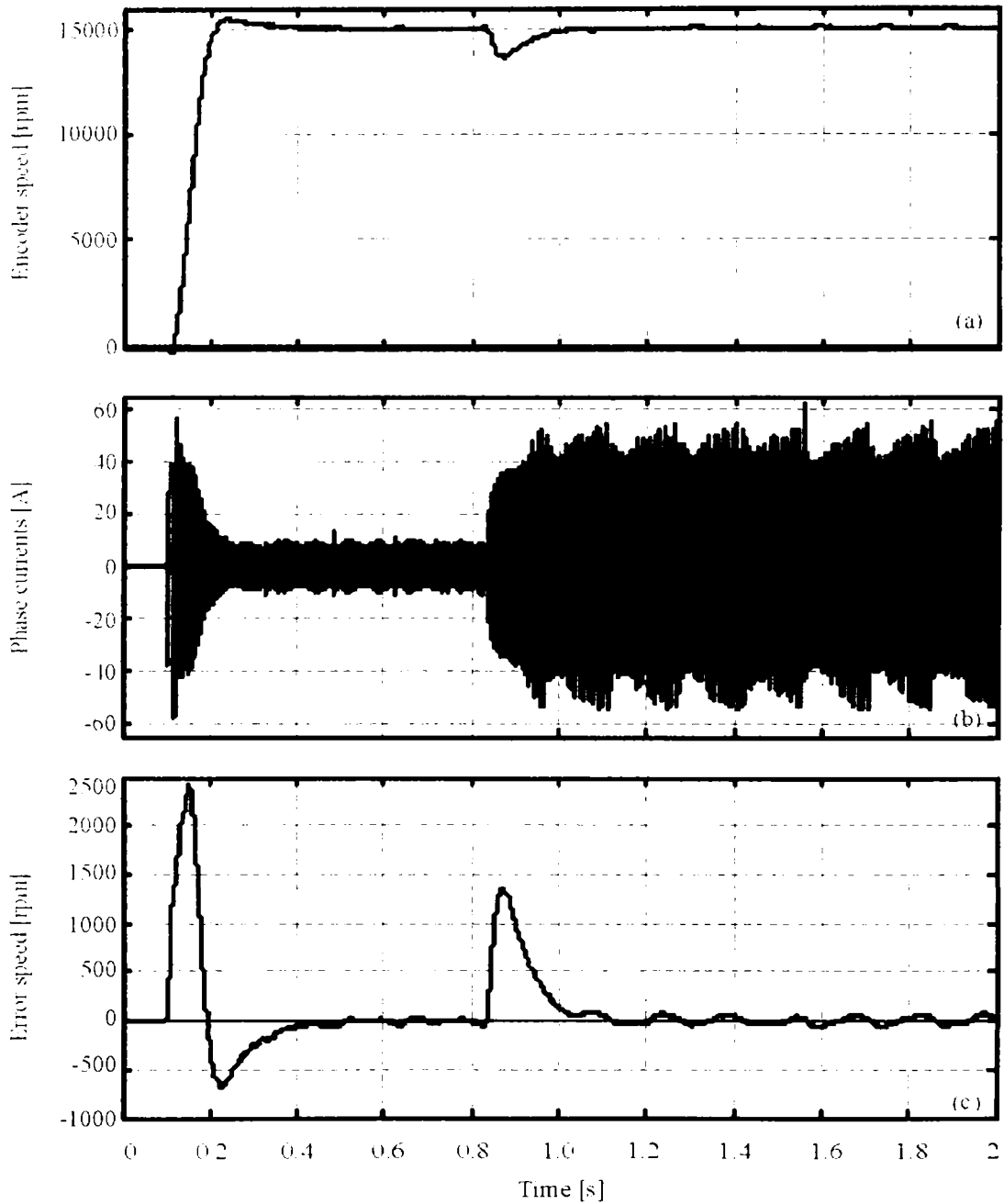


Fig. 5.15 Unload start-up at 15,000 rpm and loading at 80% of rated torque at 0.8 s:

a) Encoder speed; b) Three phase currents; c) Speed error between encoder & require speed

Fig. 5.16 illustrates the effect of the loop modifying the voltage amplitude. As it can be observed, the control system uses at startup and immediately after, the

same voltage as the standard V/f control prescribes. The next step is to regulate the voltage amplitude by decreasing it. As it was mentioned before, this could be done by accelerating the voltage vector.

As Fig. 5.16 shows, when a load occurs, automatically the voltage vector is increased.

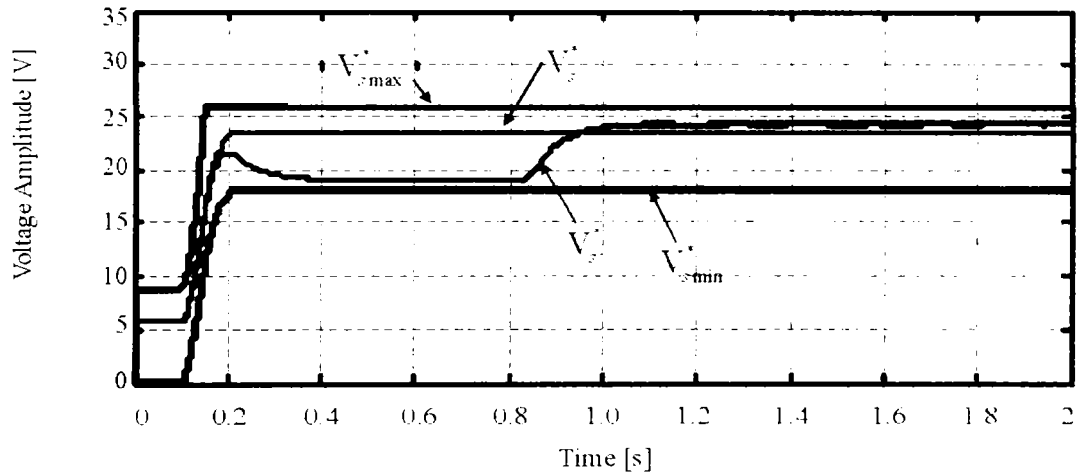


Fig. 5.16 Voltage amplitudes during dynamic tests in Fig. 5.15.

#### 5.6.4. No Load Start-Up to 20,000 rpm

The difficult test was to achieve the rated speed of 20,000 rpm. During the test the machine was driven in the same conditions as the ones described in Chapter 3 using the vector control.

As it can be seen in Fig. 5.17b, at this speed the control has some problems. Thus, the current waveforms are not perfectly sinusoidal, having some additional oscillations.

Fig. 5.17a illustrates no load system startup from 0 to +20,000 rpm. The encoder speed presented in Fig. 5.17a is the machine actual speed.

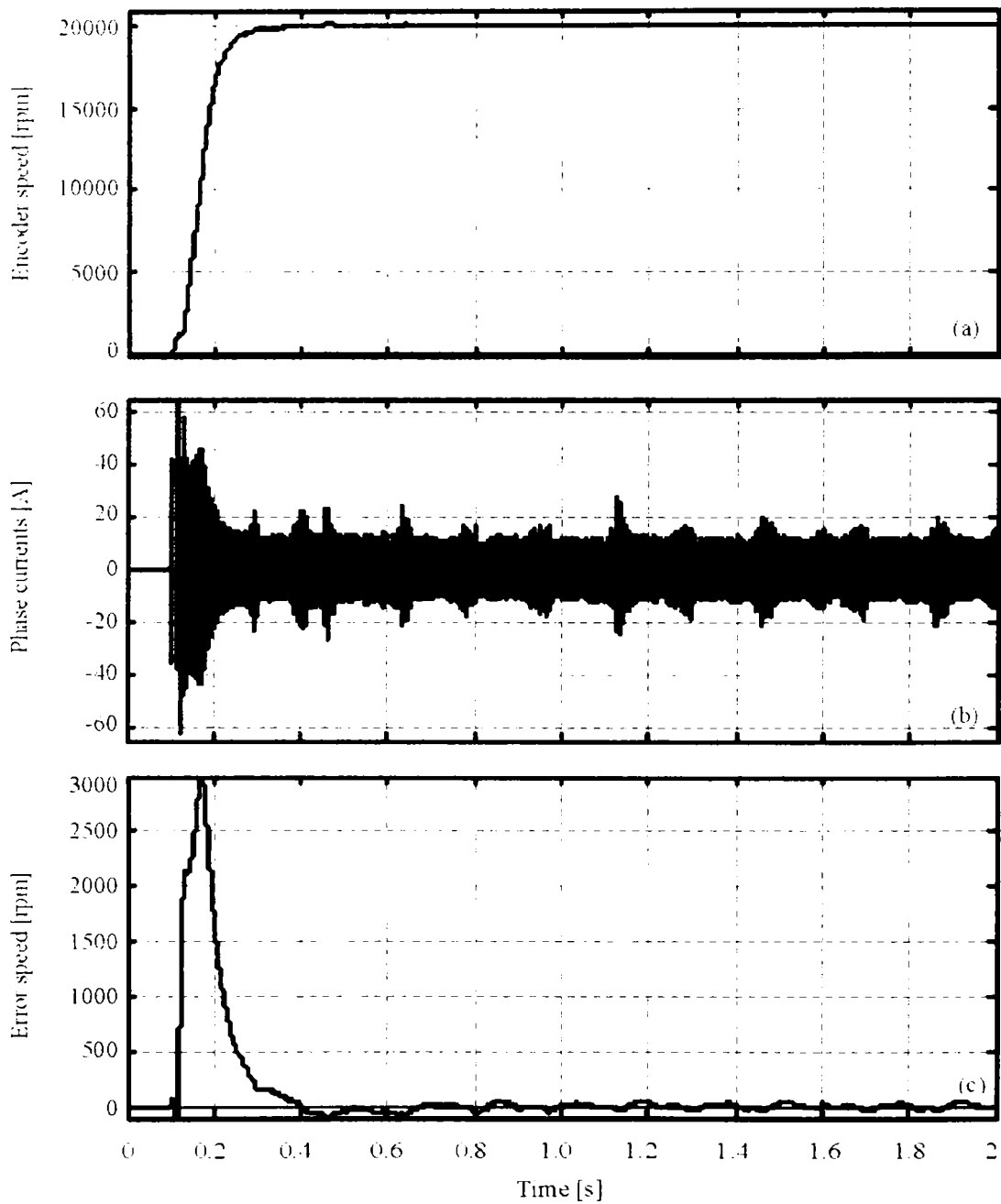


Fig. 5.17 Unload start-up at 20,000 rpm:

a) Encoder speed; b) Three phase currents; c) Speed error between encoder & require speed

It has to be noticed that, for 10,000 rpm over speed, the motor could not be driven using the standard V/f control due to the oscillations presence causing the motor stop. The motor performance over 20,000 rpm has to be remarked.

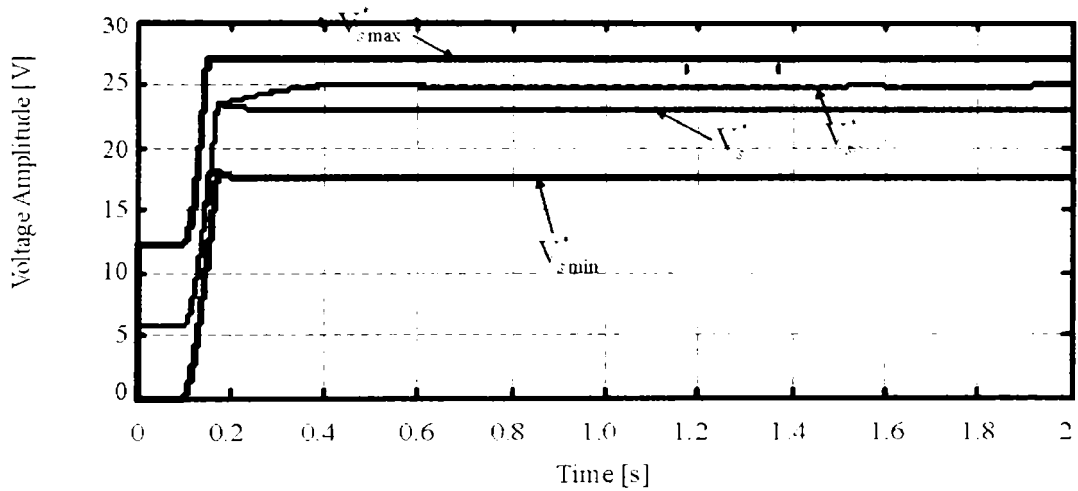


Fig. 5.18 Voltage amplitudes during dynamic tests in Fig. 5.17.

Fig. 5.18 presents how the voltage amplitude is controlled while Fig. 5.19 shows the way the voltage vector  $\vec{V}_s^*$  is accelerated.

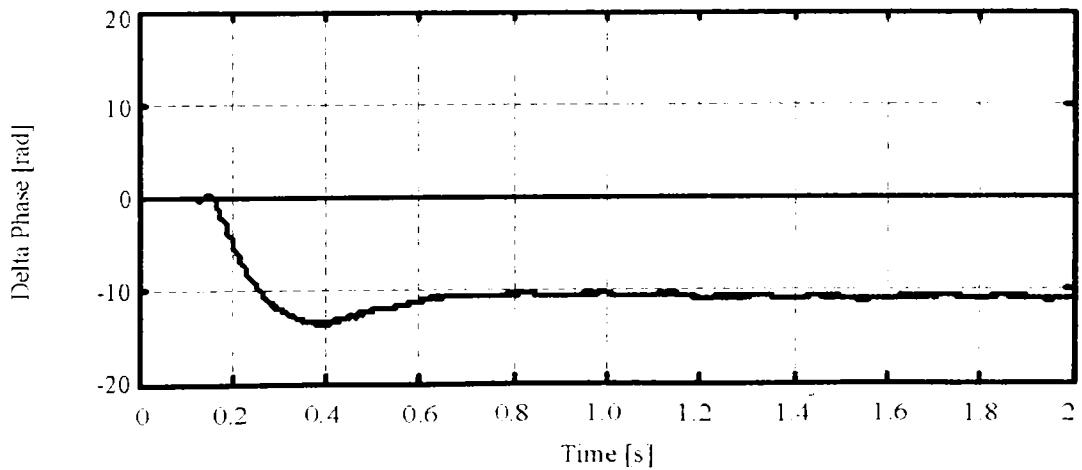


Fig. 5.19 Phase intervention of stabilizing loops regulators during dynamic tests in Fig. 5.17.

### **5.6.5. No Load Start-Up to 2,000 rpm and Speed Reversal with Step Torque Load**

Low speed operation represents a challenge for both standard sensorless vector control and proposed control system. However, the standard V/f control operates rather properly at low speed if fast load torque variation does not occur, but the current amplitudes are large, so the efficiency is decreased. Vector control operates properly at low speed when using an encoder. Even if the experiments were conducted down to 2,000 rpm only for making a comparison with the vector control system (see Fig. 5.20), the proposed control system was tested and can operate adequately down to 1,200 rpm.

The first event in Fig. 5.20 is acceleration up to 2,000 rpm. The ripples in currents and speed waveforms at low speed are larger than the ones obtained at high speed (20,000 rpm). At 0.6 s the motor is instantly loaded at 25% rated torque. At 1.2 s a speed reversal occurs. Fig. 5.20c show that the speed error during speed transients is quite large. The final test involves removing the load at 1.8 s.

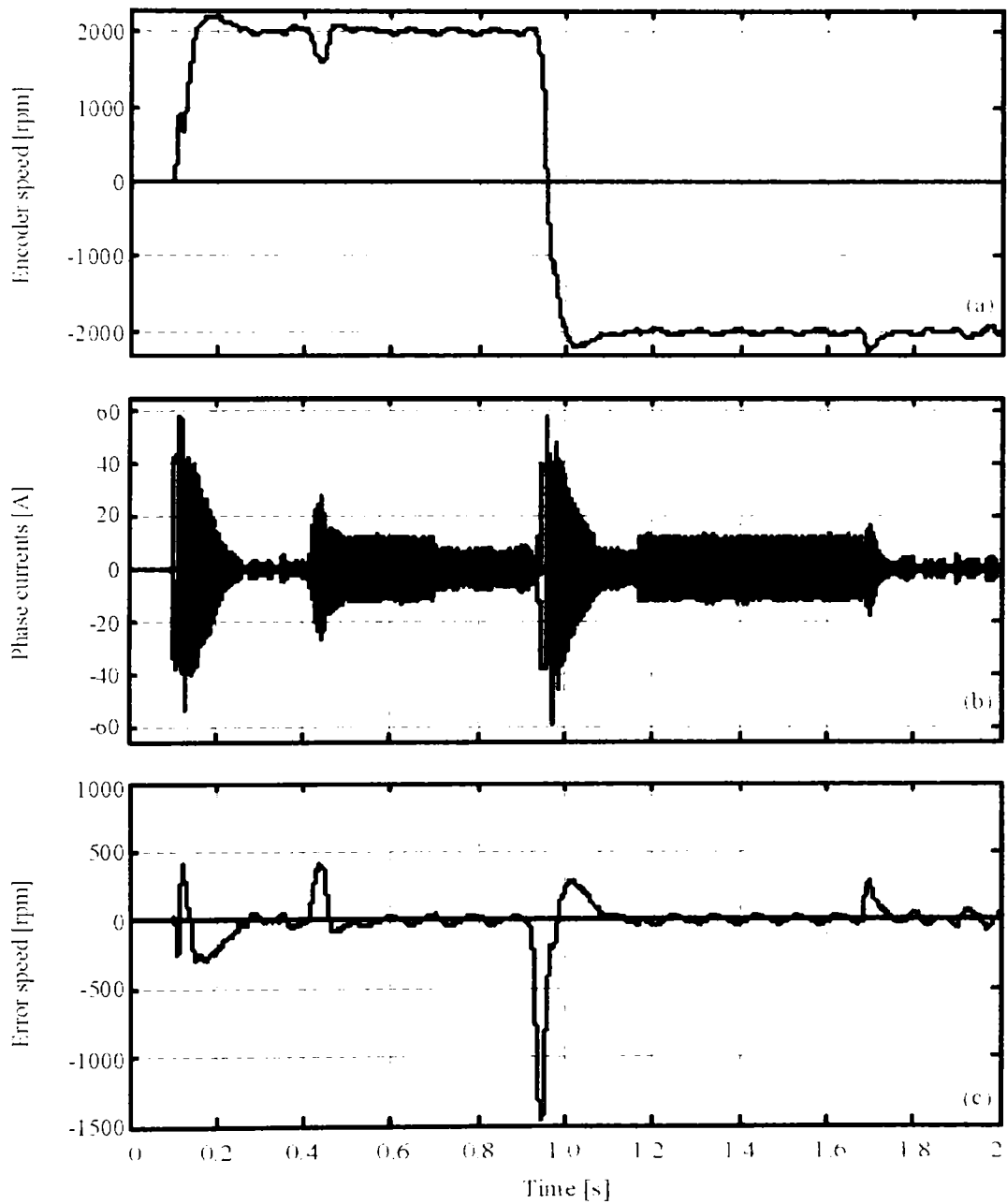


Fig. 5.20 Unload start-up at 2,000 rpm, loading at 80% of rated torque at 0.6 s, reverse speed from 2,000 rpm to -2,000 rpm at 1.2 s:

a) Encoder speed; b) Three phase currents; c) Speed error between encoder & required speed

Finally, fast speed reduction from 10,000 rpm to 5,000 rpm is demonstrated in Fig. 5.21.

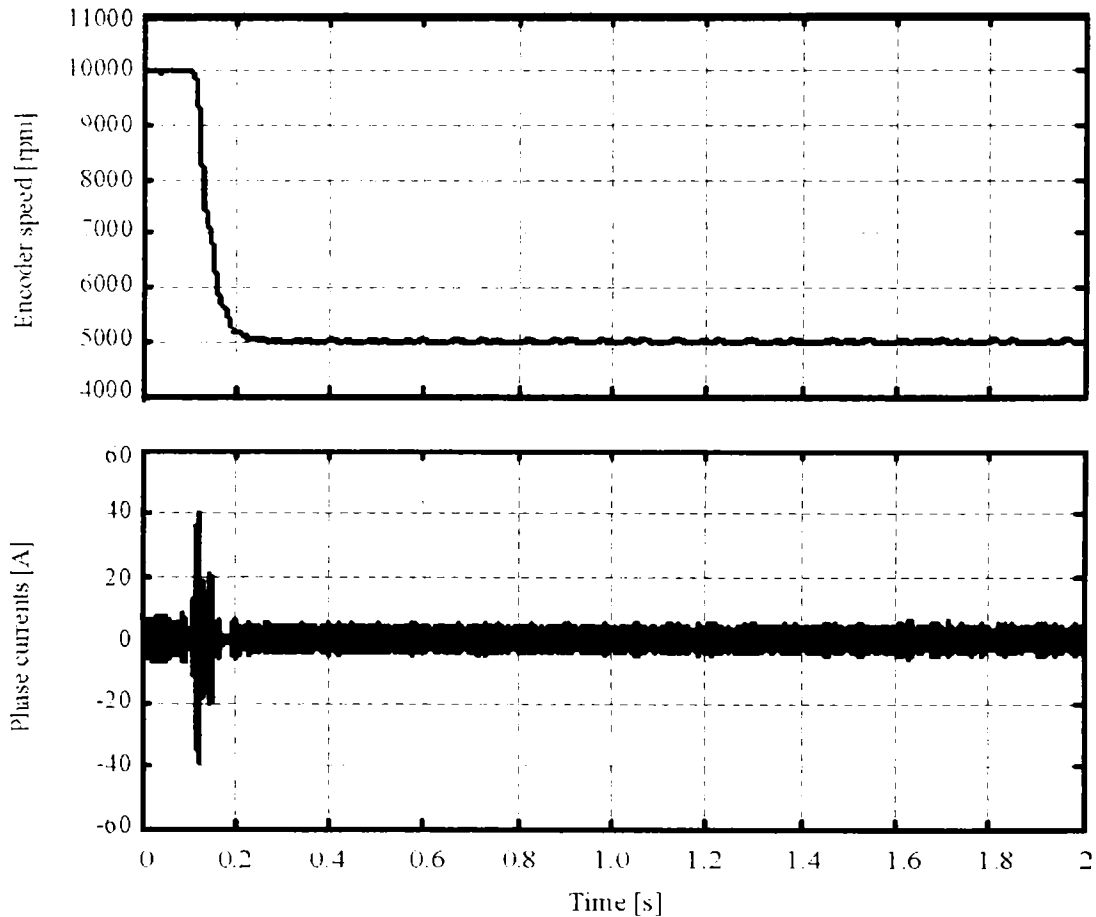


Fig. 5.21 Fast speed reductions test from 10,000 rpm to 5,000 rpm

## 5.7. Conclusion

A novel sensorless control system for high-speed SPMSM is proposed based on two stabilizing loops to correct the voltage amplitude and phase in V/f control by using a close loop for zero interior reactive power.

The advantages are the following:

- the torque and speed responses are fast;



- the online computation time cycle is shorter than the one of the sensorless vector control by using only the  $\alpha\beta$  coordinates;
- the motor can start from any rotor position;
- the motor operates without a speed loop or current controllers, for simplicity and robustness;
- the method does not ask for rotor position and speed estimators;
- the method is not influenced by the stator resistance value at all;
- the machine inductance does not have to be known exactly;
- the speed dynamics and steady state errors, operating with approximate parameter values, are comparable with those of sensorless vector control results, which operates, however, well with more exact parameters;
- no dc voltage or speed sensors are required;

## Appendix

TABLE 5.1.

GAINS USED IN REAL CONTROL

PI $\Delta V$ controller Fig. 5.4		$k_{p_v}$	10
		$k_{i_v}$	0.3
PI $\Delta\theta$ controller Fig. 5.4		$k_{p_\theta}$	10
		$k_{i_\theta}$	0.5
Voltage LPF Fig. 5.4	$\frac{1}{k_F s + 1}$	$k_{FV}$	0.1
Angle LPF Fig. 5.4		$k_{F\theta}$	0.1
			10 (used in speed reversal)

## References

- [1] C. Zwyssig, S.D. Round, and J.W. Kolar, "An Ultrahigh-Speed, Low Power Electrical Drive System," *IEEE Trans on Ind. Electron.*, vol. 55, Feb. 2008, pp. 577–585.
- [2] J. Oyama, T. Higuchi, T. Abe, K. Shigematsu, X. Yang, and E. Matsuo, "A trial production of small size ultra-high speed drive system," in *Proc. IEEE IEMDC'03*, June 2003, vol. 1, pp. 31–36.
- [3] R. M. Kennel, "Ultra high speed drive with permanent magnet synchronous motors and hardware based field orientated control," in *Proc. ACEMP-Electromotion'07*, Bodrum, Turkey, Sept. 2007, pp. 116–124.
- [4] L. Zhao, C. Ham, L. Zheng, T. Wu, K. Sundaram, J. Kapat, and L. Chow, "A highly efficient 200 000 rpm permanent magnet motor system," *IEEE Trans. Magnetics*, vol. 43, no. 6, pp. 2528–2530, June 2007.
- [5] Y. Nakamura, T. Kudo, F. Ishibashi, and S. Hibino, "High-efficiency drive due to power factor control of a permanent magnet synchronous motor," *IEEE Trans. Power Electron.*, vol. 10, pp. 247–253, Mar. 1995.
- [6] K. Suzuki, S. Saito, T. Kudor, A. Tanaka, and Y. Andoh, "Stability improvement of V/f controlled large capacity voltage-source inverter fed induction motor," in *Conf. Record IEEE-IAS 2006*, vol. 1, pp. 90–95, Oct. 2006.
- [7] P. D. C. Perera, F. Blaabjerg, J. K. Pedersen, and P. Thogersen, "A sensorless, stable V/f control method for permanent-magnet synchronous motor drives," *IEEE Trans. Ind. Appl.*, vol. 39, no. 3, pp. 783–791, May/Jun. 2003.
- [8] L. B. Brahim, "Improvement of the stability of the V/f controlled induction motor drive systems," in *Proc. IEEE-IECON'98*, Sept. 1998, vol. 2, pp. 859–864.
- [9] L. Zhao, C. H. Ham, Q. Han, T. X. Wu, L. Zheng, K. B. Sundaram, J. Kapat, and L. Chow, "Design of an optimal V/f control for a super high speed permanent magnet synchronous motor," in *Proc. IEEE-IECON 2004*, Nov. 2004, vol. 3, pp. 2260–2263.
- [10] Jee-Hoon Jung, Gang-Youl Jeong, and Bong-Hwan Kwon, "Stability improvement of V/f-controlled induction motor drive systems by a dynamic

- current compensator," *IEEE Trans. Ind. Electron.*, vol. 51, no. 4, pp. 930–933, Aug. 2004.
- [11] R. S. Colby and D. W. Novotny, "An efficiency-optimizing permanent-magnet synchronous motor drive," *IEEE Trans. Ind. Appl.*, vol. 24, no. 3, pp. 462–469, May-June 1988.
- [12] R. Ancuti and I. Boldea, "V/f control of PM-SM super high speed drives with flux and power angle stabilizing loops," in *Conf. Record OPTIM 2006*, Brasov, May 2006, vol. 3.
- [13] H. Luo, Q. Wang, X. Deng and S. Wan, "A novel V/f scalar controlled induction motor drives with compensation based on decoupled stator current," in *Proc. Industrial Technology Conf. IEEE-ICIT 2006*, Dec. 2006, pp. 1989–1994.
- [14] L. Xu and C. Wang, "Implementation and experimental investigation of sensorless control scheme for PMSM in super-high variable speed operation," in *Conf. Rec. IEEE-IAS 1998*, Oct. 1998, vol. 1, pp. 483–489.
- [15] B.-H. Bae, S.-K. Sul, J.-H. Kwon, and J.-S. Byeon, "Implementation of sensorless vector control for super-high-speed PMSM of turbo-compressor," *IEEE Trans. Ind. Appl.*, vol. 39, no. 3, pp. 811–818, May/June 2003.
- [16] J.-I. Itoh, N. Nomura, and H. Ohsawa, "A comparison between V/f control and position-sensorless vector control for the permanent magnet synchronous motor," in *Proc. Power Conversion Conf. PCC Osaka 2002*, April 2002, vol. 3, pp. 1310–1315.
- [17] T. Halkosaari, "Optimal U/f-control of high speed permanent magnet motors," in *Proc. IEEE Industrial Electronics Symposium ISIE 2006*, July 2006, vol. 3, pp. 2303–2308.
- [18] R. Ancuti, I. Boldea, G.-D. Andreescu, and D. Iles-Klumpner, "Novel motion sensorless control of high-speed small-power surface mount PMSM drives: With experiments," in *Proc. OPTIM 2008*, Brasov, May 2008, vol. 3, pp. 11-18.
- [19] Y. S. Kim, Y. K. Choi, and J. H. Lee, "Speed-sensorless vector control for permanent-magnet synchronous motors based on instantaneous reactive power in the wide-speed region," *IEEE Proc.- Electr. Power Appl.*, vol. 152, no. 5, pp. 1343–1349, Sept. 2005.

- [20] Maiti, S.; Chakraborty, C.; "Reactive Power Based Speed Sensorless Controller for Permanent Magnet Synchronous Motor Drive" IEEE Industrial Technology, ICIT 2006. 15-17 Dec. 2006 pp. 247 – 252
- [21] Hyoung-Seok Kang; Young-Seok Kim; "A Sensorless Speed Control of an Interior Permanent Magnet Synchronous Motor based on an Instantaneous Reactive Power and a fuzzy logic controller" IEEE Power Electronics Specialists Conference, PESC . June 2006 pp. 1 - 7
- [22] Viawan, F.A.; Karlsson, D.; "Voltage and Reactive Power Control in Systems With Synchronous Machine-Based Distributed Generation Power Delivery", IEEE Trans. April 2008 pp. 1079 - 1087
- [23] \*\*\*\* "Transient angular stability of three parallel connected synchronous generators with large load changes and control of active and reactive power" OPTIM, May 2008 pp. 131 - 136
- [24] Jasinski, Marek; Swierczynski, Dariusz; Kazmierkowski, Marian P.; "Direct Active and Reactive Power Control of AC/DC/AC Converter with Permanent Magnet Synchronous Generator for Sea Wave Converter" Power Engineering, Energy and Electrical Drives, POWERENG 2007. 12-14 April 2007 pp. 78 - 83
- [25] Zou Ji-yan; Ding Fu-hua; Duan Xiong-ying; "An intelligent reactive power compensator based on synchronous vacuum circuit breaker" Discharges and Electrical Insulation in Vacuum, ISDEIV. Sept. 27 - Oct. 1, 2004 pp. 354 - 358
- [26] D. W. Novotny and T. A. Lipo, "d, q modeling of induction and synchronous machines," in *Vector Control and Dynamics of AC Drives*, ch. 2, Oxford Univ. Press, London, UK, 1998.
- [27] M. Jansson, L. Harnefors, O. Wallmark, and M. Leksell, "Synchronization at startup and stable rotation reversal of sensorless nonsalient PMSM drives," *IEEE Trans. on Ind. Electron.*, vol. 53, , no. 2, pp. 379–387, April 2006.
- [28] R. Ancuti, I. Boldea, G. D. Andreescu "Sensorless V/f Control of Surface PMSM with Two Novel Stabilizing Loops for High Speed Dynamics" will be publish at IEEE TEC.

# Chapter 6

## The test bench setup

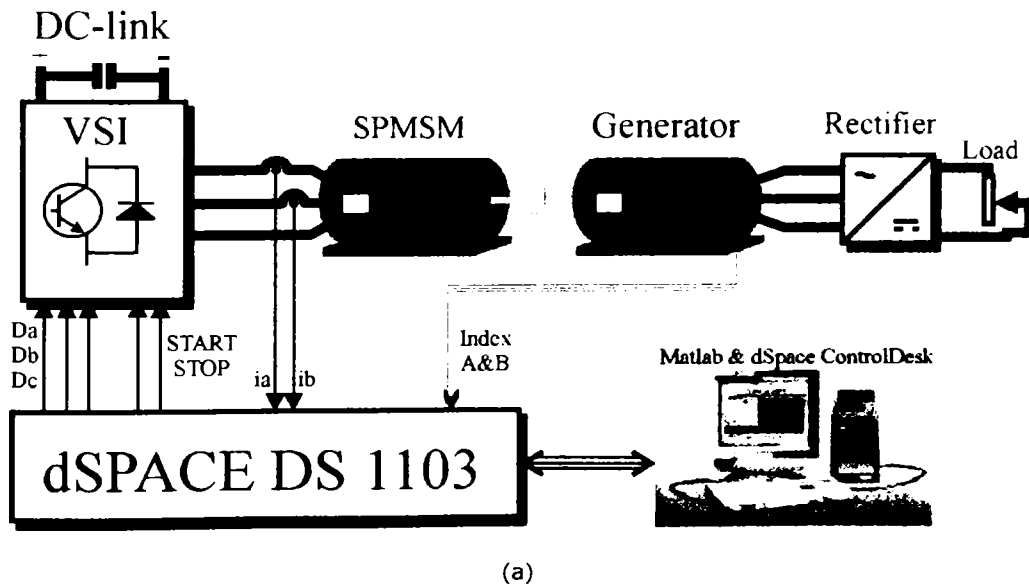
### Abstract

This chapter deals with the extended description of the laboratory setup used for all the tests presented in Chapters 3 and 5.

It was build up in the Intelligent Motion Control Lab, Faculty of Electrical Engineering Timisoara, with the intended purpose to prove that simulated control algorithms related to the high speed PMSM are really working.

### 6.1. Introduction

The schematic principle of the test bench setup is presented in Fig. 6.1a. The setup consists of two identical 0.8 kW, 20,000 rpm, 4 pole SPMSMs with sinusoidal back-emf which are mechanically coupled (Fig. 6.1b).



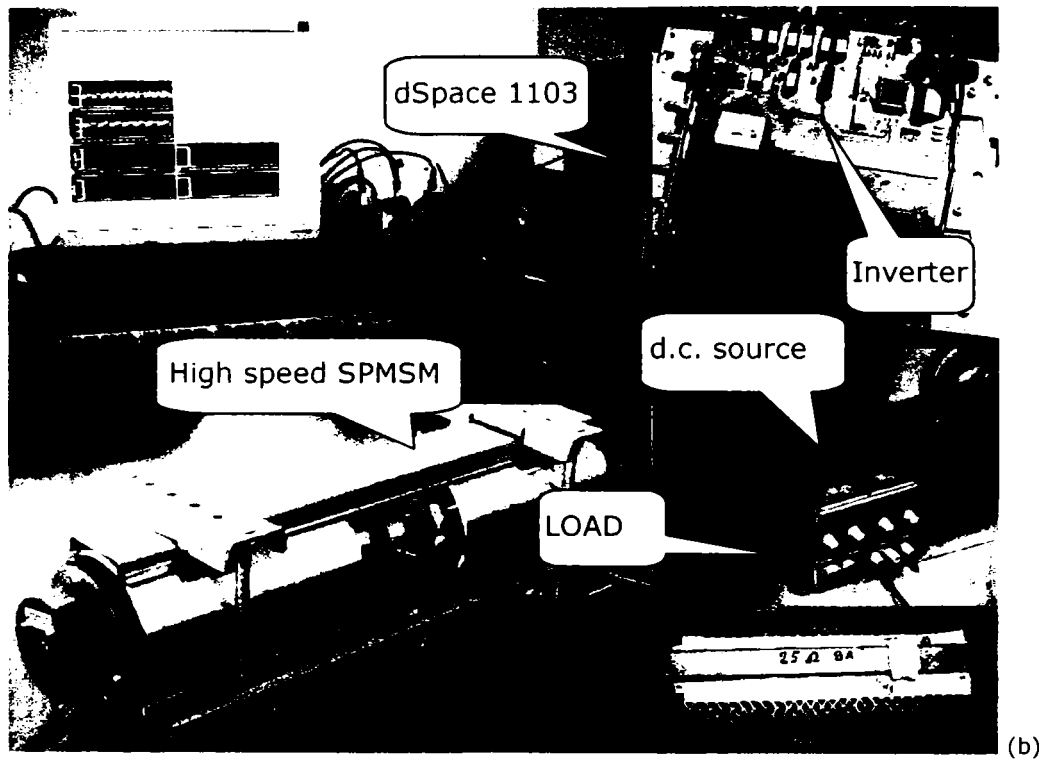


Fig. 6.1 Experimental system setup for high speed SPMSM

a) the scheme b) the actual setup containing in the two identical SPMSM, batteries, inverter and the dSpace platform.

The motor data are presented in TABLE 6.1. The motor is fed by a 50V/300A MOSFET inverter with 20 kHz switching frequency. The encoder has 500 pulses-per-revolution and provides the actual rotor position and speed only for comparisons. All control algorithms, using 10 KHz sampling frequency, are developed in Matlab-Simulink and implemented on a dSpace platform.

## 6.2. Hardware specifications

### 6.2.1. The twin permanent magnet synchronous machines

The main components of the system are the twin high speed SPMSM motors manufactured by Ebm Papst, Germany. These motors were assembled in our Intelligent Motion Control Lab, Faculty of Electrical Engineering Timisoara.

The motors are 2-poles machines, star connected in the stator. In the rotor the machine has rare earth permanent magnets. The nominal stator voltage is 30 V and the nominal current is  $I_n = 28.5$  A.

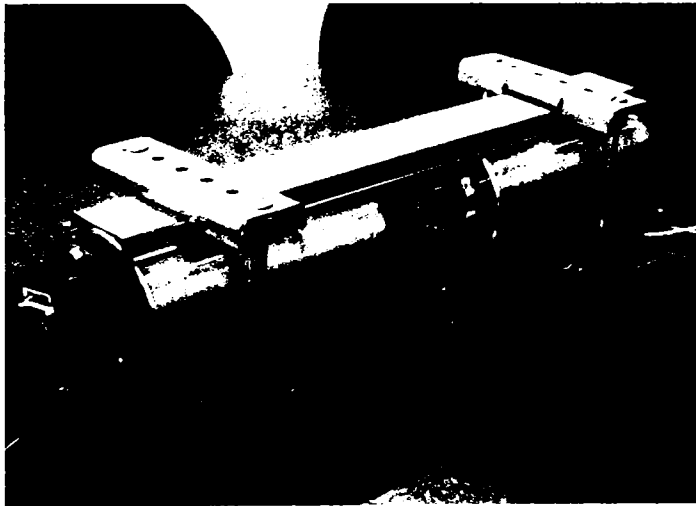


Fig. 6.2 High speed PMSM coupled machines: the motor and the generator used for load.

Each motor has attached two position sensors: an incremental encoder with 500 pulses-per-revolution, used as motor in the presented controls, and three Hall sensors, working together, which are cheaper than the encoder.

This gives the possibility to test each control with two different position sensors: the encoder or the Hall sensors.

TABLE 6.1.

## SPMSM SPECIFICATIONS

Number of pole pairs ( $p_1$ )	2
Rated speed	20,000 rpm
Rated frequency	667 Hz
Rated torque	0.4 Nm (at 20,000 rpm)
Rated phase to phase voltage	39 V(rms)
Rated phase current	29.5 A(rms) (at 20,000 rpm)
Stator resistance per phase ( $R_s$ )	0.083 $\Omega$
Inductance ( $L_s$ )	0.0425 mH
Rotor permanent-magnet ( $\lambda_{PM}$ )	0.00635 Vsrad <sup>-1</sup>
Inertia of rotating system ( $J$ )	40 <sup>*</sup> 10 <sup>-6</sup> kgm <sup>2</sup>
Viscous friction coefficient ( $B_m$ )	10 <sup>-6</sup> Nms/rad

## 6.2.2. dSpace DS1103

The **DS1103 PPC** is a very flexible and powerful system featuring both high computational capability and comprehensive I/O periphery [1]. Additionally, it features a software SIMULINK interface that allows all applications to be developed in the MATLAB ® /Simulink friendly environment. All compiling and downloading processes are carried out automatically in the background. Experimenting software, called Control Desk, allows real-time management of the running process by providing a virtual control panel with instruments and scopes (Fig. 6.3).



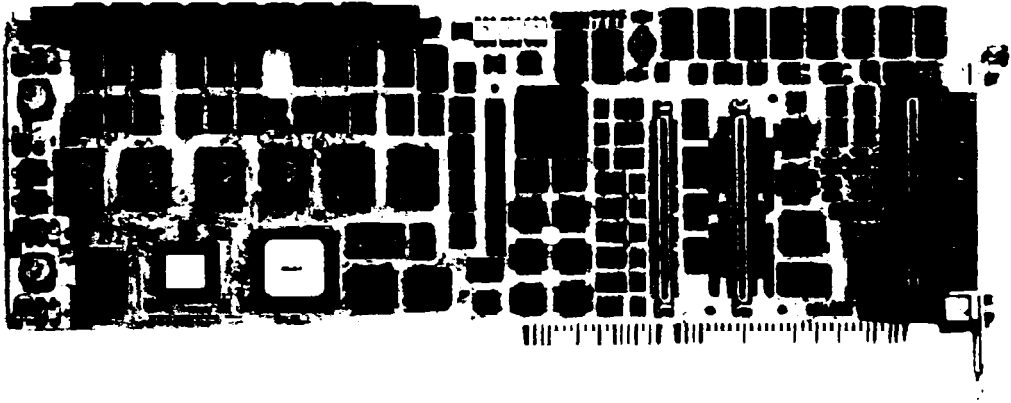
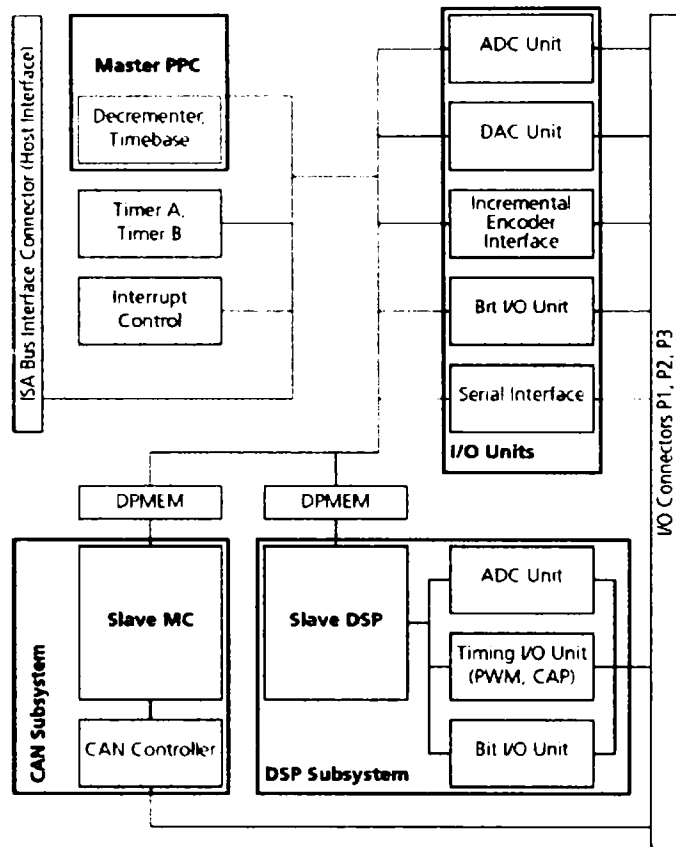


Fig. 6.3 The single board control system dSpace DS1103.

The DS1103 is a single board system based on the **Motorola PowerPC 604e/333MHz** processor (PPC), which forms the main processing unit.

Fig. 6.3 gives an overview of the functional units of the DS1103.



Legend:

ADC	Analog/Digital Converters
MC	CAN Microcontroller 80C164
CAP	Capture
DAC	Digital/Analog Converters
DPMEM	Dual-Port Memory
DSP	Digital Signal Processor TMS320F240
PPC	Power PC 604e Processor
PWM	Pulse Width Modulation

Fig. 6.4 DS1103 internal functional block diagram

### **6.2.2.1. I/O Units**

A set of on-board peripherals frequently used in digital control systems has been added to the PPC. They include: analog-digital and digital-analog converters, digital I/O ports (Bit I/O), and a serial interface. The PPC can also control up to six incremental encoders, in this way it allows the development of advanced controllers for robots.

### **6.2.2.2. DSP Subsystem**

The DSP subsystem, based on the Texas Instruments TMS320F240 DSP fixed-point processor, is especially designed for the control of electric drives. Among other I/O capabilities, the DSP provides 3-phase **PWM generation** making the subsystem useful for **drive applications**.

### **6.2.2.3. CAN Subsystem**

A further subsystem, based on Siemens 80C164 micro-controller (MC), is used for connection to a CAN bus.

### **6.2.2.4. Master PPC Slave DSP Slave MC**

The PPC has access to both the DSP and the CAN subsystems. Spoken in terms of inter-processor communication, the PPC is the master, whereas the DSP and the CAN MC are slaves.

The DS1103 PPC Controller Board provides the following features summarized in alphabetical order:

- **A/D Conversion**

ADC Unit providing:

- 4 parallel A/D-converters, multiplexed to 4 channels each, 16-bit resolution, 4  $\mu$ s sampling time,  $\pm 10$ V input voltage range
- 4 parallel A/D-converters with 1 channel each, 12-bit resolution, 800 ns sampling time  $\pm 10$ V input voltage range

Slave DSP ADC Unit providing:

- 2 parallel A/D converters, multiplexed to 8 channels each, 10-bit resolution, 6  $\mu$ s sampling time  $\pm 10$ V input voltage range

- **Digital I/O**

Bit I/O Unit providing:

- 32-bit input/output, configuration byte-wise

Slave DSP Bit I/O-Unit providing:

- 19-bit input/output, configuration bit-wise

- **CAN Support**

Slave MC fulfilling CAN Specifications 2.0 A and 2.0 B, and ISO/DIS 11898.

- **D/A Conversion**

DAC Unit providing:

- 2 D/A converters with 4 channels each, 14-bit resolution  $\pm 10$  V voltage range

- **Incremental Encoder Interface**

Incremental Encoder Interface comprising:

- 1 analog channel with 22/38-bit counter range,
- 1 digital channel with 16/24/32-bit counter range, and
- 5 digital channels with 24-bit counter range

- **Interrupt Control - Interrupt Handling.**

- **Serial I/O**

Serial Interface providing:

- standard UART interface, alternatively RS-232 or RS-422 mode.

- **Timer Services**

Timer Services comprising:

- 32-bit downcounter with interrupt function (Timer A),
- 32-bit upcounter with pre-scaler and interrupt function
- 32-bit downcounter with interrupt function (PPC built-in Decrementer)
- 32/64-bit timebase register (PPC built-in Timebase Counter).

- **Timing I/O**

Slave DSP Timing I/O Unit comprising:

- 4 PWM outputs accessible for standard Slave DSP PWM Generation,
- 3 x 2 PWM outputs accessible for Slave DSP PWM3 Generation and Slave DSP PWM-SV Generation,
- 4 parallel channels accessible for Slave DSP Frequency Generation, and
- 4 parallel channels accessible for Slave DSP Frequency Measurement (F2D) and Slave DSP PWM Analysis (PWM2D).

### 6.2.3. Position sensor

The PMSM motor was equipped with an incremental encoder to prove the sensorless position estimation techniques. The encoder has 500 pulses-per-revolution (ppr) and provides the real rotor position and speed (Fig. 6.5).

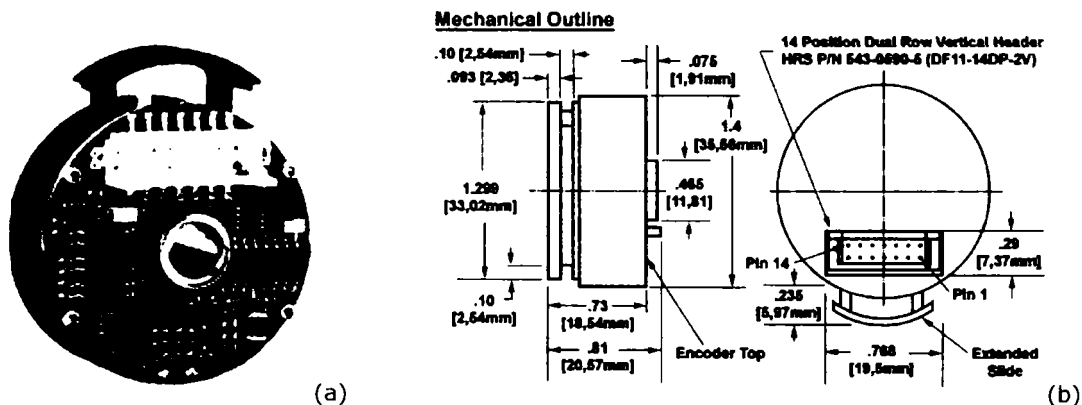


Fig. 6.5 Commutation encoder attached to the PMSM machines

(a) Encoder 3D Model (b) Mechanical outline

The device was a RENCO encoder type RCM15. The features of this encoder are:

- 2 data channels in quadrature
- Once around index marker pulse.
- 3 commutation channels optically & electrically isolated.
- RS-422 interface (data & comm.).
- Self aligning. Self centering. Self gapping.
- Frequency response to 300 KHz.
- Differential Index, commutation, and data channels.
- PC Board connector for easy installation.

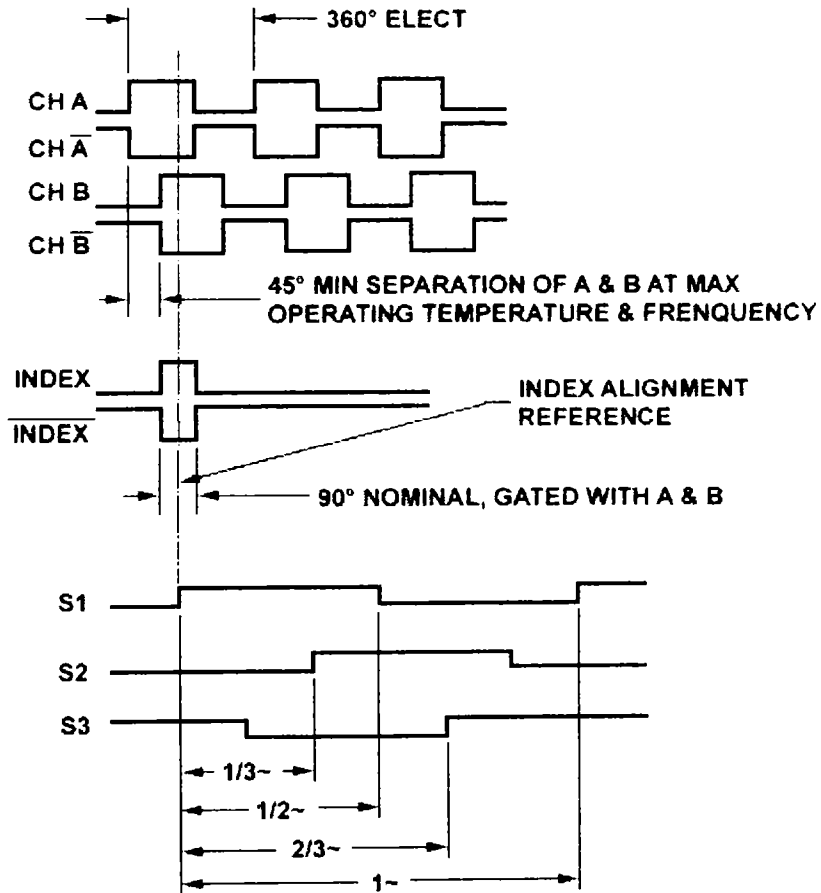


Fig. 6.6 Output configuration of the encoder

In the same time it is important to have the encoder datasheet which has to specify the position of the encoder output pins. Knowing the pins position the encoder can be attached to the controller device.

Pin	Function	Color Codes
1	CH A	Yel
3	CH A NOT	Wht/Yel
5	CH B	Blu
7	CH B NOT	Wht/Blu
9	INDEX	Orn
11	INDEX NOT	Wht/Orn
13	VCC	Red
14	GND	Blk
-----		
2	S1	Grn
4	S2	Brn
6	S3	Wht
8	GND2	
10	VCC2	
12	N/C	

Fig. 6.7 Output pins terminations (Refer to Mechanical Outline Drawing in Fig. 6.5b)

So the encoder provides differential RS442 signals (A+, A-, B+, B-, INDEX+, INDEX-) which can be directly connected to the control system. The dSpace platform can be connected to the encoder in differential mode (see Fig. 6.8) or in single-ended TTL mode (see Fig. 6.9).

This RENCO feature reduces the cost while improving the performance and reliability of the brushless motor/encoder package.

Any encoder should have at least three signals to be used in the control. This encoder has two data channels in quadrature and furthermore three Hall sensors as it can be seen in Fig. 6.6. So the device provides nine signals which can be used in the control.



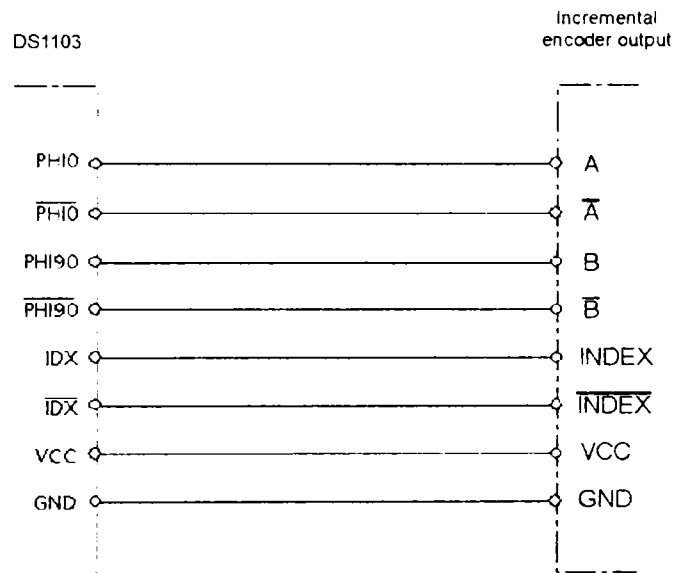


Fig. 6.8 Encoder providing differential RS422 signals

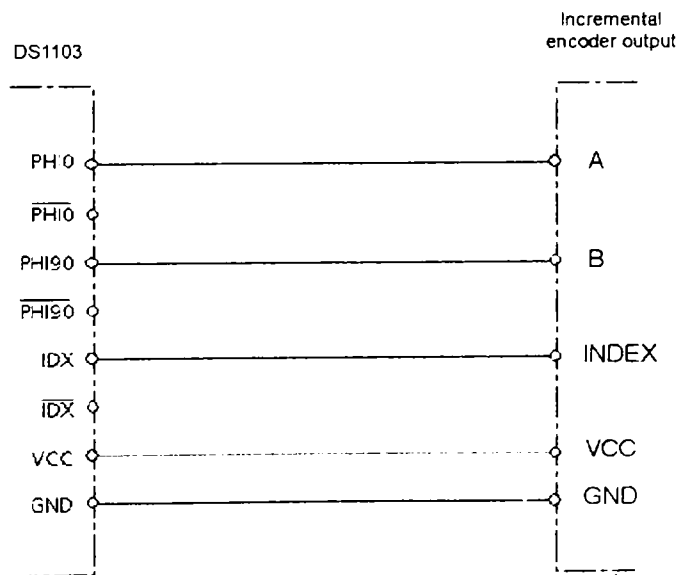


Fig. 6.9 Encoder providing single-ended TTL modes

Another important thing is to connect the encoder to the dSpace platform. The dSpace platform can work simultaneous with seven encoders (CP 32 ... CP 37 and CP 39) corresponding to channels 1 to 7.

Because the pin numbering of the Sub-D is not standardized the following figure shows the incremental encoder interface connector.

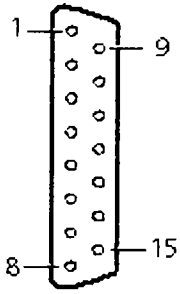
Connector (CP32 ... CP37, CP39)		Pin	Signal	Pin	Signal
	1	VCC (+5 V)			
	2	PHI0(x)	9	VCC (+5 V)	
	3	$\overline{\text{PHI0(x)}}$	10	GND	
	4	$\overline{\text{PHI90(x)}}$	11	GND	
	5	$\overline{\text{PHI90(x)}}$	12	GND	
	6	INDEX(x)	13	GND	
	7	$\overline{\text{INDEX(x)}}$	14	GND	
	8	GND	15	GND	

Fig. 6.10 dSpace incremental encoder interface connector

The last step is to set the software so that to know the encoder channel number (1 to 7) and to know if the encoder provides singleended TTL modes or differential RS422 signals.

### 6.2.4. Interface system

An interface board was designed in order to use the PWM outputs of the slave DSP unit for controlling the MOSFET drivers of the inverter.

It contains 5 pieces SFH750 fiber optic emitters (3 SPWM+ 1 ENABLE +1 PAUSE) and a SN74HCT541 non-inverting octal buffer to increase the DS1103 PWM signals current capability according to SFH750 optic fiber driver requirements (see Fig. 6.11). Additionally, series connected LED mounted on the front panel display the logic state of the optic fiber signals.

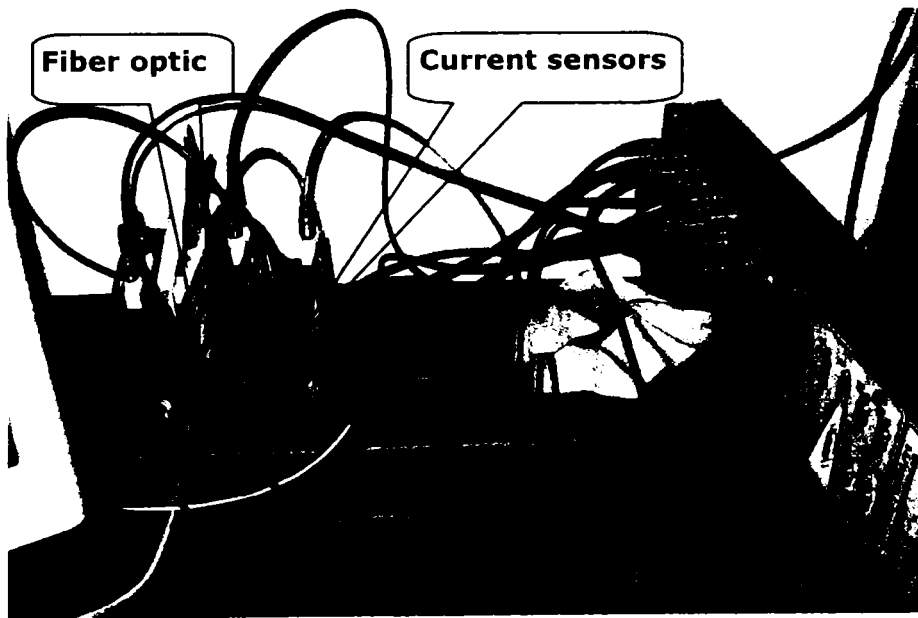


Fig. 6.11 The interface system

## 6.3. Software

The entire software was developed under **Matlab 6.5 Simulink** environment, compiled automatically using Microtec C compiler for Motorola Power PC and Texas Instruments C compiler and built/downloaded automatically in **Control Desk Developer** specialized interface software using the dSpace platform.

### 6.3.1. Matlab Simulink

The **Matlab 6.5 Simulink** software is divided in:

- measure and protection software where acquisition, software signal conditioning and software protection are made
- control and estimation algorithms

#### 6.3.1.1. Measure and protection software

The measure and protection is the first part of the developed software and has three main parts:

- acquisition scaling and digital filtering of the signals
- encoder interface
- protection

In the acquisition software the ADC channels are settled for acquiring the two currents in Fig. 6.12. The rotor currents are acquired on the 2 nonmultiplexed A/D channels with 12-bit resolution, 800 ns sampling time.

The software has the facility to acquire multiplexed channels with 16-bit resolution, 4  $\mu$ s sampling time. These are not used in the system.

Afterwards the measured quantities are scaled taking into account the scaling factors of the sensors. Also the third current is here calculated from the other two measured.

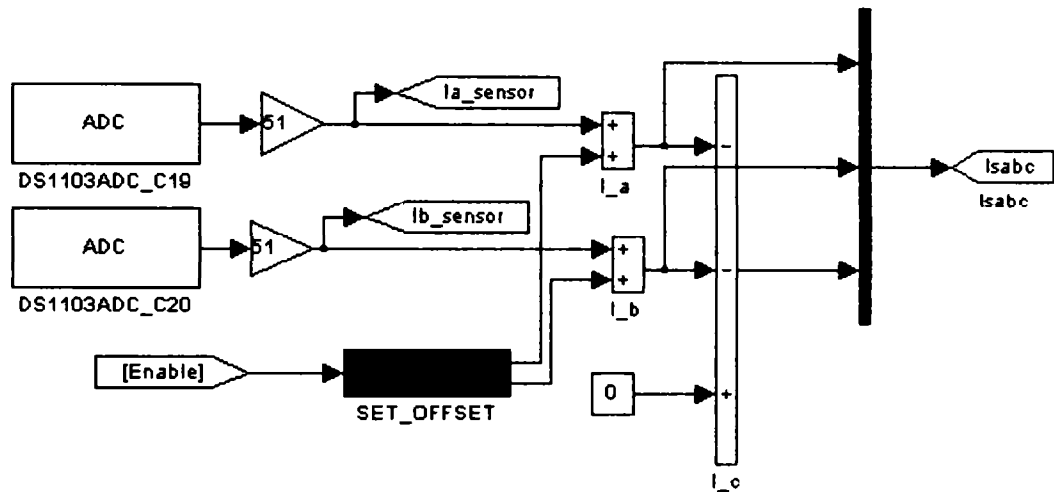


Fig. 6.12 Acquisition signals process

It is important to set in the software the input channel as it is in the dSpace terminal.

In the encoder interface (Fig. 6.13) the position of the rotor and its speed are computed. This could be obtained by counting the pulses coming on the dedicated hardware interface and knowing the encoder resolution (number of the pulses for one revolution) and the system sampling time.

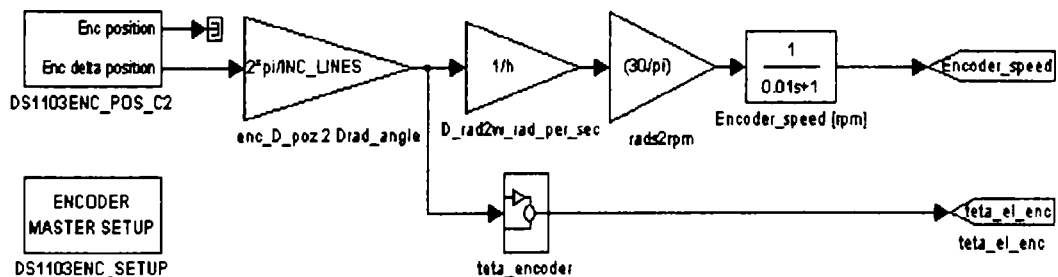


Fig. 6.13 Blocks for incremental encoder

In the software protection part, the entire inverter/motor protection is designed.

In the present case, two protections were implemented: the overcurrent protection and the overspeed protection (see Fig. 6.14). The implementation is done as follows: the measured quantities are compared with the threshold values and the negated output of the comparators passed through an OR gate together with the ENABLE signal. Thus, the output is inhibited by any of the measured values exceeding its threshold value.

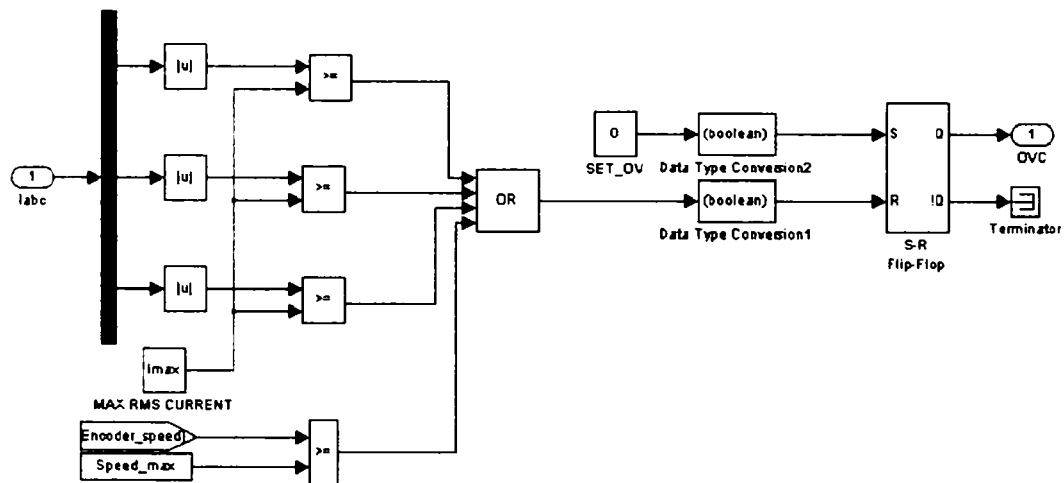


Fig. 6.14 Overcurrent and overspeed protection implementation

### 6.3.1.2. Control and estimation algorithms

The software also includes a control algorithm which can be built taking account into the user rules.

In the case of driving a motor, it is very important to know how to choose the inverter. In our case, it is necessary that the three control signals (Overcurrent, START and PAUSE) have the right value in order to allow the proper command of the inverter.

The algorithm uses the inputs (currents, voltages, position, speed etc.) and computes the applied command voltages ( $V_{\alpha}$  and  $V_{\beta}$ ). The **svmtmpl** function (see APPENDIX) automatically provides the duty cycles  $D_a$ ,  $D_b$  and  $D_c$  - the  $t_{on}$  of

the transistor - from the command voltages. Then, these duty cycles are introduced in a dSpace special block which will provide the PWM command signals for the upside transistors (see Fig. 6.15). The inverter (in our case) is capable to automatically provide the PWM command signals for the downside transistors, taking into account the imposed dead time.

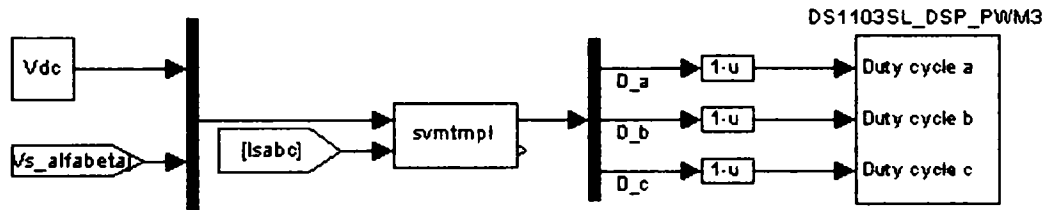


Fig. 6.15 Inverter pulses command

### 6.3.2. "Control Desk" Developer specialized real time interface software

When the soft is ready and it has no errors, it can be compiled in dSpace using the command BUILD. After the compilation, the soft is loaded in the interface called Control Desk (see Fig. 6.16). Now, this interface contains all system parameters and allows their visualization, acquisition and changing.

Thus at first, the system starts having all its variables and constants loaded from the soft developed in Matlab Simulink, and latter, if it is desired, these variables and constants can be modified in real time from the Control Desk Developer.

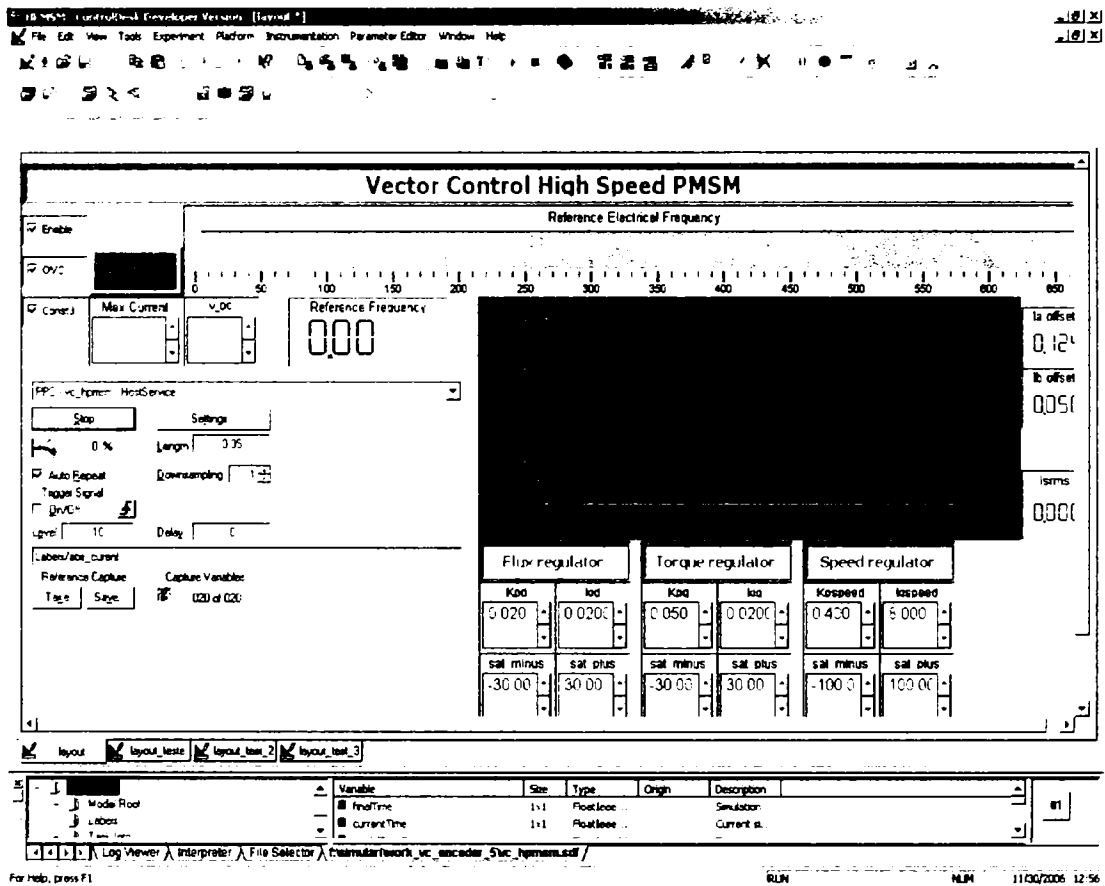


Fig. 6.16 dSpace Control Desk environment

## 6.4. From simulation to practical implementation

The simulation and the soft interacting with the hardware system are both developed in Matlab Simulink. Simulations implemented in dSpace are made in [8] to [19]. Thus, at first, a simulation can be developed and then it can be loaded in dSpace and used in practice by using specialized blocks (see Fig. 6.12, Fig. 6.13 and Fig. 6.15).

Fig. 6.17 presents the vector control simulation with encoder. In this simulation a virtual motor with the same characteristics as the real one is used.



## Vector control sensorless SPMSM

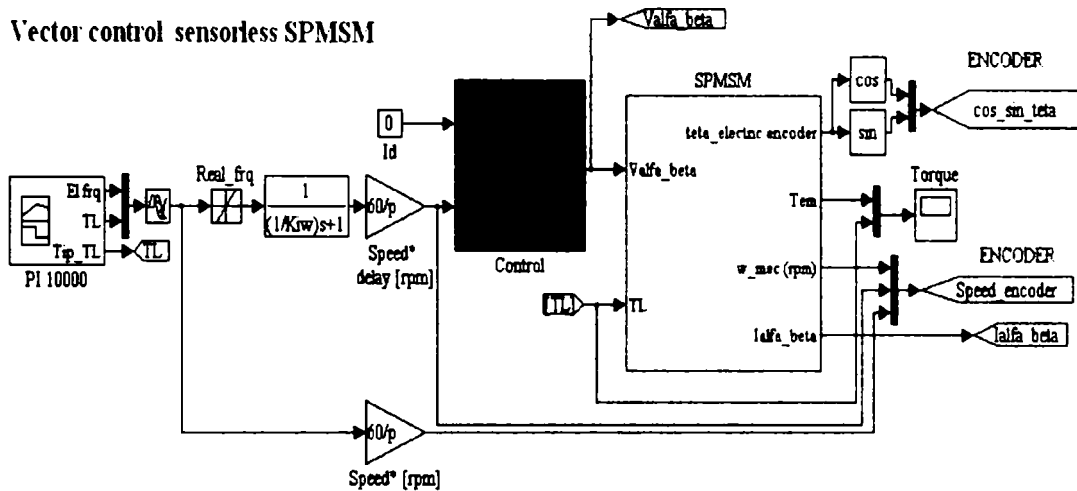


Fig. 6.17 Vector control simulation

The system from Fig. 6.17 can be easily implemented in dSpace following the next steps:

- The virtual motor is replaced by a specialized function and a dedicated block (see Fig. 6.15).
- The feedback from the virtual motor is replaced by the signals provided by the encoder mounted on the real motor shaft (see Fig. 6.13)
- The simulation currents are replaced by the signals provided by the current sensors (see Fig. 6.12)

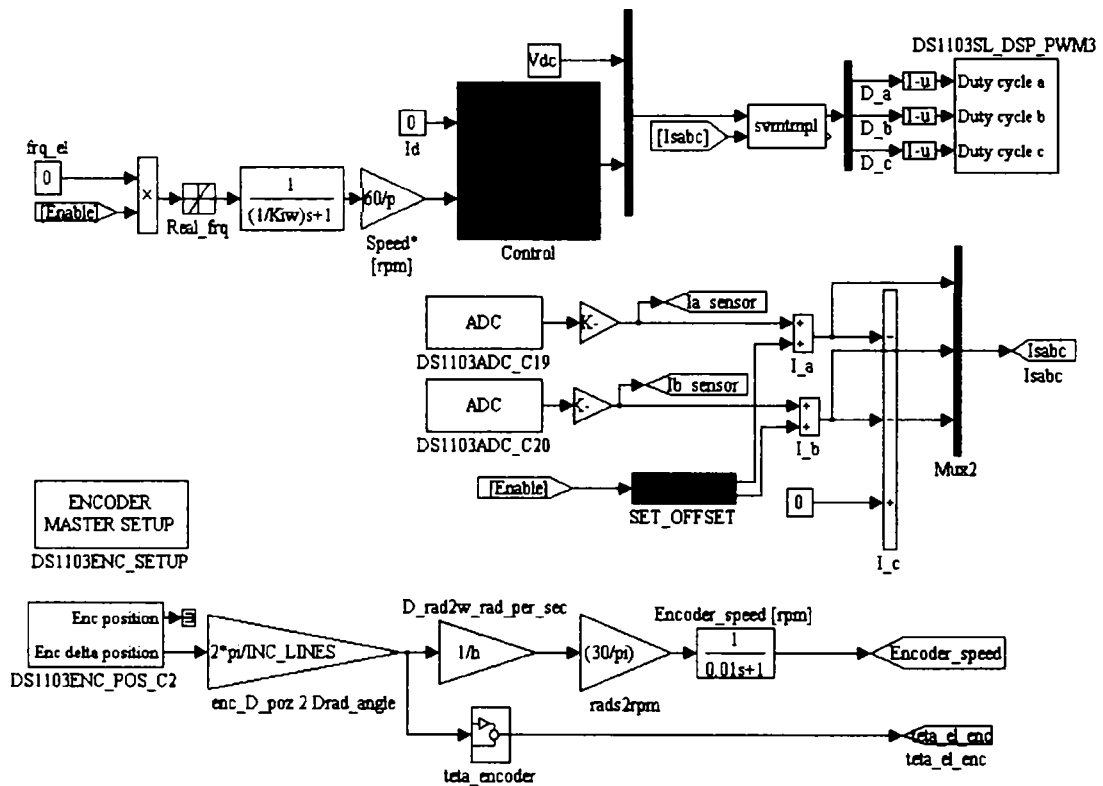


Fig. 6.18 Vector control simulation in Matlab Simulink

It has to be noticed that all these signals are real and thus, they have no ideal values, fact that could create some problems. It is recommended to use integrators with trigger (as it is shown in Fig. 6.19) in order to avoid problems.

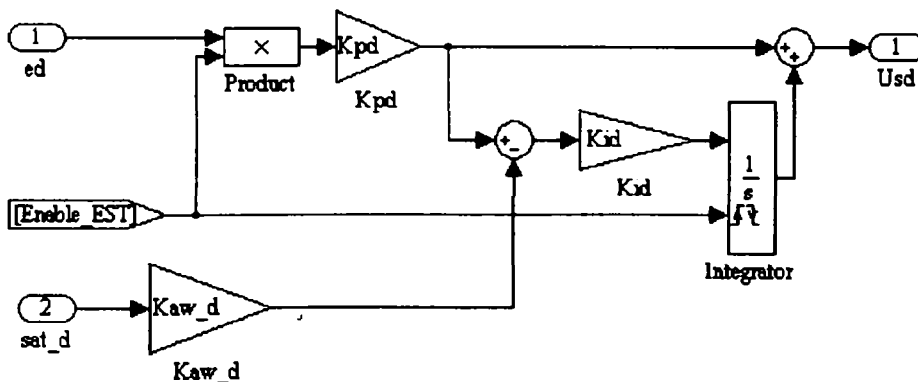


Fig. 6.19 PI implementation for dSpace system

## 6.5. The system tuning

For the HSPMSM command all the sensors must be tuned so that the transmitted data to the dSpace platform to be accordingly to the actual data and to correspond in totality with the control strategy requirements.

### 6.5.1. Current and voltage sensors tuning

The current sensors (Fig. 6.11) used in system management are 50A sensors. Their tuning consists in observation of the connection between the actual current and their output voltage. Then they are introduced into the dSpace platform. In the case of this considered situation the constant for current sensors is  $K_{ie}=51$  in (6.1). This constant depends of the resistor attached to the sensor and his value is suggested for any sensor datasheet.

$$K_{ie} = \frac{I}{U_{sensor}} \quad (6.1)$$

So, the sensor delivers to the dSpace board a voltage value but this value represents in fact a current (in the case of a current sensor).

### 6.5.2. Phase A Voltage Back Emf synchronization with incremental encoder

If a position sensor in the motor management is required, it is extremely important that phase a voltage back emf ( $U_{femfA}$ ) to be synchronized with the incremental encoder.

But in the case of an encoder embedded with the motor this is not realized. Almost anytime there is a delay between the encoder and the voltage (Fig. 6.20). In order that the system operates in suitable conditions both the encoder and the voltage  $U_{femfA}$  must reach 0 in the same time.

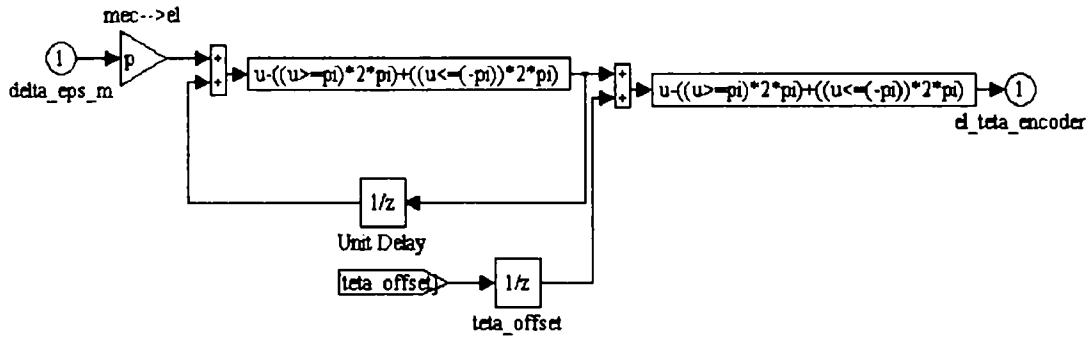
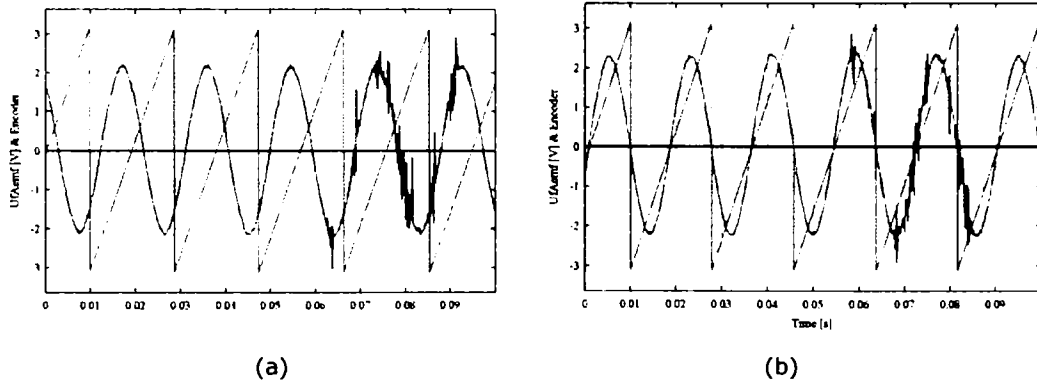


Fig. 6.20 Adding a constant value to the encoder angle

As it can be seen, in this case the delay has a relatively large value. This could be corrected by adding or extracting a constant angle from that delivered by the encoder.

This value will never be the same. The explanation is: at the moment of system start up, whatever the encoder position would be, this position is considered to be the zero position; the real zero position is in fact the one in which the permanent magnet axis d is aligned with the stator axis a (see Fig. 6.21).



(a) (b)  
 Fig. 6.21 Phase A Voltage Back Emf ( $U_{femfA}$ ) (blue line) and incremental encoder position (red line) before (a) and after (b) synchronization

### **6.5.3. Start up issues**

DSPACE is a user friendly software in which any simulation developed in Matlab Simulink can be easily implemented on a real-time system. Anyway some issues could occur. These will be discussed below. We will next refer to the control of a three phase motor (see Fig. 6.1).

#### **6.5.3.1. Optical fiber**

In the case study (see Fig. 6.1) the link between the dSPACE system and the inverter is realized by the use of 5 optic fibers. At the end of these optic fibers there are the transmitters which convert the electrical information in light signal (SFH 756) and at the other end of the optic fibers there are the receivers (SFH 551) which convert the light signal in electrical signal.

When the optic fiber is incorrectly cut (a special device for cutting is recommended to be used) the light signal could be lost.

Thus, before experimental tests start, it is important to verify the optical fibers with an oscilloscope: when a logical signal 1 is provided by dSPACE to the transmitters SFH 756V, the same logical signal 1 (3.3 V) has to be received to the optic fiber end. This can be measured on SFH 551 pins. Otherwise, the optic fiber will be cut until the right signal will appear.

#### **6.5.3.2. The congruence between the current sensors and the motor phases**

In the case of a control that uses the feedback from the current sensors (i.e. vector control), it is crucial that the signals from the current sensors to be in accordance with motor phases.

A necessary, but not sufficient condition, is to be sure that the sensor supposed to be on the phase a is truly on the motor phase a and the phase b sensor is on the phase b.

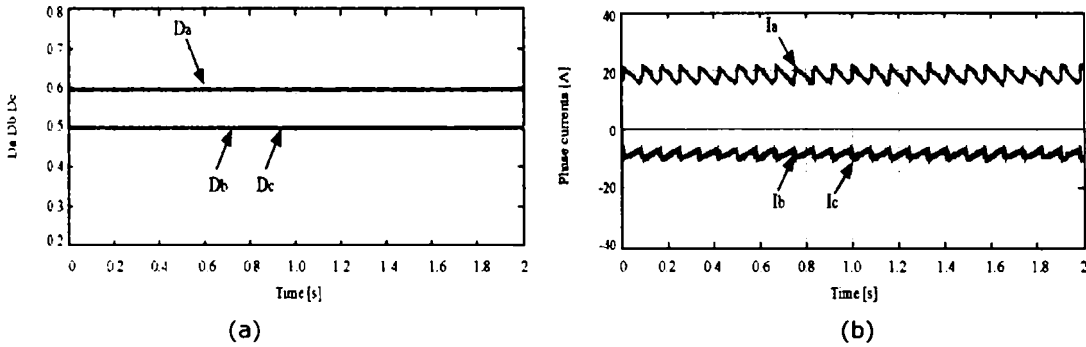


Fig. 6.22 Voltage prescription and actual current in motor for tuning the current sensors

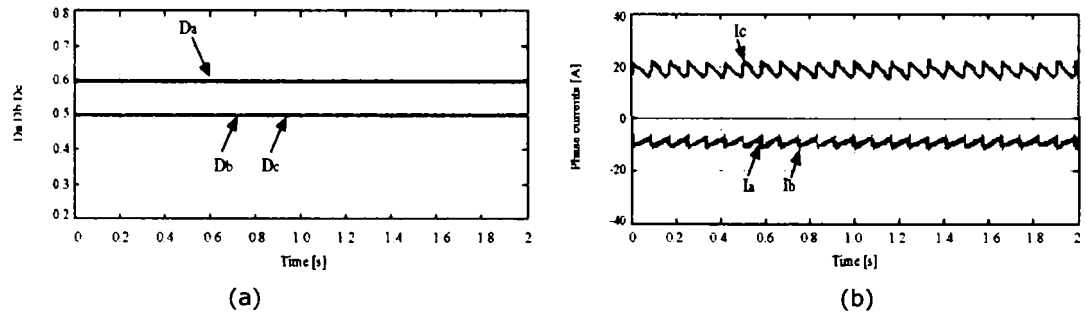


Fig. 6.23 Voltage prescription and actual current in motor for tuning the current sensors when sensors are not correctly calibrated

To be sure of that, a little test is recommended:

The voltage vectors  $V_{\alpha\beta a} > 0V$  and  $V_{\beta a} = 0V$  are applied. This is equivalent to apply the inverter pulses:  $D_a > 0.5$ ,  $D_b = 0.5$  and  $D_c = 0.5$ .

If the links are correctly, when the inverter pulses are applied, (see Fig. 6.22a), the monitored currents  $I_a$ ,  $I_b$  and  $I_c$  should appear as in Fig. 6.22b. Thus  $I_a$  should have a positive value and the other two currents should have negative equal values. Any other combination is not accepted (see for example Fig. 6.23).

If the current waveforms do not appear as in Fig. 6.22, follow the next steps:

**Step1**

Make sure that  $D_a$  corresponds to the phase a and the fiber optic links the dSpace with phase a inverter leg. Make the same checks for the other phases. If there is no problem go to the next step.

#### Step2

Measure the real phase voltage value using a voltmeter. If the current phase has not the right value, then  $D_a$ ,  $D_b$  and  $D_c$  are replaced with  $1-D_a$ ,  $1-D_b$  and  $1-D_c$  - these should be done due to the many existent inverter signals in the command board and in the inverter. If the current phase has the right value, then go to the next step.

#### Step3

Make sure that all motor phase wires pass correctly through the current sensors. If so, go to the next step. If not, change the direction through the sensors.

#### Step4

Change the sign of the sensor gain in (6.1).

Notice that combinations of these errors could occur. So, it is very important to resolve them step by step.

#### **6.5.3.3. Position sensor errors**

Another problem for the system is the position sensor device. First of all, it is important to know what kind of encoder will be used: single ended or differential. For this procedure, take in consideration Fig. 6.8 and Fig. 6.9.

In Fig. 6.1a the system has attached a differential encoder but the dSpace platform is set to use only three signals like in Fig. 6.8.

The encoder can be tested only when the system is working. For the test is important to rotate the machine with a scalar control. This encoder is worthless for the scalar control. Consequently, it will not be used.

The dSpace blocks dedicated for the encoders and the entire computation is presented in Fig. 6.13.

When the scalar control demands a positive speed on the Control Desk display should appear a positive speed according to the prescribed one. If this will not happened then:

- change two motor phases, but make sure this changes to not affect the current sensors OR
- modify the encoder dSpace links as follows: link PHI0 with phase b and PHI90 with phase a (crossover wires linking) (not recommended).

Another possible problem regarding the encoder device is that this one could be affected by mechanical vibrations or electromagnetic perturbations.

## 6.6. Conclusion

The experimental test platform used during the tests of state observers and sensorless control of a variable speed SPMSM system was presented in this chapter.

The main application of this system is for high speed machines, but the platform is suitable to investigate the motion control of any kind of machine with or without encoder.

All the hardware components of the system were presented, discussed and analyzed. The software used for measurements and protections, signal conditioning, vector control, flux estimators and position-speed observation is explained.

The software developed in Matlab Simulink and the interface "Control Desk" Developer from the dSpace platform and the way these two interact was also presented.

The tuning method for different kinds of sensors was described.

The possible errors and some methods to avoid them were discussed.



## References

- [1] R. Teodorescu, "Getting Started with dSpace system," *Flexible Drives System Laboratory (FDSL) Reference Manual*, Version 1.0, Institute of Energy Technology, Aalborg University, Denmark
- [2] B. Maurice, G. Izzo, T. Castagnet "Comparison Of Mosfet And Igbt Transistors in Motor Drive Applications" <http://www.st.com/stonline/products/literature/an/3717.pdf>
- [3] Longya Xu and Changjiang Wang, "Implementation and experimental implementation of sensorless control schemes for PMSM drives," *IEEE Trans. Ind. Appl.*, vol. 39, no. 3, pp. 783–791, May-June 2003.
- [4] Kenjo T. Power electronics for the Microprocessor Control. Oxford: Clarendon Press. 1990
- [5] P. D. C. Perera, F. Blaabjerg, J. K. Pedersen, and P. Thogersen, "A sensorless, stable V/f control method for permanent-magnet synchronous motor drives," *IEEE Trans. Ind. Appl.*, vol. 39, no. 3, pp. 783–791, May/Jun. 2003.
- [6] Jacek F. Gieras and Mitchell Wing "Permanent Magnet Motor Technology"
- [7] Mongeau P. "High torque/high power density permanent magnet motors." Naval Symp on Electr Machines, Newport, RI, USA, 1997
- [8] Lapusan, C.; Matis, V.; Balan, R.; Hancu, O.; Stan, S.; Lates, R. "Rapid control prototyping using matlab and dSpace. application for a planar parallel robot", IEEE International Conference on Automation, Quality and Testing, Robotics, 2008. AQTR 2008. Vol. 2, May 2008 pp, 361 - 364
- [9] Sefa, I.; Altin, N.; Ozdemir, S.; Demirtas, M.; "dSPACE based control of voltage source utility interactive inverter" International Symposium on Power Electronics, Electrical Drives, Automation and Motion, SPEEDAM 2008. 11-13 June 2008 Page(s):662 - 666
- [10] Meah, Kala; Hietpas, Steven; Ula, S.; "Rapid Control Prototyping of a Permanent Magnet DC Motor Drive System using dSPACE and Mathworks Simulink", Applied Power Electronics Conference, APEC March 2007 pp. 856 - 861
- [11] Salam, Z.; Soon, T.L.; Ramli, M.Z.; "Hardware Implementation of the High Frequency Link Inverter Using the dSPACE DS1104 Digital Signal Processing

- Board" IEEE International Power and Energy Conference, PECon '06. Nov. 2006 pp. 348 - 352
- [12] Venkatesa Perumal, B.; Chatterjee, J.K.; "SVPWM Implementation in dSPACE for Generalized Impedance Controller Used for Self Excited Induction Generation System" Power Electronics, Drives and Energy Systems, PEDES '06. Dec. 2006 pp. 1 - 6
- [13] Yang Luo; Hui Li; Mingyong Shen; "Speed Control of BLDCM for Industrial Sewing Machine Based on dSPACE" Mechatronics and Automation, Proc. of IEEE International Conference June 2006 pp. 2127 - 2132
- [14] Rubaai, A.; Ofoli, A.; Castro, M.; "dSPACE DSP-Based Rapid Prototyping of Fuzzy PID Controls for High Performance Brushless Servo Drives" Record of the 2006 IEEE IAS Annual Meeting. Conference Vol. 3, Oct. 2006 pp. 1360 - 1364
- [15] Nie, Z.; Emadi, A.; Chin, Y.; "A dSPACE control implementation for the standard three-phase boost rectifier" 30th Annual Conference of IEEE Industrial Electronics Society, 2004. IECON 2004. Vol. 1, Nov. 2004 pp. 1 - 5 Vol. 1
- [16] Laakkonen, O.; Rauma, K.; Saren, H.; Luukko, J.; Pyrhonen, O.; "Electric drive emulator using dSPACE real time platform for VHDL verification" The 2004 47th Midwest Symposium Circuits and Systems, 2004. MWSCAS July 2004 pp. iii - 279-82 vol.3
- [17] Jebali, T.; Jemli, M.; Boussak, M.; Gossa, M.; Kamoun, M.B.T.; "Dspace based experimental results of indirect field oriented control (IFOC) PWM VSI fed induction motor" Industrial Technology, IEEE ICIT '04. Dec. 2004 pp. 569 - 573 Vol. 2
- [18] Yang Luo; Hui Li; Mingyong Shen; "Speed Control of BLDCM for Industrial Sewing Machine Based on dSPACE" Mechatronics and Automation, IEEE International Conference June 2006 pp. 2127 - 2132
- [19] Hao Leo Li; Hu, A.P.; Jinfeng Gao; Xin Dai; "Development of a Direct AC-AC Converter Based on a DSPACE Platform" International Conference on Power System Technology, PowerCon 2006. Oct. 2006 pp. 1 - 6

# Chapter 7

## Conclusion and contributions

Due to the attractive efficiency, PMSMs are good candidates for pumps, micro-turbine started generation units, centrifugal compressors, grinding machines, textile machines, drill, dental drills, aerospace technologies drives. This thesis has been focused on control of PMSMs for such drives.

In order to provide synchronization between machine excitation frequency and rotor frequency, the rotor position is essential during PMSM vector control. The direct approach to obtain the rotor position information is an encoder position sensor. Because of the cost and of the reduced reliability, a rotor mounted angular position sensor is not desirable especially at high speed. In this situation a sensorless control is needed. Two sensorless controls for high speed drives have been investigated in this thesis.

Based on the results presented in the thesis, the main conclusions can be summarized as below.

### 7.1. Mathematical model and control properties

- For the SPMSM, the rotor  $d, q$  model is the most convenient since the vector control strategy is made in this reference frame.
- The stator reference frame was used to develop estimators for SPMSM machine and also for the novel control strategy.
- To understand the electrical machine behavior the machine equations, in both rotor and stator coordinate, are shortly presented in Chapter 2.

### 7.2. Sensorless vector control

- The vector control uses cascade control type, incorporating two inner current loops in rotor reference frame and an outer speed controller loop. The torque control is achieved by controlling the currents in  $d, q$  reference frame. The control system requires rotor position feedback in order to

perform self-synchronization. The basic PI controllers are sufficient for current and speed control in this system.

- In order to achieve sensorless operation of the drive, the position and angle estimators are required. It is important to consider the type of the machine (SPMSM or IPMSM) in the estimator architecture.
- The investigated rotor position estimator employs a phase-locked loop (PLL) state-estimator. It extracts the rotor position and speed estimations from the vector  $\bar{E}$ . The estimator receives the measured stator currents  $(I_a, I_b)$ , the reference voltages in stator coordinates  $(V_\alpha^*, V_\beta^*)$  and generates at the output both the rotor position  $\hat{\theta}_{er}$  and rotor speed  $\hat{\omega}_r$ .
- The voltage drop compensation of the inverter semiconductor devices is important in voltage amplitude especially at startup and low speed.
- Almost the same tests were performed both by simulations and on motor presented in Chapter 6.

### 7.3. Sensorless V/f control with two stabilizing loops

- Two solutions are presented in Chapter 4. The first solution is based on maintaining constant power angle while the second one brings to zero the internal reactive power. Both solutions have two stabilizing loops which lead the system to speed oscillations compensation. Furthermore, the second solution provides fast dynamic speed response.
- The stabilization of open loop V/f controlled PMSMs is achieved by using the two loops which provide voltage amplitude and angle corrections. To implement these stabilizing loops no position and d.c. link voltage sensors are required. In the system, these loops can also be seen as signals, which provide synchronization between the machine excitation and the rotor mechanical frequency.
- With the proposed voltage control method, making zero the interior reactive power was the best solution for drive stabilization. No rotor angle position sensor has been used to implement the complete drive system and the performance has shown that the drive is suitable for fast response high speed applications in Chapter 5.

- The sensorless control does not need the stator resistance value at all. The only necessary parameter to be known with approximation is the stator inductance.
- It can be said that the control system operates efficient knowing only the approximated values of the machine parameters.

## 7.4. Comparison of control methods

- The sensorless V/f control with two stabilizing loops calculation requires a shorter time compared with vector control strategy. This is due to the fact that the novel control system does not use rotor position, speed estimators and the Park transformations, in which the trigonometric functions  $\sin$  and  $\cos$  added a computation effort. That's why the overall calculation power required for implementation of the novel sensorless control method is less compared to the sensorless vector control method.
- The overall performance of the sensorless V/f control with two stabilizing loops is almost the same compared to the investigated sensorless vector control as it is illustrated by simulation results in Chapter 4.
- The novel V/f control starts from any rotor position without other supplementary startup strategy.
- The novel control system operates without a speed loop or current controllers for simplicity and robustness and does not use rotor position and speed estimators.
- No d.c. voltage or speed sensors are required in all studied sensorless control systems.
- The speed dynamics and steady state errors of novel control system, operating with approximated parameters values, are comparable with those of sensorless vector control which operates well with more exact parameters values.
- Considering the implementation simplicity and the overall performance of the drive, in conclusion, it can be said that the proposed V/f control method is a good alternative for vector control and could be a solution for high speed drive system where fast dynamic response is a necessity.

## 7.5. Original contributions

The main contributions in the thesis can be summarized as below:

- Operation using the vector control with encoder has no problems because the encoder provides accurate rotor angle position and speed. Due to the very small time constant, estimating the rotor position and speed is quite a challenging process. The practical testing of four rotor position and speed estimators for the high speed and fast dynamic sensorless vector control was performed in Chapter 2. The results from all estimators are compared with encoder sensor position. The estimator that answers better in the requirements has been chosen in the practical sensorless control presented in Chapter 3.
- Simulation and practical testing of the vector control with encoder and sensorless with selected estimator were performed (Chapter 2 and 3)
- A start-up procedure based on the automatically align of the motor in a known rotor position and voltage drop compensation of the inverter semiconductor devices was developed and implemented (Chapter 3).
- Two novel V/f controls with stabilizing loops with significant improvements of classical V/f control were proposed (Chapter 4 and 5).
- Development of one of this V/f control system performing as well as vector control system, but which has the advantage of less on line computation effort was developed, simulated and implemented in practice in Chapter 4 and Chapter 5. This novel control system does not need the exact values of the motor parameters in order to operate correctly. The startup is performed without knowing the machine initial position as for the standard V/f control, but having the same general dynamics as vector control (Chapter 4 and 5).
- The novel developed control does not need any position sensor and neither uses the rotor position and speed estimations. However, using this novel control, the prescribed speed is closely followed by the actual speed. The errors between the two speeds are similar to the ones obtained for the vector control (Chapter 5).

## 7.6. Future work

Even through several topics have been addressed in the thesis, there are some other, which are interesting for future research. Some of those topics are summarized below:

- Testing the motor at nominal speed and torque. This test could be performed increasing the voltage magnitude of the inverter d.c. link.
- Speed reversing at +/-20,000 rpm using the novel proposed control system, but also the sensorless vector control system. We mention that this test is the hardest test in which the motor can be tested. The first step was the performed speed reversal at  $I_a$  +/-10,000 rpm with the motor loaded at 80% of nominal torque (see Chapter 5).

## Summary in Romanian

### Sumar

Teza de față este dedicată controlului de înaltă performanță al motoarelor sincrone cu magneți permanenți de mare viteză și în mod particular al celor cu magneți de suprafață. Lucrarea oferă câteva soluții de control al acestor mașini și prezintă mai în detaliu o comparație, în capitole separate, a celui mai performant control existent, cel vectorial, cu un control nou propus.

Mașinile de mare viteză sunt răspândite în industrie ca: pompe, micro turbine, mașini din industria textilă, compresoare centrifugale, în domeniul stomatologic și aerospațial etc.

Această răspândire, de altfel din ce în ce mai mare, s-a datorat eficienței ridicate față de mașinile de inducție. Astfel în ultimii ani s-a încercat pe de o parte înlocuirea (acolo unde era cazul și rentabil ca și cost) a unor mașini de inducție cu mașini sincrone (și aici ne referim la tot domeniul de viteze) iar pe de altă parte propunerea de acționari noi care să aibă la bază mașinile sincrone a început să fie din ce în ce mai des întâlnită.

Totuși impedimentul major al impunerii pe piață al acestor mașini a fost în primul rând prețul iar mai apoi controlul performant al acestora. Dat fiind faptul că prețul magneților s-a ieftinit din ce în ce mai mult prin producția de serie s-a ajuns la o accesibilitate a acestor mașini care foloseau asemenea materiale. În ceea ce privește controlul au fost de la început și mai există probleme.

Problemele controlului erau de mai multe feluri. Pe de o parte era necesar ca mașina condusă să nu iasă din sincronism în timpul conducerii ei. Acest lucru presupunea folosirea unui traductor de turație (encoder) care indică poziția exactă a rotorului față de câmpul electric învârtitor creat în statorul mașinii. Controalele folosite au fost aceleași ca și la mașina de inducție cu unele mici modificări. Trebuie amintit aici controlul cel mai performant explicat în literatură și folosit și la mașinile de inducție și anume cel vectorial. Astfel mașinile sincrone cărora li se atașează un encoder pot funcționa foarte bine conduse prin controlul vectorial.

În Capitolele 2 și 3 se propune studiul controlului vectorial (atât în simulare cât și în implementare experimentală) cu și fără encoder, punându-se în evidență problemele apărute și soluții la acestea.



În lucrarea de față studiul s-a făcut pe o mașină cu magneți permanenți de suprafață (SPMSM) la viteza de 20,000 rpm și cu parametrii dați în Capitolul 6 al tezei. Dificultățile suplimentare întâmpinate s-au datorat și faptului că mașina controlată era de mare viteză cu o constantă de timp de aproximativ 0.5 ms. Astfel au fost făcute simulări cu această mașină dar și implementare experimentală pe un sistem de laborator. Provocarea majoră a fost atunci când s-a încercat conducerea fără senzor de mișcare (sensorless). Datorită faptului că mașina are nevoie de poziția exactă în fiecare moment a rotorului un estimator de mare precizie era necesar. Au fost testate patru estimatoare rapide de unghi și viteză pentru a fi implementate ulterior în controlul fără senzor de mișcare. S-a ajuns la concluzia că estimatorul care avea la baza tensiunile induse din stator și care ține cont de regim dinamic al acestora era cel mai potrivit. S-au făcut experimente complexe cu estimatorul ales prezentate în Capitolul 2 (simulare) și Capitolul 3 (implementare practică). În ceea ce privește implementarea practică a fost necesară aflarea poziției exacte a rotorului dar și compensarea tensiunii pierdută pe semiconductoarele din invertor pentru a avea o pornire corectă. Probleme mari au fost întâmpinate la reversare care pentru a putea fi realizată corect avea nevoie cu adevărat de o estimare a unghiului extrem de precisă.

Date fiind problemele apărute la controlul vectorial, s-a considerat oportun a se studia și propune un nou control, ca o alternativă la cel prezentat și existent în literatura de specialitate.

Ideea de a propune și introduce un control nou a venit de la problemele indicate în literatură apărute la motoarele de viteză mare relative la ciclul de calcul tot mai redus o dată cu creșterea vitezei dar și a problemelor legate de estimatorul de unghi și poziție.

În Capitolele 4 și 5 este prezentat noul control care are la baza controlul simplu cunoscut în literatura sub denumirea V/f standard numit și controlul scalar. Acestui control standard, extrem de simplu, i se atașează două bucle de corecție a amplitudinii și unghiului vectorului de tensiune prescris.

În Capitolul 4, care tratează simulările, sunt propuse două controale. În primul caz este tratat controlul unei mașini de viteză foarte mare (80000 rpm) care ține constant unghiul dintre vectorul fluxului statoric al mașinii (estimat) și vectorul curentului (calculat). Acest unghi este de dorit a fi mai mare de  $60^{\circ}$  pentru a garanta un factor de putere de 0.86. Acest control a redus oscilațiile de viteză existentele la controlul scalar îmbunătățit și randamentul mașinii dar nu și-a propus dinamicii mari ca și la controlul vectorial. Al doilea control simulat avea la bază tot

controlul standard V/f introducând două bucle de stabilizare. Controlul ține constantă puterea reactivă internă a mașinii lucru echivalent cu a conduce mașina, la un cuplu de încărcare dat, cu un curent minim deci randament maxim. Simulările s-au făcut cu o mașina de 20000 rpm și s-au remarcat prin rezultate excelente. Astfel nu numai că s-a îmbunătățit stabilitatea mașinii și randamentul dar s-a remarcat și prin faptul că mașina a putut fi accelerată și decelerată în timpi comparativi cu cei obținuți la controlul vectorial. Mai mult mașina pornește din orice poziție. Mai trebuie menționat faptul că ambele controale nu folosesc unghiul rotorului și viteza acestuia deloc în reglaj. Mașina funcționează fără a treia buclă, de turație, existentă la controlul vectorial dar nici nu folosește transformata Park deci, ambele controale, sunt mai rapide prin prisma calculelor făcute.

Ulterior controlul care monitorizează și ține constantă puterea reactivă internă este implementat pe un stand din laborator cu un motor existent de 0.4 Nm și 20000 rpm. Rezultatele experimentale obținute au confirmat simulările și au scos în evidență faptul că noul control poate conduce la fel de bine mașina ca și controlul vectorial deși nu folosește transformata Park, nu are nici un estimator de poziție sau unghi dar nici encoder folosind (numai cu aproximație) valoarea inductanței mașinii și curenții.

Sistemul experimental în ansamblu dar și unele probleme apărute în timpul punerii în funcțiune dar și rezolvarea acestora sunt prezentate într-un capitol separat.

## Organizarea tezei

Teza este organizată în șapte capitole după cum urmează:

În *primul capitol* este prezentată o viziune de ansamblu asupra mașinilor actuale cu magneți permanent și controlul acestora. Este făcută o clasificare a domeniilor în care se folosesc mașinile sincrone și sunt date câteva exemple. Avantajele folosirii mașinilor sincrone în comparație cu mașinile de inducție sunt puse în evidență. Sunt date detalii în ceea ce privește controlul lor și dificultățile care apar atunci când acestea sunt conduse la viteza mare.

În *capitolul doi* este prezentat un model de simulare dezvoltat pentru analiza controlului unei mașini sincrone cu magneți permanenți de viteza mare condusa cu

ajutorul controlului vectorial. Tot aici sunt prezentate și patru estimatoare de unghi și viteză necesare în controlul vectorial fără senzor de poziție.

În *capitolul trei* sunt prezentate rezultate experimentale detaliate obținute cu motorul și controlul simulat la capitolul precedent. Controlul vectorial a fost făcut cu estimatorul care se bazează pe tensiunea indusă obținută în regim dinamic, ales din cele patru estimatoare prezentate și simulate la capitolul precedent considerat a fi cel mai bun în regim dinamic cu timpul de răspuns rapid. Importanța căderii de tensiune pe elementele semiconductoare ale invertorului a fost demonstrată în special la pornire și s-a utilizat o compensare a acestei căderi de tensiune bazate pe poziția vectorului curent.

În *capitolul patru* este prezentată simularea a două controale propuse în conducerea mașinilor de mare viteză. Unul din controale se bazează pe menținerea unui factor de putere constant prin monitorizarea unghiului dintre vectorul curentului și a fluxului total statoric. A doua metoda monitorizează încontinuu puterea reactivă internă ținând-o la zero. Acest lucru este echivalent cu a funcționa la un cuplu de încărcare dat cu un curent minim deci cu randament maxim.

Controlul propus se bazează pe controlul scalar  $V/f$  care este îmbunătățit prin adăugarea a două bucle. Aceste bucle acționează asupra amplitudinii și fazei vectorului de tensiune prescris al mașinii. Efectul introducerii acestor bucle se regăsește în stabilizarea oscilațiilor mașinii dar și în dinamica acesteia. Practic controlul scalar este îmbunătățit în așa măsură încât performanțele obținute pot concura performanțele sistem vectorial studiat și prezentat în capitolele precedente.

În *capitolul cinci* sunt prezentate rezultate experimentale ale controlului nou propus care s-a axat pe reglajul puterii reactive interne. Acestea confirmă simulările făcute în capitolul precedent. În același timp sunt scoase încă o dată în evidență asemănările cu controlul vectorial implementat în capitolul trei.

În *capitolul șase* este prezentat în detaliu standul experimental cu motor, invertor, dar și sistemul de dezvoltare pentru aplicații în timp real cu software și echipamentul de control. Tot în acest capitol s-a considerat util a se face o mică prezentare a problemelor care pot apărea la punerea în funcțiune, pentru prima dată, a sistemului de control al unui motor trifazat. Pe acest stand experimental pot fi testate mai multe tipuri de motoare și implementate mai multe strategii de control.

*Capitolul șapte*, este rezervat concluziilor finale și contribuțiilor tezei.

## Contribuțiile tezei

Principalele contribuții ale tezei sunt punctate mai jos:

- Controlul vectorial cu encoder nu are probleme în ceea ce privește pornirea sau răspunsul în cuplu pentru că encoderul furnizează precis atât unghiul cât și poziția. Dat fiind faptul că motorul testat are constantă de timp foarte mică apar dificultăți la estimarea poziției sau a vitezei rotorice. Simularea a patru estimatoare de unghi și viteză cu dinamică rapidă necesare pentru controlul vectorial de mare viteză și compararea cu traductorul de poziție considerat ca martor s-a făcut în Capitolul 2. Estimatorul care a răspuns cel mai bine cerințelor a fost ales și îmbunătățit pentru conducerea practică fără senzor de poziție a motorului în Capitolul 3
- S-a simulat și implementat practic control vectorial cu encoder și sensorless cu ajutorul celui mai bun estimator (Capitolul 2 și 3)
- Implementarea unei proceduri de start prin compensarea tensiunii și alinierea automată a motorului într-o poziție cunoscută utilă la pornirea controlului vectorial fără senzor de mișcare (Capitolul 3).
- Propunerea a două noi metode sensorless de tip V/f cu bucle stabilizatoare diferite care îmbunătățesc evident controlul clasic V/f (Capitolul 4 și 5)
- Dezvoltarea uneia dintre metodele studiate ajungând să aibă performanțe relativ asemănătoare cu cele ale controlului vectorial dar care are nevoie de mai puțină putere de calcul a fost simulat și implementat practic în Capitolul 4 și 5. Sistemul nu are nevoie de parametri exacti ai mașinii pentru a funcționa corect. Pornirea se face fără a fi nevoie de poziția inițială ca și în cazul controlului standard V/f, având însă aceeași dinamică cu cea a controlului vectorial (Capitolul 4 și 5).
- Sistemul nou dezvoltat nu are nevoie de senzor de poziție dar nici nu folosește deloc în control poziția și viteză estimată pentru că nu are nevoie de acestea. Totuși controlul face ca viteză prescrisă să fie urmărită îndeaproape cu erori asemănătoare cu cele obținute la controlul vectorial (Capitolul 5).

**Author's papers related to the Ph. D. thesis**

- [1] R. Ancuti and I. Boldea, "V/f control of PM-SM super high speed drives with flux and power angle stabilizing loops," in *Proc. OPTIM 2006*, Brasov, May 2006, CD-ROM (index ISI Proc.).
- [2] R. Ancuti, G.-D. Andreescu, and I. Boldea, "Four rotor position and speed simplified estimators for vector control of high-speed SPMSM with test comparisons," *Journal of Electrical Engineering, JEE*, vol. 7, no. 4, Politehnica Publishing House, Timisoara, 2007 (index INSPEC).
- [3] R. Ancuti, I. Boldea, G.-D. Andreescu, and D. Iles-Klumpner, "Novel motion sensorless control of high-speed small-power surface mount PMSM drives: With experiments," in *Proc. OPTIM 2008*, Brasov, May 2008, vol. 3, pp. 11-18.(index ISI Proc.).
- [4] R. Ancuti, I. Boldea, G.-D. Andreescu and D. Iles "Fast Response Sensorless Control of High Speed Surface PM-SM: With Experiments" Nat. Conf. on Electric Drives, Romania, Timisoara 2008.
- [5] R. Ancuti, I. Boldea, G.-D. Andreescu "Sensorless V/f Control of Surface PMSM with Two Novel Stabilizing Loops for High Speed Dynamics" sent for publication to *IEEE Trans. on Energy Conversion* vol. EC, 2008 (ISI journal).

## Author's CV

# Ancuți Răzvan

### Office

S.C. BEESPEED Automatizari SRL  
Timisoara

Tel: 0256 204402

E-mail: [razvan@beespeed.ro](mailto:razvan@beespeed.ro)

### Home

Liviu Rebreanu 134/A, Timisoara

Tel: 0767 350550

E-mail: [ancuti\\_r@yahoo.com](mailto:ancuti_r@yahoo.com)

### Education

2002 – 2008 Ph.D. Student, University „Politehnica” of Timisoara

2002 Dipl. degree in Electrical Engineering

1997 – 2002 University „Politehnica” of Timisoara, Timisoara, Romania  
Department of Electrical Engineering

1993 – 1997 Computers High School “Grigore Moisil” of Timișoara

### Personal Experience

Aug. – Oct. 2006 Institute of Energy Technology, Aalborg University, (Denmark)  
Guest Researcher

### Personal Data

Born: July 11<sup>th</sup> 1978

Family: Unmarried

# APPENDIX

The used Space Vector Modulation (SVM) program (s-function implemented in MATLAB ® /Simulink) – created by Assist. Prof. Dr. **Cristian Lascu**.

## Symbols

### “svmtmpl.c” file

```
*Space Vector Modulation S-Function Template
* Project: PMSM Sensorless DTC drive
* Autor: Cristian Lascu, 2004
* Continut: Space Vector Modulation S-Function template for Simulink *
*Input: Vdc, Ualfa, Ubeta
*Output: Da, Db, Dc

#define S_FUNCTION_NAME svmtmpl
#define S_FUNCTION_LEVEL 2
#include "simstruc.h"
#include "svm.c"

static void mdlInitializeSizes(SimStruct *S)
{
    ssSetNumSFcnParams(S, 1); /* Number of expected parameters */
    if (ssGetNumSFcnParams(S) != ssGetSFcnParamsCount(S)) {
        /* Return if number of expected != number of actual parameters */
        return;
    }

    ssSetNumContStates(S, 0);
    ssSetNumDiscStates(S, 0);

    if (!ssSetNumInputPorts(S, 2)) return;
    ssSetInputPortWidth(S, 0, 3);
    ssSetInputPortDirectFeedThrough(S, 0, 1);
    ssSetInputPortWidth(S, 1, 3);
    ssSetInputPortDirectFeedThrough(S, 1, 1);
    if (!ssSetNumOutputPorts(S, 2)) return;
    ssSetOutputPortWidth(S, 0, 3);
    ssSetOutputPortWidth(S, 1, 2);
```

```

ssSetNumSampleTimes(S, 1);

/* Take care when specifying exception free code - see sfuntmpl.doc */
ssSetOptions(S, SS_OPTION_EXCEPTION_FREE_CODE);
//ssSetOptions(S, 0);
}

static void mdlInitializeSampleTimes(SimStruct *S)
{
//ssSetSampleTime(S, 0, CONTINUOUS_SAMPLE_TIME);
ssSetSampleTime(S, 0, INHERITED_SAMPLE_TIME);
ssSetOffsetTime(S, 0, 0.0);

}

static void mdlOutputs(SimStruct *S, int_T tid)
{
    InputRealPtrsType uPtr = ssGetInputPortRealSignalPtrs(S,0);
    InputRealPtrsType iPtr = ssGetInputPortRealSignalPtrs(S,1);
    real_T          *d = ssGetOutputPortRealSignal(S,0);
    real_T          *y = ssGetOutputPortRealSignal(S,1);
    real_T          *k = mxGetPr(ssGetSFcnParam(S,0));
    real_T u[3],i[3];
    u[0]=*uPtr[0];
    u[1]=*uPtr[1];
    u[2]=*uPtr[2];
    i[0]=*iPtr[0];
    i[1]=*iPtr[1];
    i[2]=*iPtr[2];
    SVM(u,i,d,y,k);
}

static void mdlTerminate(SimStruct *S){
}
#ifdef MATLAB_MEX_FILE /* Is this file being compiled as a MEX-file */
#include "simulink.c" /* MEX-file interface mechanism */
#else
#include "cg_sf.h" /* Code generation registration function */
#endif

```

### "svm.c" file

```

*Space Vector Modulation
*Project: PMSM Sensorless DTC drive
*Autor: Cristian Lascu, 2004

```



\*Continut: Space Vector Modulation

\*Input: Us.alfa, Us.beta, Vdc

\*Output: Da, Db, Dc

```
#include <math.h>
```

```
#include "vector.h"
```

```
#define R3 1.732051
```

```
#define Dmax 0.98
```

```
#define Dmin 0.02
```

```
// Space Vector Modulation
```

```
void SVM(real_T *u, real_T *i, real_T *d, real_T *y, real_T *k)
```

```
{
```

```
    struct Vector{real_T alfa,beta;} Us;
```

```
    real_T K>(*k)*tdead/h;
```

```
    real_T Umax=R3/u[0];
```

```
    real_T Da,Db,Dc;
```

```
    real_T T1,T2;
```

```
    int sector;
```

```
    Us.alfa = R3*Umax*u[1]; //normalizare - Holtz
```

```
    Us.beta = Umax*u[2];
```

```
// Sectorul tensiunii si timpii de modulare
```

```
if (Us.beta>0)
```

```
if (Us.alfa>Us.beta)
```

```
{
```

```
    sector=0;
```

```
    T1=0.5*(Us.alfa-Us.beta);
```

```
    T2=Us.beta;
```

```
}
```

```
else if (-Us.alfa<Us.beta)
```

```
{
```

```
    sector=1;
```

```
    T1=0.5*(Us.alfa+Us.beta);
```

```
    T2=0.5*(Us.beta-Us.alfa);
```

```
}
```

```
else
```

```
{
```

```

        sector=2;
        T1=Us.beta;
        T2=-0.5*(Us.alfa+Us.beta);
    }
else if (Us.alfa<Us.beta)
{
    sector=3;
    T1=0.5*(Us.beta-Us.alfa);
    T2=-Us.beta;
}
else if (-Us.alfa>Us.beta)
{
    sector=4;
    T1=-0.5*(Us.alfa+Us.beta);
    T2=0.5*(Us.alfa-Us.beta);
}
else
{
    sector=5;
    T1=-Us.beta;
    T2=0.5*(Us.alfa+Us.beta);
}

// Supramodularea Holtz
if (T1>1.0) T1=1.0,T2=0.0; //bang-bang
else if (T2>1.0) T2=1.0,T1=0.0; //bang-bang
else if (T1+T2>1.0) if (T1>T2) T2=1.0-T1; else T1=1.0-T2;//OVM

//Factorii de umplere - SVM
switch (sector) {
case 0: Da=0.5*(1.0+T1+T2);
        Db=0.5*(1.0-T1+T2);
        Dc=0.5*(1.0-T1-T2);
        break;
case 1: Da=0.5*(1.0+T1-T2);
        Db=0.5*(1.0+T1+T2);
        Dc=0.5*(1.0-T1-T2);
        break;
case 2: Da=0.5*(1.0-T1-T2);
        Db=0.5*(1.0+T1+T2);
        Dc=0.5*(1.0-T1+T2);
        break;
case 3: Da=0.5*(1.0-T1-T2);

```

```

        Db=0.5*(1.0+T1-T2);
        Dc=0.5*(1.0+T1+T2);
        break;
    case 4:    Da=0.5*(1.0-T1+T2);
        Db=0.5*(1.0-T1-T2);
        Dc=0.5*(1.0+T1+T2);
        break;
    case 5:    Da=0.5*(1.0+T1+T2);
        Db=0.5*(1.0-T1-T2);
        Dc=0.5*(1.0+T1-T2);
        break;
    default:
        Da=0.0;Db=0.0;Dc=0.0;
}

// Stator voltage
y[0] = u[0]*(2.0*Da-Db-Dc)/3.0;
y[1] = u[0]*(Db-Dc)/R3;

// Dead-time compensation
Da = Da + K*sat(i[0],zone);
Db = Db + K*sat(i[1],zone);
Dc = Dc + K*sat(i[2],zone);

// Pulse drop
if (Da>Dmax) Da=1.0; else if (Da<Dmin) Da=0.0;
if (Db>Dmax) Db=1.0; else if (Db<Dmin) Db=0.0;
if (Dc>Dmax) Dc=1.0; else if (Dc<Dmin) Dc=0.0;

// Duty cycles
d[0] = Da;
d[1] = Db;
d[2] = Dc;
}

```

## "vector.h" file

```

*Global Variables and Constant Definitions
* Project: PMSM Sensorless DTC drive
* Autor: Cristian Lascu, 2004
* Continut: Global Variables and Constant Definitions

```

```

#ifndef VECTOR
#define VECTOR

```

```
// Sampling time
const real_T h=0.0002;           //           [s]

// SVM parameters
const real_T tdead = 2e-6;       // dead time [s]
const real_T zone = 1.0; // linear zone [A]

// Constante matematica
const real_T pi=3.1415926;

// Saturation function
real_T sat(real_T x, real_T z)
{
    if (x>z) return 1.0;
    else if (x<-z) return -1.0;
    else return x/z;
}

#endif
```